Technische Universität München

Fakultät für Physik

Lehrstuhl für Theoretische Physik IV (T31)

Flavour Physics Beyond the Standard Model in Top and Bottom Quarks

Emmanuel Stamou

Vollständiger Abdruck der von der Fakultät für Physik der Technischen Universität München zur Erlangung des akademischen Grades eines

Doktors der Naturwissenschaften (Dr. rer. nat.)

genehmigten Dissertation.

Vorsitzende:		Univ.-Prof. Dr. Laura Fabbietti
Prüfer der Dissertation:	1.	Univ.-Prof. Dr. Andrzej J. Buras (i.R.)
	2.	Univ.-Prof. Dr. Alejandro Ibarra

Die Dissertation wurde am 18.09.2013 bei der Technischen Universität München eingereicht und durch die Fakultät für Physik am 02.10.2013 angenommen.

Contents

1 Introduction **1**

I Foundations **4**

Minimal Flavour Violation 5

2 Gauged Flavour Symmetries **6**

2.1 Maximally Gauged Flavour 7
2.2 Composite See-Saw Mechanism 9
2.3 The Departure from MFV 10
2.4 Flavour-gauge Bosons 11

3 New Strong Interactions in Top Physics **14**

3.1 The Hypercolour Model 15

4 The Decays $B_q \to \ell^+\ell^-$ **18**

4.1 Experimental Status 18
4.2 The Standard Model Prediction 19

II Theoretical Implications **22**

5 Gauged Flavour Symmetries **23**

5.1 Effective Lagrangians 23
5.1.1 $\Delta F = 2$ Transitions 24
5.1.2 $\overline{B} \to X_s\gamma$ 24
5.2 Wilson Coefficients from MGF 26
5.2.1 $\Delta F = 2$ Transitions 26
5.2.2 $\overline{B} \to X_s\gamma$ 28
5.3 Renormalisation Group Effects 30
5.3.1 $\Delta F = 2$ Transitions 30
5.3.2 $\overline{B} \to X_s\gamma$ 32

6 New Strong Interactions in Top Physics **37**

6.1 Hypercolour Resonances and Interactions 37
6.1.1 Pseudoscalar Pseudo-Goldstone Bosons 37
6.1.2 Vectors and Axial Vectors 38
6.1.3 Composite Quarks 41
6.1.4 P-wave Vector Mesons 44
6.2 $t\bar{t}$ Pair Production with Hypercolour Resonances 46

7 Electroweak Corrections to $B_q \to \ell^+\ell^-$ **51**
7.1 Matching Calculation of NLO Electroweak Corrections . . . 51
7.1.1 Standard Model Calculation . . . 53
7.1.2 Effective Theory Calculation . . . 55
7.2 Renormalisation Group Evolution . . . 58

III Phenomenology **60**

8 Flavour Phenomenology with Maximally Gauged Flavour **61**
8.1 Observables . . . 61
8.2 The Spectrum . . . 65
8.3 Flavour Analysis . . . 66
8.4 Comparison to alternative NP Scenarios and Summary . . . 71

9 New Strong Interactions in Top Physics **74**
9.1 $t\bar{t}$ Asymmetries at Tevatron and LHC . . . 74
9.2 The χ^2 Fit . . . 76
9.3 Benchmarks . . . 77

10 The Standard Model $B_q \to \ell^+\ell^-$ Prediction **85**
10.1 The Impact of the Electroweak Corrections on $\mathcal{C}_{10}$ . . . 85
10.2 The Branching Ratio for $B_q \to \ell^+\ell^-$ . . . 91

IV Conclusions **94**

Appendix **98**

A Gauge Flavour Symmetries **98**
A.1 Feynmann Rules for MGF . . . 98
A.1.1 Couplings to SM Bosons . . . 98
A.1.2 Couplings to Flavour Gauge Bosons . . . 100
A.2 Couplings of the Lightest Flavour Gauge Boson . . . 100

B New Strong Interactions in Top Physics **104**
B.1 Flavour Symmetry Breaking . . . 104
B.2 Vector Meson Dominance . . . 106

C Electroweak Corrections to $B_q \to \ell^+\ell^-$ **107**
C.1 Details on the Standard Model Calculation . . . 107
C.2 Details on the Effective Theory Calculation . . . 108
C.3 Threshold Corrections for α_e . . . 110
C.4 Details on the Renormalisation Group Evolution . . . 111
C.5 Numerical Study of $\mathcal{C}_{10}$ in the OS-1 Scheme . . . 114

Bibliography **116**

1 Introduction

Cosmos, from the greek "*κόσμος*", has the etymological meaning of order but also jewel. It is the perfect word for physicists to name the universe. We want to believe that the physical cosmos is comprehensible. That it has regular structures and principles that we can observe, model and, in our own limitations, comprehend. We call this process understanding.

Particle physics aims to understand physical phenomena at microscopic distances. So far, the field has been most successful in combining experimental observations with appropriate mathematical descriptions that lead to discoveries shaping the way we perceive our physical cosmos. Quantum mechanics is arguably the most prominent discovery. Together with the principles of special relativity it builds today's particle physics language, quantum field theory (QFT), which provides a common theoretical framework within which we find accurate descriptions of physics in vastly separated length scales or, equivalently, energy scales: from the scale of atoms, 10^{-10} meters, down to the scale probed currently in the Large Hadron Collider (LHC) experiments, 10^{-20} meters.

The standard model of particle physics (SM) is the most successful description of the properties of observed particles. It provides a unified description of the strong and electroweak interactions and predicted the existence of a new scalar particle, the Higgs boson. In July 2012, the ATLAS and CMS collaborations at the LHC announced the observation of a 126-GeV heavy particle with the properties of the SM Higgs boson [1, 2]. The last missing part of the SM seems to have been found - a triumph for the LHC program and a turning point for the field of particle physics.

LHC was expected to discover some new dynamics at the TeV scale responsible for unitarising weak-boson scattering. The observation of a Higgs boson basically established that this is realised through a weakly-coupled scalar. This may be just the SM Higgs, in which case a lot of questions are left unanswered, as we know from observations that physics beyond the SM exists: The SM has massless neutrinos contradicting experimental evidence for neutrino masses from neutrino oscillations. It does not have a viable candidate for dark matter, whose existence we infer from its gravitational effects on luminous matter. It does not have enough sources of CP violation to explain the observed ratio of abundances of matter and antimatter. It predicts a vacuum energy density 120 times larger than observed. These are all phenomenological reasons for the existence of new physics (NP), but not necessarily for NP at the TeV scale.

There are also more theoretical, and as such more debatable, reasons to go beyond the SM. We single out two: the flavour puzzle and the hierarchy problem.

In the SM, the Higgs boson couples to the fermions through Yukawa interactions. Their strength controls the low-energy fermion masses and the mixings between different generations. The SM merely provides a parametric description of these masses and mixings, which is deemed unsatisfactory due to the vast hierarchies present in the mass spectrum, e.g. the top-quark Yukawa coupling is of $\mathcal{O}(1)$, while the electron Yukawa coupling is of $\mathcal{O}(10^{-6})$. This is the so called flavour puzzle. In particle physics, we often understand regular structures and large hierarchies using symmetries. For instance, we observe a hierarchy in the low-energy spectrum of quantum chromo dynamics (QCD), where pions are much lighter than all other resonances.

We have a dynamical explanation for this hierarchy: the spontaneous breaking of a global symmetry in the fundamental QCD Lagrangian. The hope is that also the flavour puzzle has a dynamical explanation that answers why fermions come in three generations. However, the energy scale of this new flavour dynamics is unknown.

The hierarchy problem is related to the Higgs particle, which has a singular role in the SM, because it is the one fundamental scalar particle of the theory. The presence of NP at some scale Λ associated with particles that interact with the Higgs has a striking consequence. The Higgs mass receives corrections proportional to Λ, i.e. its mass is dictated by the high scale, which renders the observation of a light Higgs unnatural. Fermions and gauge bosons are fundamentally different in this respect. Chiral and gauge symmetries, respectively, protect their masses. Whether Λ is the Planck scale, where gravitational interactions become large, or some other NP scale is not important for the argument. This naturalness issue of the SM is referred to as the hierarchy problem. Its most popular solution is to introduce low-scale supersymmetry to relate bosons to fermions and therefore scalars to fermions. The chiral-symmetry protection of the fermions transmits itself to the scalars and stabilises their mass under radiative corrections. Alternatively, the notion of a fundamental scalar is abandoned, replaced by a composite particel held together by new strong interactions. The same interactions account for electroweak symmetry breaking and are therefore expected to be detectable at the LHC. Taking the naturalness problem of the SM seriously implies NP close to the TeV scale.

The search for physics beyond the SM is pursued in two complementary approaches. In the high-energy frontier the new degrees of freedom are directly produced in high-energy collisions of SM particles. In the intensity frontier low-energy properties of SM particles are investigated that are indirectly sensitive to heavy degrees of freedom via radiative corrections. The absence of clear deviations from the SM in both direct and indirect searches means that an extension of the SM is only viable if its low-energy limit is close to the SM. Indirect searches for flavour violation beyond the SM probe energy scales far beyond those accessible in colliders. For this reason, flavour physics poses the most stringent constraints on extensions of the SM that solve the hierarchy problem. A phenomenologically viable low-scale extension of the SM needs to have a flavour sector closely aligned to the SM one. At the same time, in the era of small SM deviations, accurate SM predictions are imperative to disentangle NP effects from the SM background.

This is the theoretical perspective of the research presented in this thesis. It is a quest for flavourful low-scale new physics in the quark sector motivated by the hierarchy and the flavour problem, which we shall pursue in three parallel approaches:

Low-Scale Flavour Symmetries: Extending the SM gauge symmetries to include gauged flavour symmetries is a step towards the solution of the flavour puzzle and is not necessarily incompatible with a NP scale close to the TeV. New exotic quarks and flavour-gauge bosons enrich the SM spectrum and provide new sources of flavour and CP violation. The virtue of these constructions is the small number of new parameters and, thus, their predictivity. We investigate the predictions of a minimal construction on low-energy flavour observables in the bottom and kaon sector, which allow the scenario to be distinguished from the SM and alternative extensions.

New Strong Interactions in Top Physics: The top sector of the SM is closely linked to Higgs physics through the large top Yukawa couplings and is one of the least explored sectors of

the SM. It is currently being probed at the LHC, but the Tevatron experiments may have already glimpsed the first NP effects in the measurement of a anomalously large asymmetry in $t\bar{t}$ pair production. Nevertheless, the absence of further nonstandard signals at Tevatron and LHC puts strong constraints on extensions of the SM that account for the $t\bar{t}$ asymmetry. We construct a renormalisable extension of the SM with new strong QCD-like interactions and demonstrate that this hypercolour sector naturally accounts for the measured $t\bar{t}$ asymmetry without violating present collider and low-energy constraints.

The $B_s \to \mu^+\mu^-$ Prediction: The first observation of the $B_s \to \mu^+\mu^-$ decay from LHCb in 2012 was the highlight of the LHC flavour program so far. The good agreement of the SM prediction with the measured branching ratio marks yet another success for the SM and forbids large NP effects. The agreement and the prospects of a reduced experimental error render the improvement of the SM prediction pressing. The two main theoretical uncertainties in the prediction originate from a non-perturbative hadronic quantity, the decay constant of the B meson, and a perturbative scheme and scale dependence from, hitherto, missing electroweak corrections. We compute the full next-to-leading-order electroweak corrections to the $B_q \to \ell^+\ell^-$ decays within the SM, eliminating this previously major source of uncertainty to a large extent and update its SM prediction.

Since the three topics share a common structure we have decided to present them in parallel and not split, finding this beneficial for the understanding. For each topic we devote a chapter to each one of the three Parts of this thesis.

In Part I we lay out the foundations for the research. We present the gauged-flavour and hypercolour extensions of the SM, analyse the underlying theoretical motivation concentrating on their key elements. We discuss the current experimental and theoretical status of the $B_q \to \ell^+\ell^-$ decays and the level of improvement we expect from the calculation of the two-loop electroweak corrections.

In Part II we build on the foundations of Part I and look into their theoretical implications in more detail. We derive the effects of the gauged-flavour model to low-energy flavour observables. We work within an effective QFT, so some results are applicable to a larger class of extensions of the SM. For the hypercolour model we discuss its low-energy spectrum and the way we imitate QCD to gain insight on the strongly coupled regime of the theory. For the $B_q \to \ell^+\ell^-$ decays we present the computation of the next-to-leading-order electroweak corrections.

In Part III we apply our results and make contact with experiment. We present an extensive flavour analysis of the gauge-flavour model, analyse its flavour signatures and identify ways to distinguish the model from alternative extensions of the SM. In the hypercolour model we discuss benchmarks and explicitly demonstrate that the model can naturally account for the measured $t\bar{t}$ asymmetries without contradicting collider constraints from Tevatron and LHC. Finally, we update the SM predictions for the $B_q \to \ell^+\ell^-$ decays and assess the residual theoretical uncertainties after the electroweak corrections.

Part I

Foundations

Minimal Flavour Violation

The modern way of understanding dynamics at different energy scales is through a tower of effective theories, in which each theory has a validity range within which it is a good description of physics. As we increase the scale close to the high-energy validity limit of a given theory, the effects of new heavy degrees of freedom become important and can be parametrisable by contributions from nonrenormalisable operators. We can think of the SM as an effective theory, whose high-energy cutoff scale is yet unknown, but is expected to be close to the TeV scale if the next theory of the tower addresses the hierarchy problem.

Any such extension of the SM with a NP scale close to the TeV needs to have a very specific flavour structure to evade the stringent constraints from indirect searches of flavour and CP violation beyond the SM. Since all flavour and CP violation in the SM is described by the Yukawa couplings, this means that the effects of a viable low-scale extension of the SM, which are parametrisable nonrenormalisable operators involving only SM fields, should be approximately aligned to the SM Yukawas. Minimal Flavour Violation (MFV) [3, 4, 5, 6] is the effective field theory setup proposing that all flavour and CP violation can be parametrised entirely by the SM Yukawas, i.e. that the only sources of flavour breaking are the SM Yukawas. In Refs. [7, 8, 9], this criterion has been rigorously defined in terms of flavour symmetries by constructing nonrenormalisable operators that fulfil the MFV criterion.

We focus here on the quark sector. In the limit of vanishing Yukawa couplings, the SM quark Lagrangian is invariant under a global flavour symmetry, which is the product of non-abelian SU(3) terms,

$$G_f = \mathrm{SU}(3)_{Q_L} \times \mathrm{SU}(3)_{U_R} \times \mathrm{SU}(3)_{D_R}\,, \tag{1.1}$$

and three U(1) factors, that correspond to baryon number, hypercharge and a phase transformation on the right-handed down-type quarks. The $\mathrm{SU}(2)_L$-doublet Q_L and the $\mathrm{SU}(2)_L$-singlets U_R and D_R transform under G_f as

$$Q_L \sim (\mathbf{3},\mathbf{1},\mathbf{1})\,, \qquad U_R \sim (\mathbf{1},\mathbf{3},\mathbf{1})\,, \qquad D_R \sim (\mathbf{1},\mathbf{1},\mathbf{3})\,. \tag{1.2}$$

In order to write the usual SM Yukawa terms

$$\mathcal{L}_Y = \overline{Q}_L \mathcal{Y}_d D_R H + \overline{Q}_L \mathcal{Y}_u U_R \tilde{H} + \text{h.c.}\,, \tag{1.3}$$

where $\tilde{H} = i\tau_2 H^*$, manifestly invariant under G_f, the Yukawa couplings are promoted to dimensionless non-dynamical fields (spurions) with non-trivial transformation properties under G_f

$$\mathcal{Y}_u \sim (\mathbf{3},\overline{\mathbf{3}},\mathbf{1})\,, \qquad \mathcal{Y}_d \sim (\mathbf{3},\mathbf{1},\overline{\mathbf{3}})\,. \tag{1.4}$$

With the aid of these spurion fields, the SM operator basis can be systematically extended to include nonrenormalisable operators that are formally invariant under the flavour symmetry maintaining that the only sources of flavour breaking are the SM Yukawas. Note however, that MFV is just an *ansatz* for the flavour structure of unknown physics and not a theory of flavour.

We shall encounter MFV twice in the current work: In the next chapter, we consider a model that addresses the flavour puzzle and attempts to provide a dynamical understanding for MFV. In chapter 3, we will employ the MFV prescription on the hypercolour model to allow the scale to be as low as the TeV and simultaneously evade flavour constraints.

2 Gauged Flavour Symmetries

The flavour symmetry $\mathrm{U}(3)_{Q_L} \times \mathrm{U}(3)_{U_R} \times \mathrm{U}(3)_{D_R}$ is an approximate symmetry of the SM, broken by the Yukawa couplings, and is a fundamental element of the MFV prescription. A step towards a theory for quark masses and mixings is to explore extensions of the SM in which the flavour symmetry is a "fundamental" symmetry and explore dynamical explanations for its breaking. Such models have new flavour dynamics and the crucial question is then whether they can evade the strong constraints from indirect searches of NP but still be discovered at the LHC. This depends on the explicit construction and the nature of the symmetry.

The flavour symmetry may be part of a global symmetry that is spontaneously broken, similar to the spontaneous breaking of the $\mathrm{SU}(2)_A$ axial symmetry in two-flavour QCD. In this case, the spectrum of the theory is enriched by new massless modes, the Goldstone bosons, which have not been observed so far. Bounds on the existence of such massless states come from flavour physics and more importantly from hadron decays and astrophysics. Explicit sources of symmetry breaking could be introduced to evade such bounds, in which case the models lose predictivity.

Instead of explicitly breaking the symmetry, we can hide the Goldstone bosons of the global breaking by promoting the global to a local symmetry. This is a drastic modification of the theory with interesting phenomenological consequences. There is a new massless bosonic degree of freedom for each broken generator of the gauge group that is absorbed in the longitudinal components of the new gauge fields. Thus, the theory has massive gauge bosons that are charged under flavour and as such mediate flavour-changing-neutral currents (FCNC). For some time such a construction was considered incompatible with a low NP scale or at least challenging to achieve without violating the stringent bounds from flavour observables [10]. In Ref. [11] a general framework was presented that achieved exactly this in a natural way. Before we introduce it, we first sketch the naive argument against a low-scale flavour symmetry.

In the MFV *ansatz* the Yukawa interactions can be understood as effective interactions from nonrenormalisable operators built out of the SM fermion fields, the Higgs boson field and the flavon fields, φ. The flavons φ obtain vacuum expectations values that generate together with the NP scale Λ the Yukawa couplings y. The operators are invariant under the SM gauge group and suppressed by powers of Λ:

$$\mathcal{L}_{\text{Yukawa}} \propto y\, \bar{F} F H \propto \left(\frac{\varphi}{\Lambda}\right)^n \bar{F} F H\,. \tag{2.1}$$

This translates to a F-φ-F coupling of the strength

$$\left(\frac{\langle\varphi\rangle}{\Lambda}\right)^{n-1} \frac{\langle H\rangle}{\Lambda} \equiv \frac{m}{\langle\varphi\rangle}\,, \tag{2.2}$$

where m is the mass of the fermion and angle brackets indicate vacuum expectation value of scalar fields. $\langle\varphi\rangle$ controls the strength of the coupling, as opposed Λ. Since the flavon field is itself a source of flavour-symmetry breaking we expect $m_\varphi \approx \langle\varphi\rangle$. Integrating out the flavon

field we obtain flavour-changing four-fermion operators. In the $\Delta S = 2$ sector we have

$$\frac{1}{\Lambda^2}\frac{\langle H\rangle^2}{\langle\varphi\rangle^2}(\bar{s}\,\Gamma d)\;(\bar{d}\,\Gamma s)\,. \tag{2.3}$$

The measured value of ϵ_K gives a strong constraint on the coefficient $\frac{1}{\Lambda^2}\frac{\langle H\rangle^2}{\langle\varphi\rangle^2}$. $\langle\varphi\rangle$ must be small to reproduce the small down-quark masses via Eq. (2.1). Therefore, the bound forces the scale of the NP, Λ, to be much larger that the TeV scale, $\Lambda \sim 10^3 - 10^4$ TeV.

There is a way to evade this naive estimate against a low-scale flavour symmetry. If the masses of the fermions were not controlled by positive powers of $\langle\varphi\rangle$ as in Eq. (2.1), but instead by negative powers, Λ could be brought down to the electroweak scale without huge modifications of flavour observables. In such a setup, the SM fermion masses are inversely proportional to the masses of the flavon or gauge-boson fields; we obtain an inverted hierarchy of mass scales. Refs. [12, 13, 14] first presented models with inverted hierarchies, while more recently the authors of [11] identified a minimal and natural way of implementing the inverted hierarchy, while gauging the full non-abelian flavour symmetry of the SM quark sector. The minimality and predictivity of the setup in [11] stirred the interest of the community: In Ref. [15] the embedding of the gauge flavour symmetry in an SU(5) Grand Unified Theory was considered. The authors of Ref. [16] implemented the mechanism in the presence of a left-right symmetry. And in Ref. [17] the case of gauging the U(2) parts of the quark flavour symmetry was analysed. We focus on the most minimal model of [11], introducing it in the next section and identifying its predictions and signatures in chapters 5 and 8.

2.1 Maximally Gauged Flavour

The most minimal construction presented in [11] limits itself to the quark sector. The full non-abelian part of the SM quark-flavour symmetry, namely

$$G_f = \mathrm{SU}(3)_{Q_L} \times \mathrm{SU}(3)_{U_R} \times \mathrm{SU}(3)_{D_R}\,, \tag{2.4}$$

is gauged and the mechanism of inverse hierarchies is implemented. We refer to the construction as the "Maximally Gauged Flavour" (MGF) model. In Tab. 2.1, we list the matter content of the MGF model and the transformation properties of the fields under the SM and flavour symmetries.

Two ingredients are necessary to construct the model:

- cancelling anomalies of the flavour symmetries by introducing exotic quarks that are vectorlike under the SM gauge symmetries,
- forbidding the traditional Yukawa term Eq. (2.1) by the choice of the flavour charges.

In a gauge theory, quantum corrections respect the symmetries of the classical Lagrangian, as long as the theory is free of anomalies. Four dimensional theories, are anomaly free as long as the sum of all one-loop fermionic-triangle diagrams of all gauge-boson three-point functions cancels. This is always possible if the fermions transform under vectorlike representations of the gauge symmetries in question. We achieve this by introducing the exotic fields Ψ_{u_R}, Ψ_{d_R}, Ψ_{u_L} and Ψ_{d_L} with flipped chirality but with the same transformation properties under the flavour groups of G_f. The new quark fields are two right-handed $\mathrm{SU}(3)_{Q_L}$-triplets, one left-handed

	Q_L	U_R	D_R	H	Ψ_{u_R}	Ψ_{d_R}	Ψ_{u_L}	Ψ_{d_L}	Y_u	Y_d
$\mathrm{SU}(3)_c$	**3**	**3**	**3**	**1**	**3**	**3**	**3**	**3**	**1**	**1**
$\mathrm{SU}(2)_L$	**2**	**1**	**1**	**2**	**1**	**1**	**1**	**1**	**1**	**1**
$U(1)_Y$	$+1/6$	$+2/3$	$-1/3$	$+1/2$	$+2/3$	$-1/3$	$+2/3$	$-1/3$	0	0
$\mathrm{SU}(3)_{Q_L}$	**3**	**1**	**1**	**1**	**3**	**3**	**1**	**1**	$\overline{\mathbf{3}}$	$\overline{\mathbf{3}}$
$\mathrm{SU}(3)_{U_R}$	**1**	**3**	**1**	**1**	**1**	**1**	**3**	**1**	**3**	**1**
$\mathrm{SU}(3)_{D_R}$	**1**	**1**	**3**	**1**	**1**	**1**	**1**	**3**	**1**	**3**

Table 2.1: *The transformation properties of the matter fields under the SM and flavour gauge symmetries.*

$\mathrm{SU}(3)_{U_R}$-triplet and one left-handed $\mathrm{SU}(3)_{D_R}$-triplet, all of which are singlets under $\mathrm{SU}(2)_L$ and triplets of $\mathrm{SU}(3)_c$. Requiring also the mixed anomalies to cancel fixes the hypercharges of the exotics rather uniquely[1].

In the spirit of MFV we introduce two flavon fields Y_u and Y_d that transform as bifundamentals under the flavour symmetry and obtain vevs that break the flavour symmetry. The difference to MFV is that we choose their flavour charges such that we forbid the standard Yukawa term in the Lagrangian. This choice is the key point to obtain the mechanism of inverted hierarchies discussed above. With this matter content, the most general renormalisable Lagrangian invariant under the SM and flavour gauge groups splits into three parts

$$\mathcal{L} = \mathcal{L}_{\text{kin}} + \mathcal{L}_{\text{int}} - V\left[H, Y_u, Y_d\right] . \tag{2.5}$$

$\mathcal{L}_{\text{kin}}$ contains the kinetic terms of all the fields and the couplings of fermions and scalar bosons to the gauge bosons. The covariant derivative in $\mathcal{L}_{\text{kin}}$ accounts for the interactions of the SM gauge bosons with the fermions as well as the new flavour interactions of the flavour-gauge bosons with the fermions:

$$D_\mu \supset \sum_{f=Q,U,D} i\, g_f\, (A_f)_\mu\,, \qquad \text{with} \qquad (A_f)_\mu \equiv \sum_{a=1}^{8} (A_f^a)_\mu \frac{\lambda^a_{\mathrm{SU}(3)_f}}{2}\,. \tag{2.6}$$

$\{g_f\}$ are the three new flavour-gauge coupling constants, A_f^a are the flavour-gauge bosons in the flavour basis and $\lambda^a_{\mathrm{SU}(3)_f}$ the Gell-Mann matrices. Fermions charged under the flavour symmetry $\mathrm{SU}(3)_f$ get contracted with $\lambda^a_{\mathrm{SU}(3)_f}$ and therefore interact with A_f^a. The breaking of the flavour symmetry gives vevs to Y_u and Y_d that generate the masses of the flavour-gauge bosons through the kinetic terms of Y_u and Y_d.

$\mathcal{L}_{\text{int}}$ contains the quark-mass terms and the quark-scalar interactions:

$$\begin{aligned} \mathcal{L}_{\text{int}} = \quad & \lambda_u\, \overline{Q}_L \tilde{H}\, \Psi_{u_R} + \lambda'_u \overline{\Psi}_{u_L} Y_u\, \Psi_{u_R} + M_u\, \overline{\Psi}_{u_L} U_R \\ & + \lambda_d\, \overline{Q}_L H\, \Psi_{d_R} + \lambda'_d \overline{\Psi}_{d_L} Y_d\, \Psi_{d_R} + M_d\, \overline{\Psi}_{d_L} D_R + \text{h.c.}\,. \end{aligned} \tag{2.7}$$

$M_{u,d}$ are universal mass parameters and $\lambda^{(\prime)}_{u,d}$ are universal coupling constants that can be chosen real and positive through a redefinition of the fields.

[1] Ref. [11] briefly discusses an alternative hypercharge assignment.

The last term in Eq. (2.5) is the scalar potential of the model. It has not been constructed in Ref. [11] and it is not the aim of the present work to provide it. For a complete perturbative description of the masses and mixings we would have to specify the potential that spontaneously breaks both the electroweak and flavour symmetry and minimise it (see Ref. [18] for a recent analysis). The explicit construction of such a potential is an involved and model-dependent problem. Nevertheless, as shown in [11], low-scale phenomenology is insensitive to the flavon sectors. The mechanism of inverse hierarchies suppresses the low-energy effects of dynamical flavons even more than it suppresses the effects of the flavour-gauge bosons. Therefore, we assume that the spontaneous breaking of the electroweak symmetry proceeds as in the SM through the Higgs mechanism and that the spontaneous breaking of the flavour symmetry drives the flavon fields to develop the vevs

$$\langle Y_d \rangle = \hat{Y}_d \qquad \text{and} \qquad \langle Y_u \rangle = \hat{Y}_u \, V \,. \tag{2.8}$$

$\hat{Y}_{u,d}$ are diagonal 3×3 matrices and V is a unitary matrix. It is always possible to rotate all sources of flavour violation into the matrix V of the up-quark sector by appropriate (unphysical) field rotations of the exotic and SM quark fields. Despite the similarity to the corresponding MFV relation the matrix V is not the CKM matrix and the vevs $\langle Y_{u,d} \rangle$ do not coincide with the SM Yukawa matrices. The reason is the see-saw mechanism of the model that we discuss next.

2.2 Composite See-Saw Mechanism

After flavour- and electroweak-symmetry breaking the SM and exotic quarks mix, their mass matrix is not diagonal. In what follows we focus on the up-quark sector, but analogous formulae apply to the down-quark sector. From the interactions in Eq. (2.7) we obtain after electroweak- and flavour-symmetry breaking the mass matrix

$$\mathscr{L}_{\text{int}} \supset \begin{pmatrix} \overline{U}_L \\ \overline{\Psi}_{u_L} \end{pmatrix}^T \begin{pmatrix} 0 & \lambda_u \frac{v}{\sqrt{2}} \times \mathbb{I} \\ M_u \times \mathbb{I} & \lambda'_u \langle Y_u \rangle \end{pmatrix} \begin{pmatrix} U_R \\ \Psi_{u_R} \end{pmatrix} + \text{h.c.} \tag{2.9}$$

This is a mass matrix that resembles the see-saw neutrino mass matrix. The one-one entry is per construction exactly zero due to the charge assignment of Y_u and Y_d. We diagonalise the up- and down-type mass matrices by separately rotating the left- and right-handed fields by

$$\begin{pmatrix} u^i_{R,L} \\ u'^i_{R,L} \end{pmatrix} = \begin{pmatrix} c_{u_{(R,L)i}} & -s_{u_{(R,L)i}} \\ s_{u_{(R,L)i}} & c_{u_{(R,L)i}} \end{pmatrix} \begin{pmatrix} U^i_{R,L} \\ \Psi^i_{u_{R,L}} \end{pmatrix} . \tag{2.10}$$

u^i and u'^i denote the mass eigenstates with the masses m^i_u and m'^i_u, respectively and $c_{u_{(R,L)i}}$ and $s_{u_{(R,L)i}}$ the cosines and sines of the mixing angles in question. The see-saw relation then reads [19]

$$m_{u^i} \, m_{u'^i} = M_u \, \lambda_u \, \frac{v}{\sqrt{2}} \,. \tag{2.11}$$

In this way, the smallness of the SM masses is "explained" through their mixing with heavy fermions (see [20] and references therein and the discussion in [21]).

We express the masses in terms of the flavour symmetry breaking parameters

$$m_{u^i} = \frac{s_{u_{Ri}} \, s_{u_{Li}}}{c^2_{u_{Ri}} - s^2_{u_{Li}}} \lambda'_u (\hat{Y}_u)_i \,, \qquad m_{u'^i} = \frac{c_{u_{Ri}} \, c_{u_{Li}}}{c^2_{u_{Ri}} - s^2_{u_{Li}}} \lambda'_u (\hat{Y}_u)_i \,, \tag{2.12}$$

and obtain the mixings

$$s_{u_{Li}} = \sqrt{\frac{m_{u^i}}{M_u}\left|\frac{\lambda_u\, v\, m_{u'^i} - \sqrt{2}\, M_u\, m_{u^i}}{\sqrt{2}\,\left(m_{u'^i}^2 - m_{u^i}^2\right)}\right|}, \qquad s_{u_{Ri}} = \sqrt{\frac{m_{u^i}}{\lambda_u\, v}\left|\frac{\sqrt{2}\, M_u\, m_{u'^i} - \lambda_u\, v\, m_{u^i}}{m_{u'^i}^2 - m_{u^i}^2}\right|}. \quad (2.13)$$

These results are exact and valid for all quark generations. Taking the limit $m_{u'^i} \gg m_{u^i}$, we find simpler formulae that transparently expose the mechanism of inverted hierarchies. In this limit

$$m_{u^i} \approx \frac{v}{\sqrt{2}}\frac{\lambda_u\, M_u}{\lambda'_u\,(\hat{Y}_u)_i}, \qquad m_{u'^i} \approx \lambda'_u\,(\hat{Y}_u)_i, \quad (2.14)$$

$$s_{u_{Li}} \approx \sqrt{\frac{m_{u^i}}{m_{u'^i}}\frac{\lambda_u\, v}{\sqrt{2}\, M_u}}, \qquad s_{u_{Ri}} \approx \sqrt{\frac{m_{u^i}}{m_{u'^i}}\frac{\sqrt{2}\, M_u}{\lambda_u\, v}}, \quad (2.15)$$

as in the case of the usual see-saw scheme in which $(\hat{Y}_u)_i \gg M_u\,, v$. These simplified relations are valid for all quarks, with the exception of the top quark for which the condition $m_{t'} \gg m_t$ is not necessarily satisfied in which case Eq. (2.15) receives large corrections.

Eq. (2.14) illustrates the inverted hierarchy of the $\langle Y\rangle$ with respect to the SM Yukawas. This inverted proportionality is a result of the implemented see-saw mechanism and allows us to lower the scale of NP without saturating the strong bounds from FCNCs of light-quark generations. Apart from $\mathcal{O}(1)$ couplings two mass parameters, M_u and M_d, control the up- and down-sector separately.

2.3 The Departure from MFV

The presence of new exotic quarks mixing with the SM quarks modifies the couplings of the light mass eigenstates to the SM gauge and scalar sector with respect to the SM. The modifications are discussed in [11]. We collect in App. A.1.1 the Feynman rules for all modified interactions in $R_\xi = 1$ gauge.

Here, we focus on the modifications of the charged current-current interactions with SM and exotic quarks, since they control the new pattern of flavour violation. The couplings of the Z and Higgs boson to quarks also change, but they remain flavour diagonal, i.e. only transitions within a generation of SM and exotic quarks are possible (see App. A.1.1). The case of the W boson couplings is different. Whereas the unitary CKM matrix describes all flavour violation in the SM, this is no longer true in the MGF construction.

We adopt a matrix notation and construct a 6×6 non-unitary matrix from:

- the unitary 3×3 matrix V of Eq. (2.8) and
- the mixings $c_{u_{Li}}$, $c_{d_{Li}}$, $s_{u_{Li}}$ and $s_{d_{Li}}$ with $(i = 1, 2, 3)$ introduced in Eq. (2.13).

The non-unitary 6×6 matrix is a generalised CKM matrix parametrising the flavour violation between the six up-type and the six down-type quarks. The 3×3 submatrices

$$c_{u_L}\, V\, c_{d_L} \quad \text{and} \quad s_{u_L}\, V\, s_{d_L} \quad (2.16)$$

describe the charged (W^+) current-current interactions within the light and heavy systems, respectively. The analogous matrices

$$c_{u_L}\, V\, s_{d_L} \quad \text{and} \quad s_{u_L}\, V\, c_{d_L} \quad (2.17)$$

describe the charged current-current interactions between light and heavy fermions. In this notation, c_{u,d_L} and s_{u,d_L} are diagonal matrices with the entries $c_{u,d_{Li}}$ and $s_{u,d_{Li}}$, respectively.

The matrix $c_{u_L} V c_{d_L}$ is the experimentally measured CKM matrix even though it is not a unitary matrix. This is one way of understanding why the MGF model goes beyond the original MFV prescription. The amount of mixing, parametrised by the sines and cosines in Eq. (2.13), controls the extent of the departure from the unitary CKM picture. In the decoupling limit of no mixing $c_{(u,d)_{(L,R)}} \to 1$ and $s_{(u,d)_{(L,R)}} \to 0$ the 6×6 matrix reduces to

$$\begin{pmatrix} V & 0 \\ 0 & 0 \end{pmatrix} . \tag{2.18}$$

In this case, the CKM matrix coincides with the unitary matrix V and we recover the SM. As soon as the mixing is switched on, the CKM is modified to include c_{u,d_L} and unitarity is broken. These deviations from unitarity are quite small (see Sec. 8.2) due to the mechanism of inverted hierarchies. Moreover, no new CP-violating phases enter the resulting CKM matrix. At first sight this suggests that the CP-violating observables $S_{\psi K_s}$ and $S_{\psi\phi}$ should remain unaffected by the NP. However, this is not the case due to the presence of the exotic fermions matrix and the flavour-gauge bosons that we discuss in the next Section.

Another consequence of the modification of the CKM matrix is the breaking of the GIM mechanism if we consider only SM quarks in loop-induced processes. The GIM mechanism is recovered only after including also the exotic quarks. We explicitly demonstrate this in Sec. 5.2.

2.4 Flavour-gauge Bosons

The mechanism of inverted hierarchies suppresses large effects from the flavour-gauge bosons. Nevertheless, if the NP scale is close to the TeV scale and accessible at the LHC also the lighter flavour-gauge bosons should not be unnaturally heavier that the TeV scale. In this case, low-energy precision observables, which are very sensitive to tree-level flavour violation, could be the first to feel the effects of the new flavour sector. This makes the detailed study of the flavour-gauge-boson sector necessary to understand the phenomenological consequences and viability of the MGF model.

The few $\mathcal{O}(1)$ couplings and the two mass parameters M_u and M_d in Eq. (2.7) determine all masses and couplings of the gauge-boson sector. Once the flavour symmetry is spontaneously broken the flavons settle to their vevs and their kinetic terms reduce to mass terms for the flavour-gauge bosons. Similarly to the SM W_1^μ, W_2^μ, W_3^μ and B^μ gauge fields also the fields A_f^μ from Eq. (2.6) are not mass eigenstates, but mix with each other.

We use a vector notation and summarise the three types of flavour-gauge bosons, A_Q^a, A_U^a, and A_D^a in one flavour eigenstate vector

$$\chi = \left(A_Q^1, \ldots, A_Q^8, A_U^1, \ldots, A_U^8, A_D^1, \ldots, A_D^8\right)^T . \tag{2.19}$$

The corresponding term in the Lagrangian reads [19]

$$\mathcal{L}_{\text{mass}} = \frac{1}{2}\, \chi^T\, \mathcal{M}_A^2\, \chi\,, \qquad \text{with} \qquad \mathcal{M}_A^2 = \begin{pmatrix} M_{QQ}^2 & M_{QU}^2 & M_{QD}^2 \\ M_{UQ}^2 & M_{UU}^2 & 0 \\ M_{DQ}^2 & 0 & M_{DD}^2 \end{pmatrix} \tag{2.20}$$

and

$$\begin{aligned}
\left(M^2_{QQ}\right)_{ab} =& \frac{1}{4}\, g_Q^2\, \mathrm{Tr}\left[\langle Y_u\rangle \left\{\lambda^a_{\mathrm{SU}(3)}, \lambda^b_{\mathrm{SU}(3)}\right\} \langle Y_u\rangle^\dagger + \langle Y_d\rangle \left\{\lambda^a_{\mathrm{SU}(3)}, \lambda^b_{\mathrm{SU}(3)}\right\} \langle Y_d\rangle^\dagger\right] ,\\
\left(M^2_{UU}\right)_{ab} =& \frac{1}{4}\, g_U^2\, \mathrm{Tr}\left[\langle Y_u\rangle \left\{\lambda^a_{\mathrm{SU}(3)}, \lambda^b_{\mathrm{SU}(3)}\right\} \langle Y_u\rangle^\dagger\right] ,\\
\left(M^2_{DD}\right)_{ab} =& \frac{1}{4}\, g_D^2\, \mathrm{Tr}\left[\langle Y_d\rangle \left\{\lambda^a_{\mathrm{SU}(3)}, \lambda^b_{\mathrm{SU}(3)}\right\} \langle Y_d\rangle^\dagger\right] ,\\
\left(M^2_{QU}\right)_{ab} =& \left(M^2_{UQ}\right)_{ba} = -\frac{1}{2}\, g_Q\, g_U\, \mathrm{Tr}\left[\lambda^a_{\mathrm{SU}(3)} \langle Y_u\rangle^\dagger \lambda^b_{\mathrm{SU}(3)} \langle Y_u\rangle\right] ,\\
\left(M^2_{QD}\right)_{ab} =& \left(M^2_{DQ}\right)_{ba} = -\frac{1}{2}\, g_Q\, g_D\, \mathrm{Tr}\left[\lambda^a_{\mathrm{SU}(3)} \langle Y_d\rangle^\dagger \lambda^b_{\mathrm{SU}(3)} \langle Y_d\rangle\right] .
\end{aligned} \tag{2.21}$$

The mass matrix $\mathcal{M}_A$ is specific to the number and transformation properties of the flavon fields; we restricted ourselves here to the case of two bifundamentals Y_u and Y_d.

Next, we move to the mass-eigenstate basis

$$\varphi = (\hat{A}^1, \ldots, \hat{A}^{24})^T , \tag{2.22}$$

where $\{\hat{A}^m\}$ are the twenty-four mass eigenstates of the gauge bosons. Flavour basis χ and mass basis φ are connected through the transformation

$$\chi = \mathcal{W}\varphi . \tag{2.23}$$

We obtain $\mathcal{W}$ by diagonalising numerically $\mathcal{M}_A$ such that:

$$\hat{\mathcal{M}}^2_A = \mathcal{W}^T \mathcal{M}^2_A \mathcal{W} , \tag{2.24}$$

with $\hat{\mathcal{M}}_A$ the diagonal mass-matrix.

At last, we can calculate the couplings to quarks. We define the notation

$$U^T \equiv (u, c, t, u', c', t') \qquad \text{and} \qquad D^T \equiv (d, s, b, d', s', b') \tag{2.25}$$

such that the couplings of the flavour eigenstates to quarks is given by the Lagrangian terms

$$\mathcal{L} \supset + \overline{U}_i \gamma_\mu (\mathcal{G}^u_L + \mathcal{G}^u_R)_{ij,m} U_j \cdot \chi^\mu_m \tag{2.26}$$

$$+ \overline{D}_i \gamma_\mu (\mathcal{G}^d_L + \mathcal{G}^d_R)_{ij,m} D_j \cdot \chi^\mu_m . \tag{2.27}$$

m is understood to run from 1 to 24 and the tensors $\mathcal{G} \equiv \mathcal{G}[C_{L,R},\, g_{Q,U,D}]$ can be read off from the couplings of the flavour eigenstates A_Q, A_U, and A_D to the quarks listed in App. A.1.2. For instance

$$(\mathcal{G}^u_L)_{13,1} = \frac{g_Q}{2}\, c_{u_{L1}}\, (\lambda^1_{\mathrm{SU}(3)})_{13}\, c_{u_{L3}} \quad \text{and} \quad \left(\mathcal{G}^d_R\right)_{42,18} = \frac{g_D}{2}\, s_{d_{L1}}\, (\lambda^2_{\mathrm{SU}(3)})_{12}\, c_{d_{L2}} .$$

The rotation to the mass eigenstates of the heavy gauge bosons redefines the couplings:

$$\mathcal{L} \supset + \overline{U}_i \gamma_\mu (\hat{\mathcal{G}}^u_L + \hat{\mathcal{G}}^u_R)_{ij,k} U_j \cdot \varphi^\mu_k \tag{2.28}$$

$$+ \overline{D}_i \gamma_\mu (\hat{\mathcal{G}}^d_L + \hat{\mathcal{G}}^d_R)_{ij,k} D_j \cdot \varphi^\mu_k , \tag{2.29}$$

where

$$\left(\hat{\mathcal{G}}^\alpha_{L,R}\right)_{ij,m} = \sum_k \mathcal{W}(\varphi_m,\, \chi_k)\, \left(\mathcal{G}^\alpha_{L,R}\right)_{ij,m} , \qquad \text{with} \qquad \alpha = u, d . \tag{2.30}$$

In following chapters we shall either use $\{i,\, j\} \in \{1, \ldots, 6\}$ or refer directly to the SM or exotic quark flavour, i.e.

$$\left(\hat{\mathcal{G}}^{u}_{L,R}\right)_{15,m} \equiv \left(\hat{\mathcal{G}}^{u}_{L,R}\right)_{uc',m} , \qquad \left(\hat{\mathcal{G}}^{d}_{L,R}\right)_{23,m} \equiv \left(\hat{\mathcal{G}}^{d}_{L,R}\right)_{sb,m} . \tag{2.31}$$

The existence of flavour-violating gauge bosons in the MGF model is another non-MFV aspect of the MGF model. In the original MFV, setting the SM Yukawa to zero restores the complete flavour symmetry and forbids any flavour violation. Here, this is not the case. As seen from Eq. (2.14) we can set the SM Yukawas to zero without setting the spurion vevs $\langle Y_u \rangle$ and $\langle Y_d \rangle$ to zero. In this way, the flavour symmetry remains broken and the gauge bosons still account for flavour violation even though the SM Yukawas vanish.

3 New Strong Interactions in Top Physics

The nature of electroweak symmetry breaking is a central question in current particle physics and is being explored by the LHC experiments. An attractive mechanism to stabilise the Higgs mass under radiative corrections, is dynamical electroweak symmetry breaking via new strong interactions. Theories with a low, less than 1 TeV, strong-interaction scale are a particularly exciting possibility in the LHC era, due to the large number of resonances that may be experimentally accessible. In view of the recent discovery of a Higgs-like particle, an interesting possibility is low-scale bosonic technicolour [22], such as for instance superconformal technicolour presented in Refs. [23, 24]. Here, the Higgs vacuum expectation value is induced by strong dynamics and thus unnatural fine-tunings are avoided (for a perturbative realisation of this idea see also [25]). A first hint for a low strong-interaction scale may be the measurement of an anomalously large top-quark forward-backward asymmetry ($A_{FB}^{t\bar{t}}$) at the Tevatron.

Among the many explanations proposed [26], only a small subset satisfies all flavour constraints without fine-tuning. These are models in which the new vector or scalar fields transform non-trivially under flavour symmetries [27, 28]. Going through the list of possibilities, the best agreement with experiment is arguably achieved with relatively light vector particles, with masses of $\mathcal{O}(300\text{ GeV})$ and large couplings to right-handed up quarks. There are two possibilities for flavourful vector fields in a renormalisable theory: either they are gauge bosons of flavour symmetries or they are composite. While theories with light gauge-flavour bosons are a logical possibility, as we discussed in chapter 2, they must have a very particular structure to have a low NP scale and simultaneously satisfy flavour constraints. Also, they may require a complicated and potentially fine-tuned flavon-sector, see e.g. [11], however, this is still an open question. Thus, in this chapter we explore the second option. It implies a new strong-interaction scale of approximately 1/2 TeV, accompanied by sub-TeV hypercolour (HC) resonances, some of which may be charged under ordinary colour. Surprisingly, this possibility is not excluded by existing collider searches.

We build an explicit model with a confining HC gauge group, $\mathrm{SU}(N)_{\mathrm{HC}}$. From the fundamental particle-content point of view the model is very minimal. HC matter consists of three flavours of vectorlike fermions and one flavour-singlet scalar. We shall identify the flavour of the new fermions with the flavours of the ordinary right-handed up quarks. A hallmark of the model is the existence of new flavour-nonet vector resonances, as well as a flavour triplet of composite vectorlike up quarks (u', c', t') after confinement. The latter mix with ordinary right-handed up-quark fields, rendering up-type quarks partially composite, while down-type quarks remain fundamental. This is a phenomenologically attractive feature as it permits NP effects in the up sector, e.g. $A_{FB}^{t\bar{t}}$, without affecting the down-sector. It will follow directly from the SM gauge-symmetry charge assignments of the HC matter. The model is not constructed to provide a natural explanation for electroweak symmetry breaking - the Higgs field remains a fundamental scalar with a mass unstable under radiative corrections. The motivation for model is to naturally account for the measured $t\bar{t}$ asymmetries through light vectors with $\mathcal{O}(1)$ couplings to up and top quarks without violating collider and flavour constraints. The model and its phenomenology will appear in an upcoming publication [29].

3.1 The Hypercolour Model

QCD provides the prototype for a confining theory with a spectrum that contains flavoured vector mesons. Using QCD as a guide, we introduce an asymptotically free confining $\mathrm{SU(N)_{HC}}$ hypercolour gauge group. The anomaly-free matter content consists of three copies of vectorlike hypercolour quarks $\mathcal{Q}_{Li}, \mathcal{Q}_{Ri}$ $(i = 1, 2, 3)$ and a flavour-singlet hypercolour scalar $\mathcal{S}$, that transform under the HC and SM gauge symmetries as[1]

	$\mathcal{Q}_{L,i}$	$\mathcal{Q}_{R,i}$	$\mathcal{S}$
$\mathrm{SU}(N)_{\mathrm{HC}}$	N	N	$\overline{N}$
$\mathrm{SU}(3)_c$	1	1	3
$\mathrm{SU}(2)_L$	1	1	1
Y	a	a	b

We fix the hypercharge (and electric charge) to satisfy $a + b = 2/3$ and shall consider the specific case

$$a = 0 \qquad \text{and} \qquad b = 2/3\,.$$

The fermionic degrees of freedom are singlets under the SM gauge group and only the scalar $\mathcal{S}$ interacts through its colour and hypercharge with the SM gauge fields.

With this matter content, the most general renormalisable NP Lagrangian is

$$\begin{aligned}\mathscr{L}_{\mathrm{HC}} = \mathscr{L}_{\mathrm{kinetic}} &+ \left(\mathbf{h}_{ij}\, \bar{u}_{R,i}\, \mathcal{Q}_{L,j}\, \mathcal{S} \;+\; \mathrm{h.c.}\right) \\ &+ \mathbf{m}_{\mathcal{Q}ij}\, \overline{\mathcal{Q}}_i\, \mathcal{Q}_j \\ &+ m_{\mathcal{S}}^2\, |\mathcal{S}|^2 \;+ \lambda |\mathcal{S}|^4 \;+ \lambda' |\mathcal{S}|^2 |H|^2\,,\end{aligned} \tag{3.1}$$

where $u_{R,i}$ are the SM right-handed up quarks. Direct couplings to the left-handed SM quarks are not allowed by the hypercharge assignments. The "strong" Yukawa couplings $\mathbf{h}_{ij}$ couple the HC fermion sector to the up-quark sector of the SM. After confinement, $\mathcal{S}$ and $\mathcal{Q}$ form bound states with the quantum numbers of the SM up-type quarks, which induces mixing with the SM up sector.

The Yukawa couplings $\mathbf{h}_{ij}$ are new sources of flavour violation to which we apply the principle of MFV. At some high scale, we impose the global flavour symmetry $\mathrm{U}(3)_{U_R}$, under which (u_{R1}, u_{R2}, u_{R3}) and $(\mathcal{Q}_1, \mathcal{Q}_2\,, \mathcal{Q}_3)$ transform as flavour triplets, or its subgroup $\mathrm{U}(2)_{\mathrm{U_R}}$, under which the first two components transform as doublets. In the SM, the top and bottom Yukawa couplings break the global flavour-symmetry group $G_f = \mathrm{U}(3)_{U_R} \times \mathrm{U}(3)_{D_R} \times \mathrm{U}(3)_{Q_L}$ to its subgroup $\mathrm{H}_f = \mathrm{U}(2)_{U_R} \times \mathrm{U}(2)_{D_R} \times \mathrm{U}(2)_{Q_L} \times \mathrm{U}(1)_3$. Thus, in either case, at low energies we expect the strong Yukawa couplings and mass terms to be approximately

$$\mathbf{h} = \mathrm{diag}(h_1, h_1, h_3), \qquad \mathbf{m}_{\mathcal{Q}} = \mathrm{diag}(m_{\mathcal{Q}1}, m_{\mathcal{Q}1}, m_{\mathcal{Q}3}). \tag{3.2}$$

H_f is broken in the SM due to the (small) quark Yukawa couplings of light quarks and the CKM mixing angles. Therefore, the H_F breaking is small. We assume that this is the case in our model as well, i.e. we make use of the MFV hypothesis and align the new sources of flavour breaking to the SM Yukawas. In this way, the approximate $\mathrm{U}(2)_{U_R}$ symmetry protects against dangerous flavour violation and HC-contributions to $D - \overline{D}$ mixing as well as single

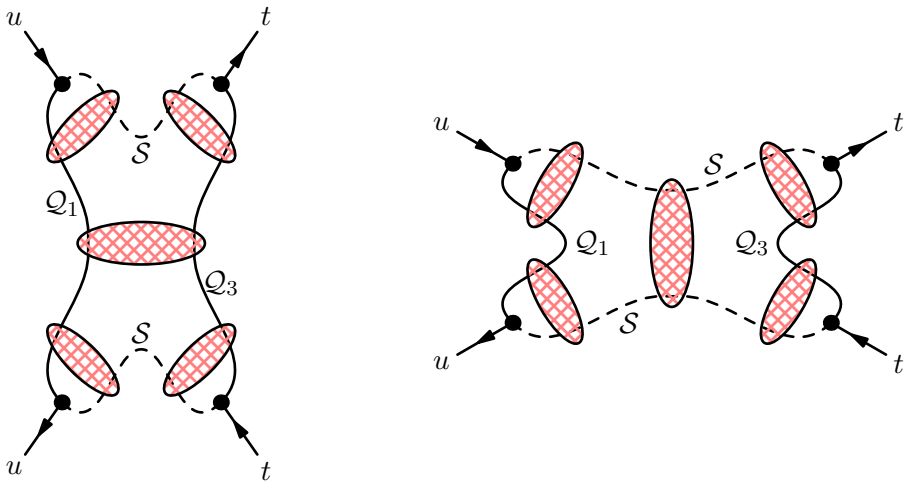

Figure 3.1: *$t\bar{t}$ pair production through HC matter in the UV description of the model. The flavour symmetry forbids single and same-sign top production. HC matter condenses to resonances indicated by ellipses. In the IR description, resonances contribute through both t- and s-channel $t\bar{t}$ production, left and right panel, respectively. All HC interactions to SM quarks proceed through the mixing with the composite up quarks.*

and same-sign top production are negligible. Our focus here is the top sector. Thus, the small breaking of H_F is not relevant for our discussion and we work in the limit of Eq. (3.2).

We stress the following:

- The fact that the HC-matter sector couples only to the right-handed up quarks is purely due to our choice of representations (hypercharge assignments). Were we to change the hypercharge of the $\mathcal{Q}_i$'s to $-1/3$ the HC sector would couple to the right-handed down quarks, or it would only couple to the left-handed quarks if the $\mathcal{Q}_i$'s were taken to be $SU(2)_L$ doublets.

- The set-up is compatible with generation of the quark-mass and mixing hierarchies via spontaneous breaking of a horizontal non-abelian symmetry at some high UV scale, e.g., U(3), or $\mathrm{U}(2)\times\mathrm{U}(1)$, or a discrete group, under which both SM and HC quarks transform (see chapter 2). In such a scenario, the MFV structure of the $\mathrm{U}(3)_{\mathrm{U_R}}$ or $\mathrm{U}(2)_{\mathrm{U_R}}$ global symmetry of the hypercolour sector would be an accidental consequence of the underlying horizontal symmetry, rather than being imposed explicitly. The strong Yukawa couplings and mass terms in Eq. (3.1) are dimension-four, whereas their MFV breaking corrections would be due to suppressed higher-dimensional operators.

- The flavour structure of the resonance mass spectrum, which we discuss in chapter 6, can provide a hint for the existence of such a fundamental horizontal symmetry in the UV (see also [30]).

The HC model is a minimal renormalisable extension of the SM with a very simple structure. Since we do not observe any free HC matter, at low energies the HC model has to be in its

[1] A less minimal alternative, which we do not pursue, is that the fermions are colour triplets and the scalar is a colour singlet.

strongly-coupled regime and the connection of the UV to the IR picture is distorted by non-perturbative dynamics. HC matter confines to bound states described by resonances in the same way that quarks confine to hadrons and mesons at low energies in QCD. The appropriate description of phenomena below the HC chiral-symmetry breaking scale is the IR picture. Fig. 3.1 illustrates $t\bar{t}$ production in both UV and IR picture. Light quarks mix with bound states of $\mathcal{Q}$ and $\mathcal{S}$ to produce the $t\bar{t}$ pair through exchange of t- and s-channel resonances.

In chapter 6 we discuss the resonance spectrum. Using QCD as an analogy, we relate the UV parameters of the theory, i.e. h_1, h_3, $m_{\mathcal{Q}_1}$, $m_{\mathcal{Q}_3}$ and $m_{\mathcal{S}}$, to properties of the low-energy particles and compute their contribution to the $t\bar{t}$ cross section. In chapter 9 we discuss the predictions of phenomenologically viable benchmarks. Some details on flavour breaking and scaling arguments are deferred to App. B.

4 The Decays $B_q \to \ell^+\ell^-$

The decays of the axial pseudo-scalars B_q with $q = d,\ s$ to two charged leptons are of particular importance for current particle physics phenomenology. In the SM, FCNCs mediate the decays and therefore there are no tree-level contributions; the decays are loop-induced. In addition, the decays are helicity suppressed, i.e. they are kinematically forbidden in the limit of zero masses for the charged leptons. For these reasons, the decays are very suppressed in the SM. At the same time, their decay rate can be predicted with high accuracy since the helicity structure of initial and final states forbids photonic-mediated one-loop amplitudes and because only one hadronic quantity enters the prediction, the decay constant of B_q.

The suppression of the $B_q \to \ell^+\ell^-$ rates and the theoretical cleanness of their SM prediction makes them powerful probes of the SM and extensions of it. Most prominent is the case of scenarios with two higgs-doublets, like supersymmetry. There, the decay rate is highly sensitive to Higgs penguins if $\tan\beta$ is large, with $\tan\beta$ the parameter controlling the hierarchy of the two vacuum expectation values. The large-$\tan\beta$ case predicts an enhanced branching ratio for the $B_q \to \ell^+\ell^-$ modes. The helicity suppression of the $B_q \to e^+e^-$ modes is too strong to experimentally access them at the moment and while the $B_q \to \tau^+\tau^-$ modes are much less suppressed, their experimental determination is challenging and unlikely to be possible in the near future. However, the decays $B_q \to \mu^+\mu^-$ are currently investigated by the LHC experiments with the highlight of the LHC flavour-program being the first observation of the $B_s \to \mu^+\mu^-$ mode from LHCb [31]. An observation close to what the SM predicts and another missed chance for supersymmetry to be found. In view of the current experimental status, the experimental prospects, and the importance of the decays in testing extensions of the SM it is of paramount importance to understand and improve the SM prediction.

At the moment, the two main sources of uncertainty in the SM are the decay constant f_{B_q} and hitherto unknown electroweak (EW) corrections. The precise calculation of f_{B_q} is actively pursued by the lattice community. In this part of the thesis, we focus on the calculation of the EW corrections. In the next Sections, we present the experimental status and the SM prediction for the $B_q \to \ell^+\ell^-$ decays. In chapter 7 we calculate the two-loop EW corrections for $B_q \to \ell^+\ell^-$ and in chapter 10 we present their branching ratio predictions and assess the residual uncertainties.

4.1 Experimental Status

In November 2012, LHCb reported the first experimental evidence of the decay $B_s \to \mu^+\mu^-$ with a signal significance of $3.5\,\sigma$ and the time-integrated and CP-averaged branching ratio [31]

$$\overline{\mathrm{BR}}(B_s \to \mu^+\mu^-) = \left(3.2^{+1.4}_{-1.2}(\mathrm{stat})^{+0.5}_{-0.3}(\mathrm{sys})\right) \cdot 10^{-9}\,, \tag{4.1}$$

well in agreement with SM predictions. For the decay $B_d \to \mu^+\mu^-$ LHCb provided the upper limit [31]

$$\overline{\mathrm{BR}}(B_d \to \mu^+\mu^-) < 9.0 \cdot 10^{-10}\,, \tag{4.2}$$

at 95% confidence-level.

LHCb raised the signal significance to $4.0\,\sigma$ in the summer 2013 after analysing the, at the time, full data set of 1 fb^{-1} at $\sqrt{s} = 7$ TeV and 2 fb^{-1} at $\sqrt{s} = 8$ TeV, with the result [32]

$$\overline{\mathrm{BR}}(B_s \to \mu^+\mu^-) = \left(2.9^{+1.1}_{-1.0}(\mathrm{stat})^{+0.3}_{-0.1}(\mathrm{sys})\right) \cdot 10^{-9}\,. \tag{4.3}$$

CMS confirmed the result independently utilizing its complete data set of 5 fb^{-1} at $\sqrt{s} = 7$ TeV and 20 fb^{-1} at $\sqrt{s} = 8$ TeV [33] reporting

$$\overline{\mathrm{BR}}(B_s \to \mu^+\mu^-) = \left(3.0^{+0.9}_{-0.8}(\mathrm{stat})^{+0.6}_{-0.4}(\mathrm{sys})\right) \cdot 10^{-9} \tag{4.4}$$

and the slightly higher signal significance of $4.3\,\sigma$. The weighted average of the two measurement is [34]

$$\overline{\mathrm{BR}}(B_s \to \mu^+\mu^-) = (2.9 \pm 0.7) \cdot 10^{-9}\,. \tag{4.5}$$

Both experiments also improved the upper 95% confidence limit on the $B_d \to \mu^+\mu^-$ decay:

$$\overline{\mathrm{BR}}(B_d \to \mu^+\mu^-) < 7.4 \cdot 10^{-10} \qquad \text{from LHCb [32] and} \tag{4.6}$$

$$\overline{\mathrm{BR}}(B_d \to \mu^+\mu^-) < 1.1 \cdot 10^{-9} \qquad \text{from CMS [33].} \tag{4.7}$$

The large decay width difference $\Delta\Gamma_s$ of the B_s system implies that the instantaneous branching ratio at time $t = 0$, $\mathrm{BR}^{[t=0]}(B_q \to \ell^+\ell^-)$, deviates from the time-integrated branching ratio, $\overline{\mathrm{BR}}(B_q \to \ell^+\ell^-)$. Neglecting for a moment cuts on the lifetime in the experimental determination of $\overline{\mathrm{BR}}$, the fully time-integrated and the instantaneous branching ratios are related in the SM as [35]

$$\overline{\mathrm{BR}} = \frac{\mathrm{BR}^{[t=0]}}{1 - y_q}\,, \qquad \text{with} \qquad y_q = \frac{\Delta\Gamma_q}{2\Gamma_q}\,. \tag{4.8}$$

In the B_s system, LHCb measured $y_s = 0.088 \pm 0.014$ [36, 37] and established a SM-like sign for $\Delta\Gamma_s$ [38]. The current world average for $\Delta\Gamma_s$ yields $y_s = 0.062 \pm 0.009$ [39].

By 2018, the experimental accuracy in LHCb in the B_s system is expected to reach $0.5 \cdot 10^{-9}$ and with 50 fb^{-1} $0.15 \cdot 10^{-9}$ [40]. The latter corresponds to an error at the 5% level with respect to the current central value. Results of comparable precision may be expected from CMS, and perhaps also from ATLAS.

4.2 The Standard Model Prediction

In the SM, the decay $B_q \to \ell^+\ell^-$ is governed by the effective $\Delta B = 1$ Lagrangian, in which the heavy degrees of freedom of the SM – the top quark, the weak gauge bosons and the Higgs boson – are decoupled. At lowest order in EW interactions, a single operator P_{10} contributes to the $B_q \to \ell^+\ell^-$ decay and the effective Lagrangian reduces to:

$$\mathscr{L}_{\mathrm{eff}} = \mathscr{L}^{(5)}_{\mathrm{QCD}\times\mathrm{QED}} + V_{tb}V^*_{tq}\,\mathcal{C}_{10}P_{10} + \mathrm{h.c.} \tag{4.9}$$

$P_{10} = [\bar{q}_L\,\gamma_\mu\,b_L][\bar{\ell}\,\gamma^\mu\gamma_5\,\ell]$ and $\mathcal{C}_{10}$ is its Wilson coefficient. $\mathscr{L}^{(5)}_{\text{QCD}\times\text{QED}}$ contains all QED and QCD interactions of the leptons and the five light quarks. V_{ij} denotes the relevant elements of the CKM quark mixing matrix. In these conventions the instantaneous branching ratio is

$$\text{BR}^{[t=0]}(B_q \to \ell^+\ell^-) = \mathcal{N}\left|\mathcal{C}_{10}\right|^2, \tag{4.10}$$

with the renormalisation-scheme-independent normalisation factor

$$\mathcal{N} = \frac{\tau_{B_q} M_{B_q}^3 f_{B_q}^2}{8\,\pi}|V_{tb}V_{tq}^*|^2\frac{m_\ell^2}{M_{B_q}^2}\sqrt{1-4\,m_\ell^2/M_{B_q}^2}\,. \tag{4.11}$$

$\text{BR}^{[t=0]}$ exhibits the helicity suppression from the smallness of m_ℓ and depends on the lifetime τ_{B_q} and the mass M_{B_q} of the B_q meson. A single hadronic parameter enters the prediction, f_{B_q}, the B_q decay constant defined by the matrix element

$$\left\langle 0|\bar{q}\,\gamma_\mu\gamma_5\,b|\bar{B}_q(p)\right\rangle = i f_{B_q} p_\mu\,. \tag{4.12}$$

f_{B_q} is nowadays subject to lattice calculations with errors at a few percent level eliminating this previously major source of uncertainty [41, 42, 43, 44]. The uncertainties due to f_{B_q}, τ_{B_q} and y_q approach a level of below 3% [45] in $\overline{\text{BR}}$.

Next, we consider perturbative uncertainties from the expansion of $\mathcal{C}_{10}$ in powers of QCD and electromagnetic couplings. In Eq. (4.9) we deviated from the usual convention to factor out combinations of EW parameters[1], such as the Fermi constant, G_F, the QED fine structure constant, α_e, the W-boson mass, M_W, or the sine of the weak mixing angle $s_W \equiv \sin(\theta_W)$. The most common normalisations are

$$\mathcal{C}_{10} = \frac{4G_F}{\sqrt{2}}\,c_{10}\,, \qquad\qquad \mathcal{C}_{10} = \frac{G_F^2 M_W^2}{\pi^2}\,\widetilde{c}_{10}\,, \tag{4.13}$$

with the LO Wilson coefficients

$$c_{10} = -\frac{\alpha_e}{4\pi}\frac{Y_0(x_t)}{s_W^2}\,, \qquad\qquad \widetilde{c}_{10} = -Y_0(x_t)\,. \tag{4.14}$$

They depend on the gauge-independent function Y_0 [46], where $x_t = (M_t/M_W)^2$ denotes the ratio of top-quark to W-boson mass and

$$Y_0(x) = \frac{x}{8}\left(\frac{4-x}{1-x} + \frac{3x}{(1-x)^2}\ln x\right)\,. \tag{4.15}$$

We shall refer to the choice c_{10} and $\widetilde{c}_{10}$ as the "single-G_F" and "quadratic-G_F" normalisation, respectively. The former choice is the standard convention of the $\Delta B = 1$ effective theory in the literature, whereas the latter choice removes the dependence on α_e and s_W in favour of G_F and M_W [47]. The virtue of the quadratic-G_F normalisation is that the LO Wilson coefficient depends only on G_F, M_t and M_W. It is therefore insensitive to the scheme of s_W or α_e.

As far as pure QCD corrections are concerned the two normalisation choices are equivalent. $\mathcal{C}_{10}$ depends at LO strongly on the renormalisation scheme for M_t under QCD. The NLO QCD

[1] We shall not vary the EW renormalisation scheme of the CKM factor $V_{tb}V_{tq}^*$. Thus, we keep it as a common factor to have a universal $\mathcal{C}_{10}$ for both $q = d$ and $q = s$.

contribution to $\mathcal{C}_{10}$ [48, 49, 50, 51] greatly reduced this major uncertainty and the upcoming calculation of these QCD corrections at NNLO [52] will render them negligible.

The two normalisations may also be considered equivalent at the lowest order in EW interactions due to the tree-level relation $G_F = \pi\alpha_e/(\sqrt{2}M_W^2 s_W^2)$. In practice, however, their LO numerical values vary by a lot if numerical input for the EW parameters is used that corresponds to different renormalisation schemes. For instance, the choice of $s_W^2 = 0.2231$ in the on-shell scheme [39] versus $s_W^2 = 0.2314$ in the $\overline{\text{MS}}$ [39] shifts the LO numerical value of the branching ratios by 7%. At higher orders in the EW interactions, the analytic form of $\mathcal{C}_{10}$ depends both on the normalisation choice and the EW renormalisation scheme. The power of G_F affects the matching, whereas the choice of the EW renormalisation scheme changes the finite counterterms for the parameters. By including these EW corrections, the overall numerical differences among the different choices of normalisations and EW schemes become much smaller and the large uncertainty present at lowest order is removed.

So far the full NLO EW corrections we unknown. In this work we close this gap and calculate them with a two-loop EW matching calculation. Being usually ignored in the budget of theoretical uncertainties of the branching ratios, the importance of a complete calculation was emphasized in Ref. [53]. There, the NLO EW corrections were employed in the limit of large top-quark mass [54], which is known to be insufficient at the level of accuracy aimed at Ref. [55], where analogous corrections to the $K \to \pi\nu\bar{\nu}$ decays were calculated. Ref. [53] estimated the residual EW uncertainties to be at least 5% on the branching ratio.

The Wilson coefficient $\mathcal{C}_{10}$ is evaluated at the scale where the heavy degrees of freedom are integrated out, the matching scale. The renormalisation group of the five-flavour theory evolves $\mathcal{C}_{10}$ down to the scale at which the matrix element in Eq. (4.12) is computed on the lattice. Under QCD, no operators mix with P_{10} and the Renormalisation Group Evolution (RGE) is trivial. This is not the case in QED. Operators in the effective Lagrangian mix into P_{10} and their Wilson coefficients enter the branching ratio prediction. Ref. [47] first considered these EW RGE corrections and we revisit them in light of our new EW matching calculation.

In chapter 7 we present the technical details of the calculation. We derive $\mathcal{C}_{10}$ at NLO in the EW interactions adopting the two normalisation choices and three EW renormalisation schemes. We solve the RGE and obtain $\mathcal{C}_{10}$ at the low-energy scale, of the order of the bottom-quark mass, at NLO order in the QED expansion. In chapter 10, we assess the numerical effect of the EW corrections on $\mathcal{C}_{10}$ and update the SM predictions for the branching ratios of the $B_q \to \ell^+\ell^-$ decays.

Part II

Theoretical Implications

5 Gauged Flavour Symmetries

In this chapter we take a closer look into the consequences of the MGF model. We make the connection to low-energy observables that are sensitive to the new flavour-violating sector focussing on $\Delta\mathrm{F}=2$ observables and the branching ratio of $\overline{B}\to X_s\gamma$. Our goal is to transparently separate the effects of exotic quarks from the flavour-gauge bosons to quantify their importance in the phenomenological analysis.

A complementary analysis including collider constraints and electroweak oblique corrections is performed in [11]. Their analysis does not include the effects from the flavour-gauge bosons that we discuss here in detail. The main constraint from Ref. [11] comes from the tree-level modification of the bottom-quark coupling to the Z boson. This affects its precisely measured width. However, as discussed in chapter 2, different parameters control the down- and the up-sector; they can be tuned independently from each other to evade the bound and still have light top partners in the spectrum.

In Sec. 5.1 we present the effective Lagrangians for $\Delta\mathrm{F}=2$ transitions and $\overline{B}\to X_s\gamma$ after integrating out the heavy degrees of freedom, e.g. W, Z, H bosons, top quark and all exotic quarks and flavour-gauge bosons. In Sec. 5.2 we calculate the contributions to the Wilson coefficients from exotic quarks and flavour-gauge bosons. In Sec. 5.3 we connect the high matching scale with the low meson-mass scales at which the hadronic matrix elements are evaluated by solving the Renormalisation Group. The results in Sec. 5.3 do not depend on the details of the MGF model, they apply to all UV completions that generate the same operators.

5.1 Effective Lagrangians

The notion of an effective QFT as a good description of physics for a limited range of energy scales is well suited to connect phenomena of different energy scales through a tower of effective QFTs. Here, we make use of such an effective theory to mediate the effects of the new heavy flavour sector down to the scales of the mesons. We match the MGF theory to the five-flavour theory of QED and QCD supplemented with nonrenormalisable operators, whose Wilson coefficients incorporate all effects from the electroweak and NP sector.

If the sole difference between the MGF model and the SM were the exotic quarks the matching would generate the same operators in both cases, since all flavour violation would still come from the left-handed coupling of the W bosons. The difference would be so-called matching corrections, i.e. modified Wilson coefficients of the SM operator basis. The presence of flavour violating bosons coupling to both left- and right-handed quarks changes this. Integrating them out generates new operators with non-zero Wilson coefficients.

5.1.1 $\Delta F = 2$ Transitions

The effective Lagrangian that describes $\Delta F = 2$ transitions of down-type quarks at LO in both the electroweak and flavour-gauge interactions reads

$$\mathscr{L}_{\text{eff}}^{\Delta F=2} = \mathscr{L}_{\text{QCD}\times\text{QED}}(u,d,s,c,b) - \frac{G_F^2\, M_W^2}{4\pi^2} \sum_i C_i(\mu) Q_i \,. \tag{5.1}$$

M_W is the mass of the W boson, Q_i are the relevant nonrenormalisable operators for the transitions given below and $C_i(\mu)$ their Wilson coefficients evaluated at a scale μ; we specify them in the next section.

In the SM the only operator generated is $Q_1^{\text{VLL}}(M)$, while here more dimension-six operators have non-zero Wilson coefficients. We neglect the effects from the flavon exchanges in which case the relevant operator basis for the $M - \overline{M}$ ($M = K^0, B_d^0, B_s^0$) systems reads [56]

$$\begin{aligned}
Q_1^{\text{VLL}}(K) &= (\bar{s}^\alpha \gamma_\mu P_L d^\alpha)(\bar{s}^\beta \gamma^\mu P_L d^\beta)\,, & Q_1^{\text{VLL}}(B_q) &= (\bar{b}^\alpha \gamma_\mu P_L q^\alpha)(\bar{b}^\beta \gamma^\mu P_L q^\beta)\,,\\
Q_1^{\text{VRR}}(K) &= (\bar{s}^\alpha \gamma_\mu P_R d^\alpha)(\bar{s}^\beta \gamma^\mu P_R d^\beta)\,, & Q_1^{\text{VRR}}(B_q) &= (\bar{b}^\alpha \gamma_\mu P_R q^\alpha)(\bar{b}^\beta \gamma^\mu P_R q^\beta)\,,\\
Q_1^{\text{LR}}(K) &= (\bar{s}^\alpha \gamma_\mu P_L d^\alpha)(\bar{s}^\beta \gamma^\mu P_R d^\beta)\,, & Q_1^{\text{LR}}(B_q) &= (\bar{b}^\alpha \gamma_\mu P_L q^\alpha)(\bar{b}^\beta \gamma^\mu P_R q^\beta)\,,\\
Q_2^{\text{LR}}(K) &= (\bar{s}^\alpha P_L d^\alpha)(\bar{s}^\beta P_R d^\beta)\,, & Q_2^{\text{LR}}(B_q) &= (\bar{b}^\alpha P_L q^\alpha)(\bar{b}^\beta P_R q^\beta)\,.
\end{aligned} \tag{5.2}$$

$P_{L,R} = (1 \mp \gamma_5)/2$ and the indices α and β indicate the colour of the quark fields. All new operators have a trivial colour structure, since the flavour-gauge bosons are not charged under $\text{SU}(3)_c$.

5.1.2 $\overline{B} \to X_s\gamma$

The decay $\overline{B} \to X_s\gamma$ is mediated by the photonic dipole operators $Q_{7\gamma}$ and $Q'_{7\gamma}$ and through QCD mixing also by the gluonic dipoles Q_{8g} and Q'_{8g}. In our conventions the dipole operators read

$$\begin{aligned}
Q_{7\gamma} &= \frac{e}{16\pi^2}\, m_b\, \bar{s}_\alpha\, \sigma^{\mu\nu}\, P_R\, b_\alpha\, F_{\mu\nu}\,,\\
Q_{8g} &= \frac{g_s}{16\pi^2}\, m_b\, \bar{s}_\alpha\, \sigma^{\mu\nu}\, P_R\, T^a_{\alpha\beta}\, b_\beta\, G^a_{\mu\nu}\,,
\end{aligned} \tag{5.3}$$

where e and g_s are the electromagnetic and chromomagnetic coupling consants, respectively. The primed operators are the operators in which we substitute the right-handed projector, P_R, with the left-handed one, P_L. In the SM the contributions of the primed operators are suppressed by m_s/m_b relative to those coming from $Q_{7\gamma}$ and Q_{8g} and are therefore negligible.

Dimension-six four-quark operators mix into $Q_{7\gamma}$ and their Wilson coefficients contribute in this way also to the branching ratio. This mixing is very important in the SM, it enhances the rate by a factor of $2-3$ [57]. MGF generates two sorts of dimension-six operators:

- Operators present also in the SM after integrating out W and Z bosons, namely two charged current-current operators, $Q^{cc} = \{Q_1, Q_2\}$, and four QCD-penguin operators,

$Q_P = \{Q_3, Q_4, Q_5, Q_6\}$, with their primed counterparts ($P_L \leftrightarrow P_R$),

$$\begin{aligned}
Q_1 &= (\bar{s}_\alpha \gamma_\mu P_L c_\beta)(\bar{c}_\beta \gamma^\mu P_L b_\alpha) , & Q_2 &= (\bar{s}_\alpha \gamma_\mu P_L c_\alpha)(\bar{c}_\beta \gamma^\mu P_L b_\beta) , \\
Q_3 &= (\bar{s}_\alpha \gamma_\mu P_L b_\alpha) \sum_{q=u,d,s,c,b} \left(\bar{q}_\beta \gamma^\mu P_L q_\beta\right) , & Q_4 &= (\bar{s}_\alpha \gamma_\mu P_L b_\beta) \sum_{q=u,d,s,c,b} \left(\bar{q}_\beta \gamma^\mu P_L q_\alpha\right) , \\
Q_5 &= (\bar{s}_\alpha \gamma_\mu P_L b_\alpha) \sum_{q=u,d,s,c,b} \left(\bar{q}_\beta \gamma^\mu P_R q_\beta\right) , & Q_6 &= (\bar{s}_\alpha \gamma_\mu P_L b_\beta) \sum_{q=u,d,s,c,b} \left(\bar{q}_\beta \gamma^\mu P_R q_\alpha\right) .
\end{aligned} \tag{5.4}$$

- New neutral current-current operators Q^{nn} and $Q^{nn\prime}$ generated by integrating out the flavour-gauge bosons [21]. The first forty-eight of them contain the neutral currents $(\bar{s}\,\gamma_\mu P_{L,R}\, b)$ and the flavour conserving currents $(\bar{f}\,\gamma_\mu P_{L,R}\, f)$, with $f = u, c, t, d, s, b$. We introduce the general notation for the Q^{nn} and $Q^{nn\prime}$ operators in question

$$Q^f_{1,2}(A, B) , \qquad \text{for} \quad A, B = \{L, R\} . \tag{5.5}$$

  For instance

$$Q^u_1(L,R) = (\bar{s}_\alpha \gamma_\mu P_L b_\beta)(\bar{u}_\beta \gamma^\mu P_R u_\alpha) , \quad Q^u_2(L,R) = (\bar{s}_\alpha \gamma_\mu P_L b_\alpha)(\bar{u}_\beta \gamma^\mu P_R u_\beta) . \tag{5.6}$$

  There are another eight neutral current-current operators with a different colour and flavour structure than in $Q^f_{1,2}(A, B)$:

$$\begin{aligned}
\hat{Q}^d_1(A,B) &= (\bar{s}_\alpha \gamma_\mu P_A d_\beta)\left(\bar{d}_\beta \gamma^\mu P_B b_\alpha\right) , \\
\hat{Q}^d_2(A,B) &= \left(\bar{s}_\alpha \gamma_\mu P_A d_\alpha\right)(\bar{d}_\beta \gamma^\mu P_B b_\beta) .
\end{aligned} \tag{5.7}$$

  In this classification, we refer to Q^{nn} $[Q^{nn\prime}]$ as the operators $Q_{1,2}(A, B)$ with $A = L$ $[A = R]$ and $B = L, R$ $[B = R, L]$.

  The operator basis in Eqs. (5.5), (5.7) and (5.4) is reducible by Fierz transformations. Yet we work with all operators and do not use Fierz relations for the RG analysis to keep the anomalous dimensions in a transparent form. As discussed in [58, 59], one can use a linearly dependent operator basis for the RG evolution and only at the end apply Fierz relations if required. In the case of $C_{7\gamma}(\mu_b)$ at LO this is not necessary.

We have collected all operators, whose Wilson coefficients contribute to the rate of $\overline{B} \to X_s\gamma$. We adopt the overall SM normalisation for the effective Lagrangian:

$$\begin{aligned}
\mathscr{L}_{\text{eff}}^{\overline{B}\to X_s\gamma} =& \mathscr{L}_{\text{QCD}\times\text{QED}}(u,d,s,c,b) \\
&+ \frac{4G_F}{\sqrt{2}} \sum_{\{Q^{cc}, Q_P^{(\prime)}, Q^{nn(\prime)}\}} C_i(\mu) Q_i \\
&+ \frac{4G_F}{\sqrt{2}} \Big[C_{7\gamma}(\mu) Q_{7\gamma} + C_{8g}(\mu) Q_{8g} + C'_{7\gamma}(\mu) Q'_{7\gamma} + C'_{8g}(\mu) Q'_{8g} \Big] .
\end{aligned} \tag{5.8}$$

The effective Lagrangians of this section are not specific to the MGF model. All extensions of the SM with flavour violating vectors, which are not charged under the SM gauge groups, generate the same operator bases. What is model dependent are the Wilson coefficients that we present next.

5.2 Wilson Coefficients from MGF

5.2.1 $\Delta F = 2$ Transitions

At LO in the weak and flavour-gauge interactions there are two competing contributions to the $\Delta F = 2$ amplitudes.

- One-loop contributions from box diagrams with W-boson and up-type-quark exchanges. Due to the mixing among light and heavy quarks, there are three different types of diagrams: with light quarks only, with heavy quarks only, or with both light and heavy quarks running in the box, i.e. for the case of $K^0 - \bar{K}^0$ mixing:

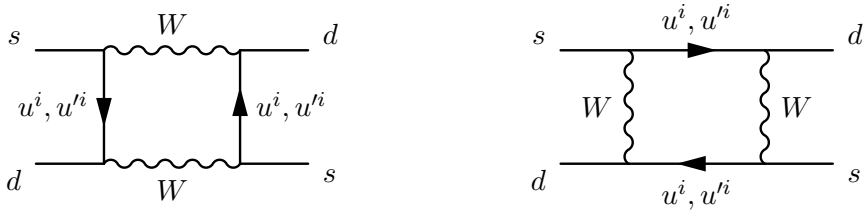

  If we only consider exchanges of SM quarks, the GIM mechanism is broken in these contributions. This means that even if we identify all SM-quark masses the contribution does not cancel as it would in the SM. The GIM is recovered when we include the exchanges of heavy quarks, as we shall see explicitly below.

- Tree-level contributions from flavour-gauge-boson exchanges that generate the new neutral current-current operators and violate flavour, i.e. for the case of $K^0 - \bar{K}^0$ mixing:

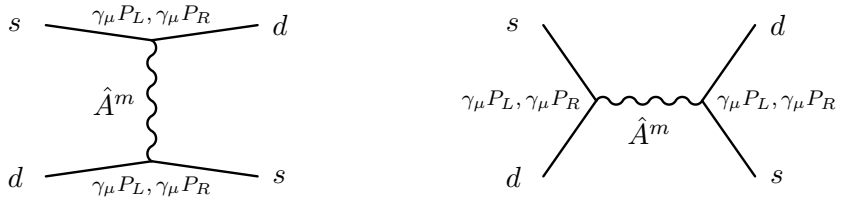

  Box diagrams with flavour-boson exchanges are NLO in the flavour interactions and thus subleading.

Therefore, we separate the Wilson coefficients in Eq. (5.1) in their box-diagram and tree-level contributions as:

$$C_i(\mu) = \Delta^{(M)}_{\text{box}} C_i(\mu) + \Delta^{(M)}_{A} C_i(\mu)\,, \tag{5.9}$$

where $M = \{K, B_d, B_s\}$.

Contributions from Box Diagrams

The operator Q_1^{VLL} is the only one with an initial condition from boxes. We calculate it by integrating out W bosons, top quarks and all exotic quarks at the scale $\mu_t \approx m_t$ according to the Feynman rules in App. A.1. The results are

$$\Delta^{(M)}_{\text{Box}} C_1^{VLL}(\mu_t) = \Delta_1(\mu_t, M) + \Delta_2(\mu_t, M) + \Delta_3(\mu_t, M)\,, \tag{5.10}$$

where for the kaon system we have

$$\begin{aligned}
\Delta_1(\mu_t, K) &= (c_{d_{L1}}\, c_{d_{L2}})^2 \sum_{i,j=1,2,3} \lambda_i(K)\, \lambda_j(K)\, c^2_{u_{Li}}\, c^2_{u_{Lj}}\, F(x_i, x_j)\,, \\
\Delta_2(\mu_t, K) &= (c_{d_{L1}}\, c_{d_{L2}})^2 \sum_{i,j=1,2,3} \lambda_i(K)\, \lambda_j(K)\, s^2_{u_{Li}}\, s^2_{u_{Lj}}\, F(x'_i, x'_j)\,, \\
\Delta_3(\mu_t, K) &= (c_{d_{L1}}\, c_{d_{L2}})^2 \sum_{i,j=1,2,3} \lambda_i(K)\, \lambda_j(K)\, \left[c^2_{u_{Li}}\, s^2_{u_{Lj}}\, F(x_i, x'_j) + s^2_{u_{Li}}\, c^2_{u_{Lj}}\, F(x'_i, x_j)\right]\,,
\end{aligned} \tag{5.11}$$

and similarly for the B_d and B_s systems. We have introduced the notation

$$\lambda_i(K) \equiv V^*_{is} V_{id}, \qquad \lambda_i(B_q) \equiv V^*_{ib} V_{iq}, \tag{5.12}$$

where $q = d, s$ and V is the unitary matrix of Eq. (2.8) and not the experimentally measured CKM matrix. The arguments of the box-functions F are

$$x_i = \left(\frac{m_{u^i}}{M_W}\right)^2, \qquad x'_j = \left(\frac{m_{u'^j}}{M_W}\right)^2 \tag{5.13}$$

and the loop function $F(x_i, x_j)$ is

$$F(x_i, x_j) = \frac{1}{4}\Big[\,(4 + x_i\, x_j)\; I_2\,(x_i,\, x_j) - 8\, x_i\, x_j\, I_1\,(x_i,\, x_j)\,\Big] \tag{5.14}$$

with

$$\begin{aligned}
I_1(x_i,\, x_j) = &\quad \frac{1}{(1-x_i)(1-x_j)} + \left[\frac{x_i\, \ln(x_i)}{(1-x_i)^2(x_i - x_j)} + (i \leftrightarrow j)\right]\,, \\
I_2(x_i,\, x_j) = &\quad \frac{1}{(1-x_i)(1-x_j)} + \left[\frac{x_i^2\, \ln(x_i)}{(1-x_i)^2(x_i - x_j)} + (i \leftrightarrow j)\right].
\end{aligned} \tag{5.15}$$

We consider all terms in the sums of Eq. (5.11) with the same $\lambda_i\lambda_j$ coefficient, e.g. the same "CKM" coefficients:

$$\mathcal{F}_{ij} \equiv c^2_{u_{Li}} c^2_{u_{Lj}} F(x_i, x_j) + s^2_{u_{Li}} s^2_{u_{Lj}} F(x'_i, x'_j) + c^2_{u_{Li}} s^2_{u_{Lj}} F(x_i, x'_j) + s^2_{u_{Li}} c^2_{u_{Lj}} F(x'_i, x_j). \tag{5.16}$$

If all fermion masses were degenerate, this combination would be independent of i, j and the unitarity of the matrix V would assure the vanishing of FCNC currents. This is what one expects from the GIM mechanism. In this decomposition we arrange the function $\mathcal{F}$ to match the usual notation. Namely for the kaon system we write

$$\begin{aligned}
S_0(x_t) &\longrightarrow S_t^{(K)} \equiv (c_{d_{L1}}\, c_{d_{L2}})^2\, (\mathcal{F}_{33} + \mathcal{F}_{11} - 2\mathcal{F}_{13})\,, \\
S_0(x_c) &\longrightarrow S_c^{(K)} \equiv (c_{d_{L1}}\, c_{d_{L2}})^2\, (\mathcal{F}_{22} + \mathcal{F}_{11} - 2\mathcal{F}_{12})\,, \\
S_0(x_c, x_t) &\longrightarrow S_{ct}^{(K)} \equiv (c_{d_{L1}}\, c_{d_{L2}})^2\, (\mathcal{F}_{23} + \mathcal{F}_{11} - \mathcal{F}_{13} - \mathcal{F}_{12})\,.
\end{aligned} \tag{5.17}$$

For the B_q systems we define similar functions $S_i^{(B_q)}$ derived from the previous ones by substituting $c_{d_{L1}}\, c_{d_{L2}}$ with $c_{d_{L1}}\, c_{d_{L3}}$ $(c_{d_{L2}}\, c_{d_{L3}})$ in the case of $q = d$ $(q = s)$. To recover the S_0 functions from the $S_i^{(M)}$ expressions we decouple the exotic quarks, i.e. we take the limit in which all the cosines are equal to one and all the sines are zero. The mixings c_i and s_j introduce a new flavour dependence, which implies a departure from the strict MFV picture even in the absence of new CP-violating phases.

Contributions from Tree-level Flavour-gauge-boson Exchanges

The contribution from flavour-gauge-boson exchanges are generated at the high scale $\mu_H \approx \hat{M}_{A^m}$, around the mass of the boson in question. In the notation of Sec. 2.4 we obtain for the kaon system

$$\Delta_A^{(K)} C_1^{VLL} = \frac{4\pi^2}{G_F^2 M_W^2} \sum_{m=1}^{24} \frac{1}{2\,\hat{M}_{A^m}^2} \left[\left(\hat{\mathcal{G}}_L^d \right)_{ds,m} \right]^2 , \tag{5.18}$$

$$\Delta_A^{(K)} C_1^{VRR} = \frac{4\pi^2}{G_F^2 M_W^2} \sum_{m=1}^{24} \frac{1}{2\,\hat{M}_{A^m}^2} \left[\left(\hat{\mathcal{G}}_R^d \right)_{ds,m} \right]^2 , \tag{5.19}$$

$$\Delta_A^{(K)} C_1^{LR} = \frac{4\pi^2}{G_F^2 M_W^2} \sum_{m=1}^{24} \frac{1}{2\,\hat{M}_{A^m}^2} \left[2 \left(\hat{\mathcal{G}}_L^d \right)_{ds,m} \left(\hat{\mathcal{G}}_R^d \right)_{ds,m} \right] , \tag{5.20}$$

where the indices d and s stand for the flavour of the external quarks and the index m refers to the $\hat{A}^m$ gauge-boson mass eigenstate. The expressions for the B_d and B_s systems are the previous ones after substituting ds with db and sb, respectively.

The flavour-gauge bosons have flavour-violating couplings that are strongly hierarchical due to the mechanism of inverse hierarchies discussed in Sec. 2.2:

$$\left(\hat{\mathcal{G}}_{L,R}^d \right)_{sb} \gg \left(\hat{\mathcal{G}}_{L,R}^d \right)_{db} \gg \left(\hat{\mathcal{G}}_{L,R}^d \right)_{ds} , \qquad \left(\hat{\mathcal{G}}_{L,R}^u \right)_{ct} \gg \left(\hat{\mathcal{G}}_{L,R}^u \right)_{ut} \gg \left(\hat{\mathcal{G}}_{L,R}^u \right)_{uc} . \tag{5.21}$$

In App. A.1.2 we explicitly present these couplings for the lightest gauge boson. The reason for this hierarchy is both the mixings among SM and exotic quarks and the sequential breaking of the flavour symmetry encoded in the flavon vevs.

There are no purely new CP-violating phases in this model. The CP-odd phase of unitary matrix V is the only one and controls both box and tree-level contributions. Nevertheless, with respect to the SM there can be large modifications to the mixing induced CP-asymmetries $S_{\psi K_S}$ and $S_{\psi\phi}$ of the $B_d^0 - \bar{B}_d^0$ and the $B_s^0 - \bar{B}_s^0$ system, respectively. Similarly, also the mass differences $\Delta M_{B_{d,s}}$ and ϵ_K are affected. The small number of new parameters in the MGF construction is the reason for the strict correlations between the new physics contributions within these observables. We discuss them in the phenomenological analysis.

5.2.2 $\overline{B} \to X_s\gamma$

Similarly to the $\Delta F = 2$ Wilson coefficients we decompose the Wilson coefficients for the dipole operators mediating $\overline{B} \to X_s\gamma$ into two parts. The SM-like W boson and the new flavour-gauge-boson exchange:

$$\begin{aligned} C_{7\gamma}(\mu) &= \Delta_{\rm SM} C_{7\gamma}(\mu) + \Delta_A C_{7\gamma}(\mu) , \\ C_{8g}(\mu) &= \Delta_{\rm SM} C_{8g}(\mu) + \Delta_A C_{8g}(\mu) . \end{aligned} \tag{5.22}$$

- $\Delta_{\rm SM} C$'s are the SM-like contributions from diagrams with W bosons with modified couplings to both SM and exotic quarks of charge $+2/3$:

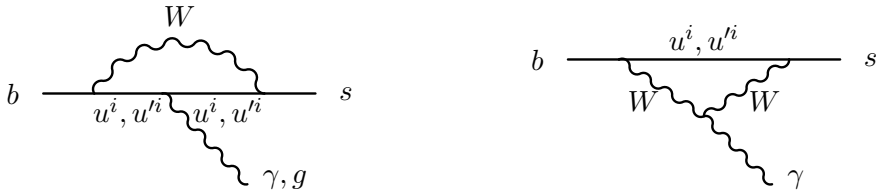

$$\Delta_{\rm SM} C_{7\gamma}(\mu_t) = c_{d_{L2}}\, V_{ts}^* V_{tb}\, c_{d_{L3}} \left(c_{u_{L3}}^2 C_{7\gamma}^{SM}(x_t) + s_{u_{L3}}^2 C_{7\gamma}^{SM}(x_t') \right) , \tag{5.23}$$

$$\Delta_{\rm SM} C_{8g}(\mu_t) = c_{d_{L2}}\, V_{ts}^* V_{tb}\, c_{d_{L3}} \left(c_{u_{L3}}^2 C_{8g}^{SM}(x_t) + s_{u_{L3}}^2 C_{8g}^{SM}(x_t') \right) , \tag{5.24}$$

with the SM Inami-Lim functions [46]

$$C_{7\gamma}^{\rm SM}(x) = \frac{3x^3 - 2x^2}{4(x-1)^4} \ln x - \frac{8x^3 + 5x^2 - 7x}{24(x-1)^3} , \tag{5.25}$$

$$C_{8g}^{\rm SM}(x) = \frac{-3x^2}{4(x-1)^4} \ln x - \frac{x^3 - 5x^2 - 2x}{8(x-1)^3} . \tag{5.26}$$

The Wilson coefficients of the corresponding primed operators are also given by the previous expressions, but with an extra suppression factor of m_s/m_b.

- $\Delta_A C$'s are the contributions of neutral-gauge-boson exchanges with virtual SM and exotic quarks of charge $-1/3$:

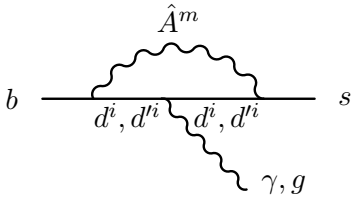

Contrary to the $\Delta F = 2$ transitions there is no tree-level contribution to the $\overline{B} \to X_s\gamma$ decay from the flavour-gauge interactions. Both SM-like and flavour-gauge contributions are loop induced and since the flavour-gauge bosons are typically much heavier than the W boson we expect smaller effects from the former. However, unlike the W boson, the flavour-gauge bosons couple to both left- and right-handed quark chiralities. The RL part of this contribution is thus chirally enhanced and comes with a linear dependence on the internal down-type-quark mass, which may compensate the suppression from the mass of the flavour-gauge bosons. Therefore, we can expect potentially large effects from the heavy exotic down-type quarks, which we analysed in a model-independent manner in Ref. [21]. The result of the analysis is that in models with a see-saw explanation for the light quark masses, like here, the smallness of the flavour-violating couplings of the flavour-gauge bosons is sufficient to suppress large effects to the $\overline{B} \to X_s\gamma$ rate. We shall therefore not list these Wilson coefficients here and refer to the original publication in which we computed them [21].

We also need the initial conditions at μ_H for the new neutral-current-current operators discussed in Sec. 5.1. We present here the result for the simplified case in which only one neutral flavour-gauge boson $\hat{A}^m$ contributes to the initial conditions. The generalisation to all

flavour-gauge bosons is straightforward. In the normalisation of Eq. (5.8) the initial conditions for the $Q_2^f(A,B)$ and $\hat{Q}_2^d(A,B)$ operators read

$$\Delta^{AB} C_2^f(\mu_H) = -2\frac{s_W^2}{e^2}\frac{M_W^2}{\hat{M}_{A^m}^2}\left(\hat{\mathcal{G}}_A^d\right)^*_{sb,m}\left(\hat{\mathcal{G}}_B^d\right)_{ff,m}, \tag{5.27}$$

$$\Delta^{AB} \hat{C}_2^d(\mu_H) = -2\frac{s_W^2}{e^2}\frac{M_W^2}{\hat{M}_{A^m}^2}\left(\hat{\mathcal{G}}_A^d\right)^*_{sd,m}\left(\hat{\mathcal{G}}_B^d\right)_{bd,m}, \tag{5.28}$$

where s_W is the weak mixing angle in the SM. The operators $Q_1^f(A,B)$ and $\hat{Q}_1^d(A,B)$ receive no contributions to their Wilson coefficient at the matching scale.

5.3 Renormalisation Group Effects

The effective Lagrangians in Sec. 5.1 are good perturbative descriptions of the physics from the matching scale down to the scales at which the QCD coupling begins to grow and confinement takes place. The Wilson coefficients are effective couplings that we calculated at the matching scale and serve as initial conditions for the RGE down to $\Lambda_{\rm QCD}$ or, more precise, the mass of the mesons. At this scale particles carrying colour charges confine to mesons and hadrons that we observe as free external states. Computations on the lattice are the only way we know how to evaluate their matrix elements. The RGE is necessary to quantitatively understand the effect the NP scenario in question has on experimentally accessible properties of the low-energy degrees of freedom, in our case the B and K mesons. In this section we solve the RGE for the $\Delta\mathrm{F}=2$ and $\overline{B}\to X_s\gamma$ effective Lagrangians of Sec. 5.1.

5.3.1 $\Delta\mathrm{F}=2$ Transitions

We calculate amplitudes order by order in perturbation theory using dimensional regularisation, which introduces an artificial dependence on the unphysical regulator scale μ. In the case of the $\Delta\mathrm{F}=2$ effective theory both the Wilson coefficients and the matrix elements are μ dependent; a dependence that only cancels in their combination. Therefore, to connect the matching scale to the meson scale we can either evolve the Wilson coefficients down to the meson scale or directly evaluate the matrix elements at the matching scale μ_H. For the $\Delta\mathrm{F}=2$ analysis we follow Ref. [60] and do the latter. At μ_H the amplitude for the $M-\overline{M}$ mixing ($M=K^0$, B_d^0 and B_s^0) reads

$$\mathcal{A}(M\to\overline{M}) = \frac{G_F^2 M_W^2}{4\pi^2}\sum_{i,a} C_i^a(\mu_H)\langle\overline{M}|Q_i^a(\mu_H)|M\rangle\,. \tag{5.29}$$

The sum runs over all the operators listed in Eq. (5.2) and the matrix element for $M-\overline{M}$ mixing is

$$\langle\overline{M}|Q_i^a(\mu_H)|M\rangle = \frac{2}{3}\, m_M^2\, F_M^2\, P_i^a(\mu_H, M). \tag{5.30}$$

m_H denotes the mass of the meson and F_M its decay constant. The coefficients $P_i^a(\mu,M)$ collect compactly all RG effects from scales below μ_H as well as hadronic matrix elements obtained by lattice methods at low-energy scales. They explicitly depend on QCD RGE factors and non-perturbative parameters $B_i^a(\mu_L)$ given in Eqs. (7.28)–(7.34) of Ref. [60]. μ_L denotes the low-energy scale and takes the value 2 GeV and 4.6 GeV for the K and B_q system, respectively.

μ_H	500 GeV	1 TeV	3 TeV	10 TeV
$P_1^{VLL}(\mu_H,\, K)$	0.392	0.384	0.373	0.363
$P_1^{LR}(\mu_H,\, K)$	−35.7	−39.3	−45.0	−51.4
$P_1^{VLL}(\mu_H,\, B_d)$	0.675	0.662	0.643	0.624
$P_1^{LR}(\mu_H,\, B_d)$	−2.76	−2.97	−3.31	−3.69
$P_1^{VLL}(\mu_H,\, B_s)$	0.713	0.698	0.678	0.659
$P_1^{LR}(\mu_H,\, B_s)$	−2.76	−2.97	−3.31	−3.69

Table 5.1: *Central values for the P_i factors at different scales $\mu_H = \{0.5,\, 1,\, 3,\, 10\}$ TeV.*

The bag parameters $B_i^a(\mu_L)$ are subject to considerable uncertainties. The exception is B_1^{VLL} for which significant progress has been made in the recent years through lattice calculations. In the SM analysis, the RG invariant parameters $\hat{B}_1^{VLL}$ are usually denoted by $\hat{B}_K$ and $\hat{B}_{B_q}$. We report their values in Tab. 8.1. The B_1^{VLL} values that we then extract from recent lattice simulations are:

$$\begin{aligned} B_1^{VLL} &= 0.515(14)\,, && \text{for the } K \text{ system} \\ B_1^{VLL} &= 0.825(72)\,, && \text{for the } B_d \text{ system} \\ B_1^{VLL} &= 0.871(39)\,, && \text{for the } B_s \text{ system}\,. \end{aligned} \tag{5.31}$$

We combine the VLL and VRR contributions as their bag parameters are the same.

Our NLO RG analysis involves also the values of the coefficients $P_1^{LR}(\mu_H, K)$, $P_1^{LR}(\mu_H, B_d)$ and $P_1^{LR}(\mu_H, B_s)$. For their calculation we neglect intermediate thresholds of exotic quarks. The smallness of α_s at these scales as well as the absence of flavour dependence in the LO anomalous dimensions of the contributing operators renders these threshold effects negligible. Their values depend on B_1^{LR} and B_2^{LR} that we report below for the NDR scheme[1] [61, 62]:

$$\begin{aligned} B_1^{LR} &= 0.562(39)(46)\,, & B_2^{LR} &= 0.810(41)(31)\,, & &\text{for the } K \text{ system} \\ B_1^{LR} &= 1.72(4)(^{+20}_{-6})\,, & B_2^{LR} &= 1.15(3)(^{+5}_{-7})\,, & &\text{for the } B_d \text{ system} \\ B_1^{LR} &= 1.75(3)(^{+21}_{-6})\,, & B_2^{LR} &= 1.16(2)(^{+5}_{-7})\,, & &\text{for the } B_s \text{ system}\,. \end{aligned} \tag{5.32}$$

In Tab. 5.1 we collect the numerical values for the $P_i^a(\mu, M)$ factors for some indicative values of μ_H. The numerical value of the P_1^{LR} factors is large compared to its VLL and VRR counterparts. The contributions from LR operators generated by heavy vectors is thus enhanced by the QCD RGE and may have important phenomenological consequences.

The complication of the MGF model is that there is not only one relevant high scale, but several, rather different ones: the electroweak scale, the scale of the exotic fermions and the scale of each neutral gauge boson. Depending on the contribution we choose different high scales to appropriately account for the RGE effects:

- For SM box diagrams involving W bosons and SM quarks the scale is $\mu_t = \mathcal{O}(m_t)$.
- For the tree-level contributions mediated by the neutral heavy gauge bosons we choose the scale to be the mass of the gauge boson in question.

[1] In Refs. [61, 62] B_1^{LR} and B_2^{LR} are referred to as B_5 and B_4, respectively.

- For the case of contributions from box-diagrams that involve simultaneously heavy and light particles, the correct procedure is to integrate out first the heavy fermions and construct an effective field theory not involving them as dynamical degrees of freedom. However, since the most relevant contribution comes from the lightest exotic fermion[2], the t', whose mass is relatively close to m_t, we set the matching scale also here to μ_t. This procedure is a sufficiently good approximation to the exact one as the dominant RGE effects come from low scales in which α_s gets large.

5.3.2 $\overline{B} \to X_s\gamma$

In Sec. 5.1.2 we extended the SM operator basis to account for flavour-gauge-boson effects on $\overline{B} \to X_s\gamma$. Here, we also extend the SM RGE analysis to consider the QCD effects of the new neutral current-current operators at scales $\mu_b \leq \mu \leq \mu_H$. This mixing is controlled by hitherto unknown LO anomalous dimension matrices that we derive [21]. Our analysis takes into account the QCD mixing of the neutral current-current operators: into dipole operators, among themselves, and into QCD-penguin operators.

QCD- and QED-penguin operators are loop induced in both electroweak and flavour-gauge interactions; the QCD or QED coupling and the loop order suppresses their Wilson coefficients. However, contrary to the SM, the penguins compete here with the new tree-level generated current-current operators. Thus, for all practical purposes the contributions of QCD penguins are negligible and even more so the effects from QED penguins. Even though the main effect does come from the mixing into the dipole operators we include the full mixing for completeness.

The results go beyond the specific MGF model that we consider here. They have been applied in left-right symmetric extensions of the SM [63] and in models with flavour-violating Z and Z' bosons [64]. The same QCD analysis is relevant for processes other than $\overline{B} \to X_s\gamma$, e.g. non-leptonic two-body B decays and ϵ'/ϵ.

We denote the charged current-current, QCD-penguin, dipole, neutral current-current operators and the corresponding primed operators respectively by

$$Q^{cc}\,, \qquad Q_P\,, \qquad Q_D\,, \qquad Q^{nn}\,, \qquad Q'_P\,, \qquad Q'_D\,, \qquad Q^{nn\prime}\,, \tag{5.33}$$

and arrange the NP RG analysis to be independent from the SM evolution:

$$\begin{aligned} C_i^{\rm SM}(\mu_b) &= U_{ij}(\mu_b,\,\mu_W)\, C_j^{\rm SM}(\mu_W)\,, \\ C_i^{\rm NP}(\mu_b) &= W_{ij}(\mu_b,\,\mu_H)\, C_j^{\rm NP}(\mu_H)\,, \\ C_i^{\rm total}(\mu_b) &= C_i^{\rm SM}(\mu_b) + C_i^{\rm NP}(\mu_b)\,, \end{aligned} \tag{5.34}$$

where U_{ij} and W_{ij} are the elements of the RG evolution matrices. The evolution matrices depend on the anomalous dimension matrices and the QCD-β functions [65]. Here, we extract

[2] This is strictly true only for the B_q systems. Our numerical analysis shows that in the K system also the contribution from c' may be non-negligible due to the different CKM structure. The most relevant contribution is still the t' one, though.

the unknown elements of the anomalous-dimension matrix:

$$\hat{\gamma}(\alpha_s) = \frac{\alpha_s}{4\pi}\hat{\gamma}^0 = \left(\begin{array}{c|cccc|ccc} & Q^{cc} & Q_P & Q_D & Q^{nn} & & & \\ \hline Q^{cc} & X_1 & X_2 & X_3 & 0 & & & \\ Q_P & 0 & X_4 & X_5 & 0 & & & \\ Q_D & 0 & 0 & X_6 & 0 & & & \\ Q^{nn} & 0 & Y_1 & Y_2 & Y_3 & & & \\ \hline & & & & & X_4 & X_5 & 0 \\ & & & & & 0 & X_6 & 0 \\ & & & & & Y_1 & Y_2 & Y_3 \\ \hline & & & & & Q'_P & Q'_D & Q^{nn\prime} \end{array}\begin{array}{c} \\ \\ \\ \\ \\ Q'_P \\ Q'_D \\ Q^{nn\prime} \end{array}\right), \tag{5.35}$$

where X_i denote entries known from the SM analysis [66, 67] and Y_i the entries that we calculate here. In the following we drop the index (0) to simplify the notation.

Anomalous Dimensions

The inspection of the loop diagrams contributing to the anomalous dimension matrices shows that considering sixteen operators is sufficient to determine the full matrix. These are

$$\begin{array}{llll} Q^u_{1,2}(L,L)\,, & Q^d_{1,2}(L,L)\,, & Q^s_{1,2}(L,L)\,, & \hat{Q}^d_{1,2}(L,L)\,, \\ Q^u_{1,2}(L,R)\,, & Q^d_{1,2}(L,R)\,, & Q^s_{1,2}(L,R)\,, & \hat{Q}^d_{1,2}(L,R)\,. \end{array} \tag{5.36}$$

The anomalous dimensions for u replaced by c and t are equal to those of $Q^u_{1,2}$ and the ones for $Q^b_{1,2}$ are equal to the ones of $Q^s_{1,2}$. The anomalous dimensions of the remaining twenty-eight primed operators, are the same as those of the corresponding unprimed operators (see Eq. (5.35)).

We extract the mixing of the Q^{nn} into Q_D operators, i.e. Y_2, from [68, 66] by inspecting the mixing of QCD-penguin to dipole operators. For the transposed matrices we obtain

$$\hat{\gamma}^T_D(L,L) = \begin{array}{c|cccccccc} & Q^u_1 & Q^u_2 & Q^d_1 & Q^d_2 & Q^s_1 & Q^s_2 & \hat{Q}^d_1 & \hat{Q}^d_2 \\ \hline Q_{7\gamma} & \frac{416}{81} & 0 & -\frac{232}{81} & 0 & -\frac{232}{81} & -\frac{232}{81} & 0 & -\frac{232}{81} \\ Q_{8g} & \frac{70}{27} & 3 & \frac{70}{27} & 3 & \frac{151}{27} & \frac{151}{27} & 3 & \frac{70}{27} \end{array}, \tag{5.37}$$

$$\hat{\gamma}^T_D(L,R) = \begin{array}{c|cccccccc} & Q^u_1 & Q^u_2 & Q^d_1 & Q^d_2 & Q^s_1 & Q^s_2 & \hat{Q}^d_1 & \hat{Q}^d_2 \\ \hline Q_{7\gamma} & -\frac{448}{81} & 0 & \frac{200}{81} & 0 & \frac{200}{81} & \frac{16}{9} & -\frac{80}{3} & -\frac{32}{9} \\ Q_{8g} & -\frac{119}{27} & -3 & -\frac{119}{27} & -3 & -\frac{173}{27} & -\frac{16}{3} & -4 & \frac{8}{3} \end{array}. \tag{5.38}$$

The mixing among neutral current-current operators Y_3 is universally given by two 2×2 matrices:

$$\hat{\gamma}^{nn}(L,L) = \begin{array}{c|cc} & Q_1 & Q_2 \\ \hline Q_1 & -2 & 6 \\ Q_2 & 6 & -2 \end{array} \quad \text{and} \quad \hat{\gamma}^{nn}(L,R) = \begin{array}{c|cc} & Q_1 & Q_2 \\ \hline Q_1 & -16 & 0 \\ Q_2 & -6 & 2 \end{array}, \tag{5.39}$$

in such a way that only operators with the same flavour-conserving structure $(\overline{f}\,\gamma_\mu\,P_{L,R}\,f)$ mix with each other.

Finally, for Y_1 there is a universal mixing of the operator P^{nn} into the QCD-penguin operators:

$$\hat{\gamma}_P = \begin{array}{|c||c|c|c|c|}\hline & Q_3 & Q_4 & Q_5 & Q_6 \\ \hline\hline P^{nn} & -\frac{2}{9} & \frac{2}{3} & -\frac{2}{9} & \frac{2}{3} \\ \hline\end{array} \tag{5.40}$$

where

$$P^{nn} = \left\{Q_1^{u,c,t,d,s,b}(L,L),\, Q_2^{s,b}(L,L),\, \hat{Q}_2^{d}(L,L),\, Q_1^{u,c,t,d,s,b}(L,R)\right\}. \tag{5.41}$$

The remaining operators do not mix into QCD-penguin operators.

QCD evolution of $C_{7\gamma}$

Having all Wilson coefficients at μ_H and the full anomalous-dimension matrix at LO we evolve the $\Delta_A C_{7\gamma}^{(\prime)}$ in the 6-flavour effective theory down to μ_W, include $\Delta_{\rm SM} C_{7\gamma}^{(\prime)}$ and subsequently run the total Wilson coefficient in the 5-flavour theory down to μ_b. For our numerical analysis we fix the pure SM contribution such that we reproduce the NNLO SM prediction [57, 69, 70]. For $\mu_b = 2.5$ GeV this translates to $C_{7\gamma}^{\rm SM}(\mu_b) = -0.3523$. We then summarise all NP effects in the down-scaled Wilson coefficient

$$\begin{aligned}\Delta C_{7\gamma}(\mu_b) = \;& \kappa_7\;\Delta C_{7\gamma}(\mu_H) + \kappa_8\;\Delta C_{8g}(\mu_H) + \\ & + \sum_{\substack{A=L,R\\ f=u,c,t,d,s,b}} \kappa_{LA}^{f}\;\Delta^{LA} C_2^f(\mu_H) + \sum_{A=L,R} \hat{\kappa}_{LA}^{d}\;\Delta^{LA}\hat{C}_2^d(\mu_H)\,,\end{aligned} \tag{5.42}$$

where κ's are RGE factors, the so-called NP "magic numbers". We list them in Tab. 5.2 for some indicative scales μ_H using $\alpha_s(M_Z) = 0.118$.

We obtain $C'_{7\gamma}(\mu_b)$ by interchanging $L \leftrightarrow R$ and taking the initial conditions of the primed Wilson coefficients. The NP magic numbers listed in Tab. 5.2 are the same for the primed case, since QCD is blind to the fermion chirality. Inspecting Tab. 5.2 we observe that:

- Similarly to the SM, the "magic numbers" κ_7 and κ_8 suppress the initial values $\Delta C_{7\gamma}(\mu_H)$ and $\Delta C_{8g}(\mu_H)$. The suppression increases with μ_H.
- Provided $\Delta^{AB} C_2^f(\mu_H)$ and $\Delta^{AB}\hat{C}_2^d(\mu_H)$ are sufficiently larger than $\Delta C_{7\gamma}(\mu_H)$, the additive QCD corrections from the mixing of the neutral current-current operators into the dipoles dominate. Also these QCD factors κ_i increase in most cases with μ_H. The most prominent one is $\hat{\kappa}_{LR}^d$ that reaches $\mathcal{O}(1)$ values.
- The SM and NP primed dipole Wilson coefficients are suppressed by m_s/m_b and are numerically negligible. This suppression is absent in the Wilson coefficients of the primed neutral current-current operators $Q^{nn\prime}$; they should be considered in the determination of the branching ratio.

The NLO and NNLO QCD corrections in the SM prediction render its dependence on μ_b negligible. This is not the case for the NP contribution at LO. When the NP contribution enhances the SM value by 20%, the μ_b dependence in the total branching ratio amounts to

μ_H	200 GeV	1 TeV	5 TeV	10 TeV	M_Z
κ_7	0.524	0.457	0.408	0.390	0.566
κ_8	0.118	0.125	0.129	0.130	0.111
$\kappa_{LL}^{u,c}$	0.039	0.057	0.076	0.084	0.030
κ_{LL}^{t}	−0.002	−0.003	−0.002	−0.001	-
κ_{LL}^{d}	−0.040	−0.057	−0.072	−0.079	−0.032
$\kappa_{LL}^{s,b}$	0.087	0.090	0.090	0.090	0.084
$\hat{\kappa}_{LL}^{d}$	0.128	0.147	0.163	0.168	0.116
$\kappa_{LR}^{u,c}$	0.085	0.128	0.173	0.193	0.065
κ_{LR}^{t}	0.004	0.012	0.023	0.028	-
κ_{LR}^{d}	−0.015	−0.025	−0.036	−0.041	−0.011
$\kappa_{LR}^{s,b}$	−0.078	−0.092	−0.106	−0.111	−0.070
$\hat{\kappa}_{LR}^{d}$	0.473	0.665	0.865	0.953	0.383

Table 5.2: *The NP "magic numbers" for $\Delta C_{7\gamma}(\mu_b)$ defined in Eq. (5.42) for different high scales. In the last column we include for completeness the case of a flavour-violating Z.*

a 3% uncertainty if $\mu_b \in [2.5, 5]$ GeV. The uncertainty further reduces for smaller deviations with respect to the SM prediction, which is sufficiently small for our purposes.

Similarly to Eq. (5.42) we also evolve ΔC_{8g} down to $\mu_b = 2.5$ GeV to obtain

$$\begin{aligned}\Delta C_{8g}(\mu_b) = \;& \rho_7\, \Delta C_{7\gamma}(\mu_H) + \rho_8\, \Delta C_{8g}(\mu_H) + \\ & + \sum_{\substack{A=L,R \\ f=u,c,t,d,s,b}} \rho_{LA}^{f}\, \Delta^{LA} C_2^{f}(\mu_H) + \sum_{A=L,R} \hat{\rho}_{LA}^{d}\, \Delta^{LA} \hat{C}_2^{d}(\mu_H),\end{aligned} \tag{5.43}$$

with the NP "magic numbers" ρ_i listed in Tab. 5.3.

μ_H	200 GeV	1 TeV	5 TeV	10 TeV	M_Z
ρ_7	0	0	0	0	0
ρ_8	0.568	0.504	0.456	0.439	0.607
$\rho_{LL}^{u,c}$	−0.124	−0.138	−0.147	−0.150	−0.115
ρ_{LL}^{t}	−0.015	−0.033	−0.046	−0.050	-
ρ_{LL}^{d}	−0.124	−0.138	−0.147	−0.150	−0.115
$\rho_{LL}^{s,b}$	−0.243	−0.279	−0.307	−0.318	−0.222
$\hat{\rho}_{LL}^{d}$	−0.119	−0.141	−0.160	−0.168	−0.107
$\rho_{LR}^{u,c}$	0.184	0.229	0.270	0.287	0.160
ρ_{LR}^{t}	0.015	0.037	0.055	0.062	-
ρ_{LR}^{d}	0.184	0.229	0.270	0.287	0.160
$\rho_{LR}^{s,b}$	0.311	0.382	0.447	0.474	0.272
$\hat{\rho}_{LR}^{d}$	−0.064	−0.052	−0.034	−0.025	−0.067

Table 5.3: *The NP "magic numbers" for $\Delta C_{8g}(\mu_b)$ in Eq. (5.43) for different high scales. In the last column we include for completeness the case of a flavour-violating Z.*

6 New Strong Interactions in Top Physics

In this chapter we discuss the IR behaviour of the HC model constructed in chapter 3 using QCD as a guide to model and estimate the underlying non-perturbative dynamics. QCD with u, d and s quarks, has the global chiral $\mathrm{SU}(3)_L \times \mathrm{SU}(3)_R$ symmetry that is spontaneously broken by the strong interactions to $\mathrm{SU}(3)_V$ isospin symmetry. The chiral symmetry is also explicitly broken by the masses of the quarks. We consider the HC gauge group $\mathrm{SU}(3)_{\mathrm{HC}}$, in which case the main fundamental differences of the HC model to QCD are isospin-breaking effects due to electromagnetism that we shall neglect, and the HC scalar $\mathcal{S}$. The chiral symmetry of the HC theory is unrelated to $\mathcal{S}$ and we thus also expect the HC chiral symmetry to be spontaneously broken by the HC dynamics. This will be our working assumption.

We estimate the HC condensates, resonance masses and couplings via naive dimensional analysis (NDA), vector-meson dominance (VMD) and scaling from QCD. $t\bar{t}$ phenomenology will require the $\mathcal{Q}$ and $\mathcal{S}$ masses to satisfy $m_{\mathcal{Q}_1} < m_{\mathcal{Q}_3} \ll \Lambda_{\mathrm{HC}}$ and $m_{\mathcal{S}} > \Lambda_{\mathrm{HC}}$, where Λ_{HC} is the HC chiral-symmetry breaking scale. We compare constituent quark masses relative to the chiral-symmetry breaking scale, in the HC theory and in QCD, to find that: the HC quarks $\mathcal{Q}_1$ and $\mathcal{Q}_2$ roughly correspond to light quarks in QCD, $\mathcal{Q}_3$ to the strange quark and the mass of $\mathcal{S}$ is close to the charm-quark mass.

The low-energy phenomenology is dominated by the lowest lying HC resonances. We thus consider the following resonances

- the flavour octet of pseudo-Goldstone pseudoscalar resonances, π^a_{HC},
- the set of vector, ρ^a_{HC}, and axial vector, $a^a_{1,HC}$, resonances,
- the flavour-triplet of vectorlike composite quarks, u'_i, and
- the P-wave vector mesons, V_o (colour octet) and V_s (colour singlet) that are bound states of the HC scalar.

We discuss them in turn in the next section.

6.1 Hypercolour Resonances and Interactions

6.1.1 Pseudoscalar Pseudo-Goldstone Bosons

In the $\mathrm{U}(3)_{U_R}$ symmetric limit, the $\mathcal{Q}_i$ form equal condensates, $\langle\overline{\mathcal{Q}}\mathcal{Q}\rangle \neq 0$, which break the approximate HC chiral symmetry to the diagonal "isospin" subgroup, $\mathrm{SU}(3)_L \times \mathrm{SU}(3)_R \to \mathrm{SU}(3)_V$. This gives rise to a flavour octet of pseudo-Nambu-Goldstone bosons π^a_{HC}, with $a = 1, \ldots, 8$. In NDA we have $\Lambda_{\mathrm{HC}} \sim 4\pi f_\pi^{\mathrm{HC}}$ and the condensate

$$\langle\overline{\mathcal{Q}}\mathcal{Q}\rangle \sim 4\pi (f_\pi^{\mathrm{HC}})^3 \,, \tag{6.1}$$

where f_π^{HC} is the HC-pion decay constant defined through the matrix element

$$\langle\pi^a|\,\overline{\mathcal{Q}}T^a\gamma_\mu\gamma_5\mathcal{Q}\,|0\rangle = -if_\pi^{\mathrm{HC}}p_\mu \,. \tag{6.2}$$

The normalisation of flavour octet Gell-Mann matrices is $\mathrm{Tr}[T^a T^a] = 1/2$.

The explicit breaking of the chiral symmetry generates masses for the pions that proportional to the symmetry breaking parameters, the masses $m_{\mathcal{Q}}$. In the case of $m_{\mathcal{Q}_1} \neq m_{\mathcal{Q}_3}$ the pion states are no longer degenerate. Adopting the notation in QCD we have:

$$\begin{aligned}
|\pi^{\rm HC}_{1,2,3}\rangle &= |\overline{\mathcal{Q}}_1\mathcal{Q}_2\rangle, \quad |\overline{\mathcal{Q}}_2\mathcal{Q}_1\rangle, \quad \frac{1}{\sqrt{2}}(|\overline{\mathcal{Q}}_1\mathcal{Q}_1\rangle - |\overline{\mathcal{Q}}_2\mathcal{Q}_2\rangle), \\
|K^{\rm HC}_{1,2}\rangle &= |\overline{\mathcal{Q}}_{1,2}\mathcal{Q}_3\rangle, \quad |\overline{K}^{\rm HC}_{1,2}\rangle = |\overline{\mathcal{Q}}_3\mathcal{Q}_{1,2}\rangle, \\
|\eta^{\rm HC}_8\rangle &= \frac{1}{\sqrt{6}}(|\overline{\mathcal{Q}}_1\mathcal{Q}_1\rangle + |\overline{\mathcal{Q}}_2\mathcal{Q}_2\rangle - 2|\overline{\mathcal{Q}}_3\mathcal{Q}_3\rangle), \\
|\eta^{\rm HC}_0\rangle &= \frac{1}{\sqrt{3}}(|\overline{\mathcal{Q}}_1\mathcal{Q}_1\rangle + |\overline{\mathcal{Q}}_2\mathcal{Q}_2\rangle + |\overline{\mathcal{Q}}_3\mathcal{Q}_3\rangle)\,.
\end{aligned} \tag{6.3}$$

For simplicity, we neglect $\eta^{\rm HC} - \eta'^{\rm HC}$ mixing throughout, assuming that the flavour singlet $\eta^{\rm HC}_0$ is too heavy to be pair produced in decays of the vectors, just like the $\eta'^{\rm QCD}$ in QCD. The small coupling of the Goldstone bosons to the SM quarks and the large mass of the $\eta'^{\rm HC}$ justify this approximation.

If we ignore potential differences between HC quark condensates, $\langle\bar{\mathcal{Q}}_i\mathcal{Q}_i\rangle$, for $i = 1, 2$ and $i = 3$, the NDA estimates for the pseudoscalar masses are

$$\begin{aligned}
m^2_{\pi^{\rm HC}} &\sim 4\pi f^{\rm HC}_\pi \; 2m_{\mathcal{Q}_1}\,, \\
m^2_{K^{\rm HC}} &\sim 4\pi f^{\rm HC}_\pi \; (m_{\mathcal{Q}_1} + m_{\mathcal{Q}_3})\,, \\
m^2_{\eta^{\rm HC}_8} &\sim 4\pi f^{\rm HC}_\pi \; 2(m_{\mathcal{Q}_1} + 2m_{\mathcal{Q}_3})/3\,.
\end{aligned} \tag{6.4}$$

Recent lattice simulations compute the QCD condensate [71] and correct the NDA estimate in Eq. (6.4) to $4\pi f^{\rm QCD}_\pi \to 29.8 f^{\rm QCD}_\pi$, where $f^{\rm QCD}_\pi \simeq 92$ MeV in our conventions. Requiring vector resonances with mass approximately 200 GeV fixes the value of $f^{\rm HC}_\pi \simeq 20$ GeV. In this case for $m_q \in [1, 30]$ GeV the masses of the pseudoscalars range in $m_{\pi^{\rm HC}} \in [30, 160]$ GeV.

6.1.2 Vectors and Axial Vectors

As in QCD, the $[\mathcal{Q}\overline{\mathcal{Q}}]$ condensate gives rise to vector and axial-vector resonances that are flavour nonets, with the lowest lying states denoted by $\rho^a_{\rm HC}$ and $a^a_{1\,\rm HC}$ ($a = 1, .., 9$), respectively. $\rho^9_{\rm HC}$ and $a^9_{1\,\rm HC}$ are the flavour-singlet states. The $\rho^a_{\rm HC}$ and $a^a_{1\,\rm HC}$ decay constants are defined as

$$\langle\rho^a_{\rm HC}|\overline{\mathcal{Q}}\,T^a\,\gamma_\mu\,\mathcal{Q}|0\rangle = -if^{\rm HC}_\rho m^{\rm HC}_\rho \epsilon_\mu, \tag{6.5}$$

$$\langle a^a_{1\,\rm HC}|\overline{\mathcal{Q}}\,T^a\,\gamma_\mu\gamma_5\,\mathcal{Q}|0\rangle = -if^{\rm HC}_{a_1} m^{\rm HC}_{a_1} \epsilon_\mu, \tag{6.6}$$

with the flavour-singlet matrix $T^9 \equiv \mathbb{1}_{3\times3}/\sqrt{6}$.

The ρ decay constant in QCD is $f^{\rm QCD}_\rho \simeq 148$ MeV [72] and a recent light-cone sum-rule determination of the a_1 decay constant yields $f^{\rm QCD}_{a_1} \simeq 168$ MeV [73][1]. We estimate the decay constants of the corresponding HC resonances via the scaling relations

$$\frac{f^{\rm HC}_\pi}{f^{\rm QCD}_\pi} \sim \frac{f^{\rm HC}_\rho}{f^{\rm QCD}_\rho} \sim \frac{f^{\rm HC}_{a_1}}{f^{\rm QCD}_{a_1}} \tag{6.7}$$

[1] the quoted values have been reduced by a factor $1/\sqrt{2}$ to conform to our normalisation.

neglecting corrections due to the masses $m_{\mathcal{Q}_i}$ that are expected to be small for $m_{\mathcal{Q}_i} \ll \Lambda_{\rm HC}$.

Breaking the flavour symmetry by $m_{\mathcal{Q}_1} \neq m_{\mathcal{Q}_3}$ splits the flavour nonet. Similarly to Eq. (6.3), we follow the QCD notation and define the vector states in the flavour basis as

$$\begin{aligned}
|\rho^{\rm HC}_{1,2,3}\rangle &= |\overline{\mathcal{Q}}_1\mathcal{Q}_2\rangle, \quad |\overline{\mathcal{Q}}_2\mathcal{Q}_1\rangle, \quad \frac{1}{\sqrt{2}}(|\overline{\mathcal{Q}}_1\mathcal{Q}_1\rangle - |\overline{\mathcal{Q}}_2\mathcal{Q}_2\rangle), \\
|K^{*\rm HC}_{1,2}\rangle &= |\overline{\mathcal{Q}}_{1,2}\mathcal{Q}_3\rangle, \quad |\overline{K}^{*\rm HC}_{1,2}\rangle = |\overline{\mathcal{Q}}_3\mathcal{Q}_{1,2}\rangle, \\
|\rho^{\rm HC}_8\rangle &= \frac{1}{\sqrt{6}}(|\overline{\mathcal{Q}}_1\mathcal{Q}_1\rangle + |\overline{\mathcal{Q}}_2\mathcal{Q}_2\rangle - 2|\overline{\mathcal{Q}}_3\mathcal{Q}_3\rangle), \\
|\rho^{\rm HC}_9\rangle &= \frac{1}{\sqrt{3}}(|\overline{\mathcal{Q}}_1\mathcal{Q}_1\rangle + |\overline{\mathcal{Q}}_2\mathcal{Q}_2\rangle + |\overline{\mathcal{Q}}_3\mathcal{Q}_3\rangle)\,.
\end{aligned} \tag{6.8}$$

The analogous states for the axial-vectors are denoted by $a^{\rm HC}_1$, $K^{A\,\rm HC}_{(1,2)}$, $\overline{K}^{A\,\rm HC}_{(1,2)}$, $\rho^{A\,\rm HC}_8$ and $\rho^{A\,\rm HC}_9$. Breaking the flavour symmetry generates the non-degenerate mass eigenstates $\rho^{\rm HC}$, $K^{*\rm HC}$, $\overline{K}^{*\rm HC}$, V_L and V_H, where the last two are produced by $\rho^{\rm HC}_8 - \rho^{\rm HC}_9$ mixing. We refer to the corresponding axial-vector mass eigenstates as A_L and A_H.

In QCD, $\rho^{\rm QCD}_8 - \rho^{\rm QCD}_9$ mixing produces the mass eigenstates $\omega^{\rm QCD}$ and $\phi^{\rm QCD}$ that are close to being "ideally mixed", i.e. $\omega^{\rm QCD}$ is a linear combination of states with u and d quarks, while $\phi^{\rm QCD}$ is a pure s-quark state. This is the behaviour we expect if we slowly decouple the s quark in QCD: by increasing m_s above $\Lambda_{\rm QCD}$, $\omega^{\rm QCD}$ becomes the singlet of the left-over $\mathrm{SU}(2)_V$ isospin symmetry. The interesting point is that this decoupling of the s-quark happens already for $m_s \sim \Lambda_{\rm QCD}/3$. We use this dynamical input from QCD to model $\rho^{\rm HC}_8$-$\rho^{\rm HC}_9$ mixing. In which case, the HC sector is to a good approximation also ideally mixed

$$\begin{aligned}
|V^{\rm HC}_L\rangle &\simeq \quad |\omega^{\rm HC}\rangle = \frac{1}{\sqrt{2}}(|\overline{\mathcal{Q}}_1\mathcal{Q}_1\rangle + |\overline{\mathcal{Q}}_2\mathcal{Q}_2\rangle)\,, \\
|V^{\rm HC}_H\rangle &\simeq -|\phi^{\rm HC}\rangle = -|\overline{\mathcal{Q}}_3\mathcal{Q}_3\rangle\,,
\end{aligned} \tag{6.9}$$

where we follow the notation from Ref. [74]. In App. B.1 we discuss the extent of deviation from ideal mixing in the HC model for vectors and axial vectors.

Ideal mixing is an important property of the HC theory with direct consequences on $t\bar{t}$ phenomenology. When V_L and V_H are not ideally mixed states they couple to both light and top quarks producing $t\bar{t}$ pairs in s-channel channel. Such light s-channel $t\bar{t}$ mediators have to have $\mathcal{O}(1)$ widths in order to not appear as peaks in the differential invariant-mass spectrum of the $t\bar{t}$ pairs measured by Tevatron and LHC experiments. Thus, a large departure from ideal mixing is phenomenologically disfavoured.

We shall consider cases in which the mass hierarchies of the HC quarks $\mathcal{Q}$ are not the same as in QCD. In this case, scaling the QCD vector and axial-vector masses to the HC scale is not a good description, and therefore, we estimate the masses of the vectors and axial-vectors using a naive model for a generalised QCD-like theory presented in Ref. [74]. The model relates vector and axial-vector masses to the constituent quark masses and accounts for deviations from ideal mixing.

We find the model parameters by fitting the QCD masses and then rescale the fit results to the HC scale. In this naive model the masses for the three $\rho^{\rm HC}$ and four $K^{*\rm HC}_{1,2}$ and $\overline{K}^{*\rm HC}_{1,2}$ vectors are

$$\begin{aligned}
m^2_{\rho^{\rm HC}} &= m^2_{\rho^{\rm HC},\,[m_{\mathcal{Q}}=0]} + \mu^{\rm HC}\; 2m_{\mathcal{Q}_1}\,, \\
m^2_{K^{*\rm HC}} &= m^2_{\rho^{\rm HC},\,[m_{\mathcal{Q}}=0]} + \mu^{\rm HC}\; (m_{\mathcal{Q}_1} + m_{\mathcal{Q}_3})\,,
\end{aligned} \tag{6.10}$$

with an analogous prescription for axial-vectors. $\mu^{\rm HC}$ is a fit parameter rescaled from the corresponding value in QCD, $\mu^{\rm QCD} \simeq 2.1$ GeV. The masses with the subscript $[m_{\mathcal{Q}} = 0]$ indicate the chiral-limit masses rescaled from QCD. Similarly to Eq. (6.10), the model also parametrises the V_L and V_H masses and deviations from ideal mixing, which remain small for the constituent masses that we consider (see App. B.1). In the following we drop the "HC" super/subscript, with the understanding that we are referring to HC resonances and decay constants.

In Ref. [75] it was demonstrated that NP scenarios can account for the measurement of an unexpectedly large $A_{FB}^{t\bar{t}}$ at the Tevatron and simultaneously agree with the SM-like measurement of A_C at LHC. If the $t\bar{t}$ mediators are approximately 200-GeV heavy t-channel vectors or scalars the $A_{FB}^{t\bar{t}} - A_C$ correlation is broken by associated $t\bar{t}$ production. However, for this to be a viable scenario, the mediators need to have an approximately 25% branching ratio to quarks, i.e. they cannot decay primarily to quarks. In the HC model, these t-channel vectors are the mass eigenstates of the vectors $K^*_{(1,2)}$ and $\overline{K}^*_{(1,2)}$, and the axial-vectors $K^A_{(1,2)}$ and $\overline{K}^A_{(1,2)}$. The HC dynamics naturally provide a dominant decay channel for them, other than their decay to quarks, namely their decay to pseudo-Goldstone bosons.

In the flavour symmetric limit, the flavour octet ρ^a primarily decays to pairs of HC pions, with decay widths

$$\Gamma_{\rho\to\pi\pi} = \frac{g^2_{\rho\pi\pi}}{32\pi}\, m_\rho \left(1 - \frac{4m_\pi^2}{m_\rho^2}\right)^{\frac{3}{2}} , \tag{6.11}$$

where $g_{\rho\pi\pi}$ is the ρ-π-π coupling in the Lagrangian interaction

$$\mathscr{L}_{\rho\pi\pi} = -g_{\rho\pi\pi}\, f_{abc}\, \rho^a_\mu\, \pi^b \partial^\mu \pi^c , \tag{6.12}$$

with $a = 1, \ldots, 8$. We use the VMD estimate

$$g_{\rho\pi\pi} \simeq m_\rho / f_\rho . \tag{6.13}$$

In QCD, it agrees with the NDA estimate $g_{\rho\pi\pi} \sim \mathcal{O}(4\pi)$ within a factor of two and lies only 16% below the measured value. VMD is a phenomenologically driven argument stating that the electromagnetic or chromomagnetic form factors of bound states are dominated at low-momentum transfer ($q^2 \to 0$) by the lowest lying vector resonance. In App. B.2 we briefly discuss the argument and the underlying assumptions.

We assume the flavour singlet η' has a mass $m_{\eta'} \sim \Lambda_{\rm HC}$, as in QCD, and is therefore too heavy to be pair produced in decays of the vector nonet. Thus, in the flavour symmetric limit the decay width of the flavour singlet $\rho^9_{\rm HC}$ is suppressed and only its decays to ordinary quark $u_i\bar{u}_i$ final states are kinematically allowed. The expressions for the vector nonet decay widths have to be modified to take into account the non-degeneracy of the vector and pseudoscalar masses in the different decays, and $\rho^8 - \rho^9$ mixing. We list them in App. B.1.

The decays widths of the axial vectors require a more sophisticated analysis than the widths of the vectors. In QCD, the $A(^3P_1)$ axial-vector multiplet decays primarily through $A \to VP$, as well as $A \to VV$, if the latter is kinematically allowed (V denotes vectors and P pseudoscalars). The $A \to VP$ decays were discussed in a phenomenological analysis in the SU(3) symmetric limit in Ref. [76]. Their results may be used to estimate the decay widths of the HC axial-vectors and we shall discuss them in the upcoming publication [29]. We do not present this estimate in this work as the axial-vector widths do not have a large impact on $t\bar{t}$ phenomenology. In the analysis we find that viable benchmarks exist independent of the choice of the axial-vector widths.

6.1.3 Composite Quarks

The HC quarks, $\mathcal{Q}_i$, and the scalar, $\mathcal{S}$, form a flavour-triplet of composite vectorlike weak-singlet up-type quarks,

$$u'_1 \sim [\mathcal{S}\,\mathcal{Q}_1], \qquad u'_2 \sim [\mathcal{S}\,\mathcal{Q}_2], \qquad u'_3 \sim [\mathcal{S}\,\mathcal{Q}_3]\,. \tag{6.14}$$

The composite quarks mix with the ordinary up quarks via the flavour-diagonal Yukawa couplings $\mathbf{h}_{ij} = h_i\delta_{ij}$ in Eqs. (3.1) and (3.2). The mass mixing terms are ($u_i = u, c, t$),

$$\sqrt{2}\,h_i\,f_{u'_i}\,\bar{u}_{Ri}\,u'_{Li}, \tag{6.15}$$

where the composite quark decay constants $f_{u'_i}$ are defined by the matrix element

$$\langle u'_i|\overline{\mathcal{Q}}_i\,\mathcal{S}^*|0\rangle = \sqrt{2}f_{u'_i}\,\bar{u}'_i\,, \tag{6.16}$$

with u'_i Dirac spinors.

The composite quarks and the vectors are both S-wave radial ground states, so we naively expect their masses and decay constants to be of the same order,

$$f_{u'_i} \sim f_\rho^{\rm HC} \quad \text{and} \quad M_{u'_i} \sim m_\rho^{\rm HC}\,, \tag{6.17}$$

up to potentially large differences due to the short-distance masses $m_\mathcal{Q}$ and $m_\mathcal{S}$. We shall consider the case where $m_\mathcal{S} > \Lambda_{\rm HC}$ and model the composite-quark masses by a linear dependence of $M_{u'}$ on $m_\mathcal{S}$ and small corrections from $m_{\mathcal{Q}_i}$

$$M_{u'_i} \simeq M_{\rm chiral} + m_\mathcal{S} + m_{\mathcal{Q}_i}\,. \tag{6.18}$$

$M_{\rm chiral}$ is the $\rho^{\rm HC}$ chiral-limit mass $m_{\rho^{\rm HC},\,[m_\mathcal{Q}=0]}$. The composite quarks are thus much heavier than the vectors with masses above $\Lambda_{\rm HC}$; their analogue in QCD are D mesons.

In this case, the estimate $f_{u'_i} \sim f_\rho^{\rm HC}$ is not an appropriate description of their decay constants. Therefore, we use QCD data to model these decay constants. We perform a fit of the decay constants of vectors with one light constituent quark in terms of their masses ($\rho_{\rm QCD}$, $K^*_{\rm QCD}$, $D^*_{\rm QCD}$ and $B^*_{\rm QCD}$) and rescale the result to the HC scale to obtain $f_{u'}$ in terms of $M_{u'}$:

$$f_{u'} = f_\rho^{\rm QCD}\,\frac{M_{\rm chiral}}{M_\rho^{\rm QCD}}\,\mathcal{F}\left(\frac{M_{u'}}{M_{\rm chiral}}\right)\,. \tag{6.19}$$

The function $\mathcal{F}(M_{u'}/M_{\rm chiral})$ is determined by the fit and we plot it in Fig. 6.1.

The masses and decay constants of the composite states, together with the strong Yukawas, fix the mixing of SM and composite up quarks. The 3×3 up-quark mass matrix is flavour diagonal and reads, for each flavour,

$$M_{RL} = \begin{pmatrix} m_{u_i} & \sqrt{2}\,h_i\,f_{u'_i} \\ 0 & M_{u'_i} \end{pmatrix}\,, \tag{6.20}$$

with $i = 1, 2, 3$ and m_{u_i} the ordinary $SU(2)_L$-breaking quark masses. Diagonalisation then yields the mass eigenstates

$$\begin{aligned} |u_{Ri}\rangle^{\rm phys} &= \cos\theta_{Ri}\,|u_{Ri}\rangle - \sin\theta_{Ri}\,|u'_{Ri}\rangle, \\ |u'_{Ri}\rangle^{\rm phys} &= \sin\theta_{Ri}\,|u_{Ri}\rangle + \cos\theta_{Ri}\,|u'_{Ri}\rangle\,. \end{aligned} \tag{6.21}$$

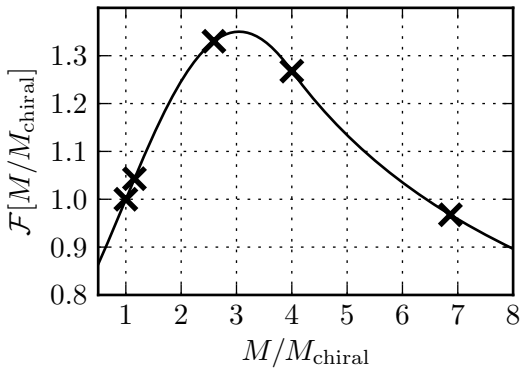

Figure 6.1: *The fit for the decay constants of vectors with one light constituent quark parametrised in terms of $M/M_{\rm chiral}$. M is the mass of the meson and $M_{\rm chiral} = m_{\rho,\,[m_{\mathcal{Q}}=0]}$, the chiral-limit mass of the ρ meson. Crosses indicate the QCD data.*

The analogous rotation with the replacement $R \to L$ gives the left-handed mass eigenstates. The SM quarks are identified with the $u_i^{\rm phys}$ states. The special case of $f_{u'_i}/M_{u'_i} \sim f_\rho/m_\rho$, as indicated by NDA where both ratios are $\mathcal{O}(1/4\pi)$, yields

$$\sin\theta_{Ri} \simeq \sqrt{2} h_i \frac{f_{u'_i}}{M_{u'_i}}\,, \qquad \sin\theta_{Li} \simeq \sqrt{2} h_i \frac{f_{u'_i} m_{u_i}}{M^2_{u'_i}}\,. \tag{6.22}$$

We observe that the mixing of left-handed up and charm quarks with the composite quarks is proportional to the light-quark mass and can be neglected.

$\mathcal{S}$ is a constituent of the u'-quarks and is typically much heavier than $4f_\pi$. Therefore, similarly to B mesons in the SM, we expect the inclusive width of the u''s to be appropriately described by the partonic width of $\mathcal{S}$

$$\Gamma_{u'_i} \simeq \Gamma_{\mathcal{S}\to u_i\bar{\mathcal{Q}}_i}\,. \tag{6.23}$$

The partonic width $\mathcal{S} \to u_i \bar{\mathcal{Q}}_i$ is

$$\frac{\Gamma_{\mathcal{S}\to u_i\bar{\mathcal{Q}}_i}}{m_{\mathcal{S}}} = \frac{|h_i|^2}{16\pi} \mathrm{PS}\left[1, \frac{m^2_{u_i}}{m^2_{\mathcal{S}}}, \frac{m^2_{\mathcal{Q}_i}}{m^2_{\mathcal{S}}}\right]\left(1 - \frac{m^2_{u_i}}{m^2_{\mathcal{S}}} - \frac{m^2_{\mathcal{Q}_i}}{m^2_{\mathcal{S}}}\right), \tag{6.24}$$

with $\mathrm{PS}\,[x,y,z] \equiv (x^2+y^2+z^2-2xy-2xz-2yz)^{1/2}$ the phase-space function. This yields typically $10\% - 20\%$ widths for the composite quarks.

Interactions with Vectors and Axial-vectors

The couplings of the vector mesons to the composite quarks are described by the Lagrangian

$$\mathscr{L} = g_\rho(\bar{u}' T^a \gamma^\mu u')\rho^a_\mu + g_{a_1}(\bar{u}' T^a \gamma^\mu \gamma_5 u') {a_1}^a_\mu\,, \tag{6.25}$$

where the composite quarks are in the interaction basis of Eq. (6.14). a are flavour indices and we consider universal couplings for simplicity. In NDA, both g_ρ and g_{a_1} are $\mathcal{O}(4\pi)$, while we

use the VMD estimate (see App. B.2)

$$g_\rho \simeq \frac{m_\rho}{f_\rho}, \qquad g_{a_1} \simeq \frac{m_{a_1}}{f_{a_1}}\,, \tag{6.26}$$

which implies $g_{\rho\pi\pi} \simeq g_\rho$ and $g_{a_1\pi\pi} \simeq g_{a_1}$. Applying the rotations in Eq. (6.21) we obtain the mass eigenstate couplings

$$\begin{aligned}\mathscr{L} =&\lambda^R_{1,ij}\,\bar{u}_{Ri}\,\gamma^\mu\,T^a_{ij}\,\rho^a_\mu\,u_{Rj} + \lambda^R_{2,ij}\,\bar{u}'_{Ri}\,\gamma^\mu\,T^a_{ij}\,\rho^a_\mu\,u'_{Rj}\\ &+(\lambda^R_{3,ij}\,\bar{u}_{Ri}\,\gamma^\mu\,T^a_{ij}\,\rho^a_\mu\,u'_{Rj} + \text{h.c.}) + (\text{R}\to\text{L})\,,\end{aligned} \tag{6.27}$$

where

$$\begin{aligned}\lambda^R_{1,ij} =&\quad g_\rho \sin\theta_{Ri}\sin\theta_{Rj},\\ \lambda^R_{2,ij} =&\quad g_\rho \cos\theta_{Ri}\cos\theta_{Rj},\\ \lambda^R_{3,ij} =&-g_\rho \sin\theta_{Ri}\cos\theta_{Rj}\,.\end{aligned} \tag{6.28}$$

For the left-handed quark couplings, $\lambda^L_{m,ij}$, substitute $R \to L$ in Eq. (6.28). We denote the corresponding axial-vector meson couplings by $\zeta^{(RL)}_1$, $\zeta^{(RL)}_2$, $\zeta^{(RL)}_3$. Their expressions follow by substituting $\gamma^\mu \to \gamma^\mu\gamma_5$ and $g_\rho \to g_{a_1}$ in Eq. (6.27). Note that the couplings to light left-handed quarks are negligible, while their right-handed equivalents are typically large.

Leaving aside corrections due to $\mathcal{F}(M_{u'}/M_{\text{chiral}}) \neq 1$, we have

$$\lambda^R_{1,ij} \simeq 2\,f_\rho^{\text{QCD}}/m_\rho^{\text{QCD}}\,h_i h_j \sim 0.4\,h_i h_j.$$

Thus, for $\mathcal{O}(1)$ Yukawa couplings the model naturally provides $\mathcal{O}(1)$ flavour-violating couplings of vector resonances to ordinary quarks, which is one of the requirements for a t-channel mediated solution to the $A^{t\bar{t}}_{FB}$.

In Eq. (6.27) the quarks are mass eigenstates and the vectors degenerate flavour eigenstates. Flavour symmetry breaking splits the flavour eigenstates to non-degenerate mass eigenstates. By explicitly evaluating T^a and rotating to the mass eigenstates of the vectors, we find the right-handed mass eigenstate coupling of K^*_1 to u and t quarks:

$$\kappa^R_{K^*_1\text{-}u\text{-}t} = \frac{1}{\sqrt{2}}\lambda^R_{1,ut} = \frac{1}{\sqrt{2}} g_\rho \sin\theta_{Ru}\sin\theta_{Rt}\,.$$

The partial decay width of the $K^* \to \bar{t}u$ then reads

$$\frac{\Gamma_{K^*\to\bar{t}u}}{m_{K^*}} = \frac{1}{16\pi}\left(\left(\lambda^R_{1,ut}\right)^2 + \left(\lambda^L_{1,ut}\right)^2\right)\text{PS}\left[1, 0, \frac{m_t^2}{m_{K^*}^2}\right]\left(1 - \frac{m_t^2}{2m_{K^*}^2} - \frac{1}{2}\left(\frac{m_t^2}{m_{K^*}^2}\right)^2\right), \tag{6.29}$$

if the decay is kinematically allowed. This should be compared to the partial width from the dominant decay channel to pseudoscalars $K^* \to K\pi$ discussed in Sec. 6.1.2 and given in App. B.1.

Interactions with Pseudoscalars

The interactions of the composite quarks with HC pions are the analogue of pion-nucleon-nucleon interaction in QCD. In the interaction basis of the quarks, it is described for the flavour-symmetric case by

$$\mathscr{L} = i\frac{g_A^{\text{HC}}}{f_\pi^{\text{HC}}}\left(\bar{u}'_{Ri}\,T^a_{ij}\,\not{\partial}\pi^a u'_{Rj} - \bar{u}'_{Li}\,T^a_{ij}\,\not{\partial}\pi^a u'_{Lj}\right), \tag{6.30}$$

We take $g_A^{\rm HC} \simeq g_A^{\rm QCD} = 1.257$. Rotating to the physical quark basis, we obtain

$$\begin{aligned}\mathscr{L} = \frac{g_A^{\rm HC}}{f_\pi^{\rm HC}}\Big(&\cos\theta_{Ri}\cos\theta_{Rj}\,\bar{u}'_{Ri}\,T^a_{ij}\,\not\partial\pi^a u'_{Rj}\\ &-\cos\theta_{Ri}\sin\theta_{Rj}\,\bar{u}'_{Ri}\,T^a_{ij}\,\not\partial\pi^a u_{Rj}\\ &-\sin\theta_{Ri}\cos\theta_{Rj}\,\bar{u}_{Ri}\,T^a_{ij}\,\not\partial\pi^a u'_{Rj}\\ &+\sin\theta_{Ri}\sin\theta_{Rj}\,\bar{u}_{Ri}\,T^a_{ij}\,\not\partial\pi^a u_{Rj}\Big) - (R\to L)\,.\end{aligned} \tag{6.31}$$

To find the strength of the interaction of pions to SM quarks we integrate by parts and use the Dirac equation. In the approximation of Eq. (6.22) and keeping only the first order terms in the masses of the SM quarks we find

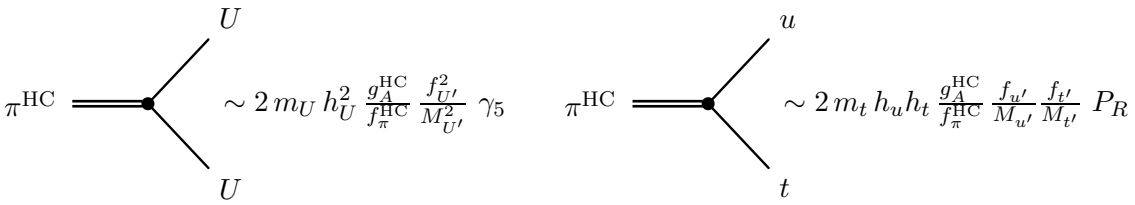

U denotes any SM up-type quark. The axial $\pi^{\rm HC}$-U-U coupling is proportional to the mass of the U quark. Thus, the pion couplings to two light quarks are always negligible. However, the $\pi^{\rm HC}$-u-t coupling of pseudoscalars ($K^{\rm HC}$) to the right-handed top and light-quark is proportional to the top-quark mass and cannot be neglected, and indeed, the hyper-kaons will contribute to the $A_{FB}^{t\bar{t}}$ in the t-channel.

6.1.4 P-wave Vector Mesons

Finally, we consider the flavour-singlet colour-octet and colour-singlet P-wave vector-meson bound states of the HC scalars, denoted $V_o[\mathcal{S}^*\mathcal{S}]$ and $V_s[\mathcal{S}^*\mathcal{S}]$, respectively. Since the scalar $\mathcal{S}$ has no analogue in QCD, there are large uncertainties in our estimation of their properties. Their interpolating currents are derivative operators for which we can define the corresponding decay constants as

$$\begin{aligned}\langle V_o^a|\mathcal{S}^*\overset{\leftrightarrow}{\partial}_\mu\mathcal{T}^a\mathcal{S}|0\rangle &= -if_{V_o}M_{V_o}\epsilon_\mu,\\ \langle V_s|\mathcal{S}^*\overset{\leftrightarrow}{\partial}_\mu\mathcal{S}|0\rangle &= -i\sqrt{6}f_{V_s}M_{V_s}\epsilon_\mu\,,\end{aligned} \tag{6.32}$$

with $\mathcal{T}^a$ the colour Gell-Mann matrices, normalized as $\mathrm{Tr}[\mathcal{T}^a\mathcal{T}^a] = 1/2$, and $\overset{\leftrightarrow}{\partial} \equiv \overset{\rightarrow}{\partial} - \overset{\leftarrow}{\partial}$.

The couplings of these vector mesons to composite quarks in the interaction basis are

$$\mathscr{L} = g_{V_o}\,\bar{u}'_i\,\mathcal{T}^a\,\gamma_\mu\,u'_i\,V_o^{a\,\mu} + g_{V_s}\,\bar{u}'_i\,\gamma_\mu\,u'_i\,V_s^\mu\,, \tag{6.33}$$

where colour indices have been suppressed and we work in the flavour symmetric limit for simplicity, i.e. universal g_{V_o} and g_{V_s}. Note that g_{V_o}, g_{V_s} are of $\mathcal{O}(4\pi)$ in NDA. We estimate these couplings using VMD, similarly to the ρ^a-composite quark couplings, yielding

$$g_{V_o} \simeq \frac{M_{V_o}}{f_{V_o}}, \qquad g_{V_s} \simeq \frac{M_{V_s}}{\sqrt{6}f_{V_s}}\,. \tag{6.34}$$

Kinetic mixing of the gluons with V_o generates universal couplings of the latter to all SM quarks, which in VMD is given by

$$\mathscr{L} = -g_s^2 \frac{f_{V_o}}{M_{V_o}} \bar{q}\, \mathcal{T}^a \gamma^\mu\, q\, V_{o\,\mu}^a \,. \tag{6.35}$$

in the quark-interaction basis; g_s is the strong coupling constant.

We can gain some insight into the magnitudes of the VMD estimates for g_{V_o} and g_{V_s} or the ratios M_V/f_V, from the QCD flavour nonet ($^3P_2$) tensor mesons: $f_2(1270)$, $f_2'(1525)$, $a_2(1320)$, $K_2^*(1430)$. Like V_o and V_s, they are P-wave bound states with interpolating currents that are derivative operators. Their decay constants f_T can be defined as [77],

$$\langle T|\frac{1}{2}(\bar{q}_1\gamma_\mu \overset{\leftrightarrow}{\partial}_\nu q_2 + \bar{q}_1\gamma_\nu \overset{\leftrightarrow}{\partial}_\mu q_2)|0\rangle = f_T m_T^2 \epsilon_{\mu\nu}\,, \tag{6.36}$$

where $\epsilon_{\mu\nu}$ is the meson polarisation tensor. Light-cone QCD sum-rule determinations of the decay constants range approximately from 102 MeV for f_2 to 126 MeV for f_2' [77] and are consistent with extractions of the decay constants from the measured $f_2 \to \pi^+\pi^-$ and $f_2' \to K^+K^-$ decay rates, which employ the tensor-meson dominance hypothesis. The ratios, $f_T^{\rm QCD}/m_T^{\rm QCD} \approx 0.08$, are significantly smaller than the corresponding QCD flavour-nonet vector-meson ratios, like f_{a_1}/m_{a_1}. This observation, as well as the fact that the QCD tensor and axial-vector mesons are approximately 50% heavier than their vector-nonet counterparts, can be attributed to them being P-wave radially first excited states. Given that V_o and V_s are also P-wave states, we shall estimate their masses to be $\sim 50\%$ larger than the flavour-nonet $\rho_{\rm HC}^a$ masses (not including potentially significant differences due to $m_{\mathcal{Q}}$, $m_{\mathcal{S}}$) and $f_{V_{o,s}}/M_{V_{o,s}} \sim f_T^{\rm QCD}/m_T^{\rm QCD} < f_\rho^{\rm QCD}/m_\rho^{\rm QCD}$.

The $V_{(o,s)}$ interactions in Eqs. (6.33) and (6.35) in the quark-mass basis are then obtained similarly to Eq. (6.27). For instance, for the right-handed up quarks, the colour-octet interactions are

$$\begin{aligned}\mathscr{L} = {}& \kappa_{1,i}^R\, \bar{u}_{Ri}\, \gamma^\mu\, \mathcal{T}^a\, V_{o\,\mu}^a\, u_{Ri} + \kappa_{2,i}^R\, \bar{u}'_{Ri}\, \gamma^\mu\, \mathcal{T}^a\, V_{o\,\mu}^a\, u'_{Ri} \\ & + (\kappa_{3,i}^R\, \bar{u}_{Ri}\, \gamma^\mu\, \mathcal{T}^a\, V_{o\,\mu}^a\, u'_{Ri} + \text{h.c.}) + (R \to L)\,,\end{aligned} \tag{6.37}$$

with

$$\begin{aligned}\kappa_{1,i}^R &= g_{V_o} \sin^2\theta_{Ri} - g_s^2 \frac{f_{V_o}}{M_{V_o}} \cos^2\theta_{Ri}, \\ \kappa_{2,i}^R &= g_{V_o} \cos^2\theta_{Ri} - g_s^2 \frac{f_{V_o}}{M_{V_o}} \sin^2\theta_{Ri}, \\ \kappa_{3,i}^R &= -\left(g_{V_o} + g_s^2 \frac{f_{V_o}}{M_{V_o}}\right) \sin\theta_{Ri} \cos\theta_{Ri}.\end{aligned} \tag{6.38}$$

The couplings to left-handed quarks $\kappa_{m,i}^L$ are obtained by substituting $R \to L$ above. For the couplings to down quarks take the limit $g_{V_o}, \theta_{Ri}, \theta_{Li} \to 0$.

The $V_{(o,s)}$ dominantly decay to pairs of SM and composite up quarks with the following chiralities

$$V_{(o,s)} \to u_{Ri}\, \bar{u}_{Li} + u_{Ri}\, \bar{u}_{Li}, \qquad V_{(o,s)} \to u'_{Ri}\, \bar{u}_{Li} + u_{Ri}\, \bar{u}'_{Li}\,. \tag{6.39}$$

This assumes that the decays are kinematically allowed, a situation easily realised given the enhanced masses of the P-wave vectors and the fact that $m_{\mathcal{S}}$ is significantly larger than $m_{\mathcal{Q}}$

in our case. Which of these channels dominate, depends on the kinematic suppression and the Yukawa couplings that control the amount of mixing of light and composite quarks.

We obtain for the general case $u_A = u_i, u_i'$ and $u_B = u_i, u_i'$ the partial width

$$\frac{\Gamma_{V_o \to \bar{u}_A u_B}}{M_{V_o}} = \frac{1}{48\pi} \mathrm{PS}\left[1, \frac{m_A^2}{M_{V_o}^2}, \frac{m_B^2}{M_{V_o}^2}\right] \Bigg\{ \left[\left(\kappa_{AB}^R\right)^2 + \left(\kappa_{AB}^L\right)^2\right] \times \left(1 - \frac{m_A^2}{2M_{V_o}^2} - \frac{m_B^2}{2M_{V_o}^2} - \frac{1}{2}\left(\frac{m_A^2}{M_{V_o}^2} - \frac{m_B^2}{M_{V_o}^2}\right)^2\right) + 6\kappa_{AB}^R \kappa_{AB}^L \frac{m_A}{M_{V_o}} \frac{m_B}{M_{V_o}} \Bigg\}, \quad (6.40)$$

where $\kappa_{(A,B)}^{(L,R)}$ correspond for a given case to the couplings defined in Eq. (6.38). Our total width is then the sum of all kinematically allowed decays. For V_s substitute $g_{V_o} \to g_{V_s}$ and multiply by 6 for the different colour structure.

Taking as a representative example $g_{V_o} = m_{V_o}/f_{V_o} = 1/0.08$, $\sin\theta_R = 0.27h$ (identifying $f_{u'}/M_{u'} \approx f_\rho/m_\rho$ in Eq. (6.22)), $M_{u'} = 550$ GeV, and $M_{V_o} = 700$ GeV (corresponding to $m_\rho \sim 300$ GeV, $M_{u'} \sim m_{\rho^{\mathrm{HC}}} + m_{\mathcal{S}}$, $M_{V_o} \approx 1.5\, m_{\rho^{\mathrm{HC}}} + 2m_{\mathcal{S}}$ and $m_{\mathcal{Q}} \ll m_{\mathcal{S}} \sim 250$ GeV) we sum over all possible final states and obtain for $h = 2$ that $\Gamma_{V_o}/M_{V_o} \approx 30\%$. Thus, we conclude that V_o can be very broad for couplings $h_i \sim 1$, i.e.

$$\Gamma_{V_o}/M_{V_o} = \mathcal{O}(1), \quad (6.41)$$

and the same applies to the V_s width.

V_o and V_s are the reason we are forced to consider $m_{\mathcal{S}} > \Lambda_{\mathrm{HC}}$. They are s-channel mediators of $t\bar{t}$-pair production at Tevatron and LHC that, typically, produce peaks in differential $m_{t\bar{t}}$ spectrum if their masses are close to the production threshold and their widths are small. This is the case when $m_{\mathcal{S}} \simeq m_{\mathcal{Q}}$; the decays to SM quark-pairs are the only kinematically permitted decay channels and are not enough to hide the resonances from the differential spectrum. By increasing $m_{\mathcal{S}}$ all channels become kinematically accessible and $V_{(os)}$ are too broad to disturb the spectra at Tevatron or LHC.

This concludes the discussion of the resonances that we consider in our analysis. For each resonance we discussed how to estimate its mass, width and couplings to ordinary quarks in terms of the UV parameters of the HC model: $m_{\mathcal{Q}}$, $m_{\mathcal{S}}$, h_1 and h_3. The HC model has many similarities to ordinary QCD, which motivated us to model the infrared behaviour of the HC theory closely to what is observed in QCD after chiral-symmetry breaking. This is the working assumption of our analysis with which we restrict the parameter space of the model. The fact that, even in this restricted QCD-like setup, phenomenological viable benchmarks exist and account for the observed $A_{FB}^{t\bar{t}}$ reinforces our point that new strong interactions at the TeV scale are possible and may have evaded direct detection so far.

6.2 $t\bar{t}$ Pair Production with Hypercolour Resonances

In the SM, at the partonic LO level, a $t\bar{t}$ pair is produced by the amplitudes, $q\bar{q} \to t\bar{t}$ and $gg \to t\bar{t}$. The HC interactions modify the $U\overline{U} \to t\bar{t}$ amplitude only by additional s- and t-channel amplitudes mediated by vector and pseudoscalar mesons. $U = u, c$, since the HC

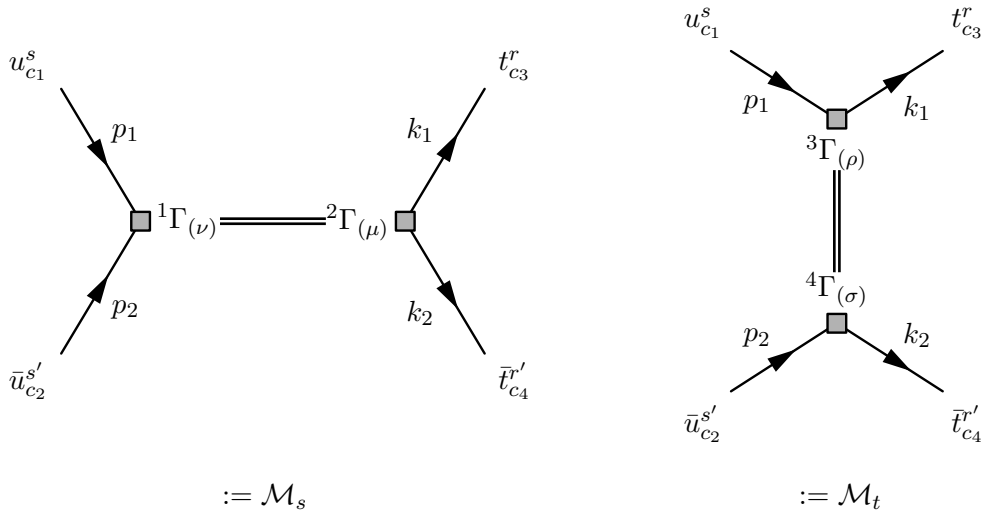

Figure 6.2: *s- and t-channel diagrams in the left and right panel, respectively, for $t\bar{t}$ production from a $u\bar{u}$ initial state. Here, arrows indicate the momentum flow. $s^{(\prime)}$ and $\tau^{(\prime)}$ are spin indices, c_i colour indices.*

resonances do not couple to the down-quark sector except from V_o, which has a small universal coupling to quarks from kinetic mixing with the gluon. Here, we consider for concreteness the NP effects in the $u\bar{u} \to t\bar{t}$ amplitude. The s-channel mediators in the HC model are: V_o, V_s, V_L, V_H, A_L and A_H. The t-channel mediators are: K_1^{HC}, $K_1^{*\mathrm{HC}}$ and $K_1^{A\,\mathrm{HC}}$. Fig. 6.2 depicts the Feynman diagrams for the s- and t-channel amplitudes. The differential partonic $q\bar{q} \to t\bar{t}$ cross section is then the squared averaged sum of all SM and HC amplitudes:

$$\frac{d\hat{\sigma}}{dz} = \frac{\beta}{32\pi s}\overline{\sum}|\mathcal{M}_{tot}|\,, \tag{6.42}$$

where s is the centre-of-mass energy, $\beta = \sqrt{1-4m_t^2/s}$ the velocity of the top-quark in the rest frame of the initial state and z the cosine of the scattering angle of the top quark in the partonic centre-of-mass frame. $\overline{\sum}$ averages over all spins and colour indices of the initial state and sums over all indices of the final state, i.e. in the notation defined in Fig. 6.2,

$$\overline{\sum} = \frac{1}{2}\frac{1}{2}\sum_{s,s',r,r'}\ \frac{1}{3}\frac{1}{3}\sum_{c_1,c_2,c_3,c_4}\left(\sum_a\right). \tag{6.43}$$

The sum over Gell-Mann indices $a = 1,\ldots,8$ applies only to the colour-octet exchange V_o. The s- and t-channel amplitudes for a given resonance then read:

$$i\mathcal{M}_s = \left(\bar{v}^{s'}_{c_2}(p_2)\,{}^1\Gamma_{(\nu)}\,u^s_{c_1}(p_1)\right)\ \cdot M_s^{(\nu\mu)} \cdot \left(\bar{u}^r_{c_3}(k_1)\,{}^2\Gamma_{(\mu)}\,v^{r'}_{c_4}(k_2)\right)\ \cdot \mathcal{J}_{c_2c_1}\mathcal{J}_{c_3c_4} \tag{6.44}$$

$$i\mathcal{M}_t = \left(\bar{u}^r_{c_3}(k_1)\,{}^3\Gamma_{(\rho)}\,u^s_{c_1}(p_1)\right)\ \cdot M_t^{(\rho\sigma)} \cdot \left(\bar{v}^{s'}_{c_2}(p_2)\,{}^4\Gamma_{(\sigma)}\,v^{r'}_{c_4}(k_2)\right)\ \cdot \mathcal{J}_{c_3c_1}\mathcal{J}_{c_2c_4} \tag{6.45}$$

with $u^s(p)$ and $v^s(p)$ Dirac spinors.

- $M^{\mu\nu}_{(st)}$ are the propagators of the resonance. In the constant width approximation, for a vector resonance with mass M_V and width Γ_V they are

$$M_s^{\nu\mu} = -i\frac{g_{\nu\mu} - q_s^\nu q_s^\mu/M_V^2}{q_s^2 - M_V^2 + iM_V\Gamma_V} \qquad \text{with} \quad q_s \equiv p_1 + p_2 \tag{6.46}$$

$$M_t^{\rho\sigma} = -i\frac{g_{\rho\sigma} - q_t^\rho q_t^\sigma/M_V^2}{q_t^2 - M_V^2 + iM_V\Gamma_V} \qquad \text{with} \quad q_t \equiv p_1 - k_1\,. \tag{6.47}$$

  For a pseudoscalar with mass M_S and width Γ_S they are

$$M_s = -i\frac{1}{q_s^2 - M_S^2 + iM_S\Gamma_S} \tag{6.48}$$

$$M_t = -i\frac{1}{q_t^2 - M_S^2 + iM_S\Gamma_S} \tag{6.49}$$

- ${}^i\Gamma_{(\mu)}$ are the chiral couplings of the resonances to the quarks:

Vector Mediators	**Scalar Mediators**
${}^1\Gamma_\nu = \gamma_\nu(\kappa^L_{uu}P_L + \kappa^R_{uu}P_R)$	${}^1\Gamma = (\kappa^L_{uu}P_L + \kappa^R_{uu}P_R)$
${}^2\Gamma_\mu = \gamma_\mu(\kappa^L_{tt}P_L + \kappa^R_{tt}P_R)$	${}^2\Gamma = (\kappa^L_{tt}P_L + \kappa^R_{tt}P_R)$
${}^3\Gamma_\rho = \gamma_\rho(\kappa^L_{tu}P_L + \kappa^R_{tu}P_R)$	${}^3\Gamma = (\kappa^L_{tu}P_L + \kappa^R_{tu}P_R)$
${}^4\Gamma_\sigma = \gamma_\sigma(\kappa^L_{ut}P_L + \kappa^R_{ut}P_R)$	${}^4\Gamma = (\kappa^L_{ut}P_L + \kappa^R_{ut}P_R)$

  Details of the couplings for each resonance to quarks are found in the last section. The $\kappa^{(LR)}$'s here include the mixings with the composite quarks $\sin\theta_{Ri}$ and $\sin\theta_{Li}$ and the explicit values of the flavour generators T_a.

- $\mathcal{J}_{c_ic_j}$ are colour factors. They are equal to the identity for all resonances except for the colour octet:

$$\begin{aligned} \mathcal{J}_{c_ic_j} &= \mathcal{T}^a_{c_ic_j} \qquad \text{for } V_o \text{ and the gluon,} \\ \mathcal{J}_{c_ic_j} &= \mathbb{1}_{c_ic_j} \qquad \text{otherwise.} \end{aligned} \tag{6.50}$$

  The colour factors control the interference among contributions of different resonances and interference with SM gluon contribution. We discuss them below.

We compute $|\mathcal{M}_{\text{tot}}|^2$ applying standard trace technology. Using $|\mathcal{M}_1 + \mathcal{M}_2|^2 = |\mathcal{M}_1|^2 + |\mathcal{M}_2|^2 + 2\,\text{Re}(\mathcal{M}_1\mathcal{M}_2^*)$ we reduce the calculation of all contributions and interferences to three traces on which we map the specific cases described above. The three general cases are

- the product of two s-channel amplitudes from two mediators, med_1 and med_2,

$$\begin{aligned} \mathcal{M}_s(\text{med}_1)\;\mathcal{M}_s^*(\text{med}_2) = &\text{Tr}\left[(\not{p}_2 - m_u)\,{}^1\Gamma_{(\nu_1)}(\not{p}_1 + m_u)\,{}^1\Gamma'_{(\nu_2)}\right] \times \\ &\text{Tr}\left[(\not{k}_1 + m_t)\,{}^2\Gamma_{(\mu_1)}(\not{k}_2 - m_t)\,{}^2\Gamma'_{(\mu_2)}\right] \times \\ &M_s^{(\nu_1\mu_1)}M_s^{(\nu_2\mu_2)*} \times \\ &\mathcal{J}_{c_2c_1}\mathcal{J}_{c_3c_4}\mathcal{J}^*_{c_2c_1}\mathcal{J}^*_{c_3c_4}\,, \end{aligned} \tag{6.51}$$

- the product of two t-channel amplitudes from two mediators, med_1 and med_2,

$$\begin{aligned}\mathcal{M}_t(\text{med}_1)\ \mathcal{M}_t^*(\text{med}_2) =& \text{Tr}\left[(\not{k}_1 + m_t)^3 \Gamma_{(\rho_1)} (\not{p}_1 + m_u)^3 \Gamma'_{(\rho_2)}\right] \times \\ & \text{Tr}\left[(\not{p}_2 - m_u)^4 \Gamma_{(\sigma_1)} (\not{k}_2 - m_t)^4 \Gamma'_{(\sigma_2)}\right] \times \\ & M_t^{(\rho_1\sigma_1)} M_t^{(\rho_2\sigma_2)*} \times \\ & \mathcal{J}_{c_3c_1} \mathcal{J}_{c_2c_4} \mathcal{J}^*_{c_3c_1} \mathcal{J}^*_{c_2c_4}\,,\end{aligned} \tag{6.52}$$

- the product of an s- and a t-channel amplitude from two mediators, med_1 and med_2,

$$\begin{aligned}\mathcal{M}_s(\text{med}_1)\ \mathcal{M}_t^*(\text{med}_2) = (-1)&\text{Tr}\left[(\not{k}_2 - m_t)^4 \Gamma'_{(\sigma_2)} (\not{p}_2 - m_u)^1 \Gamma_{(\nu_1)}\right] \times \\ & \text{Tr}\left[(\not{p}_1 + m_u)^3 \Gamma'_{(\rho_2)} (\not{k}_1 + m_t)^2 \Gamma_{(\mu_1)}\right] \times \\ & M_s^{(\nu_1\mu_1)} M_t^{(\rho_2\sigma_2)*} \times \\ & \mathcal{J}_{c_2c_1} \mathcal{J}_{c_3c_4} \mathcal{J}^*_{c_3c_1} \mathcal{J}^*_{c_2c_4}\,.\end{aligned} \tag{6.53}$$

To shorten the expressions above we introduced ${}^i\Gamma'_\mu$ and ${}^i\Gamma'$ defined by their unprimed counterparts as[2]:

$$\begin{aligned} {}^i\Gamma_\mu = \gamma_\mu(\kappa^L P_L + \kappa^R P_R) \qquad &\mapsto \qquad {}^i\Gamma'_\mu = (\kappa^{L*} P_R + \kappa^{R*} P_L)\gamma_\mu \\ {}^i\Gamma = (\kappa^L P_L + \kappa^R P_R) \qquad &\mapsto \qquad {}^i\Gamma' = (\kappa^{L*} P_R + \kappa^{R*} P_L) \end{aligned}$$

Finally, we need the colour factors from summing the few colour structures in Eq. (6.50) over all colour indices in Eq. (6.43). There are few distinct cases for two mediators $\text{M}^{\text{col}}_{\text{cha}}$ and $\text{N}^{\text{col}}_{\text{cha}}$ with col={S (colour-singlet), O (colour-octet)} and cha = {s (s-channel),t (t-channel)}.

- $\text{M}^{\text{S}}_{\text{s}}$ and $\text{N}^{\text{S}}_{\text{s}}$ or $\text{M}^{\text{S}}_{\text{t}}$ and $\text{N}^{\text{S}}_{\text{t}}$:

$$\frac{1}{9} \sum_{c_1,c_2,c_3,c_4} (\mathbb{1}_{c_2c_1} \mathbb{1}_{c_3c_4}) \left(\mathbb{1}^*_{c_2c_1} \mathbb{1}^*_{c_3c_4}\right) = \frac{1}{9}\ \text{Tr}[\mathbb{1}]\ \text{Tr}[\mathbb{1}] = 1\,.$$

- $\text{M}^{\text{O}}_{\text{s}}$ and $\text{N}^{\text{O}}_{\text{s}}$: giving the interference of gluon and V_o amplitudes,

$$\frac{1}{9} \sum_{c_1,c_2,c_3,c_4} \sum_a \left(\mathcal{T}^a_{c_2c_1} \mathcal{T}^a_{c_3c_4}\right) \left(\mathcal{T}^{a*}_{c_2c_1} \mathcal{T}^{a*}_{c_3c_4}\right) = \frac{1}{9} \sum_a \text{Tr}[\mathcal{T}^a \mathcal{T}^{a\dagger}]\ \text{Tr}[\mathcal{T}^a \mathcal{T}^{a\dagger}] = \frac{2}{9}\,.$$

- $\text{M}^{\text{S}}_{\text{s}}$ and $\text{N}^{\text{S}}_{\text{t}}$: giving the interference of all s-channel colour-singlet to t-channel colour-singlet mediated amplitudes,

$$\frac{1}{9} \sum_{c_1,c_2,c_3,c_4} (\mathbb{1}_{c_2c_1} \mathbb{1}_{c_3c_4}) (\mathbb{1}_{c_3c_1} \mathbb{1}_{c_2c_4}) = \frac{1}{9}\ \text{Tr}[\mathbb{1}] = \frac{1}{3}\,,$$

[2] The definition is not the hermitian conjugate because γ_0's have already been absorbed in the trace taking into account that $(\bar{u}_i \gamma_\mu P_L u_j)^\dagger = \bar{u}_j P_R \gamma_\mu u_i$.

- $\mathrm{M}_{\mathrm{s}}^{\mathrm{O}}$ and $\mathrm{N}_{\mathrm{s}}^{\mathrm{S}}$: yielding no interference of the gluon or V_o to s-channel colour-singlet amplitudes,

$$\frac{1}{9}\sum_{c_1,c_2,c_3,c_4}\sum_{a}\left(\mathcal{T}^a_{c_2c_1}\mathcal{T}^a_{c_3c_4}\right)\left(\mathbb{1}_{c_2c_1}\mathbb{1}_{c_3c_4}\right)=\frac{1}{9}\sum_{a}\mathrm{Tr}[\mathcal{T}^a]\ \mathrm{Tr}[\mathcal{T}^a]=0\,.$$

- $\mathrm{M}_{\mathrm{s}}^{\mathrm{O}}$ and $\mathrm{N}_{\mathrm{t}}^{\mathrm{S}}$: giving the interference of the gluon and V_o amplitudes to the t-channel amplitudes,

$$\frac{1}{9}\sum_{c_1,c_2,c_3,c_4}\sum_{a}\left(\mathcal{T}^a_{c_2c_1}\mathcal{T}^a_{c_3c_4}\right)\left(\mathbb{1}_{c_3c_1}\mathbb{1}_{c_2c_4}\right)=\frac{1}{9}\sum_{a}\mathrm{Tr}[\mathcal{T}^a\mathcal{T}^a]=\frac{4}{9}\,.$$

Adding all contributions together we calculate the $|\mathcal{M}_{\mathrm{tot}}|^2$ using `FORM` [78], which is, however, too lengthy to be included here. Some results on more restricted cases have been presented in Ref. [28], which we reproduce analytically. We also implemented all resonances in a `FeynRules` [79] model that we combine with `Madgraph` [80] to automatically evaluate the full $u\bar{u}\to t\bar{t}$ amplitude at LO. We find numerical agreement with our analytic result.

7 Electroweak Corrections to $B_q \to \ell^+\ell^-$

In this chapter we return to the decays $B_q \to \ell^+\ell^-$ and present the perturbative SM computation of the NLO EW corrections to the Wilson coefficient that controls their branching ratios, $\mathcal{C}_{10}$ from Eq. (4.9). We split the calculation in two: the matching calculation that we discuss in Sec. 7.1 and the folding with the RGE that we perform in Sec. 7.2.

7.1 Matching Calculation of NLO Electroweak Corrections

We obtain the NLO EW corrections to the Wilson coefficient $\mathcal{C}_{10}$ by matching the SM to the effective theory of EW interactions. For this purpose, we evaluate one-light-particle irreducible Greens functions with the relevant external light degrees of freedom up to the required order in the EW couplings in both theories. The Wilson coefficients are determined by requiring equality of the renormalised Greens functions order by order in perturbation theory

$$\mathcal{A}_{\text{full}}(\mu_0) \stackrel{!}{=} \mathcal{A}_{\text{eff}}(\mu_0) \tag{7.1}$$

at the matching scale μ_0. The scale is chosen to be of the order of the heavy degrees of freedom to minimise otherwise large logarithms that enter the Wilson coefficients. The Wilson coefficients have the general expansion

$$\begin{aligned}\mathcal{C}_i(\mu_0) = \mathcal{C}_i^{(00)} + \tilde{\alpha}_s\,\mathcal{C}_i^{(10)} + \tilde{\alpha}_s^2\,\mathcal{C}_i^{(20)} \\ + \tilde{\alpha}_e\left(\mathcal{C}_i^{(11)} + \tilde{\alpha}_s\,\mathcal{C}_i^{(21)} + \tilde{\alpha}_s^2\,\mathcal{C}_i^{(31)} + \tilde{\alpha}_e\,\mathcal{C}_i^{(22)}\right) + \dots\,,\end{aligned} \tag{7.2}$$

in the strong and electromagnetic $\tilde{\alpha}_{s,e} \equiv \alpha_{s,e}/(4\pi)$ running couplings of the effective theory at the scale μ_0, where we follow the convention of [81]. The expansion starts with tree-level contributions denoted by the superscript (00), has higher-order QCD corrections ($m0$) with $m > 0$, pure QED corrections (mm) with $m > 0$ and mixed QCD-QED corrections (mn) with $m > n > 0$, all of which depend explicitly on μ_0 except for (00).

For $\mathcal{C}_{10}$ the non-zero matching corrections start at order $\tilde{\alpha}_e$, i.e., for $n \geq 1$. $\mathcal{C}_{10}^{(11)}$ [46] and the NLO QCD correction $\mathcal{C}_{10}^{(21)}$ [48, 49, 50, 51] are known and the NNLO QCD correction $\mathcal{C}_{10}^{(31)}$ will soon be published [52]. Here, we calculate $\mathcal{C}_{10}^{(22)}$ [82].

Eq. (7.2) is to be understood as the definition of the components $\mathcal{C}_i^{(mn)}$ that complies with the single-G_F normalisation in the literature [81]. The comparison with Eqs. (4.13) and (4.14) yields

$$\mathcal{C}_{10}^{(11)} = \frac{4G_F}{\sqrt{2}} c_{10}^{(11)} = -\frac{4G_F}{\sqrt{2}} \frac{Y_0(x_t)}{s_W^2} \tag{7.3}$$

and

$$\mathcal{C}_{10}^{(11)} = \frac{G_F^2 M_W^2}{\pi^2} \frac{1}{\tilde{\alpha}_e} \widetilde{c}_{10}^{(11)} = -\frac{G_F^2 M_W^2}{\pi^2} \frac{1}{\tilde{\alpha}_e} Y_0(x_t) \tag{7.4}$$

for the single- and quadratic-G_F normalisation, respectively. This convention introduces an artificial factor $1/\alpha_e$ into the components of the quadratic-G_F normalisation. We prefer to introduce this artificial dependence than rearrange the expansion in Eq. (7.2). In this way, the comparison of the RGE evolution in the two normalisations is much more transparent (see Sec. 7.2). The artificial $1/\alpha_e$ factors cancel anyway in the RGE.

Although the operator P_{10} does not mix with other $\Delta B = 1$ operators under QCD, at higher order in QED interactions such a mixing does take place [83, 81]. As a consequence, the effective Lagrangian in Eq. (4.9) has to be supplemented with new operators:

$$\mathcal{C}_{10}P_{10} \quad \longrightarrow \quad \sum_i \mathcal{C}_i P_i \,. \tag{7.5}$$

Terms proportional to $\sim V_{ub}V_{uq}^*[\mathcal{C}_1(P_1^u - P_1^c) + \mathcal{C}_2(P_2^u - P_2^c)]$ do not contribute at the order that we consider.

The operators relevant for $B_q \to \ell^+\ell^-$ at the considered order in strong and EW interactions comprise the current-current operators ($i = 1, 2$), the QCD-penguin operators ($i = 3, 4, 5, 6$) and the semileptonic operators ($i = 9, 10$), where we follow the operator definition of [81]:

$$\begin{aligned}
P_1 &= (\bar{q}_L\gamma_\mu T^a c_L)(\bar{c}_L\gamma^\mu T^a b_L)\,,\\
P_2 &= (\bar{q}_L\gamma_\mu c_L)(\bar{c}_L\gamma^\mu b_L)\,,\\
P_3 &= (\bar{q}_L\gamma_\mu T^a c_L)\sum_Q(\bar{Q}_L\gamma^\mu T^a Q_L)\,,\\
P_4 &= (\bar{q}_L\gamma_\mu c_L)\sum_Q(\bar{Q}_L\gamma^\mu Q_L)\,,\\
P_5 &= (\bar{q}_L\gamma_\mu\gamma_\nu\gamma_\rho T^a c_L)\sum_Q(\bar{Q}_L\gamma^\mu\gamma_\nu\gamma_\rho T^a Q_L)\,,\\
P_6 &= (\bar{q}_L\gamma_\mu\gamma_\nu\gamma_\rho c_L)\sum_Q(\bar{Q}_L\gamma^\mu\gamma_\nu\gamma_\rho Q_L)\,,\\
P_9 &= (\bar{q}_L\gamma_\mu b_L)\sum_\ell(\bar{\ell}\gamma^\mu\ell)\,,\\
P_9 &= (\bar{q}_L\gamma_\mu b_L)\sum_\ell(\bar{\ell}\gamma^\mu\gamma_5\ell)\,,
\end{aligned} \tag{7.6}$$

with $q = d, s$, $Q = u, d, s, c, b$ and ℓ charged-lepton fields. The definition does not include a factor $\alpha_e/(4\pi)$ in $P_{(9,10)}$, which we include in the matching conditions of the Wilson coefficients at the matching scale. Only P_2 and P_9 affect the matching calculation. The remaining operators enter the RGE analysis discussed in Sec. 7.2.

There are also two evanescent operators E_9 and E_{10} [83]

$$E_9 = (\bar{q}_L\gamma_\mu\gamma_\nu\gamma_\rho b_L)\sum_\ell(\bar{\ell}\gamma^\mu\gamma^\nu\gamma^\rho\ell) - 10P_9 + 6P_{10}\,, \tag{7.7}$$

$$E_{10} = (\bar{q}_L\gamma_\mu\gamma_\nu\gamma_\rho b_L)\sum_\ell(\bar{\ell}\gamma^\mu\gamma^\nu\gamma^\rho\gamma_5\ell) + 6P_9 - 10P_{10}\,, \tag{7.8}$$

whose one-loop Wilson coefficients could contribute to the matching. Evanescent operators vanish algebraically in $d = 4$ dimensions. In our case only E_9 mixes into P_{10}, E_{10} will not contribute.

Parameter		Value	Ref.
G_F		$(1.166\,378\,7 \pm 0.000\,000\,6) \cdot 10^{-5}\,\text{GeV}^{-2}$	[39]
$\alpha_s(M_Z^{\text{pole}})$	$(N_f = 5)$	0.1184 ± 0.0007	[39]
$\alpha_e(M_Z^{\text{pole}})$	$(N_f = 5)$	$(127.944 \pm 0.014)^{-1}$	[39]
M_Z^{pole}		(91.1876 ± 0.0021) GeV	[39]
M_t^{pole}		(173.2 ± 0.9) GeV	[84, 85]
M_H^{pole}		(125.5 ± 1.5) GeV	[39, 1, 2]

Table 7.1: *The physical input. $\alpha_{s,e}$ are the running $\overline{MS}$ couplings at $\mu = M_Z^{\text{pole}}$ in the theory with dynamical W, Z and H bosons but with the top-quark decoupled. Masses are the experimentally measured pole masses.*

Beside evanescent operators also equations-of-motion vanishing operators can contribute in principle to the matching. However, in our case there are no such operators with a projection on the tree-level matrix element of P_{10} to affect the matching.

We describe the calculation of $\mathcal{A}_{\text{full}}$ and $\mathcal{A}_{\text{eff}}$ in Sections 7.1.1 and 7.1.2, respectively. In the SM calculation of $\mathcal{A}_{\text{full}}$, we apply different EW renormalisation schemes for the involved parameters to demonstrate that the renormalisation scheme dependence is rendered negligible when including $\mathcal{C}_{10}^{(22)}$. The schemes differ by finite parts of the counterterms that renormalise the bare parameters of the Lagrangian or equivalently the parameters appearing in the LO Wilson coefficient. Nevertheless, we use the same physical input in all schemes for the numerical evaluation that we have chosen to be

$$G_F, \quad \alpha_e(M_Z^{\text{pole}}), \quad \alpha_s(M_Z^{\text{pole}}), \quad V_{ij}, \quad M_Z^{\text{pole}}, \quad M_t^{\text{pole}} \text{ and } M_H^{\text{pole}}\,. \tag{7.9}$$

G_F is the Fermi constant as extracted from muon life-time experiments. It is itself a Wilson coefficient of the effective theory and plays thus a special role in the calculation of EW corrections; we postpone further discussion to Sec. 7.1.2. The couplings α_e and α_s are the $\overline{\text{MS}}$ couplings at the scale of the Z pole mass in the SM with the top-quark decoupled, but the W and Z still dynamical degrees of freedom [39]. We discuss the different definitions of α_e in App. C.3 in connection with its threshold corrections. V_{ij} are elements of the CKM matrix. M_Z^{pole}, M_t^{pole} and M_H^{pole} are the pole masses of Z boson, top quark and Higgs boson, respectively. The numerical values are summarised in Tab. 7.1. The weak mixing angle s_W and M_W are not input for our calculation, they are dependent quantities.

7.1.1 Standard Model Calculation

We keep only the leading contributions of the expansion in the momenta of external states, in which case the full amplitude for $b \to q\,\ell^+\ell^-$ takes the form

$$\mathcal{A}_{\text{full}} = \sum_i A_{\text{full},\,i}(\mu)\langle P_i(\mu)\rangle^{(0)}\,. \tag{7.10}$$

$A_{\text{full},i}$'s are coefficient functions with the electroweak expansion

$$A_{\text{full},\,i} = A_{\text{full},\,i}^{(0)} + \tilde{\alpha}_e A_{\text{full},\,i}^{(1)} + \tilde{\alpha}_e^2 A_{\text{full},\,i}^{(2)} + \dots\,, \tag{7.11}$$

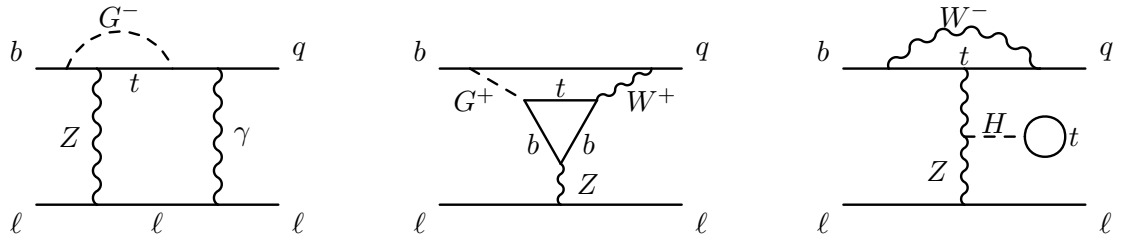

Figure 7.1: *Two-loop diagrams in the SM contributing to the $b \to q\ell^+\ell^-$ at NLO in EW interactions.*

with α_e the electromagnetic coupling in the six-flavour theory with dynamical weak gauge and Higgs bosons. $\langle P_i(\mu)\rangle^{(0)}$ denote the tree-level matrix elements. Our focus here is the calculation of the two-loop contribution $A^{(2}_{\text{full},10}$ and some parts of $A^{(1)}_{\text{full},\,i}$ that involve the evanescent operators E_9 and E_{10} and are required for the matching.

For this purpose, we calculate all two-loop EW Feynman diagrams and the corresponding one-loop diagrams with inserted counterterms, Fig. 7.1 depicts some examples. We proceed as in [55] and perform all calculations in the Feynman gauge $\xi = 1$ using two independent setups. In App. C.1 we discuss the more technical aspects of the calculation, e.g. γ-algebra in d dimensions, loop integrals and wave-function renormalisations. Here, we concentrate on the electroweak renormalisation conditions.

Having fixed the physical input, we define three renormalisation schemes and discuss the relation of their renormalised parameters to the physical input in Eq. (7.9). In all three schemes we use $\overline{\text{MS}}$ renormalisation for α_e and the top-quark mass under QCD. Additional finite terms are included into the field renormalisation constants as explained in more detail in App. C.1. Therefore, our schemes differ only by finite EW renormalisations of s_W, M_t and M_W appearing at LO in c_{10}. For $\widetilde{c}_{10}$, s_W is absorbed in the additional factor G_F and needs no further specification.

1.) On-shell scheme

In the on-shell scheme, at the order we consider, the masses of Z boson and top quark coincide with their respective pole masses. The mass of the W boson is a dependent quantity for our choice of physical input. We calculate it including radiative corrections following [86]. This relation introduces a mild higgs-mass dependence of $\mathcal{C}_{10}$ at LO. The weak mixing angle in the on-shell scheme is defined by

$$s_W^2 \to (s_W^{\text{on-shell}})^2 \equiv 1 - \left(M_W^{\text{on-shell}}/M_Z^{\text{on-shell}}\right)^2 . \tag{7.12}$$

Therefore, the only finite counterterms necessary are δM_Z^2, δM_W^2 and δM_t at one-loop, they are given in [87, 88]. We also treat tadpoles as in [87, 88]: we include tadpole diagrams (see Fig. 7.1), and a renormalisation δt to cancel the divergence and the finite part of the one-loop tadpole diagram. This way we ensure that all renormalisation constants apart from wave-function renormalisations are gauge invariant [89].

2.) $\overline{\text{MS}}$ scheme

In the $\overline{\text{MS}}$ scheme the fundamental parameters are those of the "unbroken" SM Lagrangian

$$g_1, \qquad g_2, \qquad g_3, \qquad v, \qquad \lambda \qquad \text{and} \qquad y_t. \tag{7.13}$$

Here, g_3, g_2 and g_1 are the couplings of the SM gauge group $SU(3)_c \times SU(2)_L \times U(1)_Y$, v is the vacuum expectation value of the Higgs field and λ its quartic self-coupling, whereas y_t is the top-Yukawa coupling. The parameters are renormalised by counterterms subtracting only divergences and $\log(4\pi) - \gamma_E$ terms, i.e., they are running $\overline{\text{MS}}$ parameters. We do not treat tadpoles differently in this respect, only their divergences are subtracted by the counterterm for v. By expressing the parameters of the LO Wilson coefficients in terms of the "unbroken"-phase parameters

$$\begin{aligned} s_W^2 \to \bar{s}_W^2 &\equiv g_1^2/(g_1^2+g_2^2)\,, & 4\pi\alpha_e &\equiv g_1^2 g_2^2/(g_1^2+g_2^2)\,, \\ M_W \to \overline{M}_W &\equiv v g_2/2\,, & x_t \to \bar{x}_t &\equiv 2y_t^2/g_2^2\,, \end{aligned} \tag{7.14}$$

we iteratively fix their values at the matching scale μ_0. To this end, we require that the one-loop running of the unbroken parameters in the six-flavour theory together with the appropiate counterterms reproduces the physical input of Eq. (7.9). Overlines in Eq. (7.14) indicate $\overline{\text{MS}}$ renormalisation. $\bar{s}_W$ is the $\overline{\text{MS}}$ renormalised weak mixing angle in the six-flavour theory. Ref. [39] denotes it by $\hat{s}_W^{\text{ND}}$.

3.) Hybrid scheme

For Eq. (4.14) where s_W appears at LO we adopt yet another scheme. We renormalise the couplings α_e and s_W in the $\overline{\text{MS}}$ scheme and the masses in x_t on-shell. Effectively this corresponds to including the on-shell counterterms for masses and using Eq. (7.14) instead of (7.12) for s_W. Correspondingly, we use s_W, α_e, M_t, M_W and M_H as fundamental parameters for the hybrid scheme. This scheme is a better-behaved alternative to the on-shell scheme, in which the counterterm for s_W receives large top-quark-mass dependent corrections. (see App. C.5).

Having fixed all renormalisation conditions we evaluate $A^{(2)}_{\text{full},10}$. In practice we calculate the $\overline{\text{MS}}$ amplitude and include the appropriate counterterms in $A^{(1)}_{\text{full},10}$ to shift from the $\overline{\text{MS}}$ to the on-shell or hybrid scheme. The full expression for $A^{(2)}_{\text{full},10}$ is too lengthy to be included here. We shall attach the complete analytic two-loop EW contribution in the on-shell scheme for the quadratic-G_F normalisation, $\widetilde{c}_{10}^{(22)}$, to the electronic preprint of the upcoming publication [82].

7.1.2 Effective Theory Calculation

The effective theory is described by the effective Lagrangian in Eq. (4.9) supplemented with the $\Delta B = 1$ operators from Eq. (7.6). All fields are canonically normalised in the theory. To simplify the notation we drop any indices indicating an expansion in $\tilde{\alpha}_s$ throughout this Section. The fields and couplings are $\overline{\text{MS}}$-renormalised via the redefinitions of bare quantities

$$\begin{aligned} q &\to Z_d^{1/2}\, q\,, & \ell &\to Z_\ell^{1/2}\, \ell\,, \\ e &\to Z_e\, e\,, & C_j &\to \sum_i C_i\, \hat{Z}_{i,j}\,, \end{aligned} \tag{7.15}$$

where q denotes down-type-quark fields and ℓ charged-lepton fields. Z_d and Z_ℓ are the field-renormalisation constants and Z_e the coupling-renormalisation constant. Wilson coefficients

are effective couplings that also need to be renormalised. Their renormalisation is the matrix $\hat{Z}_{i,j}$. Off-diagonal entries are due to operator mixing and diagonal entries from self-mixing. $\hat{Z}_{i,j}$ has the expansion in $\tilde{\alpha}_e$

$$\hat{Z}_{i,j} = \delta_{i,j} + \tilde{\alpha}_e \, \hat{Z}^{(1)}_{i,j} + \tilde{\alpha}_e^2 \, \hat{Z}^{(2)}_{i,j} + \dots \,. \tag{7.16}$$

Similarly, we expand Z_d, Z_ℓ and Z_e. We defer the presentation of the explicit expressions of the constants to App. C.2.

Since we employ dimensional regularisation for ultraviolet and infrared divergences, all loop diagrams in the effective theory are scaleless – no mass scale in the loop – and therefore vanish. Infrared and ultraviolet poles exactly cancel each other. As a consequence, the amplitude is entirely determined by the tree-level matrix elements $\langle P_j \rangle^{(0)}$ of the relevant operators P_j. These are proportional to the Wilson coefficients $\mathcal{C}_i$ and renormalisation constants from counterterm insertions. The divergences associated with the counterterms subtract the pure ultraviolet poles of the loop amplitudes. Since in the latter, ultraviolet and infrared divergences cancel each other, the sum of loop and counterterm amplitudes has left over divergences, namely the infrared ones. These are the same in the full theory because the low-energy behaviour of the two theories can only be the same. Therefore, the left-over infrared divergences will cancel in the matching as we shall explicitly see. The renormalised amplitude reads

$$\begin{aligned} \mathcal{A}_{\text{eff}}(\mu) &= \sum_i A_{\text{eff},\,i}(\mu) \langle P_i(\mu) \rangle^{(0)} \\ &= V_{tb} V_{tq}^* \sum_{i,j} \mathcal{C}_i(\mu) \, \hat{Z}_{i,j} Z_j \, \langle P_j(\mu) \rangle^{(0)} \,. \end{aligned} \tag{7.17}$$

Both the Wilson coefficients $\mathcal{C}_i$ and the renormalisation constants have an expansion in $\tilde{\alpha}_e$ Eqs. (7.2) and (7.16), respectively. The Z_j's summarise products of field- and charge-renormalisation constants of the operator in question, i.e., for P_{10}

$$Z_{10} = Z_d \, Z_\ell \,, \tag{7.18}$$

which is the only one required for our matching.

Only a few physical operators contribute to the part of $\mathcal{A}_{\text{eff}}(\mu)$ proportional to $\langle P_{10} \rangle^{(0)}$ since only a few mix either at one-loop or two-loop level into P_{10} and have, at the same time, a non-zero Wilson coefficient at one-loop or tree-level, respectively. These operators are: P_2, which has a non-zero Wilson coefficient $\mathcal{C}_2^{(00)}$ as well as an entry in $\hat{Z}^{(2)}_{2,10}$ and P_9 which mixes at one-loop into P_{10} and has a non-zero $\mathcal{C}_9^{(11)}$. Moreover, apart from the physical operators, also the evanescent operator E_9 mixes at one-loop with P_{10} and also has a one-loop Wilson coefficient. All contributing mixing renormalisation constants of physical operators can be extracted from the anomalous dimension in the literature [83]. We collect all constants and discuss the mixing of evanescent operators in App. C.2. Finally, at the two-loop level the amplitude reads

$$\begin{aligned} A^{(2)}_{\text{eff},P_{10}} = V_{tb} V_{tq}^* \, (\tilde{\alpha}_e)^n \Big[\;& \mathcal{C}_{10}^{(22)} + \mathcal{C}_{10}^{(11)} Z_{10}^{(1)} \\ & + \mathcal{C}_2^{(00)} \hat{Z}^{(2)}_{2,10} + \sum_{i=\{9,10,E_9,E_{10}\}} \mathcal{C}_i^{(11)} \hat{Z}^{(1)}_{i,10} \Big] \,, \end{aligned} \tag{7.19}$$

with the power $n = 2$ and $n = 1$ for the single- and quadratic-G_F normalisation, respectively.

The one-loop Wilson coefficients in Eq. (7.19), multiplied with renormalisation constants, contribute finite terms to the matching through their $\mathcal{O}(\varepsilon)$ terms. We reproduce the finite and $\mathcal{O}(\varepsilon)$ parts of $\mathcal{C}_{9,10}^{(11)}$ in Ref. [90]. For $\mathcal{C}_{E_9}^{(11)}$ only the finite terms are needed, we list them in App. C.2. For this purpose we have also matched the one-loop amplitudes proportional to the $\langle P_{9,10}\rangle^{(0)}$ and $\langle E_{9,10}\rangle^{(0)}$ up to $\mathcal{O}(\varepsilon)$.

The Fermi constant, G_F, is very precisely measured in muon decay and provides a valuable input for the determination of the EW parameters. It is an input parameter in our computation and an explicit factor of the Wilson coefficients $\mathcal{C}_i$. To match the full with the effective amplitude also G_F needs to be expanded in terms of α_e. Following [55], we define G_F to be proportional to the Wilson coefficient G_μ of the operator $Q_\mu = (\bar{\nu}_{\mu_L}\gamma_\rho\mu_L)(\bar{e}_L\gamma^\rho\nu_{e_L})$ that induces muon decay in the effective Fermi theory

$$G_F \equiv \frac{1}{2\sqrt{2}} G_\mu = \frac{1}{2\sqrt{2}} \left(G_\mu^{(0)} + \tilde{\alpha}_e G_\mu^{(1)} + \dots \right) , \tag{7.20}$$

with the tree-level matching relation

$$G_\mu^{(0)} = \frac{2\pi\alpha_e}{s_W^2 M_W^2} = \frac{2}{v^2} \tag{7.21}$$

and the NLO EW correction $G_\mu^{(1)}$ [91][1]. The normalisation of $\mathcal{C}_{10}$ is G_F and not $1/(2\sqrt{2})G_\mu^{(0)}$. Since we work at NLO in EW interactions, $G_\mu^{(1)}$ enters the effective theory amplitude (7.17). Moreover, the power of G_F in the normalisation of the effective Lagrangian affects $\mathcal{C}_i^{(22)}$ through a matching contribution proportional to $G_\mu^{(1)}/G_\mu^{(0)} \times \mathcal{C}_i^{(11)}$. Contrarily, the leading EW components $\mathcal{C}_i^{(11)}$ remain unchanged in the two normalisations. We demonstrate this explicitly by the expansion in $\tilde{\alpha}_e$. In the single-G_F normalisation

$$\begin{aligned} \mathcal{C}_{10} = \frac{4G_F}{\sqrt{2}}\, c_{10} &= \left[G_\mu^{(0)} + \tilde{\alpha}_e G_\mu^{(1)} + \cdots \right] \left[\tilde{\alpha}_e c_{10}^{(11)} + \tilde{\alpha}_e^2\, c_{10}^{(22)} + \cdots \right] \\ &= G_\mu^{(0)} \left[\tilde{\alpha}_e c_{10}^{(11)} + \tilde{\alpha}_e^2 \left(c_{10}^{(22)} + \frac{G_\mu^{(1)}}{G_\mu^{(0)}}\, c_{10}^{(11)} \right) + \cdots \right] \end{aligned} \tag{7.22}$$

and in the quadratic-G_F normalisation

$$\mathcal{C}_{10} = \frac{G_F^2 M_W^2}{\pi^2} \widetilde{c}_{10} = \frac{(G_\mu^{(0)})^2 M_W^2}{8\pi^2} \left[\tilde{\alpha}_e \widetilde{c}_{10}^{(11)} + \tilde{\alpha}_e^2 \left(\widetilde{c}_{10}^{(22)} + 2\, \frac{G_\mu^{(1)}}{G_\mu^{(0)}}\, \widetilde{c}_{10}^{(11)} \right) + \cdots \right] , \tag{7.23}$$

receiving an additional factor of two. Depending on the choice of normalisation, the according contribution proportional to $G_\mu^{(1)}/G_\mu^{(0)} \times \mathcal{C}_i^{(11)}$ is included in Eq. (7.19) in order to consistently obtain $c_{10}^{(22)}$ and $\widetilde{c}_{10}^{(22)}$. A similar procedure is also necessary for α_e. We discuss these threshold corrections in App. C.3.

The merit of defining G_F to be itself a Wilson coefficient at the matching scale is that the large uncertainties from the scale dependence of the vacuum expectation value in $G_\mu^{(0)}$ do not appear at all in the Wilson coefficient at LO.

[1] We have computed $G_\mu^{(1)}$ in Ref. [55]. More recently, the authors of Ref. [92] presented its analytic expression. A typo slipped in the preprint version, but is corrected in the journal version. Our results agree.

We described separately the calculation of the $b \to q\ell^+\ell^-$ at NLO in the EW and QED interactions in the SM and the effective five-flavour theory, respectively. By matching the parts of $A_{\text{eff}} \sim \langle P_{10}\rangle^{(0)}$ and $A_{\text{full}} \sim \langle P_{10}\rangle^{(0)}$ at NLO order in $\tilde{\alpha}_e$ we obtain for the first time $\mathcal{C}_{10}^{(22)}$. It has been known so far only in the large top-quark-mass limit [54, 93]. We verified the explicit cancellations of all left-over infrared divergences and reproduce the large top-quark-mass limit for the quadratic-G_F normalisation. More details on the large-m_t expansion were presented in Ref. [55].

7.2 Renormalisation Group Evolution

This section summarises the results of the evolution of the Wilson coefficients under the renormalisation group equations from the matching scale, μ_0, down to the low scale, μ_b. μ_0 is of the order of the masses of the decoupled heavy degrees of freedom, approximately 100 GeV and $\mu_b \sim 5$ GeV of the order of the bottom-quark mass at which matrix elements are computed. The according anomalous dimension matrices of the $\Delta B = 1$ effective theory, including NLO EW corrections, are given in Ref. [83] and the RGE is solved in Ref. [81] for the single-G_F normalised Lagrangian in Eqs. (4.9) and (4.14) including the running of α_e. These corrections were considered for the first time for $B_s \to \mu^+\mu^-$ in Ref. [47].

The evolution operator $U(\mu_b, \mu_0)$ relates the Wilson coefficients at the matching scale, see (7.2), to the ones at μ_b:

$$\mathcal{C}_i(\mu_b) = \sum_j U(\mu_b, \mu_0)_{ij}\, \mathcal{C}_j(\mu_0)\,. \tag{7.24}$$

At the low energy scale the Wilson coefficients may again be expanded in $\alpha_s(\mu_b)$ and the small ratio $\kappa \equiv \alpha_e(\mu_b)/\alpha_s(\mu_b)$:

$$\mathcal{C}_i(\mu_b) = \sum_{m,n=0}^{\infty} \left[\tilde{\alpha}_s(\mu_b)\right]^m \left[\kappa(\mu_b)\right]^n \mathcal{C}_{i,(mn)}\,. \tag{7.25}$$

We obtain the explicit expressions for the components $\mathcal{C}_{i,(mn)}(\mu_b)$ from the solution in Ref. [81] with further details and the full solution for $i = 10$ presented in App. C.4.

In the single-G_F normalisation the Wilson coefficient $c_{10}(\mu_b)$ starts at order α_e with the following non-zero contributions

$$\begin{aligned} c_{10}(\mu_b) = {} & \tilde{\alpha}_e \left(c_{10,(11)} + \tilde{\alpha}_s c_{10,(21)}\right) \\ & + \tilde{\alpha}_e^2 \left(\frac{c_{10,(02)}}{\tilde{\alpha}_s^2} + \frac{c_{10,(12)}}{\tilde{\alpha}_s} + c_{10,(22)}\right)\,. \end{aligned} \tag{7.26}$$

The components $c_{i,(mn)}$ are functions of the ratio $\eta \equiv \alpha_s(\mu_0)/\alpha_s(\mu_b)$ and the high-scale components $c_j^{(mn)}$ from Eq. (7.2). For illustration, we give here numerical results for the exemplary

values $\mu_0 = 160$ GeV and $\mu_b = 5$ GeV, yielding $\eta = 0.509$,

$$\begin{aligned}
c_{10,(11)} &= c_{10}^{(11)}\,,\\
c_{10,(21)} &= \eta\, c_{10}^{(21)}\,,\\
c_{10,(02)} &= 0.0058\, c_2^{(00)}\,,\\
c_{10,(12)} &= 0.068\, c_2^{(00)} + 0.005\, c_1^{(10)} - 0.005\, c_4^{(10)}\\
&\quad + 0.252\, c_9^{(11)} + 1.118\, c_{10}^{(11)}\,,\\
c_{10,(22)} &= 0.133\, c_1^{(10)} + 0.066\, c_4^{(10)}\\
&\quad + 0.002\, c_1^{(20)} + 0.001\, c_2^{(20)} + 0.004\, c_3^{(20)}\\
&\quad - 0.002\, c_4^{(20)} + 0.033\, c_5^{(20)} - 0.039\, c_6^{(20)}\\
&\quad - 1.593\, c_9^{(11)} - 2.226\, c_{10}^{(11)}\\
&\quad + 0.128\, c_9^{(21)} + 0.569\, c_{10}^{(21)} + c_{10}^{(22)}\,.
\end{aligned} \tag{7.27}$$

We give the explicit solution for arbitrary values of η in App. C.4.

The $c_{10,(mn)}$'s depend on the initial matching conditions of the Wilson coefficients, the $c_i^{(mn)}$ in Eq.(7.2), of various orders [90]. More specifically, they depend on:

- the tree-level coefficient of P_2,
- the one-loop α_s coefficients of P_1, P_2 and P_4,
- the one-loop α_e coefficients of P_9 and P_{10},
- the two-loop α_s^2 coefficients of P_1, P_2, P_3 , P_4 , P_5 and P_6,
- the two-loop $\alpha_e\alpha_s$ coefficients of P_9 and P_{10} as well
- the two-loop NLO EW correction for P_{10} calculated in Sec. 7.1.

We derive the equivalent expressions for the case of the quadratic-G_F normalisation from the single-G_F normalisation expansion in Eq. (7.25)

$$\widetilde{c}_i(\mu_b) = \sum_{m,n=0}^{\infty} [\tilde{\alpha}_s(\mu_b)]^{m-1}\, [\kappa(\mu_b)]^{n-1}\, \widetilde{c}_{i,(mn)}\,. \tag{7.28}$$

For $i = 10$ the lowest-order non-zero terms

$$\begin{aligned}
\widetilde{c}_{10}(\mu_b) &= \widetilde{c}_{10,(11)} + \tilde{\alpha}_s \widetilde{c}_{10,(21)}\\
&\quad + \tilde{\alpha}_e \left(\frac{\widetilde{c}_{10,(02)}}{\tilde{\alpha}_s^2} + \frac{\widetilde{c}_{10,(12)}}{\tilde{\alpha}_s} + \widetilde{c}_{10,(22)} \right)\,,
\end{aligned} \tag{7.29}$$

already start at zeroth order in α_e. The components of the initial Wilson coefficients in Eq. (7.2) are related by

$$\widetilde{c}_i^{(mn)} = s_W^2\, c_i^{(mn)}\,, \qquad \text{for} \quad n < 2 \tag{7.30}$$

where a factor $\tilde{\alpha}_e(\mu_0)$ has been pulled out and substituted by $\tilde{\alpha}_e(\mu_b)$. For cases $n \geq 2$, which is here only of concern for $\mathcal{C}_{10}$, an additional shift has to be taken into account explicitly in the matching analogously to the discussion below (7.20). Eventually, the downscaled components $\widetilde{c}_{i,(mn)}$ in Eq. (7.28) are given by Eq. (7.27) by replacing $c_i^{(mn)} \to \widetilde{c}_i^{(mn)}$ and omitting the contributions of $\widetilde{c}_{10}^{(11)}$ in $\widetilde{c}_{10,(12)}$ as well as $\widetilde{c}_{10}^{(11)}$ and $\widetilde{c}_{10}^{(21)}$ in $\widetilde{c}_{10,(22)}$.

Part III

Phenomenology

8 Flavour Phenomenology with Maximally Gauged Flavour

8.1 Observables

In this Section we discuss the observables that we consider in the phenomenological analysis of the flavour sector in the MGF model. Since the original publication [19] some of the input for the analysis has changed. The most notable changes are the values of the meson decay constants for the neutral B mesons and the bag factor $\hat{B}_K$ in the neutral kaon sector after new lattice results. Also, there have been new experimental results, e.g. the branching ratio of $B^+ \to \tau^+ \nu$. We use the updated input for quantities whose modification has a relevant impact on our analysis. We keep, however, the input for the elements of the CKM matrix as this is necessary to avoid breaking the correlation between box and flavour-gauge-boson contributions.[1] We collect the input for the analysis in Tab. 8.1 and discuss next the observables.

ΔM_K and ϵ_K

In the neutral kaon sector the amplitude for the mixing of the flavour eigenstates K^0 and $\bar{K}^0$ is:

$$2\, m_K \left(M_{12}^K\right)^* = \langle \bar{K}^0 | \mathcal{H}_{\text{eff}}^{\Delta S=2} | K^0 \rangle \,, \tag{8.1}$$

with m_K the neutral kaon mass. Out of the amplitude two observables are constructed. The K_L-K_S mass difference, ΔM_K, given to a very good approximation by the real part of the amplitude

$$\Delta M_K = 2\,\text{Re}\left(M_{12}^K\right) \,. \tag{8.2}$$

And the parameter ϵ_K describing the amount of indirect CP violation in the kaon sector

$$\epsilon_K = \frac{\kappa_\epsilon\, e^{i\,\varphi_\epsilon}}{\sqrt{2}(\Delta M_K)_{\text{exp}}}\,\text{Im}\left(M_{12}^K\right) \,, \tag{8.3}$$

with the values $\varphi_\epsilon = (43.51 \pm 0.05)^\circ$ and $\kappa_\epsilon = 0.923 \pm 0.006$. The value of κ_ϵ takes into account that $\varphi_\epsilon \neq \pi/4$ as assumed in older analyses and includes long-distance effects in $\text{Im}\,\Gamma_{12}$ [102, 105] and $\text{Im}\,M_{12}$ [101].

Using the results from Sec. 5.2 and 5.3 we obtain the expression for M_{12}^K, and therefore also

[1] A recent progress in the determination of the CKM elements has been the LHCb measurement of the CKM phase $\gamma = (67 \pm 12)^\circ$ [94]. Within the experimental errors the new value is in agreement with the one we use in the analysis. We refer to Ref. [95] for a discussion on the dependence of flavour observables on γ.

$G_F = 1.16637(1) \times 10^{-5}\,\text{GeV}^{-2}$	[96]	$m_{B_d} = 5279.5(3)$ MeV	[96]
$M_W = 80.385(15)$ GeV	[96]	$m_{B_s} = 5366.3(6)$ MeV	[96]
$\sin^2\theta_W = 0.23116(13)$	[96]	$F_{B_d} = (188 \pm 4)$ MeV	[44]
$\alpha(M_Z) = 1/127.9$	[96]	$F_{B_s} = (225 \pm 3)$ MeV	[44]
$\alpha_s(M_Z) = 0.1184(7)$	[96]	$\hat{B}_{B_d} = 1.26(11)$	[97]
$m_u(2\,\text{GeV}) = 1.7 \div 3.1$ MeV	[96]	$\hat{B}_{B_s} = 1.33(6)$	[97]
$m_d(2\,\text{GeV}) = 4.1 \div 5.7$ MeV	[96]	$F_{B_d}\sqrt{\hat{B}_{B_d}} = 227(19)$ MeV	[97]
$m_s(2\,\text{GeV}) = 100^{+30}_{-20}$ MeV	[96]	$F_{B_s}\sqrt{\hat{B}_{B_s}} = 279(15)$ MeV	[97]
$m_c(m_c) = (1.279 \pm 0.013)$ GeV	[98]	$\xi = 1.237(32)$	[97]
$m_b(m_b) = 4.19^{+0.18}_{-0.06}$ GeV	[96]	$\eta_B = 0.55(1)$	[99, 100]
$M_t = 172.9 \pm 0.6 \pm 0.9$ GeV	[96]	$\tau_{B^\pm} = (1641 \pm 8) \times 10^{-3}$ ps	[96]
$\lvert V_{us}\rvert = 0.2252(9)$	[96]	$m_K = 497.614(24)$ MeV	[96]
$\lvert V_{cb}\rvert = (40.6 \pm 1.3) \times 10^{-3}$	[96]	$F_K = 156.1(11)$ MeV	[97]
$\lvert V_{ub}^{\text{incl.}}\rvert = (4.27 \pm 0.38) \times 10^{-3}$	[96]	$\hat{B}_K = 0.7643(97)$	[97]
$\lvert V_{ub}^{\text{excl.}}\rvert = (3.38 \pm 0.36) \times 10^{-3}$	[96]	$\kappa_\epsilon = 0.94(2)$	[101]
$\gamma = (68^{+10}_{-11})^\circ$	[39]	$\varphi_\epsilon = (43.51 \pm 0.05)^\circ$	[102]
		$\eta_1 = 1.87(76)$	[103]
		$\eta_2 = 0.5765(65)$	[99]
		$\eta_3 = 0.496(47)$	[104]

Table 8.1: *Values of experimental and theoretical quantities used throughout our numerical analysis of the MGF model. $m_i(m_i)$ are $\overline{MS}$ masses and M_t is the pole top-quark mass.*

for ΔM_K and ϵ_K:

$$\begin{aligned} M_{12}^K = \quad & \frac{G_F^2\, M_W^2}{12\pi^2}\, F_K^2\, m_K \Big[\;\; \hat{B}_K\, \eta_{cc}\, \lambda_2^2(K)\, S_c^{(K)} + \hat{B}_K\, \eta_{tt}\, \lambda_3^2(K)\, S_t^{(K)} + \\ & + 2\, \hat{B}_K\, \eta_{ct}\, \lambda_2(K)\, \lambda_3(K)\, S_{ct}^{(K)} + \\ & + P_1^{VLL}(\mu_H, K)\, \Big(\Delta_A^{(K)}\, C_1^{VLL}(\mu_H) + \Delta_A^{(K)}\, C^{VRR}(\mu_H)\Big) \Big]^* \\ + & \frac{G_F^2\, M_W^2}{12\pi^2}\, F_K^2\, m_K\, P_1^{LR}(\mu_H, K)\, \big[\Delta_A^{(K)}\, C_1^{LR}(\mu_H)\big]^* . \end{aligned} \tag{8.4}$$

The first term is the complete contribution from the Wilson coefficients of LL and RR operators. It has a part proportional to the non-perturbative bag factor $\hat{B}_K$, calculated on the lattice [106, 107, 108, 109, 110], and a part proportional to P_1^{VLL}. The latter is the sum of the contributions from the flavour-gauge bosons folded with the RGE. Its parts proportional to η_{cc}, η_{tt} and η_{ct} are the contributions from the SM-like box diagrams. The η factors summarise NLO and NNLO QCD corrections in the SM as calculated in Refs. [103, 104, 99]. This way of arranging Eq. (8.4) ensures that by decoupling all NP we reproduce the SM prediction (see Eq. (5.17)). The second term summarises the LR contributions from flavour-gauge bosons. As discussed in Sec. 5.3, they are enhanced by the RGE and the numerical analysis will show that they have a considerable impact on $|\epsilon_K|$.

ΔM_{B_q} and CP Asymmetries

Analogously to the kaon amplitude we define the $B_q^0 - \bar{B}_q^0$ mixing amplitude ($q = d, s$)

$$2\, m_{B_q}\, (M_{12}^q)^* = \langle \bar{B}_q^0 | \mathcal{H}_{\text{eff}}^{\Delta B=2} | B_q^0 \rangle \, . \tag{8.5}$$

The mixing in the B_d^0 and B_s^0 sectors has some differences with respect to $K^0 - \bar{K}^0$ mixing. One is the different CKM structure which strongly suppresses the charm and charm-top contribution and renders them completely negligible compared to the top contribution. Therefore, we obtain equivalently to Eq. (8.4)

$$\begin{aligned} M_{12}^q = \quad & \frac{G_F^2\, M_W^2}{12\pi^2}\, F_{B_q}^2\, m_{B_q} \Big[\eta_B\, \hat{B}_{B_q}\, \lambda_3^2(B_q)\; S_t^{(B_q)} + \\ & + P_1^{VLL}(\mu_H, B_q)\, \Big(\Delta_A^{(B_q)} C_1^{VLL}(\mu_H) + \Delta_A^{(B_q)} C^{VRR}(\mu_H)\Big) \Big]^* , \\ + & \frac{G_F^2\, M_W^2}{12\pi^2}\, F_{B_q}^2\, m_{B_q}\, P_1^{LR}(\mu_H, B_q)\, \big[\Delta_A^{(B_q)} C_1^{LR}(\mu_H)\big]^* . \end{aligned} \tag{8.6}$$

Another difference is that in the B sector the long-distance effects are estimated to be small and $\Gamma_{12} \ll M_{12}$. This modifies the expression for the mass differences to be

$$\Delta M_{B_q} = 2\, |M_{12}^q| \, . \tag{8.7}$$

In the SM ΔM_{B_d} and ΔM_{B_s} have a large theoretical error stemming from $\sim 10\%$ uncertainties in the combination $F_{B_q}\sqrt{\hat{B}_{B_q}}$ [111, 112], but there is still room for improvement from lattice calculations. A large part of these non-perturbative uncertainties cancel in the ratio [113, 112, 114]

$$\xi = \frac{F_{B_s}^2}{F_{B_d}^2}\frac{\hat{B}_s}{\hat{B}_d} = 1.237 \pm 0.032 \, . \tag{8.8}$$

Therefore, we also consider in our analysis the ratio of the two mass differences:

$$R_{\Delta M_B} \equiv \frac{\Delta M_{B_d}}{\Delta M_{B_s}} \,. \tag{8.9}$$

Mixing in the neutral B sectors is sensitive to new CP violating phases. To expose the contributions from NP we follow [115] and define

$$M_{12}^q \equiv (M_{12}^q)_{\rm SM}\, C_{B_q}\, e^{2\,i\,\varphi_{B_q}} \,. \tag{8.10}$$

The real factors, C_{B_q}, parametrise changes in the absolute value of the amplitude and the phases, φ_{B_q}, the new sources of CP violation. The SM contributions are also complex

$$\big(M_{12}^d\big)_{\rm SM} = \big|\big(M_{12}^d\big)_{\rm SM}\big| e^{2\,i\,\beta} \,, \qquad\qquad \big(M_{12}^s\big)_{\rm SM} = \big|\big(M_{12}^s\big)_{\rm SM}\big| e^{2\,i\,\beta_s} \,, \tag{8.11}$$

where the phases $\beta \simeq 22^\circ$ and $\beta_s \simeq -1^\circ$ are defined through

$$V_{td}^{\rm SM} = |V_{td}^{\rm SM}| e^{-i\beta} \qquad \text{and} \qquad V_{ts}^{\rm SM} = -|V_{ts}^{\rm SM}| e^{-i\beta_s} \,. \tag{8.12}$$

In this notation, the experimentally accessible coefficients of $\sin(\Delta M_{B_d}\, t)$ and $\sin(\Delta M_{B_s}\, t)$ in the time-dependent asymmetries of the decays $B_d^0 \to \psi K_S$ and $B_s^0 \to \psi\phi$ are

$$S_{\psi K_S} = \sin(2\beta + 2\varphi_{B_d}) \qquad \text{and} \qquad S_{\psi\phi} = \sin(2|\beta_s| - 2\varphi_{B_s}) \,. \tag{8.13}$$

The Branching Ratio BR($B^+ \to \tau^+\nu$)

We also consider the tree-level decay $B^+ \to \tau^+\nu$. For some time now, the world average from Barbar and Belle [116, 117] was 2σ higher than the SM prediction based on a global fit of the CKM parameters. The situation changed when Belle reanalysed the data with a new hadronic tag and removed the tension with the SM [118].

In MGF the $B^+ \to \tau^+\nu$ branching ratio is:

$$\mathrm{BR}(B^+ \to \tau^+\nu) = \frac{G_F^2\, m_{B^+}\, m_\tau^2}{8\pi} \left(1 - \frac{m_\tau^2}{m_{B^+}^2}\right)^2 F_{B^+}^2\, |c_{u_{L1}}\, V_{ub}\, c_{d_{L3}}|^2\, \tau_{B^+} \,, \tag{8.14}$$

in which all NP effects come from the mixing with exotic quarks and are thus expected to be very small. Flavour-gauge bosons contribute only at the loop-level, they are negligible. We therefore use the ratio $R_{\mathrm{BR}/\Delta M}$ to cancel large hadronic uncertainties in the meson decay constants F^+ and F_{B_d} [117, 119]:

$$R_{\mathrm{BR}/\Delta M} = \frac{\mathrm{BR}(B^+ \to \tau^+\nu)}{\Delta M_{B_d}} \approx \frac{3\,\pi\,\tau_{B^+}}{4\,\eta_B\,\hat{B}_{B_d}\,S_0(x_t)} \frac{c_{u_{L1}}^2\, c_{d_{L3}}^2}{C_{B_d}} \frac{m_\tau^2}{M_W^2} \frac{|V_{ub}|^2}{\left|V_{tb}^*\, V_{td}\right|^2} \left(1 - \frac{m_\tau^2}{m_{B_d}^2}\right)^2 \,, \tag{8.15}$$

where we used $m_{B^+} \approx m_{B_d}$, which is justified considering the errors in the other quantities and the experimental error of the branching ratio.

The Branching Ratio BR($\overline{B} \to X_s\gamma$)

The SM prediction for the $\overline{B} \to X_s\gamma$ branching ratio at NNLO [57, 69, 70] is

$$\mathrm{BR}(\overline{B} \to X_s\gamma) = (3.15 \pm 0.23) \times 10^{-4}\,. \tag{8.16}$$

It has been calculated for a photon-energy cut-off $E_\gamma > 1.6$ GeV in the $\overline{B}$-meson rest frame and is to be compared with the current experimental value [96]

$$\mathrm{BR}(\overline{B} \to X_s\gamma) = (3.55 \pm 0.24 \pm 0.09) \times 10^{-4}\,, \tag{8.17}$$

for the same energy cut-off E_γ. In the presence of NP the expression for the branching ratio reads:

$$\mathrm{BR}(\overline{B} \to X_s\gamma) = R\left(|C_{7\gamma}(\mu_b)|^2 + |C'_{7\gamma}(\mu_b)|^2 + N(E_\gamma)\right)\,, \tag{8.18}$$

where $R = 2.47 \times 10^{-3}$ and $N(E_\gamma) = (3.6 \pm 0.6) \times 10^{-3}$. The parameter R is an overall factor, whose determination is discussed in [69, 70], while $N(E_\gamma)$ is a non-perturbative contribution. We calculate NP contributions at the LO including the RGE and add them to the NNLO SM contribution

$$C_{7\gamma}(\mu_b) = C_{7\gamma}^{\mathrm{SM}}(\mu_b) + \Delta C_{7\gamma}(\mu_b)\,, \tag{8.19}$$

with the central value of $C_{7\gamma}^{\mathrm{SM}}(\mu_b)$ at the NNLO corresponding to Eq. (8.16) for $\mu_b = 2.5$ GeV

$$C_{7\gamma}^{\mathrm{SM}}(\mu_b) = -0.3523\,. \tag{8.20}$$

8.2 The Spectrum

To evaluate the flavour observables we first need to calculate the spectrum of the model in terms of the SM fermion masses and the NP parameters in Eq. (2.5). The spectrum depends also on the elements of the unitary matrix V, which we determine using its relations to the experimentally measured CKM matrix defined in Eq. (2.16). From Eqs. (2.13) and (2.15) we deduce that $c_{(u,d)_L} \approx 1$, except for t and t'. As a result, in a good approximation the CKM matrix is

$$\tilde{V} \simeq \begin{pmatrix} V_{ud} & V_{us} & V_{ub} \\ V_{cd} & V_{cs} & V_{cb} \\ c_{u_{L3}} V_{td} & c_{u_{L3}} V_{ts} & c_{u_{L3}} V_{tb} \end{pmatrix}\,, \tag{8.21}$$

in which the deviation from the unitarity of the CKM matrix is

$$\left(\tilde{V}^\dagger \tilde{V}\right)_{ij} = \delta_{ij} - s^2_{u_{L3}} V^*_{ti} V_{tj}\,, \qquad \left(\tilde{V} \tilde{V}^\dagger\right)_{ij} = \delta_{ij} - s^2_{u_{L3}} \delta_{it} \delta_{jt}\,. \tag{8.22}$$

The deviations are present only when the top-quark entries are considered and are proportional to $s^2_{u_{L3}}$. All other entries of the CKM matrix coincide with the corresponding entries of the unitary matrix V up to small corrections. The phase γ in the unitary triangle is not affected by the mixing:

$$\tilde{\gamma} \equiv \arg\left(-\frac{\tilde{V}_{ud}\tilde{V}^*_{ub}}{\tilde{V}_{cd}\tilde{V}^*_{cb}}\right) = \arg\left(-\frac{V_{ud}V^*_{ub}}{V_{cd}V^*_{cb}}\right)\,. \tag{8.23}$$

Therefore, we use the tree-level experimental determinations of $|V_{us}|$, $|V_{cb}|$, $|V_{ub}|$, and γ and the unitarity of the matrix V to fix the values of all its elements. To a good approximation these determinations are insensitive to NP effects.

Having determined V, we calculate the spectrum and the couplings of the new particles. They are fixed once, in addition to the SM parameters, we fix the seven NP couplings $\lambda^{(\prime)}_{u,d}, g_Q, g_U, g_D$ and the two mass parameters M_u and M_d in Eqs. (2.6) and (2.7). Their actual determination is subtle since the energy scale at which the see-saw relations in Eqs. (2.11) hold is *a priori* not known. We identify this scale with the mass of the lightest flavour-gauge boson.

We fix the spectrum and the see-saw scale iteratively using the condition that all exotic masses are above $m_t(m_t)$. As a first step we evaluate the see-saw relation at $m_t(m_t)$ to obtain a rough estimate of the masses of exotic fermions and lightest gauge boson. With this initial spectrum we run the masses of the SM fermions to the newly defined see-saw scale including all intermediate exotic fermion thresholds. The evaluation of the see-saw relation corrects the NP spectrum. We repeat the procedure until the values of the exotic fermion masses and the see-saw scale no longer change. Finally, we evolve the exotic fermion masses down to the EW scale at which we evaluate the Wilson coefficients from box contributions.

In the numerical analysis we scan the parameter space of the model. We choose $\lambda_{u,d} \in (0, 1.5]$ and all other couplings $\{\lambda'_{u,d}, g_Q, g_U, g_D\} \in (0, 1.1]$, always staying in the perturbative regime of the theory. One way of decoupling the MGF from the SM is to reduce the coupling of the NP particles to the SM particles. By allowing small values for the couplings g_Q, g_U and g_D in the scan, we take into account the case in which the flavour-gauge bosons are decoupled from the SM, while the exotic quarks remain light. The two mass parameters are varied in the interval $M_u \in [100\,\text{GeV}, 1\,\text{TeV}]$ and $M_d \in [30\,\text{GeV}, 250\,\text{GeV}]$ following the discussion in Ref. [11]. Unphysical points of the parameter space, namely cases with $s_{u,d}$ or $c_{u,d}$ larger than 1, are not considered. Larger M_u and M_d values decouple the NP from the SM and are therefore phenomenologically irrelevant. With respect to the analysis of Ref. [11] we are scanning over all NP parameters, including $\lambda'_{u,d}$ and g_Q, g_U, g_D.

8.3 Flavour Analysis

In this Section we present the quantitative effects of the MGF model on the flavour observables from Sec. 8.1. The value of $|V_{ub}|$ is an essential input for the analysis. At the moment there are two determinations of its value that disagree with each other: one from exclusive semileptonic decays and another from inclusive ones. The disagreement is referred to as the $|V_{ub}|$ problem. The resolution of the discrepancy between the two values is an issue that should be solved in the near future. At the moment, it means that if we take the unitarity of the CKM matrix as granted and consider the good agreement of the ratio $R_{\Delta M_B}$ with the data, the inclusive and exclusive determinations imply different patterns in CP-violating observables. The value of $|V_{ub}|$ is especially relevant for the simultaneous prediction of both ϵ_K and $S_{\psi K_S}$ given the ratio $R_{\Delta M_B}$, as first discussed in Refs. [120, 102]. We therefore consider the two limiting cases:

Exclusive (small) $|V_{ub}|$:

$$|V_{ub}^{\text{excl}}| = (3.38 \pm 0.36) \times 10^{-3}$$

In this case the SM prediction of $S_{\psi K_S}$ is very close to its experimental determination, while $|\epsilon_K|$ lies somewhat below its measured value.

Inclusive (large) $|V_{ub}|$:

$$|V_{ub}^{\text{incl}}| = (4.27 \pm 0.38) \times 10^{-3}$$

In this case the SM prediction of $S_{\psi K_S}$ is larger than its experimental value by about 3σ, but the $|\epsilon_K|$ SM prediction is in perfect agreement with its experimental determination.

SM predictions for exclusive $\|V_{ub}\|$	Experimental determinations	
$\Delta M_{B_d} = 0.56\,\text{ps}^{-1}$	$\Delta M_{B_d} = 0.507(4)\,\text{ps}^{-1}$	[121]
$\Delta M_{B_s} = 19.0\,\text{ps}^{-1}$	$\Delta M_{B_s} = 17.719(43)\,\text{ps}^{-1}$	[121]
$R_{\Delta M_B} = 2.95 \times 10^{-2}$	$R_{\Delta M_B} = 2.8861(26) \times 10^{-2}$	[121]
$S_{\psi K_S} = 0.671$	$S_{\psi K_S} = 0.673(20)$	[96]
$S_{\psi\phi} = 0.0354$	$S_{\psi\phi} = -0.01(7)(1)$	[122]
$\|\epsilon_K\| = 1.86 \times 10^{-3}$	$\|\epsilon_K\| = 2.228(11) \times 10^{-3}$	[39]
$\text{BR}(\overline{B} \to X_s\gamma) = 3.15 \times 10^{-4}$	$\text{BR}(\overline{B} \to X_s\gamma) = 3.55(24)(09) \times 10^{-4}$	[39]
$\text{BR}(B^+ \to \tau^+\nu) = 0.849 \times 10^{-4}$	$\text{BR}(B^+ \to \tau^+\nu) = 0.99(25) \times 10^{-4}$	[116, 118]

Table 8.2: *The SM predictions for the observables we consider using the exclusive determination of $|V_{ub}|$ and the corresponding experimental values.*

In the past, the exclusive-$|V_{ub}|$ case came with its own serious caveats. While the SM could predict $S_{\psi K_S}$, its prediction for $|\epsilon_K|$ laid 2.5σ below the experimental determination. After our original publication [19], new lattice results increased the value of $\hat{B}_K$ by a approximately 4% and softened this tension of the SM. We present the analysis of the MGF model in view of the new results.

If the new particles in the MGF model are indeed close to the TeV scale, the model will have concrete predictions on the observables in question. The reason is that contrary to other popular extensions of the SM, like SUSY models, the Little-Higgs model, the RS-scenario and models with left-right symmetry, MGF has a much smaller number of new parameters. Since the MGF model does have new sources of CP violation transmitted from the flavour-gauge bosons, we investigate whether the model can also accommodate the inclusive-$|V_{ub}|$ case. In Tab. 8.2 we collect the SM predictions and the experimental determinations for the observables that we consider for the exclusive-$|V_{ub}|$ case.

$|\epsilon_K|$-$S_{\psi K_S}$ Correlation

In Fig. 8.1 we present the correlation between ϵ_K and $S_{\psi K_S}$ for the two cases of $|V_{ub}|$. The colour represents the percentage of the NP effect due to NP contributions from boxes and flavour-gauge bosons in blue and red, respectively. The plot demonstrates that the exclusive value of $|V_{ub}|$ is favoured in this model. Looking at both panels we make the following observations:

- The effects of exotic quarks in the boxes (blue points) typically enhances $|\epsilon_K|$.
- The same effects cannot modify $S_{\psi K_S}$, as there is no new phase in the SM-like contribution.
- The flavour-gauge bosons always reduce $|\epsilon_K|$, i.e. they can only interfere destructively with the box contributions.
- The new CP-violating phase from flavour-gauge bosons can modify $S_{\psi K_S}$ only by reducing it.

We have also decomposed the effects of the flavour-gauge bosons in contributions coming from LL, RR and LR currents to assess their quantitative importance. The decomposition shows

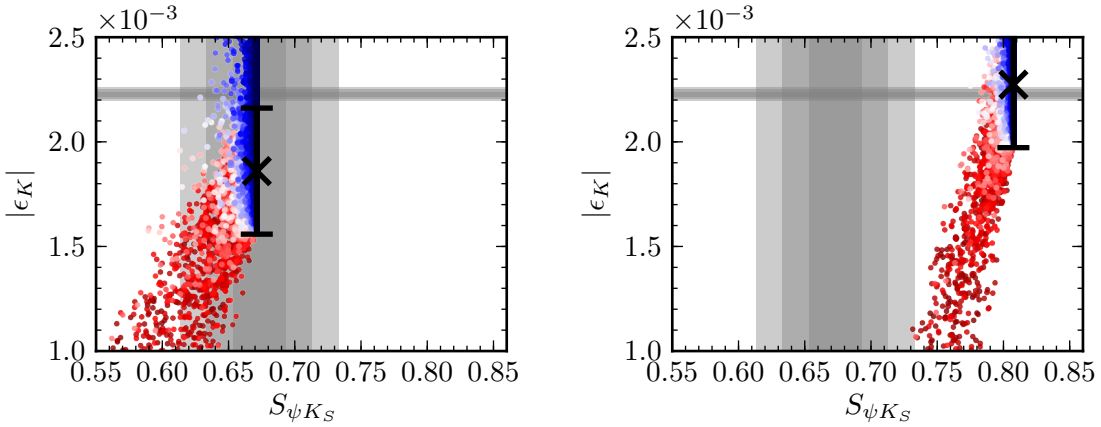

(a) Exclusive $|V_{ub}|$ **(b)** Inclusive $|V_{ub}|$

Figure 8.1: *The correlation of $|\epsilon_K|$ and $S_{\psi K_S}$. The shaded grey regions are the experimental 1σ-3σ ranges and the cross the SM prediction. The colour of the points represents the percentage of the exotic-quark and flavour-gauge boson contribution in $|\epsilon_K|$ in blue and red, respectively. We have also added the theoretical $|\epsilon_K|$ SM error in the NP points.*

that RR currents have a negligible effect, while the LL currents reduce $S_{\psi K_S}$ without affecting $|\epsilon_K|$. LR currents have no effect on $S_{\psi K_S}$, but always decrease $|\epsilon_K|$. In the model the LL currents are correlated with the LR currents and cannot be separated from each other. Their relative importance gives the "slope" of the red points in Fig. 8.1. The steepness of the "slope" comes from the fact the LR is enhanced from the RGE (see Sec. 5.3).

The numerical importance of the LR currents and the fact that they always reduce $|\epsilon_K|$ without modifying $S_{\psi K_S}$ is the reason why the model fails to describe the data in the inclusive-$|V_{ub}|$ case (Fig. 8.1b). This is a strict correlation and a non-trivial prediction of the model. As discussed in Refs. [120, 102], a negative NP phase φ_{B_d} in $B_d^0 - \bar{B}_d^0$ mixing would solve the $|\epsilon_K|$-$S_{\psi K_S}$ anomaly in the inclusive-$|V_{ub}|$ case, provided such a phase is phenomenologically allowed by other constraints. With a negative φ_{B_d}, $\sin 2\beta$ is larger than $S_{\psi K_S}$, implying a higher value on $|\epsilon_K|$, in reasonable agreement with data and a better Unitary Triangle fit. MGF provides such a phase, but it comes with contributions from LR currents which go against $|\epsilon_K|$. We thus consider the inclusive determination of $|V_{ub}|$ to disfavour the model and do not pursue it further.

The left panel with the exclusive-$|V_{ub}|$ case (Fig. 8.1a) shows the current status of the SM $|\epsilon_K|$-$S_{\psi K_S}$ anomaly. With the new value of $\hat{B}_K$ the SM is in good shape. In MGF the flavour-gauge bosons reduce $|\epsilon_K|$ and can only increase the tension. Contrarily, exotic quarks increase $|\epsilon_K|$ and improve the agreement with the data.

$|\epsilon_K|$-ΔM_B Correlation

Next, we consider in Fig. 8.2 the correlation of $|\epsilon_K|$ with the mass differences in the neutral B systems for the exclusive-$|V_{ub}|$ case. The colour coding is the same as in Fig. 8.1. The

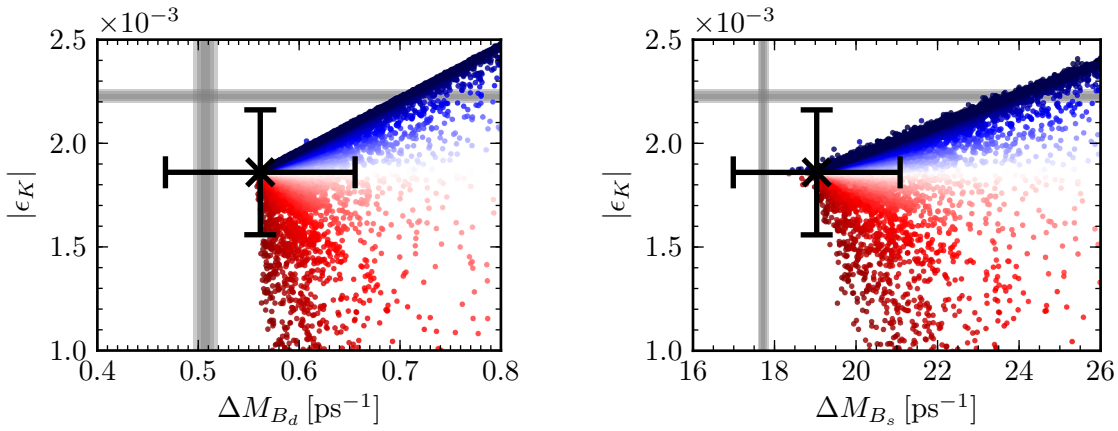

Figure 8.2: *Correlation plot for $|\epsilon_K|$ with ΔM_{B_d} and ΔM_{B_s} on the left and right panel, respectively. The colour of the points represents the percentage of the exotic-quark and flavour-gauge boson contribution in $|\epsilon_K|$ in blue and red, respectively.*

uncertainties of the hadronic quantities $F_{B_q}\sqrt{\hat{B}_{B_q}}$ dominate the theoretical errors for ΔM_{B_d} and ΔM_{B_s}. We include the error in the SM prediction, but not on each NP point to keep the presentation more transparent. Even considering the large theoretical errors the MGF construction has clear predictions.

Both exotic quarks and flavour-gauge bosons cannot decrease the mass differences, a decrease which seems to be favoured by the current values of $F_{B_q}\sqrt{\hat{B}_{B_q}}$. In contrast to the $|\epsilon_K|$-$S_{\psi K_S}$ correlation, there is an unwelcome anti-correlation from flavour-gauge bosons, which always pushes the NP prediction for both ϵ_K and ΔM_{B_q} away from their experimental values. Once again, the current data disfavour large effects from flavour-gauge bosons.

The situation here is more severe than in the $|\epsilon_K|$-$S_{\psi K_S}$ correlation. In the latter, simultaneous large effects from exotic quarks and flavour-gauge bosons could cancel each other in such a way that the combined predictions remained within the experimentally allowed range. Such a cancellation would be a fine-tuned case, but still be compatible with a low NP scale. Here, such a cancellation is impossible and large effects are completely forbidden. This is an indication that a low NP scale in the MGF model may indeed not be as viable as the construction implied. Interestingly, the indication here comes solely from indirect searches of NP and does not depend on the negative results of searches for new particles in direct searches. In the future, the theoretical uncertainties in $F_{B_q}\sqrt{\hat{B}_{B_q}}$ and $|\epsilon_K|$ will shrink and more definite statements may be possible. For now we consider quantities which are less affected by hadronic uncertainties, e.g. the ratios $R_{\Delta M_B}$ and $R_{\mathrm{BR}/\Delta M}$.

$R_{\Delta M_B}$-$R_{\mathrm{BR}/\Delta M}$ Correlation

In Fig. 8.3, we show the correlation between the ratio of the mass differences, $R_{\Delta M_B}$, and the ratio of the branching ratio $\mathrm{BR}(B^+ \to \tau^+\nu)$ to ΔM_{B_d}, $R_{\mathrm{BR}/\Delta M}$. As discussed in Sec. 8.1, a large part of the hadronic uncertainties cancel in these combinations and we expect strong constrains on the parameter space of the model.

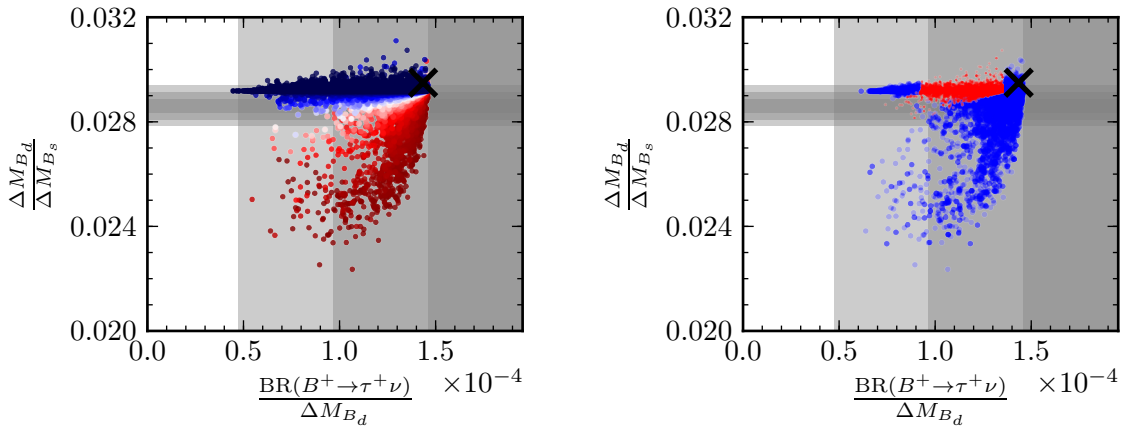

Figure 8.3: *Correlation plot for $R_{\Delta M_B}$ and $R_{BR/\Delta M}$. The grey regions refer to the experimental 1σ-3σ error ranges of the ratios $R_{\Delta M_B}$ and $R_{BR/\Delta M}$. The black cross refers to the SM values. On the left, the colour coding is the relative effect of exotic-quarks and flavour-gauge-boson contributions in blue and red, respectively. On the right, red points indicate an agreement of the ϵ_K prediction at the 3σ experimental and 1σ theoretical error range.*

The colouring in the left panel is the same as in Figs. 8.1 and 8.2. We observe that in the case of no flavour-gauge-boson contributions the ratio $R_{\Delta M_B}$ is not affected at all from NP. Exotic quarks in the boxes contribute in the same way in ΔM_{B_d} and ΔM_{B_s} such that exotic-quark contributions cancel in the ratio. Therefore, the ratio $R_{\Delta M_B}$, which has a small approximately 3% theoretical error, is the best observable to identify effects from flavour-gauge bosons. We observe that large flavour-gauge-boson effects are again disfavoured by the data.

On the right-panel, we plot in red the points that simultaneously satisfy the $|\epsilon_K|$ bound; they are within the 3σ experimental and 1σ theoretical error that we added linearly. Only part of the parameter-space with small effects from flavour-gauge bosons survives the combined bounds.

Regarding the rate of $B^+ \to \tau^+\nu$, the central value before the Belle reanalysis [118] was $\mathrm{BR}(B^+ \to \tau^+\nu) = (1.65 \pm 0.34) \times 10^{-4}$. This value lead to a serious tension for the SM and even more so for the MGF construction, which always decreases $R_{\mathrm{BR}/\Delta M}$. However, the new world average, which has still a significant experimental error, poses no longer a strong constraint on the SM or the parameter space of the MGF model.

$S_{\psi\phi}$-$S_{\psi K_S}$ Correlation

We have seen from Fig. 8.1 that a large new CP-violating phase in the neutral B_d^0 system is possible, but not phenomenologically viable due to the value of $|\epsilon_K|$. Next, we investigate the possibility of having a large phase in the neutral B_s^0 sector. In Fig. 8.4 we plot the correlated prediction of $S_{\psi K_S}$ and $S_{\psi\phi}$. In the left panel, the colour coding represents the relative amount of flavour-gauge boson to exotic-quark contributions. In the right panel, red points predict $|\epsilon_K|$, $R_{\Delta M}$ and $R_{\mathrm{BR}/\Delta M}$ to be within the 3σ experimental and 1σ theoretical range.

We observe that the effects on $S_{\psi\phi}$ are even more suppressed than in $S_{\psi K_S}$. In this respect, the MGF construction is very close to the SM and it would be very hard to differentiate the two models, even with an improved determination of $S_{\psi\phi}$.

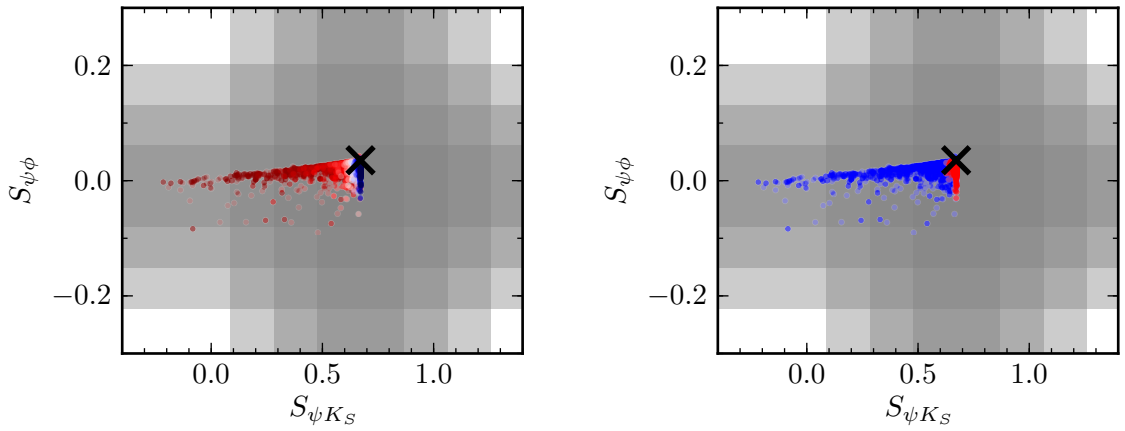

Figure 8.4: *Correlation plot for $S_{\psi K_S}$ and $S_{\psi\phi}$. The grey regions refer to the experimental 1σ-3σ error ranges. The black cross refers to the SM values. On the left, the colour coding is the relative effect of exotic-quarks and flavour-gauge-boson contributions in blue and red, respectively. On the right, red points indicate an agreement of the ϵ_K, $R_{\Delta M}$ and $R_{BR/\Delta M}$ prediction at the 3σ experimental and 1σ theoretical error range.*

$\overline{B} \to X_s\gamma$

Finally, we consider the MGF predictions for the $\overline{B} \to X_s\gamma$ rate. We plot the prediction in Fig. 8.5 in dependence of the t' mass. Using our results for the gauge-bosons from chapter 5, we find that they have a negligible effect on the rate, as anticipated from our discussion in [21]. The see-saw mechanism is enough to suppress these contributions. The exotic quarks can only enhance the rate as already pointed out in [11]. With an increasing t' mass the NP effects slowly decouple and the SM prediction is recovered. However, the effect of the t' on the $\overline{B} \to X_s\gamma$ is not large enough to provide a relevant bound on its mass.

8.4 Comparison to alternative NP Scenarios and Summary

Before we conclude, we compare the predictions of the MGF construction with alternative extensions of the SM. A complete comparison of the patterns of flavour violation requires also the study of $\Delta F = 1$ processes. However, the $\Delta F = 2$ observables that we studied here provide enough information to distinguish the MGF construction from other popular NP scenarios. We discuss here a few examples and refer to [95] for a recent extensive review on the different flavour patterns in various NP scenarios.

- The original MFV framework restricted to LL operators is called CMFV. An explicit UV implementation of this set-up is the model with a single universal extra dimension (UED) for which $\Delta F = 2$ observables have been studied in [123]. In CMFV $S_{\psi K_S}$ remains SM-like and thus, only the exclusive value of $|V_{ub}|$ is viable [124]. This is a general property of CMFV construction demonstrated in [125]. Therefore, the predictions for $\Delta F = 2$ observables in MGF and CMFV resemble each other a lot, once we impose the $|\epsilon_K|$ constraint and decouple all flavour-gauge-boson effects in MGF. $\Delta F = 1$ processes

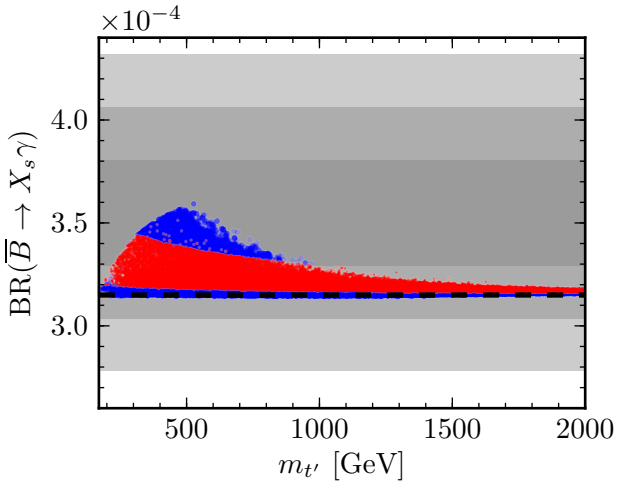

Figure 8.5: *The $BR(\overline{B} \to X_s\gamma)$ predictions as a function of m'_t. Grey regions refer to the 1σ-2σ experimental error range and the dashed black line to the SM prediction. In red are the points for which $R_{\Delta M_B}$, $R_{BR/\Delta M}$ and $|\epsilon_K|$ agree with the experiment at the 3σ experimental and 1σ theoretical level.*

can provide the distinction, though. In MGF the NP contributions uniquely enhance the BR($\overline{B} \to X_s\gamma$), while in UED they uniquely suppress it [126]. The $|\epsilon_K|$-ΔM_{B_q} correlation is similar in MGF and CMFV constructions.

- The Two-Higgs-Doublet model with MFV and flavour blind phases, 2HDM$_{\overline{\text{MFV}}}$ [127], can be distinguished from MGF if future data select the inclusive determination of $|V_{ub}|$. In 2HDM$_{\overline{\text{MFV}}}$ the contributions to $|\epsilon_K|$ are small and the interplay of the CKM phase with the flavour blind phases in the Yukawa couplings and the Higgs potential can suppress $S_{\psi K_S}$. 2HDM$_{\overline{\text{MFV}}}$ is compatible with the inclusive determination of $|V_{ub}|$, while MGF is not. In both 2HDM$_{\overline{\text{MFV}}}$ and MGF the asymmetry $S_{\psi\phi}$ is either SM-like or is reduced.

- The left-right asymmetric model (LRAM) has a large number of free parameters with respect to the MGF model. Ref. [63] presented a detailed analysis of FCNCs within the LRAM model and showed that both values of $|V_{ub}|$, inclusive and exclusive, are phenomenologically viable. The model contains many new phases and the $|\epsilon_K|$-$S_{\psi K_S}$ anomaly has more than one possible solution. It is therefore not as predictive as the MGF construction. Nevertheless, Ref. [63] demonstrated how a simple structure of the right-handed mixing matrix enhances $|\epsilon_K|$ keeping $S_{\psi K_S}$ at the SM value, while at the same time suppresses $\Delta M_{B_{d,s}}$ and significantly enhances $S_{\psi\phi}$. These signals cannot be accommodated in the MGF model. On the downside, LRAM struggles with the $|\epsilon_K|$ constraint due to huge neutral-Higgs tree-level contributions and, contrary to MGF, does not aim to explain masses and mixings.

In this work, we have performed an extensive analysis of the flavour sector of the most minimal MGF construction first presented in [11]. The model has a small number of new parameters and has thus strict patterns of flavour and CP violation that go beyond the SM.

We considered $\Delta F = 2$ observables and the branching ratios $BR(\overline{B} \to X_s\gamma)$ and $BR(B^+ \to \tau^+\nu)$ laying emphasis on separating the effects from exotic quarks and flavour-gauge bosons present in the model. We find that RR currents from flavour-gauge bosons are negligible, while LL currents provide new CP-violating phases that uniquely suppress $S_{\psi K_S}$ and $S_{\psi\phi}$. The effects on $S_{\psi\phi}$ are small compared to $S_{\psi K_S}$. The LR currents from flavour-gauge bosons do not affect $S_{\psi K_S}$, but suppress $|\epsilon_K|$. Therefore, similarly to the SM, the MGF construction can only accommodate the data for a value of $|V_{ub}|$ close to its current determination from exclusive decays. The correlation of $|\epsilon_K|$ and the mass differences ΔM_{B_d} and ΔM_{B_s} showed that a cancellation of exotic-quark and flavour-gauge contributions is not possible. Both contributions uniquely enhance ΔM_{B_d} and ΔM_{B_s} and thus, large NP effects are phenomenologically not viable.

9 New Strong Interactions in Top Physics

In this chapter, we investigate the TeV phenomenology of the HC model presented in chapter 3. By discussing the predictions of specific benchmarks of the model, we will demonstrate that the model can naturally account for anomalously large measurement of $A_{FB}^{t\bar{t}}$ and simultaneously adhere to closely related experimental constraints. The benchmark points will be the result of a χ^2 minimisation taking into account the total $t\bar{t}$ cross sections and asymmetries at Tevatron and LHC. In addition to the inclusive cross sections and asymmetries we shall present:

- the differential invariant-mass spectra of the produced $t\bar{t}$ pair at Tevatron and LHC,
- the differential $A_{FB}^{t\bar{t}}$'s in $m_{t\bar{t}}$ and the rapidity difference of the $t\bar{t}$ pair, Δy, at Tevatron,
- the dijet spectra in the invariant mass of the two jets, m_{jj}, at Tevatron and LHC, and
- the angular dijet distribution over a large range of dijet masses at Tevatron.

9.1 $t\bar{t}$ Asymmetries at Tevatron and LHC

$t\bar{t}$ asymmetries are a measure of the different probability for the top, or equivalently the anti-top quark, to be produced in a specific direction with respect to an initial $q\bar{q}$ state. If the final state of the $q\bar{q} \to t\bar{t}$ transition is symmetric under the exchange of the momentum of the t and $\bar{t}$ quark, the probabilities would be the same and the asymmetries would be zero. This is the case at LO in QCD and is why the asymmetries are small in the SM. They arise at the perturbative level and the main effect comes from interference of the one-loop box diagrams with the LO contribution and corrections from initial- and final-state radiation.

The CDF and DØ experiments at Tevatron observed an asymmetry in $p\bar{p} \to t\bar{t}$ presenting results for the partonic-level observable

$$A_{FB}^{t\bar{t}} \equiv \frac{N(\Delta y > 0) - N(\Delta y < 0)}{N(\Delta y > 0) + N(\Delta y < 0)}\,, \tag{9.1}$$

with $\Delta y = y_t - y_{\bar{t}}$, the difference of the t and $\bar{t}$ rapidities, taking the forward direction to be that of the proton[1]. In the notation from Eq. (6.42) this is equivalent to

$$A_{FB}^{t\bar{t}} = \frac{\sigma_F - \sigma_B}{\sigma_F + \sigma_B}\,, \tag{9.2}$$

with

$$\sigma_F = \int_0^1 dz \frac{d\sigma}{dz} \qquad \text{and} \qquad \sigma_B = \int_{-1}^0 dz \frac{d\sigma}{dz}\,.$$

$d\sigma/dz$ is the differential cross section convoluted with the parton distribution functions (PDF) of the proton and antiproton and integrated over a partial or the full range of the invariant

[1] Δy is invariant under boosts in the beam direction.

mass of the $t\bar{t}$ pair, $m_{t\bar{t}}$. The SM prediction for the inclusive $A_{FB}^{t\bar{t}}$ at NLO QCD including leading EW corrections [128, 129, 130, 131] is [131]

$$A_{FB}^{t\bar{t}\,\mathrm{inc\,SM}} = 0.088 \pm 0.006\,. \tag{9.3}$$

LO cross sections were used in the denominator of Eq. (9.2) and the PDF set `CTEQ6.6m` [132]. The error is the pure scale-uncertainty error for $\mu \in [m_t/2, 2m_t]$. Evidently, in the SM top quarks are preferably emitted in the forward direction while anti-top quarks in the backward direction. Note, that there is a substantial uncertainty in the SM prediction of the $A_{FB}^{t\bar{t}}$ due to missing NNLO QCD corrections. This can be seen by using the NLO QCD cross section in the denominator instead of the LO values used above. In this case, we obtain $A_{FB}^{t\bar{t}\,\mathrm{inc\,SM}} = 0.067$, which further suppresses the SM prediction and would increase the tension with the data.

The first experimental evidence for an unexpectedly large $A_{FB}^{t\bar{t}}$ came from CDF which reported an inclusive asymmetry of $A_{FB}^{t\bar{t}} = 0.158 \pm 0.075$ [133] using 5.3 fb^{-1} of data. An even larger excess was observed in the channel where both t and $\bar{t}$ decayed semileptonically $A_{FB}^{t\bar{t}} = 0.42 \pm 0.2$ [134]. The CDF result was confirmed by DØ, which reported $A_{FB}^{t\bar{t}} = 0.196 \pm 0.065$ [135]. More recently, CDF utilised its full data set of 9.4 fb^{-1} and updated its value to $A_{FB}^{t\bar{t}} = 0.164 \pm 0.047$ [136]. Naively averaging the CDF and DØ value gives

$$A_{FB}^{t\bar{t}\,\mathrm{inc\,EXP}} = 0.175 \pm 0.038\,. \tag{9.4}$$

Interestingly, CDF observes that the excess rises with the invariant mass of the $t\bar{t}$ pair $A_{FB}^{t\bar{t}\,\mathrm{low}} = 0.084 \pm 0.0046 \pm 0.030$ for $m_{t\bar{t}} \leq 450$ GeV and $A_{FB}^{t\bar{t}\,\mathrm{high}} = 0.295 \pm 0.0058 \pm 0.033$ for $m_{t\bar{t}} \geq 450$ GeV, which should to be compared to the SM predictions $A_{FB}^{t\bar{t}\,\mathrm{low\,SM}} = 0.062 \pm 0.003$ and $A_{FB}^{t\bar{t}\,\mathrm{high\,SM}} = 0.129 \pm 0.006$ [131]. DØ did not "unfold" its asymmetries so a comparison with the partonic-level asymmetries is not possible, but it appears that it does not to observe a rise with $m_{t\bar{t}}$ at least not at the detector-level asymmetries. We have collected the experimental determinations in Tab. 9.1.

At the LHC, the initial state is symmetric, so there is no fixed forward or backward direction to define an $A_{FB}^{t\bar{t}}$. The related observable is the charge asymmetry, A_C, which exploits the fact that the u valence quarks are more energetic than the $\bar{u}$ quarks from the quark gluon sea. Therefore, if in $p\bar{p}$ collisions top quarks are preferably emitted in the forward direction, in pp collisions they must be emitted preferably along the beam axis, while anti-top quarks more towards the central direction. The charge asymmetry at LHC is thus defined by

$$A_C = \frac{N(\Delta|y| > 0) - N(\Delta|y| < 0)}{N(\Delta|y| > 0) + N(\Delta|y| < 0)}\,, \tag{9.5}$$

with $\Delta|y| = |y_t| - |y_{\bar{t}}|$ and has been been observed by both ATLAS and CMS in the semileptonic and dilepton decay channel with still considerable experimental uncertainties (see Tab. 9.1). The naive average of the four measurements yields

$$A_C^{\mathrm{EXP}} = 0.010 \pm 0.008 \tag{9.6}$$

and the SM prediction for LO cross sections in the denominator is [131]

$$A_C^{\mathrm{SM}} = 0.0123 \pm 0.0005\,, \tag{9.7}$$

Observable	Value	Ref.
$A_{\rm FB}^{\rm low,\,CDF}$	0.084 ± 0.055	[136]
$A_{\rm FB}^{\rm high,\,CDF}$	0.295 ± 0.067	[136]
$A_{\rm FB}^{\rm inc,\,CDF}$	0.164 ± 0.047	[136]
$A_{\rm FB}^{\rm inc,\,D\emptyset}$	0.196 ± 0.065	[135]
$A_{\rm FB}^{\rm inc,\,average}$	0.175 ± 0.038	
$A_{\rm C}^{\rm inc,\,ATLAS,\,semileptonic}$	0.006 ± 0.010	[137]
$A_{\rm C}^{\rm inc,\,ATLAS,\,dileptons}$	0.057 ± 0.028	[138]
$A_{\rm C}^{\rm inc,\,CMS,\,semileptonic}$	0.004 ± 0.015	[139]
$A_{\rm C}^{\rm inc,\,CMS,\,dileptons}$	0.05 ± 0.06	[140]
$A_{\rm C}^{\rm inc,average}$	0.010 ± 0.008	
$\sigma_{\rm inc}^{\rm CDF}$	7.50 ± 0.48 pb	[141]
$\sigma_{\rm inc}^{\rm ATLAS}$	$177. \pm 3 \pm 8 \pm 7$ pb	[142]
$\sigma_{\rm inc}^{\rm CMS}$	$165.8 \pm 2.2 \pm 10.6 \pm 7.8$ pb	[143]
$\sigma_{\rm inc}^{\rm LHC}$	172.4 ± 8.5 pb	
$\sigma_{\rm inc}^{\rm TEV,\,NNLO}$	7.395 ± 0.544 pb	[144]
$\sigma_{\rm inc}^{\rm LHC,\,NNLO}$	172.5 ± 15.0 pb	[144]

Table 9.1: *Experimental input and SM predictions used in the evaluation of the NP χ^2.*

in good agreement with the experimental average.

The forward-backward asymmetry at Tevatron and the charge asymmetry at the LHC are closely related observables governed by the same underlying partonic process. The fact that an excess is observed in the $A_{FB}^{t\bar{t}}$ but not in A_C appears to be problematic for many extensions of the SM that account for the $A_{FB}^{t\bar{t}}$ as the two prediction are often correlated [145, 146, 147]. An increase in $A_{FB}^{t\bar{t}}$ typically also increases A_C. As briefly mentioned in Sec. 6.1.2, a way to break the correlation was presented in Ref. [75]. In models with a t-channel mediator, Z', which enhances the $A_{FB}^{t\bar{t}}$ and A_C at the Born level, the associated production of Z' in the process $gu \to tZ' \to tut\bar{t}$ (see Fig. 9.1) gives a negative contribution to A_C breaking thus the $A_{FB}^{t\bar{t}} - A_C$ correlation. We discussed candidates for the Z' in the HC theory in Sec. 6.1.

9.2 The χ^2 Fit

In the presence of NP we define the combined SM and NP prediction for $A_{FB}^{t\bar{t}}$ as

$$A_{FB}^{t\bar{t}\,SM+NP} = \frac{\Delta\sigma^{\rm SM} + \Delta\sigma^{\rm NP}}{\sigma^{\rm SM+NP}}\,. \tag{9.8}$$

Above, $\sigma^{\rm SM+NP}$ is the total inclusive LO cross section for $p\bar{p} \to t\bar{t}$, i.e. it includes associated production of t-channel mediators. $\Delta\sigma^{\rm SM} \equiv \sigma_F^{\rm SM} - \sigma_B^{\rm SM}$ at NLO QCD including EW corrections extracted for $\mu = [m_t/2, m_t, 2m_t]$ from Ref. [131]. $\Delta\sigma^{\rm NP} \equiv \sigma_F^{\rm NP} - \sigma_B^{\rm NP}$ at LO including the

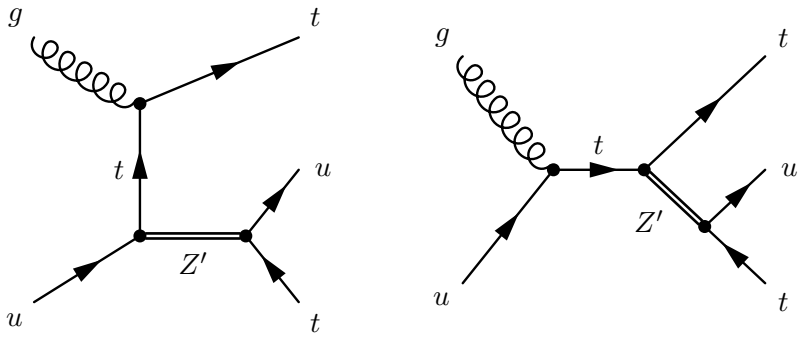

Figure 9.1: *Associated production through a t-channel mediator, Z'. In the left diagram, the decay of the Z' produces a $\bar{t}$ boosted in the direction of the initial up quark thus reducing A_C and breaking its correlation to the $A_{FB}^{t\bar{t}}$.*

interferences of NP contributions with the LO SM amplitude. We define the charge asymmetry in the presence of NP analogously. This definition ensures that decoupling the NP retrieves the SM predictions for the asymmetries.

Similarly, we combine the LO NP effects with the NNLO `CTEQ10` prediction for $t\bar{t}$ production [144]:

$$\sigma_{\text{inc}} = \sigma_{\text{inc}}^{\text{NNLO}} + \sigma_{\text{inc}}^{\text{NP}} \,, \tag{9.9}$$

where again $\sigma_{\text{inc}}^{\text{NP}}$ includes associated production and LO interferences with the SM.

Having all NP predictions for total cross sections and asymmetries we fix the scale μ in the evaluation of LO amplitudes and run a χ^2 minimisation on:

$$\chi^2 = \sum_{\text{inc, low, high}} \frac{(A_{FB}^{t\bar{t}\,\text{NP}} - A_{FB}^{t\bar{t}\,\text{EXP}})^2}{(\delta A_{FB}^{t\bar{t}\,\text{EXP}})^2} + \frac{(A_C^{\text{NP}} - A_C^{\text{EXP}})^2}{(\delta A_C^{\text{EXP}})^2} + \sum_{\text{TEV, LHC}} \frac{(\sigma_{\text{inc}} - \sigma_{\text{inc}}^{\text{EXP}})^2}{(\Delta\sigma_{\text{inc}}^{\text{EXP}})^2 + (\Delta\sigma_{\text{inc}}^{\text{NNLO}})^2} \,, \tag{9.10}$$

with the experimental input and SM predictions used for the χ^2 minimisation summarised in Tab. 9.1. Ideally, we would include also differential $m_{t\bar{t}}$ spectra and asymmetries in the χ^2, but because of the large number of resonances this is computationally too expensive.

The χ^2 fit varies the chiral mass of the ρ^{HC} meson, M_{chiral}, the masses of the HC quarks, $\mathcal{Q}$, and scalar $\mathcal{S}$, and the strong Yukawa couplings h_i. We also allow for some small perturbations around the strict QCD scaling by permitting deviations of HC couplings and decay constants around their QCD estimates. Minimizing the χ^2 in terms of this large number of variables is an algorithmically hard problem. The result is a local minimum that depends on the initial conditions and the given typical variation of the variables. The fit uses the `COBYLA` algorithm [148] for the minimisation, which allows us to apply constraints on the minimisation procedure to account for known bounds (see next section). All cross sections are automatically evaluated in `Madgraph` [80] using the NLO PDF-set `CTEQ6m` and a fixed renormalisation and α_s scale.

9.3 Benchmarks

The results of the χ^2 fit are very encouraging. We discuss one benchmark for $\mu = m_t$ and one for $\mu = 2m_t$ denoted by BM_{m_t} and BM_{2m_t}, respectively, both of which have a significantly

	$\mathbf{BM}_{m_t}$	$\mathbf{BM}_{2m_t}$
M_{chiral}[GeV]	177	171
$m_{\mathcal{Q}_1}$[GeV]	3.4	3.1
$m_{\mathcal{Q}_3}$[GeV]	30.2	30.5
$m_{\mathcal{S}}$[GeV]	520	520
h_1	2.0	2.0
h_3	4.2	4.2

	$\mathbf{BM}_{m_t}$	$\mathbf{BM}_{2m_t}$
dev. in g_ρ^{HC}	0.95	0.93
dev. in $g_{a_1}^{\text{HC}}$	0.89	0.93
dev. in $f_{u'}$	1.3	1.3
dev. in m_{a_1}	0.96	0.99

Table 9.2: *The UV parameters of the two benchmark points and the deviations from the naive QCD rescaling relations.*

	Masses [GeV]	**Widths/Masses**
π^{HC}, K^{HC}, η^{HC}	65, 146, 164	0.0%
ρ^{HC}, $K^{*\text{HC}}$, V_L, V_H	183, 218, 186, 248	6%, 0.2%, 0.1%, 0.0%
a_1^{HC}, $K^{A\,\text{HC}}$, A_L, A_H	267, 290, 276, 313	23%, 6%, 0.2%, 0.0%
V_o, V_s	1291, 1291	33%, 33%
u', c', t'	691, 691, 718	6%, 6%, 19%

Table 9.3: *The resonance mass spectrum for* BM_{m_t}. *The spectrum for* BM_{2m_t} *is insignificantly different.*

lower χ^2 than the SM:

$$\chi^2(\text{BM}_{m_t}) = 3.5 \qquad \text{to be compared with} \qquad \chi^2(\text{SM}, \mu = m_t) = 12\,,$$
$$\chi^2(\text{BM}_{2m_t}) = 3.3 \qquad \text{to be compared with} \qquad \chi^2(\text{SM}, \mu = 2m_t) = 13\,.$$

The values of the UV parameters are listed in Tab. 9.2 together with the deviations from naive QCD scaling on which the fit settled. The resulting resonance masses and widths for the benchmarks are found in Tab. 9.3.

The important facts to be taken from Tab. 9.2 are that: $m_{\mathcal{S}}$ is large, approximately 1/2 TeV, in order to hide V_o and V_s from the differential $m_{t\bar{t}}$ spectrum at Tevatron (see discussion in Sec. 6.1.4). $m_{\mathcal{Q}_3}$ is significantly larger than $m_{\mathcal{Q}_1}$ in order to kinematically suppress the decay of $K^{*\text{HC}}$ to pseudoscalars, thus increasing the associate effect in A_C. The main deviation from QCD rescaling is in the decay constant $f_{u'}$, which we increased by 30% with respect to the naive fit in Sec. 6.1.3. In this way, we globally enhanced the mixing of the composite to the SM quarks to obtain an approximately 0.3 coupling of the $K^{*\text{HC}}$ to up and top quarks. Equivalently, we could have further increased the strong Yukawa couplings (see Eq. (6.22)).

The predictions of the two benchmarks for asymmetries and cross sections are given in Tab. 9.4. We find that the $A_{FB}^{t\bar{t}}$'s are enhanced, while A_C remains SM-like, which is purely due to the associate effect. Without it, $A_{FB}^{t\bar{t}}$ and A_C would be correlated resulting in $A_C = 0.027$ and $A_C = 0.029$ for BM_{m_t} and BM_{2m_t}, respectively. The increased $m_{\mathcal{Q}_3}$ kinematically suppressed the decay of the $K^{*\text{HC}}$ to pseudoscalars resulting in an approximately 30% branching ratio to $t\bar{u}$ that corresponds to the best fit points found in Ref. [75]. In this sense, the HC model is a UV realisation of the Z' toy model from Ref. [75]. A less positive characteristic is that the benchmarks show a reduced inclusive cross section at the Tevatron, a behaviour typical for models of $A_{FB}^{t\bar{t}}$ with t-channel vector mediators [28].

	$\mathbf{BM}_{m_t}$	$\mathbf{SM}_{m_t}$	$\mathbf{BM}_{2m_t}$	$\mathbf{SM}_{2m_t}$
$A_{FB}^{t\bar{t}\,\text{inc}}$	0.185	0.088	0.191	0.082
$A_{FB}^{t\bar{t}\,\text{low}}$	0.091	0.062	0.096	0.059
$A_{FB}^{t\bar{t}\,\text{high}}$	0.314	0.129	0.327	0.123
A_C	0.014	0.123	0.018	0.012
$\sigma_{\text{inc}}^{\text{TEV}}$ [pb]	6.26	-	6.53	-
$\sigma_{\text{inc}}^{\text{LHC}}$ [pb]	180.6	-	177.4	-

Table 9.4: *The predictions of the two benchmarks for $t\bar{t}$ asymmetries and inclusive cross sections at Tevatron and LHC. For comparison also the asymmetries in the SM are listed. The NNLO SM prediction for $t\bar{t}$ production are included in Tab. 9.1.*

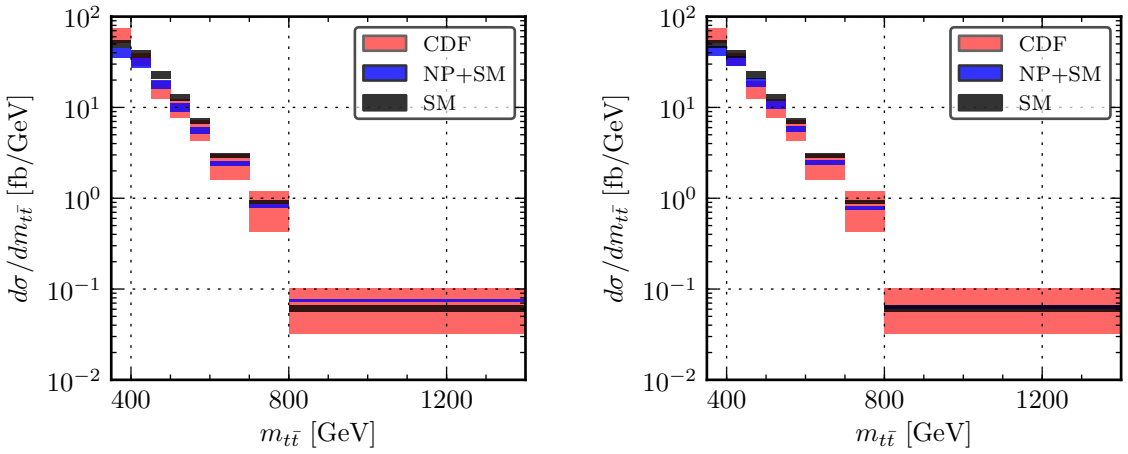

Figure 9.2: *Invariant-mass spectra for BM_{m_t} (left) and BM_{2m_t} (right) at Tevatron compared with the NLO QCD SM prediction and the measurement by CDF [149].*

Differential Spectra and Asymmetries

Next, we consider the invariant-mass spectra at Tevatron and LHC to identify possible peaks from s-channel contributions or enhancements in the high-energy tail from the dominant in our case t-channel contributions. CDF [149] presents the spectrum at the partonic level assuming the SM for the deconvolution. Thus, care is needed when comparing with NP spectra. As pointed out in Ref. [150, 151], these acceptance corrections are especially important for t-channel mediated contributions that enhance the production in forward region in contrast to the SM production, which is more central.

Using the efficiency corrections tabulated in Ref. [28] in bins of $m_{t\bar{t}}$ and Δy we correct the spectra presenting the results in Fig. 9.2. The SM contribution of the spectrum has been calculated at NLO QCD using the `aMC@NLO` utility of `Madgraph5` [80]. We observe that the NP spectra are in good agreement with the data, especially at the high-energy tail, where no enhancement is observed after the efficiency corrections have been applied. A deficit is however visible close to the threshold region, being also the reason for the reduced total cross section.

Unfortunately, the extent of the tension is difficult to judge without calculating also the NP contributions at NLO as the decrease is mainly due to destructive interference of t-channel contributions with the SM.

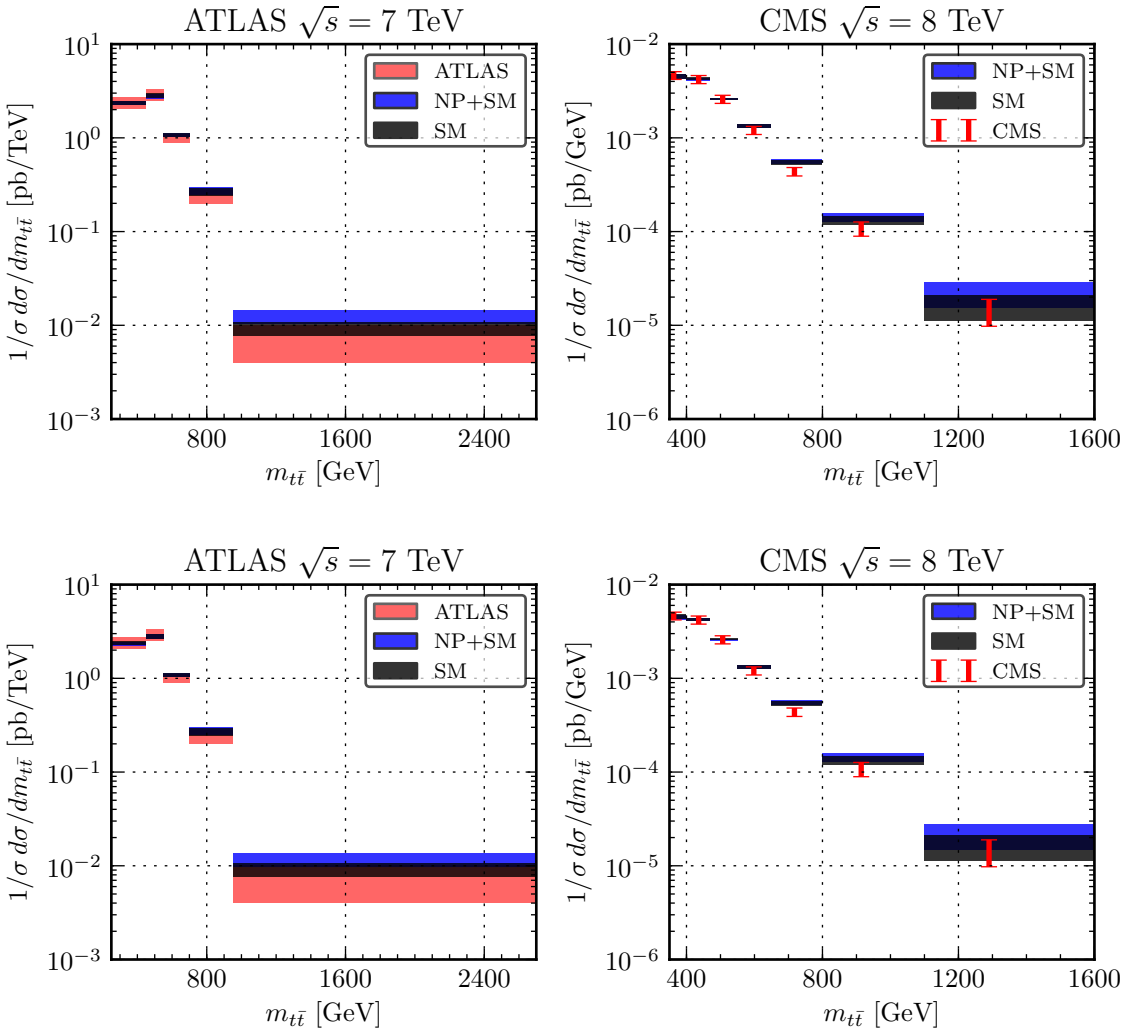

Figure 9.3: *Relative differential $m_{t\bar{t}}$ spectra for* BM_{m_t} *and* BM_{2m_t} *at LHC7 and LHC8 compared to the ATLAS [152] and CMS [153] observations. On the top, the prediction of* BM_{m_t} *and below the prediction of* BM_{2m_t}.

ATLAS and CMS report the relative $(1/\sigma)d\sigma/dm_{t\bar{t}}$ spectra at $\sqrt{s} = 7$ TeV [152] and $\sqrt{s} = 8$ TeV [153], respectively. We show the experimental measurement and the NP predictions in Fig. 9.3. We find 1σ agreement of the two benchmarks with the observed spectra at LHC with a tendency for an enhanced high-energy tail, which is attributed both to the t-channel tail and the presence of V_o and V_s at 1.2 TeV, which will thus be probed in the next LHC run.

Finally, we look into the $A_{FB}^{t\bar{t}}$'s, our main motivation for constructing the model. The improved CDF analysis including the full 9.4fb^{-1} of data presented $A_{FB}^{t\bar{t}}$ results binned in both $m_{t\bar{t}}$ and Δy, that we present for the two benchmarks in Fig. 9.4. Here, the differential

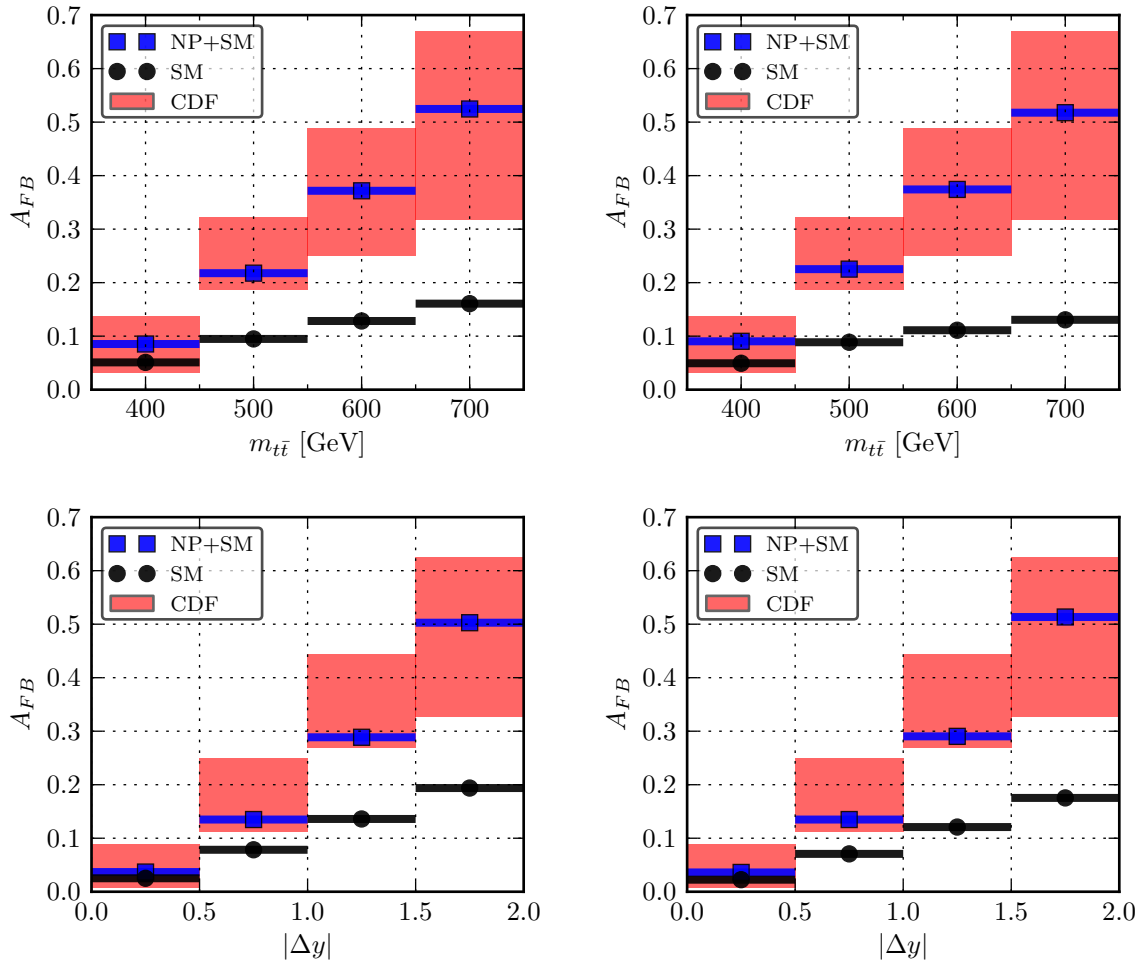

Figure 9.4: *$A_{FB}^{t\bar{t}}$ binned in $m_{t\bar{t}}$ (upper) and Δy (lower) for* BM_{m_t} *(left) and* BM_{2m_t} *(right) compared to the CDF measurements [136] and the SM NLO QCD prediction.*

$A_{FB}^{t\bar{t}}$'s have been computed at NLO QCD without the EW corrections that were included in the χ^2 minimisation. In both cases, we find that the benchmarks account for the measured enhancement in the $A_{FB}^{t\bar{t}}$. An enhancement which rises both with the invariant mass and the difference in the rapidities of the $t\bar{t}$ pair. The HC model with its tower of s- and t-channel resonances can thus naturally yield enhanced $A_{FB}^{t\bar{t}}$ without spoiling the differential mass spectra at either Tevatron or LHC.

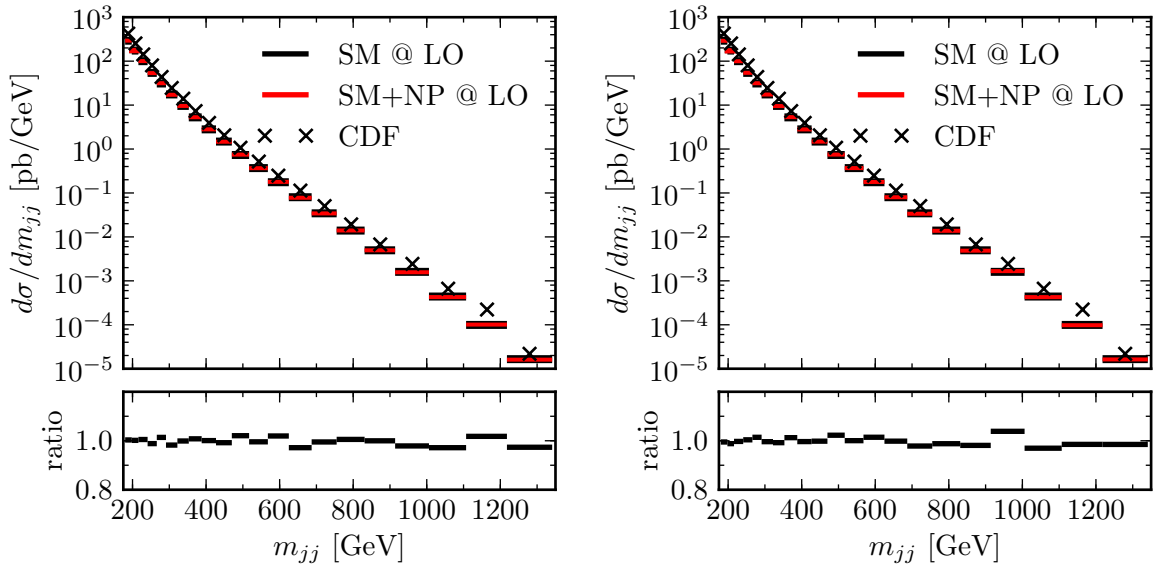

Figure 9.5: *LO differential in m_{jj} dijet spectra for BM_{m_t} (left) and BM_{2m_t} (right) at Tevatron following the CDF analysis in Ref. [156]. No significant deviations from the SM are visible. Ratio denotes the ratio of NP to SM prediction.*

Dijet Constraints

Measurements of the dijet spectrum at a hadron collider strongly constrain extensions of the SM that predict new particles with interactions to light quarks or gluons, as dijets have the largest production cross section of all processes at large momentum transfers. In the HC model there are potential candidates that may disrupt the dijet spectrum, the π^{HC}, ρ^{HC}, $V_{L(H)}$, a_1^{HC}, $A_{L(H)}$ and $V_{(os)}$. As discussed in Sec. 6.1.3, the couplings of pseudoscalars are suppressed and thus their contribution is negligible. As far as ρ^{HC} is concerned there is a related CDF search for particles that decay into two intermediate hypothesised particles, in our case the pseudoscalars, which in turn decay to four jets [154]. CDF presents bounds on this decay in dependence of the new-particle masses, which we apply as a constraint on the χ^2 minimisation. It turns out that this constraint is sufficient to find benchmarks that are also in agreement with the measured differential dijet spectra considered below.

We compare the dijet invariant-mass, $m_{t\bar{t}}$, differential spectra predicted by the two benchmarks and the SM following the CDF analysis for $\sqrt{s} = 1.96$ TeV [155]. The analysis presents partonic-level results for two jets, each with a rapidity magnitude $|\Delta y| < 1$, and reports good agreement of the SM QCD prediction with the observed spectrum. In Fig. 9.5 we present the LO result for the SM and the two benchmark points finding no deviations with respect to the SM expectations.

DØ has presented the measurement of the angular distribution of dijets for a wide spread of dijet masses $m_{jj} \in [0.25, 1.1]$ TeV [157]. The results are given in terms of the relative differential cross sections $(1/\sigma_{\mathrm{dijet}})d\sigma/d\chi_{\mathrm{dijet}}$ with $\chi_{\mathrm{dijet}} = (1+\cos\theta)(1-\cos\theta)$ and θ the polar scattering angle in the partonic centre-of-mass frame. The predictions of the two benchmarks show little deviation from the SM prediction and agree with the DØ measurements. We plot our LO predictions and the experimental observations in Fig. 9.6.

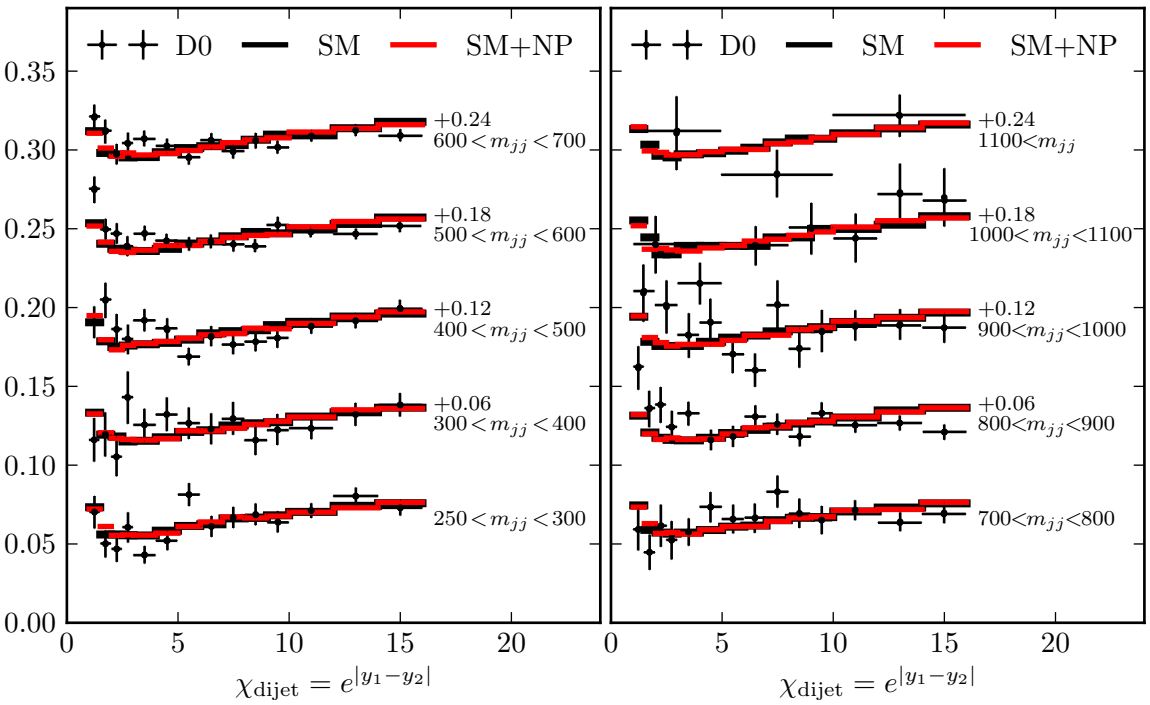

Figure 9.6: *Angular differential dijet spectrum for the* BM_{m_t} *benchmark compared with the SM and the DØ observations [157]. The spectrum for* BM_{2m_t} *shows only insignificant differences.*

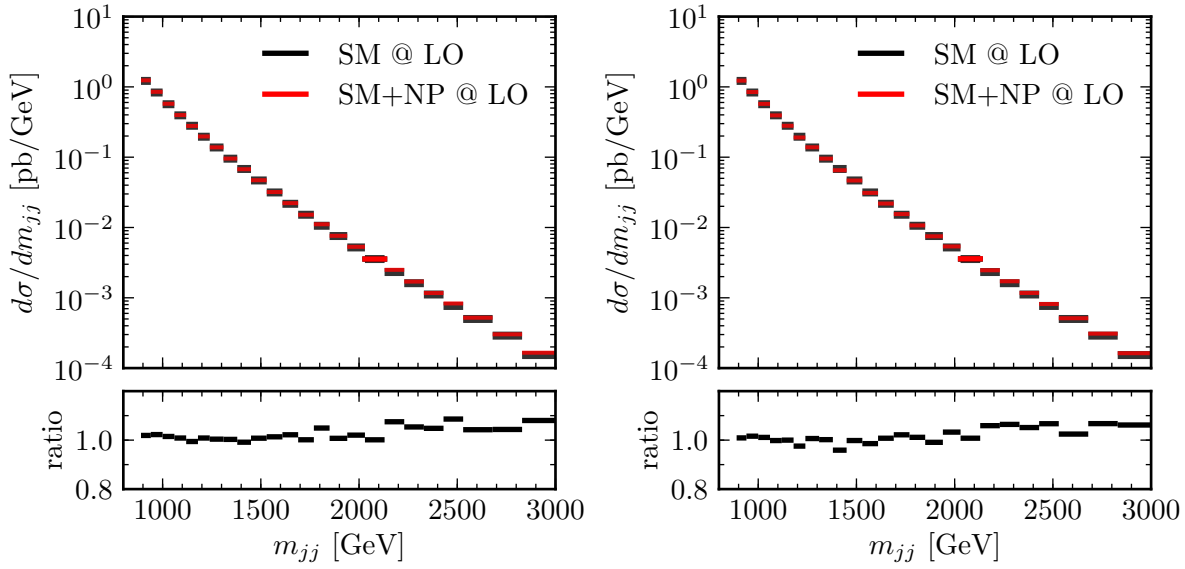

Figure 9.7: *LO differential in* m_{jj} *dijet spectra for* BM_{m_t} *(left) and* BM_{2m_t} *(right) at LHC8 following the CMS analysis in Ref. [158]. No deviations from the SM are visible. Ratio denotes the ratio of NP to SM prediction.*

Finally, we present the dijet spectrum at LHC8 as recently observed by CMS in Ref. [158]. Utilizing 4.0 fb^{-1} of data, CMS reports no significant enhancements with respect to the SM predictions. In Fig. 9.7 we present the LO spectrum for the SM and the two benchmarks finding their predictions to be compatible with the SM. Interestingly, the large decay width of V_o and V_s were sufficient to hide them from the spectrum. The high-energy tail of the spectrum is in good agreement with the SM considering the PDF uncertainties that we did not include in our analysis. However, we note that increasing h_1, while keeping the product of $h_1 \times h_3$ fixed to obtain the $A_{FB}^{t\bar{t}}$, results in an enhancement of the high-energy dijet tail at the LHC. The behaviour is similar to the $t\bar{t}$ differential spectrum at the LHC which also tends to receive enhancements from the HC resonances, that will be further probed in the next LHC run.

We have identified two benchmark points of the HC model presented in chapter 3 with a tower of resonances with masses ranging from 70 GeV to 1.2 TeV. Remarkably, the new strongly interacting HC sector is not excluded by current collider constraints and can naturally account for the anomalously large measurement of the forward-backward asymmetry. One of the predictions of the model is the occurrence of a triplet of exotic up-type quarks, which may be directly detectable at the next LHC run. The current exotic-quark searches at the LHC assume that the exotics decay to ordinary quarks and electroweak bosons, which does not apply on the HC quarks. The HC quarks decay to ordinary quarks and pseudoscalars which in turn decay to a pair of jets. Thus a more detailed analysis is necessary to assess their chances for direct detection. Also, the HC model tends to increase both the high-energy tail of $t\bar{t}$ and jj invariant-mass spectrum without showing any intermediate peak structure, both of which will be tested in the next LHC run.

10 The Standard Model $B_q \to \ell^+\ell^-$ Prediction

In this chapter we return to the SM. In chapter 7 we calculated the NLO EW matching corrections to the Wilson coefficient, $\mathcal{C}_{10}$, controlling the decays $B_q \to \ell^+\ell^-$. Here, we discuss the numerical relevance of the corrections. In Sec. 10.1 we analyse their impact on the Wilson coefficient, compare the result from different renormalisation schemes and estimate residual EW uncertainties. These results shall soon be published in Ref. [82]. In Sec. 10.2, we make the connection to the experimental measurements. We update the SM predictions of the $B_q \to \ell^+\ell^-$ branching ratios including our EW corrections and, yet unpublished, NNLO QCD corrections [52]. The updated predictions shall be presented in a joined publication [159]. I am grateful to Thomas Hermann, Mikolaj Misiak and Matthias Steinhauser for allowing me to present in this thesis the complete discussion prior to its publication.

10.1 The Impact of the Electroweak Corrections on $\mathcal{C}_{10}$

We discuss $\mathcal{C}_{10}$ at the high scale, μ_0, and the low scale, μ_b, before and after the RGE, respectively, and assess the reduction of theoretical uncertainties associated with the choices of the EW renormalisation scheme. First, we specify the level of accuracy of our numerical analysis.

Strong coupling: We use the four-loop β-function for α_s including the three-loop mixed QCD$\times$QED term given in Ref. [81]. When crossing the $N_f = 5$ to $N_f = 6$ threshold at the matching scale μ_0, we include the three-loop QCD threshold corrections using the pole-mass value for the top-quark mass [160].

Electromagnetic coupling: We implement the running of α_e in two-loop QED and three-loop mixed QED$\times$QCD precision, as presented in Ref. [81]. At the threshold $N_f = 5$ to $N_f = 6$ we include the pure QED threshold correction. The value of α_e given in Ref. [39] refers to the coupling in the SM with the top quark decoupled. From this value, we determine α_e at $\mu = M_Z$ in the full SM or in our five-flavour effective theory using the one-loop decoupling relations that we discuss in App. C.3.

Top-quark mass: We determine the running top-quark mass in the $\overline{\text{MS}}$ scheme with respect to QCD from M_t^{pole} with three-loop accuracy [160][1], $m_t(m_t) = 163.6$ GeV. We evolve it to the matching scale applying the four-loop expression of the quark-mass anomalous dimension [160]. Here, m_t denotes the top-quark mass, where QCD corrections are $\overline{\text{MS}}$-renormalised, but EW corrections are considered in the on-shell scheme. In the case that the latter are also $\overline{\text{MS}}$-renormalised, we shall choose the notation $\overline{m}_t$. The additional shift from $m_t \to \overline{m}_t$ is numerically quite significant yielding $\overline{m}_t(\overline{m}_t) = 172.7$ GeV. The shift is dominated by tadpole-diagram contributions, which cancel in the ratio $x_t = \overline{m}_t^2/\overline{M}_W^2$ that enters the LO Wilson coefficient.

[1] The choice of the matching scale has a numerically negligible impact for $\mu_0 \in [50, 300]$ GeV considered here.

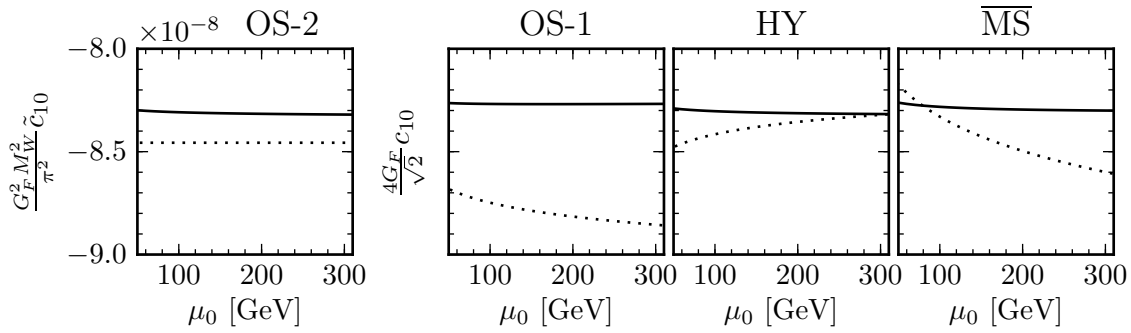

Figure 10.1: *Comparison of the matching scale, μ_0, dependence of $\mathcal{C}_{10}$ at the scale μ_0 in four renormalisation schemes (OS-2, OS-1, HY and $\overline{\text{MS}}$) at LO (dotted) and with NLO EW corrections (solid). More details in the text.*

We list the numerical input for our analysis in Tab. 7.1.

As renormalisation schemes we consider the on-shell, the $\overline{\text{MS}}$ and the hybrid scheme introduced in Sec. 7.1.1. We abbreviate them in the following as OS, $\overline{\text{MS}}$ and HY. As already emphasized in Sec. 7.1, once considering higher EW corrections, the two ways of normalising the effective Lagrangian Eq. (4.13) affect differently the NLO EW matching corrections of $\mathcal{C}_{10}$. We apply both, the single-G_F and the quadratic-G_F normalisation for the on-shell scheme, denoted as OS-1 and OS-2, respectively. For the $\overline{\text{MS}}$ and HY schemes we restrict ourselves to the single-G_F normalisation, since in the quadratic-G_F normalisation the LO Wilson coefficient does not depend on α_e or s_W.

We first consider the size and the reduction of the scheme dependences in $\mathcal{C}_{10}$ at the matching scale:

$$\mathcal{C}_{10}(\mu_0) = \begin{cases} \dfrac{4G_F}{\sqrt{2}} \tilde{\alpha}_e(\mu_0) \left[c_{10}^{(11)} + \tilde{\alpha}_e(\mu_0)\, c_{10}^{(22)}(\mu_0) \right] \\ \dfrac{G_F^2 M_W^2}{\pi^2} \left[\widetilde{c}_{10}^{(11)} + \tilde{\alpha}_e(\mu_0)\, \widetilde{c}_{10}^{(22)}(\mu_0) \right] \end{cases} , \tag{10.1}$$

for the single- and quadratic-G_F normalisation, respectively, after including the NLO EW corrections $\mathcal{C}_{10}^{(22)}$. To separate the effects of the EW calculation, we first switch off any QCD dependence. Namely, we omit the NLO QCD correction $\mathcal{C}_{10}^{(21)}$ and neglect the μ_0 dependence of the top-quark mass under QCD by fixing the QCD scale and using $m_t(m_t)$ as the on-shell top-quark mass under EW renormalisation, as far as OS-1, OS-2 and HY schemes are concerned. In the $\overline{\text{MS}}$ scheme we perform the additional shift $m_t \to \overline{m}_t$ using the value of $m_t(m_t)$ as input value. Note, that for this choice of scale, $\mu_0 = m_t$, the omitted NLO QCD correction $\mathcal{C}_{10}^{(21)}$ is particularly small [49, 50, 51], i.e. the LO result $\mathcal{C}_{10}^{(11)}$ accounts for most part of the higher-order QCD correction.

We plot the LO and (LO + NLO EW) results in Fig. 10.1 for the four renormalisation schemes. The LO $\mathcal{C}_{10}$ is μ_0 independent in the OS-2 scheme because the top-quark mass is μ_0 independent and the scheme does not depend on coupling constants at LO. The replacement $G_F \to \alpha_e(\mu_0)/(s_W^{\text{on-shell}})^2$ introduces a μ_0 dependence in OS-1 and a quite significant shift of

about 4% with respect to OS-2 that translates to a 8% modification of the LO branching ratio. The $\overline{\text{MS}}$ and HY schemes are based on the same single-G_F normalisation as the OS-1 scheme. Nevertheless, at LO they exhibit relatively large shifts with respect to it and a modified μ_0 dependence due to: the $\overline{\text{MS}}$ renormalisation of s_W in both HY and $\overline{\text{MS}}$ schemes and the EW $\overline{\text{MS}}$ renormalisation of the top-quark and W mass in the $\overline{\text{MS}}$ scheme.

We estimate the overall uncertainty due to EW corrections at LO from the variation of $\mathcal{C}_{10}$ in all four schemes. Ranging in the interval $\mathcal{C}_{10}(\mu_0) \in [-8.9, -8.2] \cdot 10^{-8}$ for $\mu_0 \in [50, 300]$ GeV, it corresponds to a $\pm 8\%$ uncertainty at the level of the branching ratio. The inclusion of the NLO EW corrections eliminates this large uncertainty, as all four schemes yield aligned (LO + NLO EW) results and the μ_0 dependence cancels to large extent in all four schemes. The residual uncertainty due to EW corrections is now confined to the small interval of $\mathcal{C}_{10}(\mu_0) \in [-8.26, -8.32] \cdot 10^{-8}$ at the scale μ_0. It is less than $\pm 0.4\%$, which gives an $\pm 0.8\%$ uncertainty on the branching ratio.

The strong reduction of the μ_0 dependence in Fig. 10.1 is due to the inclusion of the NLO corrections related to EW parameters that are formally not part of the effective theory, i.e. s_W, M_W and M_t, and hence cannot be cancelled by the RGE in the effective theory. At LO in the effective theory there is no renormalisation group mixing of $\mathcal{C}_{10}$ and this μ_0 dependence may be used directly as an uncertainty. However, as discussed in Sec. 7.2, beyond LO in QED operator mixing will reduce this residual μ_0 dependence even further.

Before proceeding, we comment on the OS-1 and $\overline{\text{MS}}$ scheme and why we shall discard them for the estimate of residual higher-order uncertainties. The OS-1 scheme exhibits the worst perturbative behavior of all four schemes, as seen in Fig. 10.1. The s_W-on-shell counterterm induces this, for an EW correction, unnaturally large shift at two-loop. As further discussed in App. C.5, the top-quark-mass dependence of the s_W-on-shell counterterm implies a significant higher-order QCD-scale dependence, which we consider artificial. On the other hand, the OS-2 and HY schemes do not exhibit this strong dependence on the top-quark mass and the estimate of the size of higher-order QCD contributions by varying the scale of m_t indicates much smaller corrections. In view of this, we restrict ourselves to schemes with reasonable convergence properties and leave OS-1 aside. In the case of the $\overline{\text{MS}}$ scheme, the application of RG equations is required for the iterative determination of the EW parameters from the input given in Eq. (7.9). For the purpose of Fig. 10.1, QCD could be ignored and lowest order RG equations were sufficient. However, in the general case the solution of the according mixed RG equations are rather involved and we shall use the comparison of the HY and OS-2 scheme to estimate higher-order EW×QCD corrections.

We now switch QCD back on and discuss $\mathcal{C}_{10}$ at the low-energy scale μ_b after applying the RGE running presented in Sec. 7.2. We express the Wilson coefficient $\mathcal{C}_{10}(\mu_b)$ as a double series in the running couplings $\tilde{\alpha}_s$ and $\tilde{\alpha}_e$, see Eqs. (7.25) and (7.27). $\mathcal{C}_{10}(\mu_b)$ has five relevant contributions $\mathcal{C}_{10,(mn)}$, $(mn = 11, 21, 02, 12, 22)$ that depend on Wilson coefficients at μ_0. So far, only the LO $\equiv (mn = 11)$ and the NLO QCD $\equiv (mn = 11 + 21)$ contributions were known. Now, we can include the full NLO EW correction with the additional contributions $(mn = 11{+}21{+}02{+}12{+}22) \equiv$ NLO (QCD + EW)[2]. For this purpose, we take into account the QCD-scale dependence of m_t in the variation of the matching scale μ_0. $\mathcal{C}_{10}(\mu_b)$ is independent

[2] These corrections were discussed in the large top-quark-mass limit including the RGE effects in [47]. The RGE effects have been neglected in [53] for $(mn = 02, 12, 22)$.

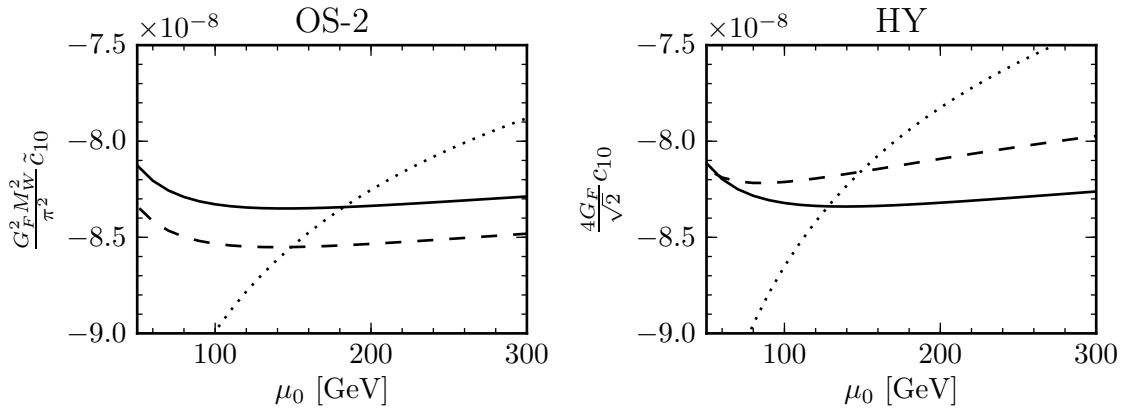

Figure 10.2: *The μ_0 dependence of the Wilson coefficient $\mathcal{C}_{10}(\mu_b = 5\,GeV)$ in two renormalisation schemes (OS-2, HY) at LO (dotted), NLO QCD (dashed) and NLO (QCD + EW) (solid). See text for more details.*

of the matching scale μ_0 up to the considered orders in the couplings due to the inclusion of the RGE evolution. However, there is a residual μ_b dependence that can only be cancelled by the according μ_b dependence of the matrix elements of the relevant operators.

Fig. 10.2 shows the μ_0 dependence of $\mathcal{C}_{10}(\mu_b = 5\,\text{GeV})$ at LO, NLO QCD and NLO (QCD + EW) in the OS-2 and HY schemes. It is clearly visible that the dependence on the renormalisation scale of m_t reduces when going from LO to NLO QCD and that the LO results coincide with the ones at NLO QCD at the scale $\mu_0 \approx 150$ GeV. A further reduction of this scheme dependence requires the inclusion of NNLO QCD corrections [52]. The NLO QCD result is quite different in the OS-2 and HY schemes. It comprises values of $\mathcal{C}_{10}(\mu_b) \in [-8.55, -7.98] \cdot 10^{-8}$. The NLO (QCD + EW) result shows again rather large shifts with respect to NLO QCD and a clear convergence of both schemes towards the same value. The results of the OS-2 and HY schemes are now confined within $\mathcal{C}_{10}(\mu_b) \in [-8.35, -8.12] \cdot 10^{-8}$ reducing the combined uncertainty due to scheme dependencies of both QCD and EW interactions to $\pm 1.4\%$. Again, we emphasise that the substantial part of this uncertainty is due to so far unknown NNLO QCD corrections. We estimate the uncertainty due to higher-order EW and QCD corrections to our two-loop EW result from: 1) the ratio of the results of HY to OS-2 scheme, thereby eliminating the numerically leading QCD μ_0-dependence of m_t, Fig. 10.3 and 2) by varying the scale μ_0 only in m_t in the two-loop EW matching corrections $c_{10}^{(22)}$ (or $\widetilde{c}_{10}^{(22)}$). From Fig. 10.3 we see that the NLO QCD ratio deviates quite strongly from 1, whereas at NLO (QCD + EW) the deviation is less than 0.3%. The ratio of the LO results coincides with the ratio of the NLO QCD ones. We find a similar μ_0 dependence of the OS-2 and HY results (about $\pm 0.1\%$) when varying the scale only in m_t in the EW two-loop matching correction. We choose the OS-2 scheme with $\mu_0 = 160$ GeV to predict the central value of $\mathcal{C}_{10} = -8.349 \cdot 10^{-8}$. The HY scheme yields $-8.339 \cdot 10^{-8}$. We assign an error due to higher-order EW corrections from the variation of μ_0 of about $\pm 0.3\%$ as suggested by the comparison of the OS-2 and HY schemes.

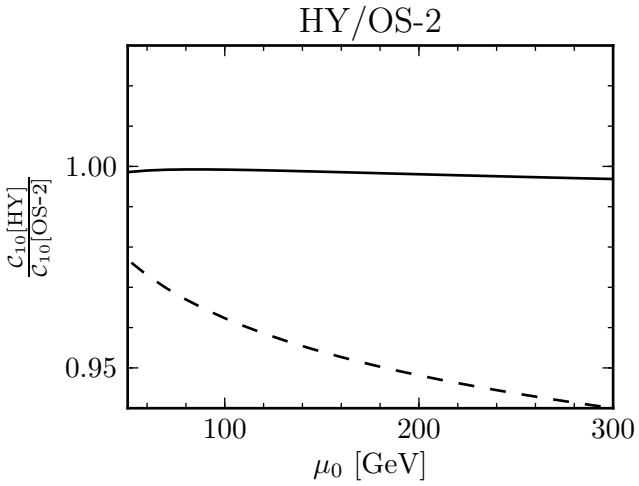

Figure 10.3: *The μ_0 dependence of the ratio of Wilson coefficient $\mathcal{C}_{10}(\mu_b = 5\,GeV)$ in the HY and the OS-2 scheme at LO and NLO QCD (dashed) and NLO (QCD + EW) (solid). The LO and NLO QCD curves coincide.*

Next, we investigate the residual μ_b dependence for the fixed value $\mu_0 = 160$ GeV. As already mentioned above, including the according matrix elements of the involved operators shall decrease this dependence further. At the moment, however, it remains an additional source of uncertainty. Fig. 10.4 shows $\mathcal{C}_{10}(\mu_b)$ at LO, NLO QCD and NLO (QCD + EW) in the OS-2 and HY schemes. Whereas the values of $\mathcal{C}_{10}(\mu_b)$ are quite different in all three schemes at NLO QCD, the inclusion of NLO (QCD + EW) corrections in the RGE yields a convergence towards the same value and a very small residual μ_b dependence in each scheme. Less than $\pm 0.2\%$ when varying $\mu_b \in [2.5, 10]$ GeV. We note that the non-perturbative uncertainty due to unknown QED corrections in the evaluation of the matrix elements is an additional source of uncertainty, not included in the above estimate.

The dependence of the EW corrections on the Higgs mass is entirely negligible. Varying $M_H \in [120, 130]$ GeV induces variations in $\mathcal{C}_{10}$ of less than $\pm 0.01\%$.

As our final result we choose for the central value the OS-2 scheme with scale settings $\mu_0 = 160$ GeV and $\mu_b = 5$ GeV:

$$\mathcal{C}_{10} = (-8.35 \pm 0.04) \cdot 10^{-8}\,, \tag{10.2}$$

where we have estimated higher-order corrections of EW origin from the scale variations of $\mu_0 \in [50, 300]$ GeV and $\mu_b \in [2.5, 10]$ GeV in two schemes, OS-2 and HY, and added linearly the two errors. The error does not include residual errors associated to higher QCD corrections that can be removed by the NNLO QCD calculation [52] nor any of the parametric errors listed in Tab. 7.1. We discuss them in the next Section in conjuction with parametric uncertainties of the branching ratio predictions.

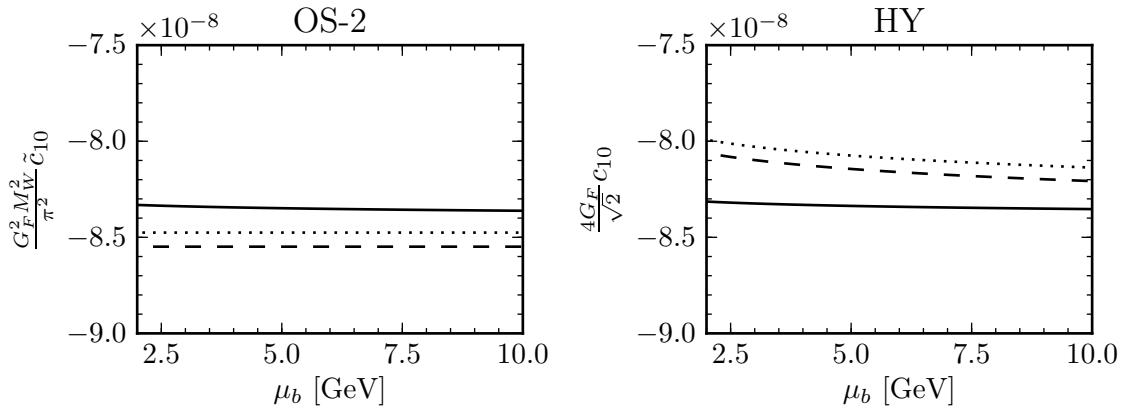

Figure 10.4: *The μ_b dependence of the Wilson coefficient $\mathcal{C}_{10}(\mu_b)$ for fixed $\mu_0 = 160$ GeV in two renormalisation schemes (OS-2, HY) at LO (dotted), NLO QCD (dashed) and NLO (QCD + EW) (solid). See text for more details.*

To illustrate the numerical relevance of the EW correction, we quote for comparison the results at NLO QCD

$$\mathcal{C}_{10}^{\mathrm{OS-2}} = -8.55 \cdot 10^{-8}\,, \qquad \mathcal{C}_{10}^{\mathrm{HY}} = -8.15 \cdot 10^{-8}\,, \tag{10.3}$$

taken from the according curves of the OS-2 and HY schemes in Fig. 10.2.

Finally, we compare our prediction with the previous estimate [53] obtained using the large-m_t approximation of $\mathcal{C}_{10}^{(22)}$ and neglecting the effects of the RGE evolution $\mathrm{BR}^{[t=0]} = 3.28 \cdot 10^{-9}$ for the HY scheme. Adopting the same numerical input ($f_{B_s} = 227$ MeV, $\tau_{B_s} = 1.466$ ps^{-1}, $M_{B_s} = 5.36677$ GeV, $|V_{tb}V_{ts}^*| = 0.0405$, $m_\mu = 105.6584$ MeV $\Rightarrow \mathcal{N} = 4.48409 \cdot 10^5$ from Eq. (4.11)) and our full result from Eq. (10.2) we obtain $\mathrm{BR}^{[t=0]} = 3.13 \cdot 10^{-9}$, which is about 5% lower, mainly due to the above mentioned approximations. The authors of [53] argued that NLO EW corrections in the HY scheme should be small and suggested a procedure, based on LO expressions that lead to the preliminary value of $\mathrm{BR}^{[t=0]} = 3.23 \cdot 10^{-9}$ (see Eq. (17) of [53]), which is closer to our result and deviates only by 3%. It was suggested to use the EW parameters α_e and s_W in the $\overline{\mathrm{MS}}$ scheme[3] at the scale $M_Z \approx 90$ GeV and the LO expression $c_{10}^{(11)} \sim Y_0(x_t)$ with $m_t(m_t)$ in combination with an additional correction factor η_Y to account for the higher-order QCD corrections from $c_{10}^{(21)}$. From the third panel in Fig. 10.1, we find at $\mu_0 = 90$ GeV a deviation of about 1.5% between the LO and the NLO EW result. We close this comparison with the remark that the authors of [53] work at LO in the EW couplings. This permits them to combine values of the input parameters that are dependent beyond LO. In our case certain EW parameters, e.g. s_W and M_W, do depend on the choice of input in Eq. (7.9). As a consequence, a straightforward numerical comparison is of limited value. However, adopting the suggested procedure and using our numerical values for dependent quantities, we obtain a slightly larger value $\mathrm{BR}^{[t=0]} = 3.24 \cdot 10^{-9}$ instead of $3.23 \cdot 10^{-9}$.

[3] In [53] the $\overline{\mathrm{MS}}$ value for s_W in the theory with the top quark decoupled was used. In our definition of the HY scheme, s_W is the weak mixing angle in the six-flavour SM. Both values are reported in Ref. [39].

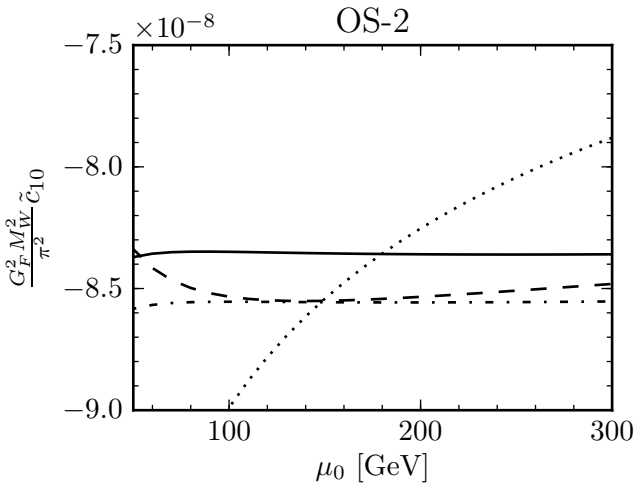

Figure 10.5: *The μ_0 dependence of $\mathcal{C}_{10}$ in the EW on-shell scheme for the quadratic-G_F normalisation. The solid line is the full (NNLO QCD + NLO EW) result and the dashed-dotted line is the NNLO QCD result. We depict the NLO QCD and LO results in dashed and dotted lines, respectively.*

10.2 The Branching Ratio for $B_q \to \ell^+\ell^-$

We computed the NLO electroweak corrections to $\mathcal{C}_{10}$ and estimated the residual uncertainties to be: $\pm 0.3\%$ from left-over EW scheme and scale dependences and again $\pm 0.2\%$ from the dependence on μ_b. The authors of Ref. [52] estimate residual perturbative QCD uncertainties on $\mathcal{C}_{10}$ after computing the NNLO QCD correction to be less that $\pm 0.1\%$. We shall not further analyse this error and await the original publication. We include it in our error budget and will also present the combination of the NNLO QCD and NLO EW calculations. I thank the authors of Ref. [52] for allowing me to include their results here, prior to their publication. Fig. 10.5 shows the combined result for $\mathcal{C}_{10}$ in the EW on-shell scheme for the quadratic-G_F normalisation (OS-2). Comparing the NLO QCD (dashed) and NNLO QCD (dashed-dotted) result, we find a clear stabilisation of $\mathcal{C}_{10}$ with respect to μ_0. Comparing the solid (NNLO QCD + NLO EW) curve to the dashed-dotted NNLO QCD curve, we observe the numerical importance of the NLO EW corrections.

For future convenience we give here an approximate formula for $\widetilde{c}_{10}$, with $\mathcal{C}_{10} = G_F^2 M_W^2/\pi^2\, \widetilde{c}_{10}$ that includes both NNLO QCD and NLO EW corrections

$$\widetilde{c}_{10} = -1.0031 \left(\frac{M_t}{173.2\,\text{GeV}}\right)^{1.480} + 1.3425\, \alpha_s^{1.425} \left(\frac{M_t}{173.2\,\text{GeV}}\right)^{0.436} . \tag{10.4}$$

The fit captures the full result for the variation $M_t \in [171.2, 175.2]$ and $\alpha_s \in [0.1164, 0.1204]$ with an accuracy better than 0.002%.

In Tab. 10.1 we summarise the numerical input for the branching ratio analysis. For the mass of the top-quark we conservatively increase the experimental error from ± 0.9 to ± 1.5 GeV to include theoretical uncertainties in the QCD conversion of the pole to the $\overline{\text{MS}}$ mass.

Parameter	Value	Ref.
G_F	$(1.166\,378\,7(6)) \cdot 10^{-5}\,\text{GeV}^{-2}$	[39]
$\alpha_s^{(5)}(M_Z)$	0.1184(7)	[39]
$\alpha_e^{(5)}(M_Z)$	$(127.944(14))^{-1}$	[39]
M_Z	91.1876(21) GeV	[39]
M_t	173.2(9) GeV	[84, 85]
M_H	125(2) GeV	[39, 1, 2]
$V_{tb}^* V_{ts}$	0.04124(64)	[161]
$V_{tb}^* V_{td}$	0.00887(20)	[161]
f_{B_s}	225(3) MeV	[44]
f_{B_d}	186(4) MeV	[44]
τ_{B_s}	$1.516(11) \cdot 10^{-12}$ s	[121]
τ_{B_d}	$1.519(7) \cdot 10^{-12}$ s	[121]
$\Delta\Gamma_s/\Gamma_s$	0.123(17)	[39]

Table 10.1: *The physical input used for the branching ratio predictions. $\alpha_{s,e}$ are the running $\overline{MS}$ couplings in the SM with the top-quark decoupled at $\mu = M_Z$. Masses are the experimentally measured pole masses. To account for the QCD uncertainty in the shift from pole to $\overline{MS}$ top-quark mass, we shall increase its uncertainty to ± 1.5 GeV.*

With this input, we predict the instantaneous branching ratios for the $B_q \to \ell^+\ell^-$ decays in the SM:

$$\text{BR}^{[t=0]}(B_s \to e^+e^-) = (7.72 \ \pm 0.38(\text{param.}) \ \pm 0.06(\text{theo.})) \times 10^{-14}\,, \tag{10.5}$$

$$\text{BR}^{[t=0]}(B_s \to \mu^+\mu^-) = (3.30 \ \pm 0.16(\text{param.}) \ \pm 0.02(\text{theo.})) \times 10^{-9}\,, \tag{10.6}$$

$$\text{BR}^{[t=0]}(B_s \to \tau^+\tau^-) = (7.00 \ \pm 0.34(\text{param.}) \ \pm 0.05(\text{theo.})) \times 10^{-7}\,, \tag{10.7}$$

for the $B_s \to \ell^+\ell^-$ decays and

$$\text{BR}^{[t=0]}(B_d \to e^+e^-) = (2.41 \ \pm 0.16(\text{param.}) \ \pm 0.02(\text{theo.})) \times 10^{-15}\,, \tag{10.8}$$

$$\text{BR}^{[t=0]}(B_d \to \mu^+\mu^-) = (1.03 \ \pm 0.07(\text{param.}) \ \pm 0.01(\text{theo.})) \times 10^{-10}\,, \tag{10.9}$$

$$\text{BR}^{[t=0]}(B_d \to \tau^+\tau^-) = (2.15 \ \pm 0.15(\text{param.}) \ \pm 0.02(\text{theo.})) \times 10^{-8}\,, \tag{10.10}$$

for the $B_d \to \ell^+\ell^-$ decays. In the parametric error we added in quadrature all relevant parametric uncertainties, f_{B_q}, τ_{B_q}, $|V_{tb}V_{tq}^*|$, M_t and α_s. We report the individual relative errors in Tab. 10.2. The theoretical error corresponds to the residual EW and QCD scheme and scale uncertainties, also added in quadrature, i.e.

$$\sqrt{0.6\%^2\ (\mu_0\ \text{EW}) + 0.4\%^2\ (\mu_b\ \text{EW}) + 0.2\%^2\ (\mu_0\ \text{QCD}))}.$$

Eqs. (10.5)–(10.10) are the instantaneous branching ratios. At the moment, LHCb [32] and CMS [33] report the time-integrated and CP-averaged branching ratio for $B_s \to \mu^+\mu^-$. The weighted average of the two measurement is [34]

$$\overline{\text{BR}}(B_s \to \mu^+\mu^-) = (2.9 \pm 0.7) \cdot 10^{-9}\,, \tag{10.11}$$

Decay	f_{B_q}	τ_{B_q}	$\lvert V_{tb}V_{tq}^*\rvert$	$M_t(\pm 1.5\,\text{GeV})$	$\alpha_s(M_Z)$
$\text{BR}^{[t=0]}(B_s \to \ell^+\ell^-)$	2.6%	0.7%	3.1%	2.7%	0.1%
$\text{BR}^{[t=0]}(B_d \to \ell^+\ell^-)$	4.3%	0.5%	4.5%	2.7%	0.1%

Table 10.2: *The dominant relative parametric uncertainties of the SM prediction of the instantaneous branching ratios for the $B_q \to \ell^+\ell^-$ decays. The central values for each mode are given in Eqs. (10.5)–(10.10)*

which should be compared with our updated prediction from Eq. (4.8)

$$\overline{\text{BR}}(B_s \to \mu^+\mu^-) = (3.52 \ \pm 0.17(\text{param.}) \ \pm 0.03(\text{theo.})) \times 10^{-9}\,. \tag{10.12}$$

The SM prediction of the time-integrated and CP-averaged rate is plagued by the additional experimental error of $y_s = 0.062 \pm 0.009$ [39], which contributes an additional 1.0% relative error. The SM prediction agrees with the experimental observation; large uncorrelated effects from physics beyond the SM are not phenomenologically viable. With the theoretical improvement of the perturbative uncertainties presented here, the future of the $B_s \to \mu^+\mu^-$ decay lies on the hands of the next LHC run and the next lattice computations that will reduce the theoretical uncertainty of f_{B_s}.

Part IV

Conclusions

Summary and Conclusions

We have clear experimental indications that the standard model of particle physics cannot be the ultimate description of physics at small distances. At the moment, our most direct probe of dynamics at high energies is the LHC machine, which, already in the first run, has achieved its main design purpose, namely, the discovery of a scalar particle very much resembling the SM Higgs boson. In doing so the LHC has basically established that the unitarisation of W and Z scattering proceeds through a weakly coupled scalar. The hierarchy problem of the SM let us expect also physics beyond the SM at the TeV scale and has motivated us to investigate observables that are directly or indirectly sensitive to new heavy degrees of freedom. The flavour structure of such low-energy extensions of the SM needs to show a highly non-generic pattern in order to evade, the severe constraints from indirect searches of flavour and CP violation. This raises the question of why and to what extent viable low-scale extensions of the SM adhere to the SM pattern of flavour and CP violation, i.e. why is Minimal Flavour Violation such a good description.

In this thesis we addressed these questions in three complementary approaches. We investigated the possibility of a dynamical realisation of Minimal Flavour Violation at the TeV scale and its predictions on low-energy flavour observables. Further, we constructed a model with new flavour-dependent strong dynamics at the TeV scale that can naturally account for the observation of an anomalously large $t\bar{t}$ forward-backward asymmetry at the Tevatron. Finally, we improved the SM prediction for the branching ratio of the recently observed $B_s \to \mu^+\mu^-$ decay by computing the next-to-leading-order electroweak corrections. Our findings are summarised below.

Gauged Flavour Symmetries: A dynamical explanation for the observed hierarchies in the masses and mixings may come from the breaking of an underlying flavour symmetry. One possibility is that the symmetry is a spontaneously broken gauge symmetry, which implies the existence of exotic quarks and massive flavour-gauge bosons that may have so far evaded detection in indirect searches, but be accessible at the LHC. We investigated the effects of these new degrees of freedom on low-energy FCNC processes in the bottom and kaon sector and found the construction to be remarkably predictive due to the gauge character of the flavour symmetry. This implies strong correlations among flavour observables and thus clear patterns of flavour violation. Combining the predictions of CP conserving and CP violating observables in the neutral bottom and kaon sector, we concluded that large effects from flavour-gauge bosons or exotic-quarks are experimentally disfavoured, i.e. they can only increase possible tensions of flavour observables in the SM, and it therefore appears challenging to distinguish the model from the SM.

New Strong Interactions in Top Physics: The top quark has a prominent role in the SM as it is the only fermion with a large coupling to the Higgs field. Top physics is thus closely linked to the mechanism of electroweak symmetry breaking and is considered to be a promising avenue for the discovery of physics beyond the SM. CDF and DØ may already have glimpsed deviations from the SM in the measurement of an unexpectedly

large forward-backward asymmetry in $t\bar{t}$ production. To account for this observation, we constructed a renormalisable extension of the SM based on an asymptotically-free confining $\mathrm{SU}(3)_{\mathrm{HC}}$ gauge symmetry. Its low-energy spectrum contains flavoured vector and scalar resonances that contribute to the forward-backward $t\bar{t}$ asymmetry. A key element of the construction was the occurrence of resonances with the quantum numbers of the SM right-handed up-type quarks, which induced mixing in the up-quark sector without modifying the down-quark sector of the SM. Along the lines of Minimal Flavour Violation we aligned new sources of flavour violation to the SM and used QCD as a guideline to model the resonance spectrum. We discussed concrete benchmark points demonstrating that new strong dynamics can both naturally account for the forward-backward asymmetry and have evaded direct detection so far.

The $B_s \to \mu^+\mu^-$ Prediction: The recent first-time observation of the rare FCNC decay $B_s \to \mu^+\mu^-$ by LHCb and subsequently by CMS has been so far the highlight of the LHC flavour program. The agreement of the SM prediction with the measurements was yet another missed chance for the discovery of large flavour-violating effects that are often predicted by extensions of the SM. This rendered the improvement of the SM prediction crucial to disentangle possible small new physics effects in the next LHC run. So far, the SM prediction was plagued by an approximately 5-7% error due to electroweak scheme and scale uncertainties. By computing the full two-loop electroweak corrections in different electroweak renormalisation schemes we achieved a reduction of this uncertainty down to approximately 0.7% and updated the SM prediction of the time-dependent and CP-averaged rate to

$$\overline{\mathrm{BR}}(B_s \to \mu^+\mu^-) = (3.52 \pm 0.17(\mathrm{param.}) \pm 0.03(\mathrm{theo.})) \times 10^{-9}\,.$$

The detailed studies presented in this work, of aspects of both the SM and two extensions of it, will be tested by the next LHC run in proton-proton collisions at 14 TeV centre-of-mass energy. Whether the overall findings of the LHC reveal new dynamics at the TeV scale or whether they reconfirm the standard model is the central question of the present era of particle physics. One thing is certain, the energy reach and thus the discovery potential of the LHC are so large that a confirmation of the SM will cast doubt upon our current notion of naturalness. In this sense, high-energy particle physics is currently at a turning point with experimental input being the only way to determine the future direction. And therein lays the challenge and excitement of this time.

Appendix

A Gauge Flavour Symmetries

A.1 Feynmann Rules for MGF

In this Appendix we list the Feynman rules for the MGF model obtained from the Lagrangian in Eq. (2.5).

A.1.1 Couplings to SM Bosons

γ coupling

The photon coupling remains unchanged; proportional to the quark charges Q_u and Q_d.

G coupling

The gluon coupling remains unchanged; proportional to the colour generators $\lambda^a_{\mathrm{SU}(3)}$.

$W^\pm$ coupling

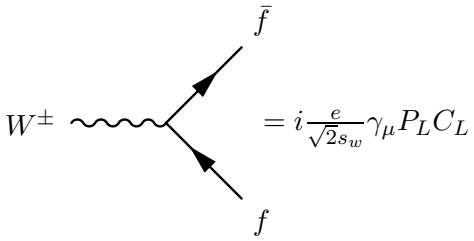

with the actual values for $\bar{f}$, f and C_L:

$$
\begin{array}{lcl}
W^+\bar{u}_i d_j & : & C_L = c_{uLi} V_{ij} c_{dLj} \\
W^+\bar{u}'_i d'_j & : & C_L = s_{uLi} V_{ij} s_{dLj} \\
W^+\bar{u}_i d'_j & : & C_L = c_{uLi} V_{ij} s_{dLj} \\
W^+\bar{u}'_i d_j & : & C_L = s_{uLi} V_{ij} c_{dLj}
\end{array}
$$

$$
\begin{array}{lcl}
W^-\bar{d}_j u_i & : & C_L = c_{uLi} V^*_{ij} c_{dLj} \\
W^-\bar{d}'_j u'_i & : & C_L = s_{uLi} V^*_{ij} s_{dLj} \\
W^-\bar{d}_j u'_i & : & C_L = s_{uLi} V^*_{ij} c_{dLj} \\
W^-\bar{d}'_j u_i & : & C_L = c_{uLi} V^*_{ij} s_{dLj}
\end{array}
$$

Z coupling

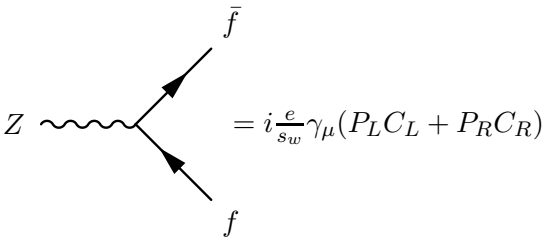

with the actual values for $\bar{f}$, f and C:

$$
\begin{array}{lcl}
Z\bar{u}_i u_i & : & C_R = -\frac{s_w^2}{c_w} Q_u \\
 & : & C_L = \frac{T^3_u c^2_{uLi} - s_w^2 Q_u}{c_w} \\
Z\bar{u}'_i u'_i & : & C_R = -\frac{s_w^2}{c_w} Q_u \\
 & : & C_L = +\frac{T^3_u s^2_{uLi} - s_w^2 Q_u}{c_w} \\
Z\bar{u}_i u'_i & : & C_R = 0 \\
 & : & C_L = +\frac{T^3_u}{c_w} c_{uLi} s_{uLi} \\
Z\bar{u}'_i u_i & : & C_R = 0 \\
 & : & C_L = +\frac{T^3_u}{c_w} c_{uLi} s_{uLi}
\end{array}
$$

$$
\begin{array}{lcl}
Z\bar{d}_i d_i & : & C_R = -\frac{s_w^2}{c_w} Q_d \\
 & : & C_L = \frac{T^3_d c^2_{dLi} - s_w^2 Q_d}{c_w} \\
Z\bar{d}'_i d'_i & : & C_R = -\frac{s_w^2}{c_w} Q_d \\
 & : & C_L = +\frac{T^3_d s^2_{dLi} - s_w^2 Q_d}{c_w} \\
Z\bar{d}_i d'_i & : & C_R = 0 \\
 & : & C_L = +\frac{T^3_d}{c_w} c_{dLi} s_{dLi} \\
Z\bar{d}'_i d_i & : & C_R = 0 \\
 & : & C_L = +\frac{T^3_d}{c_w} c_{dLi} s_{dLi}
\end{array}
$$

H coupling

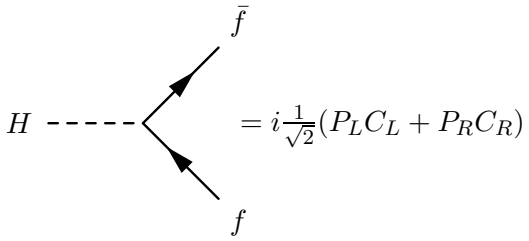

with the actual values for $\bar{f}$, f and C:

$$
\begin{array}{lcl}
H\bar{u}_i u_i & : & C_R = C_L = +\lambda_u s_{uRi} c_{uLi} \\
H\bar{u}'_i u'_i & : & C_R = C_L = -\lambda_u c_{uRi} s_{uLi} \\
H\bar{u}_i u'_i & : & C_R = C_L = -\lambda_u c_{uRi} c_{uLi} \\
H\bar{u}'_i u_i & : & C_R = C_L = +\lambda_u s_{uRi} s_{uLi}
\end{array}
$$

$$
\begin{array}{lcl}
H\bar{d}_i d_i & : & C_R = C_L = +\lambda_d s_{dRi} c_{dLi} \\
H\bar{d}'_i d'_i & : & C_R = C_L = -\lambda_d c_{dRi} s_{dLi} \\
H\bar{d}_i d'_i & : & C_R = C_L = -\lambda_d c_{dRi} c_{dLi} \\
H\bar{d}'_i d_i & : & C_R = C_L = +\lambda_d s_{dRi} s_{dLi}
\end{array}
$$

G_0 coupling

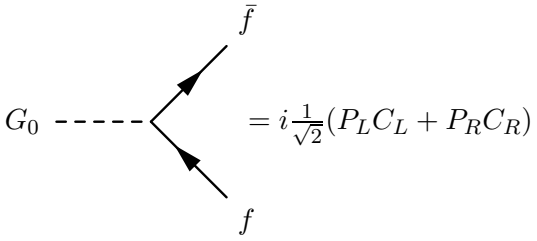

with the actual values for $\bar{f}$, f and C:

$$
\begin{array}{lcl}
G_0\bar{u}_i u_i & : & C_R = -C_L = -i\lambda_u s_{uRi} c_{uLi} \\
G_0\bar{u}'_i u'_i & : & C_R = -C_L = +i\lambda_u c_{uRi} s_{uLi} \\
G_0\bar{u}_i u'_i & : & C_R = -C_L = +i\lambda_u c_{uRi} c_{uLi} \\
G_0\bar{u}'_i u_i & : & C_R = -C_L = -i\lambda_u s_{uRi} s_{uLi}
\end{array}
$$

$$
\begin{array}{lcl}
G_0\bar{d}_i d_i & : & C_R = -C_L = +i\lambda_d s_{dRi} c_{dLi} \\
G_0\bar{d}'_i d'_i & : & C_R = -C_L = -i\lambda_d c_{dRi} s_{dLi} \\
G_0\bar{d}_i d'_i & : & C_R = -C_L = -i\lambda_d c_{dRi} c_{dLi} \\
G_0\bar{d}'_i d_i & : & C_R = -C_L = +i\lambda_d s_{dRi} s_{dLi}
\end{array}
$$

$G^{\pm}$ coupling

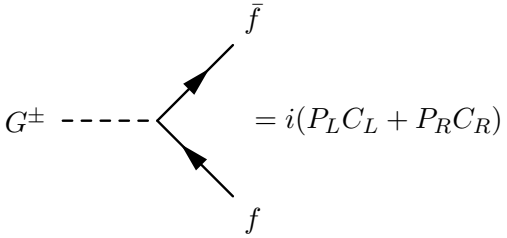

with the actual values for $\bar{f}$, f and C_L:

$$
\begin{array}{lcl}
G^+\bar{u}_i d_j & : & C_R = +\lambda_d c_{uLi} V_{ij} s_{dRj} \\
 & : & C_L = -\lambda_u s_{uRi} V_{ij} c_{dLj} \\
G^+\bar{u}'_i d'_j & : & C_R = -\lambda_d s_{uLi} V_{ij} c_{dRj} \\
 & : & C_L = +\lambda_u c_{uRi} V_{ij} s_{dLj} \\
G^+\bar{u}_i d'_j & : & C_R = -\lambda_d c_{uLi} V_{ij} c_{dRj} \\
 & : & C_L = +\lambda_u c_{uRi} V_{ij} c_{dLj} \\
G^+\bar{u}'_i d_j & : & C_R = +\lambda_d s_{uLi} V_{ij} s_{dRj} \\
 & : & C_L = -\lambda_u s_{uRi} V_{ij} s_{dLj}
\end{array}
$$

$$
\begin{array}{lcl}
G^-\bar{d}_j u_i & : & C_R = -\lambda_u s_{uRi} V^*_{ij} c_{dLj} \\
 & : & C_L = +\lambda_d c_{uLi} V^*_{ij} s_{dRj} \\
G^-\bar{d}'_j u'_i & : & C_R = +\lambda_u c_{uRi} V^*_{ij} s_{dLj} \\
 & : & C_L = -\lambda_d s_{uLi} V^*_{ij} c_{dRj} \\
G^-\bar{d}_j u'_i & : & C_R = +\lambda_u c_{uRi} V^*_{ij} c_{dLj} \\
 & : & C_L = -\lambda_d c_{uLi} V^*_{ij} c_{dRj} \\
G^-\bar{d}'_j u_i & : & C_R = -\lambda_u s_{uRi} V^*_{ij} s_{dLj} \\
 & : & C_L = +\lambda_d s_{uLi} V^*_{ij} s_{dRj}
\end{array}
$$

A.1.2 Couplings to Flavour Gauge Bosons

A_Q coupling

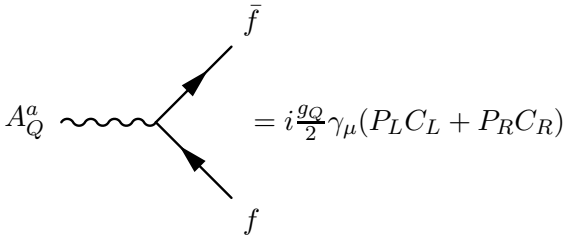

with the actual values for $\bar{f}$, f and C:

$$
\begin{aligned}
A_Q^a \bar{u}_i u_j \quad &: \quad C_R = +s_{uRi}(V\lambda^a_{\mathrm{SU}(3)}V^\dagger)_{ij}s_{uRj} \\
&: \quad C_L = +c_{uLi}(V\lambda^a_{\mathrm{SU}(3)}V^\dagger)_{ij}c_{uLj} \\
A_Q^a \bar{u}'_i u'_j \quad &: \quad C_R = +c_{uRi}(V\lambda^a_{\mathrm{SU}(3)}V^\dagger)_{ij}c_{uRj} \\
&: \quad C_L = +s_{uLi}(V\lambda^a_{\mathrm{SU}(3)}V^\dagger)_{ij}s_{uLj} \\
A_Q^a \bar{u}_i u'_j \quad &: \quad C_R = -s_{uRi}(V\lambda^a_{\mathrm{SU}(3)}V^\dagger)_{ij}c_{uRj} \\
&: \quad C_L = +c_{uLi}(V\lambda^a_{\mathrm{SU}(3)}V^\dagger)_{ij}s_{uLj} \\
A_Q^a \bar{u}'_i u_j \quad &: \quad C_R = -c_{uRi}(V\lambda^a_{\mathrm{SU}(3)}V^\dagger)_{ij}s_{uRj} \\
&: \quad C_L = +s_{uLi}(V\lambda^a_{\mathrm{SU}(3)}V^\dagger)_{ij}c_{uLj}
\end{aligned}
$$

$$
\begin{aligned}
A_Q^a \bar{d}_i d_j \quad &: \quad C_R = +s_{dRi}(\lambda^a_{\mathrm{SU}(3)})_{ij}s_{dRj} \\
&: \quad C_L = +c_{dLi}(\lambda^a_{\mathrm{SU}(3)})_{ij}c_{dLj} \\
A_Q^a \bar{d}'_i d'_j \quad &: \quad C_R = +c_{dRi}(\lambda^a_{\mathrm{SU}(3)})_{ij}c_{dRj} \\
&: \quad C_L = +s_{dLi}(\lambda^a_{\mathrm{SU}(3)})_{ij}s_{dLj} \\
A_Q^a \bar{d}_i d'_j \quad &: \quad C_R = -s_{dRi}(\lambda^a_{\mathrm{SU}(3)})_{ij}c_{dRj} \\
&: \quad C_L = +c_{dLi}(\lambda^a_{\mathrm{SU}(3)})_{ij}s_{dLj} \\
A_Q^a \bar{d}'_i d_j \quad &: \quad C_R = -c_{dRi}(\lambda^a_{\mathrm{SU}(3)})_{ij}s_{dRj} \\
&: \quad C_L = +s_{dLi}(\lambda^a_{\mathrm{SU}(3)})_{ij}c_{dLj}
\end{aligned}
$$

A_U coupling

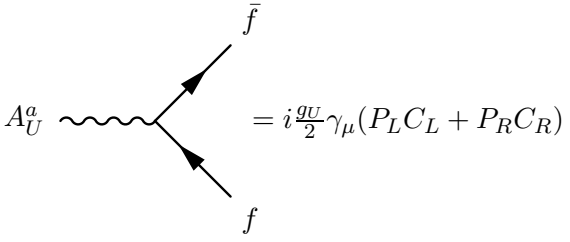

with the actual values for $\bar{f}$, f and C:

$$
\begin{aligned}
A_U^a \bar{u}_i u_j \quad &: \quad C_R = +c_{uRi}(\lambda^a_{\mathrm{SU}(3)})_{ij}c_{uRj} \\
&: \quad C_L = +s_{uLi}(\lambda^a_{\mathrm{SU}(3)})_{ij}s_{uLj} \\
A_U^a \bar{u}'_i u'_j \quad &: \quad C_R = +s_{uRi}(\lambda^a_{\mathrm{SU}(3)})_{ij}s_{uRj} \\
&: \quad C_L = +c_{uLi}(\lambda^a_{\mathrm{SU}(3)})_{ij}c_{uLj} \\
A_U^a \bar{u}_i u'_j \quad &: \quad C_R = +c_{uRi}(\lambda^a_{\mathrm{SU}(3)})_{ij}s_{uRj} \\
&: \quad C_L = -s_{uLi}(\lambda^a_{\mathrm{SU}(3)})_{ij}c_{uLj} \\
A_U^a \bar{u}'_i u_j \quad &: \quad C_R = +s_{uRi}(\lambda^a_{\mathrm{SU}(3)})_{ij}c_{uRj} \\
&: \quad C_L = -c_{uLi}(\lambda^a_{\mathrm{SU}(3)})_{ij}s_{uLj}
\end{aligned}
$$

A_D coupling

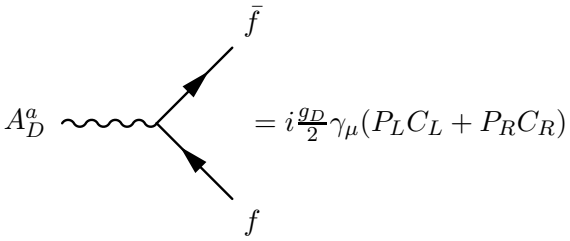

with the actual values for $\bar{f}$, f and C:

$$
\begin{aligned}
A_D^a \bar{d}_i d_j \quad &: \quad C_R = +c_{dRi}(\lambda^a_{\mathrm{SU}(3)})_{ij}c_{dRj} \\
&: \quad C_L = +s_{dLi}(\lambda^a_{\mathrm{SU}(3)})_{ij}s_{dLj} \\
A_D^a \bar{d}'_i d'_j \quad &: \quad C_R = +s_{dRi}(\lambda^a_{\mathrm{SU}(3)})_{ij}s_{dRj} \\
&: \quad C_L = +c_{dLi}(\lambda^a_{\mathrm{SU}(3)})_{ij}c_{dLj} \\
A_D^a \bar{d}_i d'_j \quad &: \quad C_R = +c_{dRi}(\lambda^a_{\mathrm{SU}(3)})_{ij}s_{dRj} \\
&: \quad C_L = -s_{dLi}(\lambda^a_{\mathrm{SU}(3)})_{ij}c_{dLj} \\
A_D^a \bar{d}'_i d_j \quad &: \quad C_R = +s_{dRi}(\lambda^a_{\mathrm{SU}(3)})_{ij}c_{dRj} \\
&: \quad C_L = -c_{dLi}(\lambda^a_{\mathrm{SU}(3)})_{ij}s_{dLj}
\end{aligned}
$$

A.2 Couplings of the lightest Flavour-gauge Boson

To illustrate the mechanism of inverted hierarchies described in Sec. 2.2, we present the couplings of the lightest flavour-gauge boson in the MGF construction. In Fig. A.1 and A.2 we give

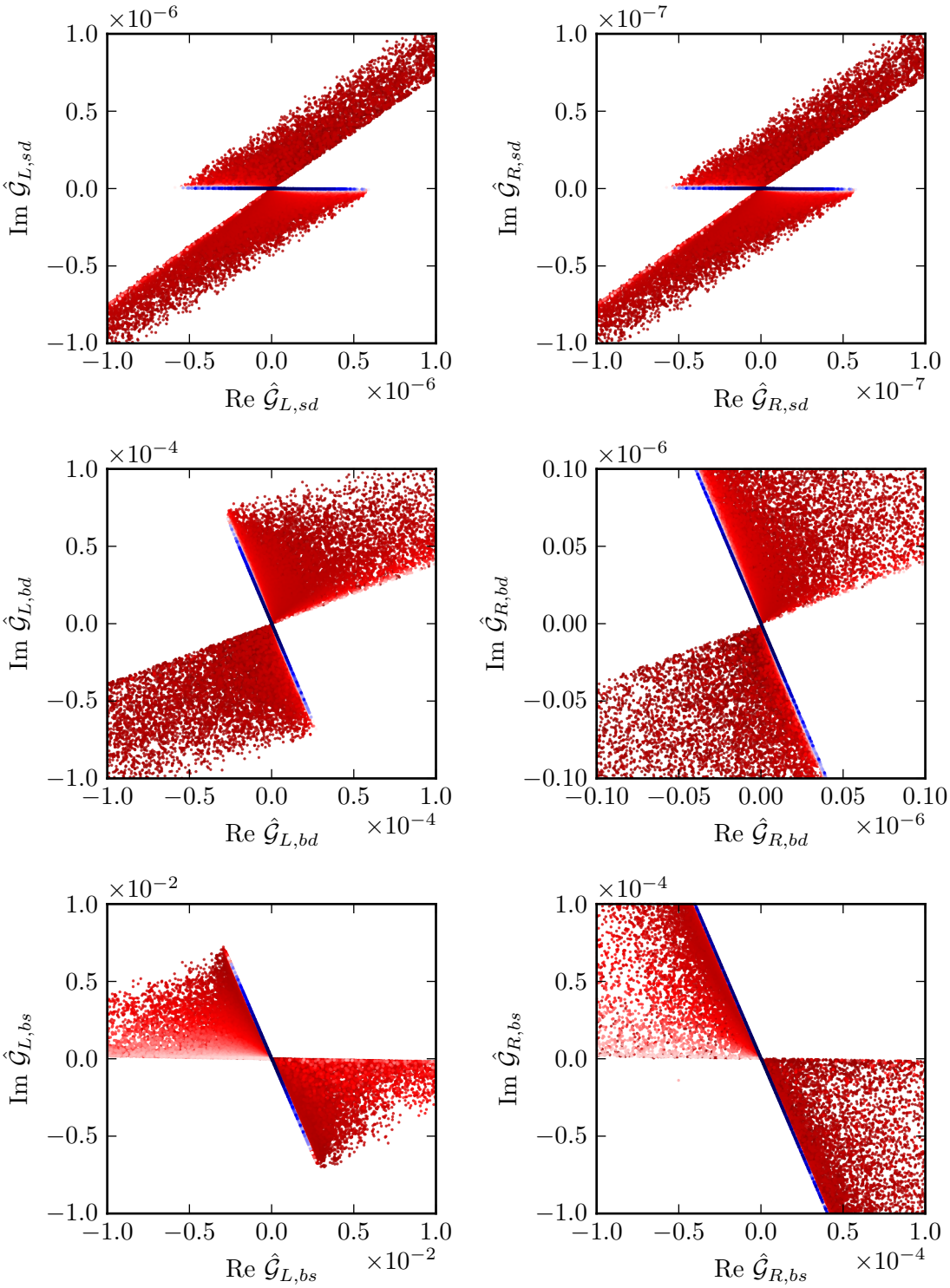

Figure A.1: *The couplings of the lightest flavour-gauge boson to the SM down-type quarks.*

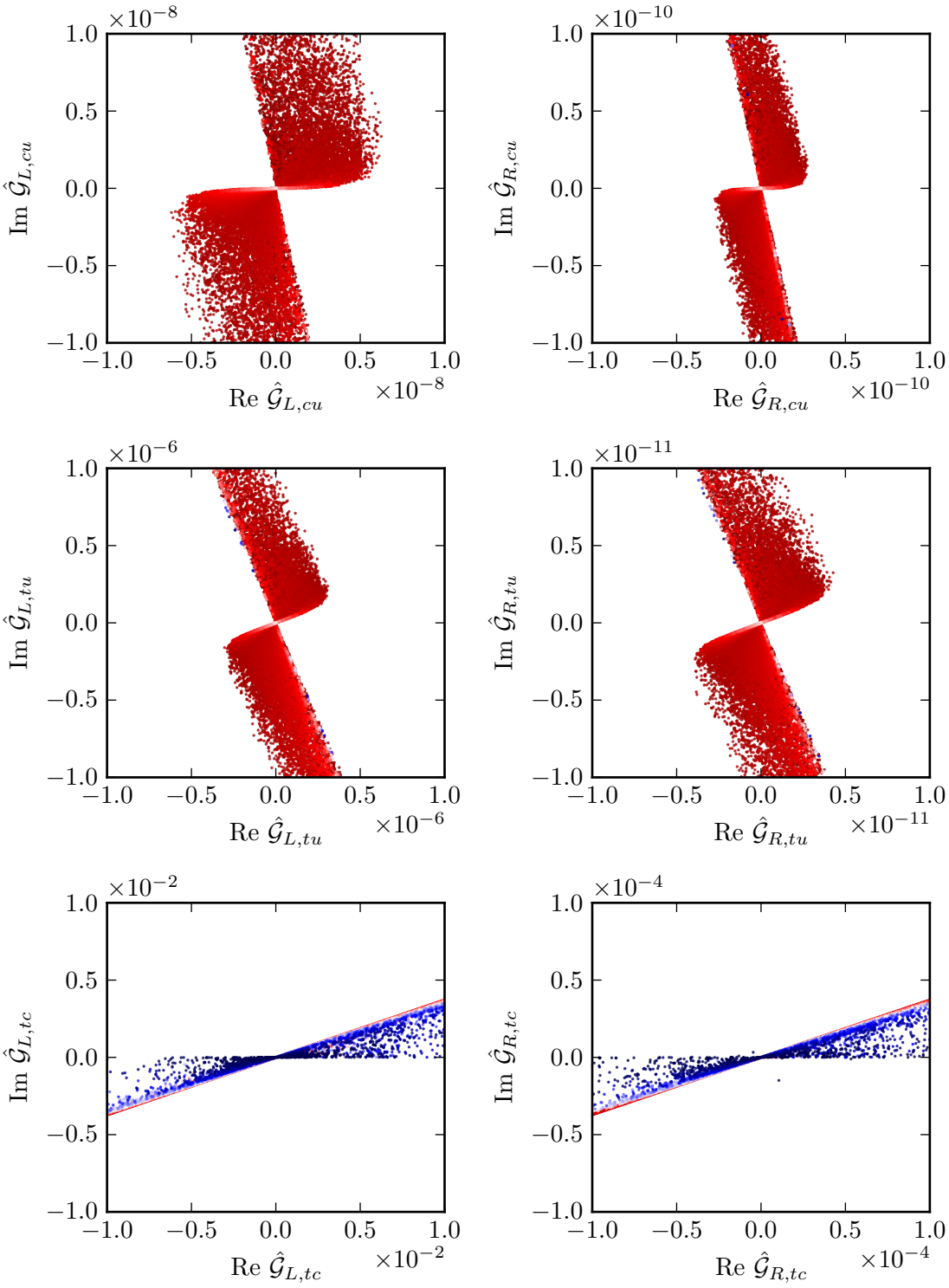

Figure A.2: *The couplings of the lightest flavour-gauge boson to the SM up-type quarks.*

the couplings of the lightest gauge boson to the light down- and up-type quarks for the exclusive V_{ub} case by scattering all the parameters of the model. The colour-coding corresponds to the mass splitting of the lightest to the next-to-lightest flavour-gauge-boson mass: red points correspond to a large splitting and blue points to complete degeneracy. We observe that the flavour-violating couplings within the first two generations are in general the smallest ones, while the opposite is true for the couplings within the last two generations. This is related to the sequential breaking of the flavour symmetry encoded into the hierarchical structure of the flavon vevs and the mechanism of inverted hierarchies.

B New Strong Interactions in Top Physics

B.1 Flavour Symmetry Breaking

Flavour symmetry breaking due to $m_{\mathcal{Q}_1} \neq m_{\mathcal{Q}_3}$ splits the vector-nonet in non-degenerate mass eigenstates and can lead to potentially large differences in their partial widths to pseudoscalars. We consider first the case of ideal mixing of $\rho_8^{\rm HC}$ and $\rho_9^{\rm HC}$ that produces the ideally-mixed states in Eq. (6.9). Dropping the HC super/subscripts, we find the partial widths to HC pseudoscalars from Eq. (6.11) to be

$$\frac{\Gamma_\rho}{m_\rho} = \frac{g^2_{\rho\pi\pi}}{48\pi}\left(1-\frac{4m_\pi^2}{m_\rho^2}\right)^{3/2} + \frac{g^2_{\rho KK}}{96\pi}\left(1-\frac{4m_K^2}{m_\rho^2}\right)^{3/2}, \tag{B.1}$$

$$\frac{\Gamma_{K^*}}{m_{K^*}} = \frac{g^2_{K^*K\pi}}{64\pi}\mathrm{PS}\left[1,\frac{m_\pi^2}{m_{K^*}^2},\frac{m_K^2}{m_{K^*}^2}\right]^3 + \frac{g^2_{K^*K\eta_8}}{64\pi}\mathrm{PS}\left[1,\frac{m_{\eta_8}^2}{m_{K^*}^2},\frac{m_K^2}{m_{K^*}^2}\right]^3, \tag{B.2}$$

$$\frac{\Gamma_\phi}{m_\phi} = \frac{g^2_{\rho^8 KK}}{48\pi}\left(1-4\frac{m_K^2}{m_\phi^2}\right)^{3/2}, \tag{B.3}$$

$$\frac{\Gamma_\omega}{m_\omega} = \frac{g^2_{\rho^8 KK}}{96\pi}\left(1-4\frac{m_K^2}{m_\omega^2}\right)^{3/2}, \tag{B.4}$$

with $\mathrm{PS}\,[x,y,z] = (x^2+y^2+z^2-2xy-2xz-2yz)^{1/2}$. For simplicity, we have neglected $\eta-\eta'$ mixing, and assumed that the flavour singlet η_0 is too heavy to be pair produced in decays of the vectors, like the η' in QCD.

We find that for $m_{\mathcal{Q}_1} < m_{\mathcal{Q}_3}$ the $\rho^{\rm HC}$ may be significantly broader than $K^{*\rm HC}$, $\phi^{\rm HC}$ and $\omega^{\rm HC}$, which decay to pseudoscalars with a $\mathcal{Q}_3$ constituent. Also, increasing $m_{\mathcal{Q}_3}$ kinematically suppresses the $K^* \to K\pi$ and $K^* \to K\eta_8$ decays and thus increases the branching ratio of $K^* \to u\bar{t}$. In this way, $m_{\mathcal{Q}_3}$ controls the magnitude of the associated production of $t\bar{t}$ pair discussed in chapter 9.

For departures from ideal mixing the mass eigenstates V_L and V_H do not coincide with ω and ϕ. In the conventions of Ref. [74], we have

$$\begin{pmatrix}|V_L\rangle\\ |V_H\rangle\end{pmatrix} = \begin{pmatrix}\cos\theta_V & \sin\theta_V\\ -\sin\theta_V & \cos\theta_V\end{pmatrix}\begin{pmatrix}|\rho^0\rangle\\ |\rho^8\rangle\end{pmatrix}, \tag{B.5}$$

where $\cos\theta_V \stackrel{!}{=} \cos\theta_{\rm dec} \equiv \sqrt{2/3}$ corresponds to ideal mixing, in which case $|V_L\rangle = |\Omega\rangle$ and $|V_H\rangle = -|\Phi\rangle$. The decay widths of V_L and V_H then read:

$$\frac{\Gamma_{V_L}}{m_{V_L}} = \frac{g_\rho^2}{32\pi}\sin^2\theta_V\left(1-4\frac{m_K^2}{m_{V_L}^2}\right)^{3/2}, \tag{B.6}$$

$$\frac{\Gamma_{V_H}}{m_{V_H}} = \frac{g_\rho^2}{32\pi}\cos^2\theta_V\left(1-4\frac{m_K^2}{m_{V_H}^2}\right)^{3/2}. \tag{B.7}$$

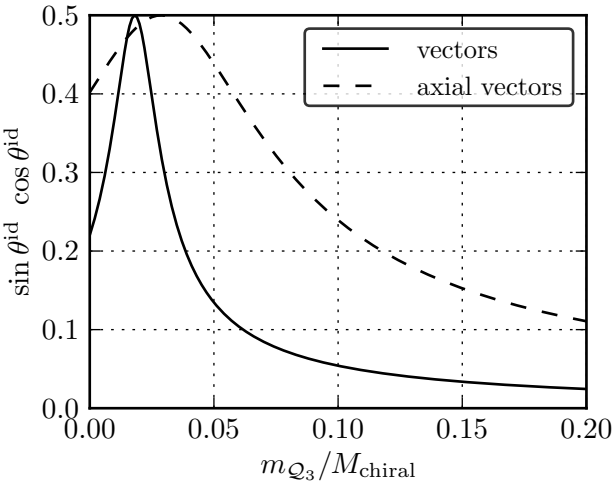

Figure B.1: *The behaviour of* $\sin\theta^{\rm id}\cos\theta^{\rm id}$ *for vectors and axial vectors in solid and dashed lines, respectively, using the quark model presented in Ref. [74] in the representative case of* $m_{\mathcal{Q}_1} = 3\ GeV$ *and* $M_{\rm chiral} = M_{\rho^{\rm HC}[m_{\mathcal{Q}}=0]} = 200\ GeV$.

We define the angle $\theta_V^{\rm id}$ as the deviation from the ideal mixing case by

$$\theta_V^{\rm id} \equiv \theta_V - \theta_{\rm dec} \tag{B.8}$$

leading to

$$\begin{aligned} \cos\theta_V^{\rm id} &= +\sqrt{2/3}\cos\theta_V + \sqrt{1/3}\sin\theta_V\,, \\ \sin\theta_V^{\rm id} &= -\sqrt{1/3}\cos\theta_V + \sqrt{2/3}\sin\theta_V\,. \end{aligned} \tag{B.9}$$

In this case, the coupling of the mass eigenstates V_L and V_H to the HC quarks, in the approximation of universal couplings of to the HC quarks ($g_\rho = g_\rho^9$), are

$$\begin{aligned} \mathcal{L} = \ & g_\rho \bar{u}_i' \left(\cos\theta_V^{\rm id}\ T_{ij}^{10} - \sin\theta_V^{\rm id}\ T_{ij}^{11}\right) \not{V}_L u_j' \\ & - g_\rho \bar{u}_i' \left(\sin\theta_V^{\rm id}\ T_{ij}^{10} + \cos\theta_V^{\rm id}\ T_{ij}^{11}\right) \not{V}_H u_j'\,, \end{aligned} \tag{B.10}$$

where we have introduced for convenience the diagonal matrices

$$T^{10} = \frac{1}{2}\begin{pmatrix} 1 & 0 & 0 \\ 0 & 1 & 0 \\ 0 & 0 & 0 \end{pmatrix} \quad \text{and} \quad T^{11} = \frac{1}{\sqrt{6}}\begin{pmatrix} 0 & 0 & 0 \\ 0 & 0 & 0 \\ 0 & 0 & 1 \end{pmatrix}$$

to best illustrate the deviations from the ideal mixing.

In Fig. B.1 we plot the product $\sin\theta^{\rm id}\cos\theta^{\rm id}$ for both vectors and axial vectors obtained from the quark model constructed in Ref. [74]. We observe that ideal mixing is rapidly obtained for values of $m_{\mathcal{Q}_3}$ that are $m_{\mathcal{Q}_3} \ll M_{\rm chiral}$. The decrease is even more rapid in the vector case.

B.2 Vector Meson Dominance

Vector meson dominance is the experimental observation that at low momentum transfer, q^2, photons do not interact with pions as if they were point-like particles, but through a form factor, which turns out to be dominated by the lowest lying vector resonance, the ρ meson [162]. Nambu had already considered the possibility of describing electron-nucleon scattering through massive vectors [163] and Sakurai [164] proposed models to describe electromagnetic interactions of pions that treated the ρ meson as a gauge field. We refer to Ref. [165] and references within for a modern, more detailed, review on aspects of VMD.

The observation of VMD means that at least the pion-photon interaction is well described by a mixing of the photon to the ρ meson and its subsequent coupling to the pions. Therefore, from the mass and decay constant of the ρ we can infer the coupling of the ρ meson to pions, which has little to do with electromagnetism.

In the HC model the situation is similar, VMD is the assumption that the form factors of resonances are dominated by the current of the interpolating vector meson. Here, we sketch a derivation of the consequence of this assumption using a pole theorem stating that amplitudes at a certain momentum transfer, q^2, factorise in two amplitudes and a pole as the momentum transfer approaches the mass of a physical state (see chapter 10 from the QFT book of Weinberg).

As an example, we consider the q^2 dependence of the "nucleon" form factor $\langle u'|J^{a\mu}|u'\rangle$, where the current is given by the interpolating current of the V_o:

$$J^{a\mu} = \mathcal{S}^* \overset{\leftrightarrow}{\partial}_\mu \mathcal{T}^a \mathcal{S}\,. \tag{B.11}$$

The current has a non-vanishing matrix element between a V_o^a state and the vacuum given by Eq. (6.32). The pole theorem states that as $q^2 \to M_{V_o}^2$:

$$\langle u'|J^{a\mu}|u'\rangle \to \langle u'|u'V_o^a\rangle \frac{1}{q^2 - M_{V_o}^2} \langle V_o^a|J^{a\mu}|0\rangle\,. \tag{B.12}$$

Inserting Eq. (6.32) and the first matrix element using the effective Lagrangian Eq. (6.33) we find for $q^2 \to M_{V_o}^2$:

$$\langle u'|J^{a\mu}|u'\rangle \to g_{V_o} \frac{f_{V_o} M_{V_o}}{q^2 - M_{V_o}^2} \bar{u}' \mathcal{T}^a \gamma_\mu u'\,. \tag{B.13}$$

Here, we used $\sum \epsilon_\mu \epsilon_\nu^* = g_{\mu\nu} + q_\mu q_\nu / M_{V_o}^2$ and the Dirac equation. The VMD hypothesis is that this limit is also a good approximation as $q^2 \to 0$. We can obtain this limiting value another way from the general parameterisation

$$\langle u'|J^{a\mu}(0)|u'\rangle = \bar{u}' \mathcal{T}^a [\gamma_\mu f_1(q^2) + \frac{i\sigma_{\mu\nu}}{2M_{u'}} q^\nu f_2(q^2)] u'\,, \tag{B.14}$$

with the normalisation condition $f_1(0) = 1$ obtained using the conservation of the current $J^{a\mu}$. Equating Eqs. (B.13) and (B.14) for $q^2 \to 0$ gives the VMD estimate for the HC coupling:

$$g_{V_o} = \frac{M_{V_o}}{f_{V_o}}\,. \tag{B.15}$$

Similarly, we can derive the VMD estimates for vector and axial-vector HC couplings to composite quarks.

C Electroweak Corrections to $B_q \to \ell^+\ell^-$

C.1 Details on the Standard Model Calculation

The two-loop EW SM calculation is similar to the analogous calculation for the $K \to \pi\nu\bar{\nu}$ decays [55]. The calculation comprises of generating and calculating all two-loop Feynman diagrams for the transition $b \to q\,\ell^+\ell^-$ (Fig. 7.1) and renormalising the amplitude.

We perform two independent calculations. We use `QGRAF` [166] to generate the topologies and a self-written `FORM` [78] program to calculate the amplitudes. In the independent calculation, Martin Gorbahn uses `FeynArts` [167] and a self-written `Mathematica` program for the respective tasks. By setting the external momenta and the masses of all fermions except for the top quark to zero, all diagrams reduce to massive vacuum diagrams with maximally three different masses. We reduce them to a few known master integrals using the recursion relations from Refs. [90, 168].

In order to match the SM to the effective theory with canonically normalised fields in a single step, it is necessary to also canonically renormalise the SM fields. We renormalise the bare fields in the Lagrangian by matrix-valued field renormalisation constants [169], e.g. for the left-handed down-type fields

$$d_{L,i}^{\text{bare}} = \sqrt{Z_{d,ij}^{L}}\, d_{L,j}\,, \tag{C.1}$$

with $i = 1, 2, 3$. The constants $Z_{d,ij}^{L}$ have an expansion in α_e and in dimensional regularisation, where $d = 4 - 2\varepsilon$, also in ε. A theory with canonically-normalised fields means that the two-point functions of two fields yield the tree-level propagator if the fields have the same flavour and vanish otherwise at all orders. As all external fields are massless in our computation, this is a renormalisation condition for the field-renormalisation constants. For two down-type quarks i and j the Feynman diagram interpretation of the renormalisation condition is:

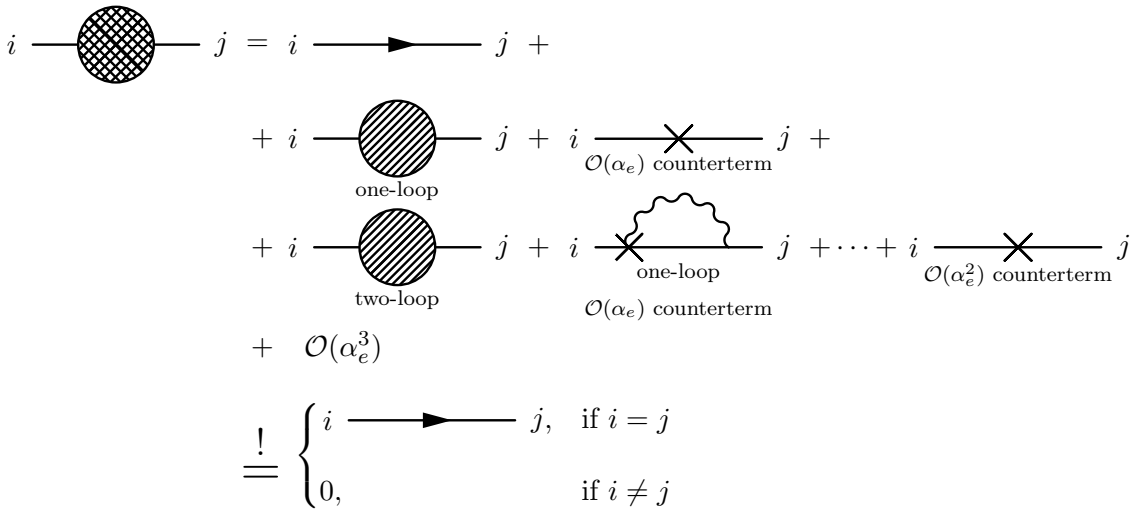

With one- and two-loop we denote the sum of all one- and two-loop diagrams. Crosses denote counterterms. Ref. [169] gives the complete set of the SM Feynman rules in $R_\xi = 1$. We evaluate all two-point functions in an expansion up to first order in external momenta. From the second line we obtain the $\mathcal{O}(\alpha_e)$ counterterms up to order $\mathcal{O}(\varepsilon)$ and from the condition in the third line we extract the $\mathcal{O}(\alpha_e^2)$ part the off-diagonal field renormalisation $Z^L_{d,ij}$ with $i \neq j$. This is the only two-loop renormalisation constant necessary for our calculation.

The counterterm of the CKM matrix is also determined by the field renormalisation constants Z^L_{ij} of the up- and down-quark fields [169]. This renormalisation prescription corresponds to a definition of the CKM elements in the effective theory where the kinetic terms of all light quark fields are canonical.

We work in dimensional regularisation, which raises the question of how to treat γ_5 in $d \neq 4$ dimensions. The naive anticommutation relation (NDR) $\{\gamma_5, \gamma_\mu\} = 0$ can lead to algebraic inconsistencies in the evaluation of traces with γ_5's. Yet, the algebraically consistent definition of γ_5 by 't Hooft-Veltman (HV) [170] leads to spurious breaking of the axial-current Ward identities and as such requires the incorporation of symmetry restoring finite counterterms. After incorporating the appropriate finite renormalisation for non-singlet axial currents, the respective diagrams computed in the HV scheme agree with the NDR calculation [171]. Accordingly, we use the HV definition of γ_5 only for diagrams with axial couplings to internal fermion loops. For these diagrams, the finite renormalisation that will restore the axial anomaly relation of diagrams with fermion traces [172] will drop out in our calculation after the sum over the complete set of SM fermions is performed. The effective theory calculation does not involve fermion traces with γ_5 and for this reason can be performed completely in the NDR scheme.

C.2 Details on the Effective Theory Calculation

To evaluate the two-loop $b \to q\,\ell^+\ell^-$ amplitude in the effective theory we need to know all Wilson coefficients and renormalisation constants appearing in Eq. (7.19). The tree-level contribution $\mathcal{C}_2^{(00)}$ and the one-loop results $\mathcal{C}_9^{(11)}$ and $\mathcal{C}_{10}^{(11)}$ are given in [90] including the $\mathcal{O}(\varepsilon)$ terms for the latter two. We reproduce their results by an explicit matching calculation. Here, we give the missing one-loop Wilson coefficients of the two evanescent operators

$$c_{E_9}^{(11)} = c_{E_{10}}^{(11)} = \frac{1}{16 s_W^2} \frac{x_t}{(x_t-1)^2} \left(1 - x_t + \log x_t\right) + \mathcal{O}(\varepsilon)\,. \tag{C.2}$$

The $\mathcal{O}(\varepsilon)$ terms of $c_{E_9}^{(11)}$ and $c_{E_{10}}^{(11)}$ do not contribute to the matching as the mixing renormalisation constants $\hat{Z}^{(1)}_{E_9,10}$ and $\hat{Z}^{(1)}_{E_{10},10}$ carry no divergent terms, only finite ones. $c_{E_9}^{(11)}$ and $c_{E_{10}}^{(11)}$ come solely from one-loop box diagrams in the SM. Z-penguin diagrams do not contribute because of their simpler Dirac algebra.

Having all relevant Wilson coefficients, we return to the renormalisation constants. We fix field- and coupling-renormalisation constants by extracting the UV poles of the appropriate photonic one-loop diagrams in the five-flavour theory. The results are:

$$Z_i = 1 + \tilde{\alpha}_e\, Z_i^{(1)} + \ldots \tag{C.3}$$

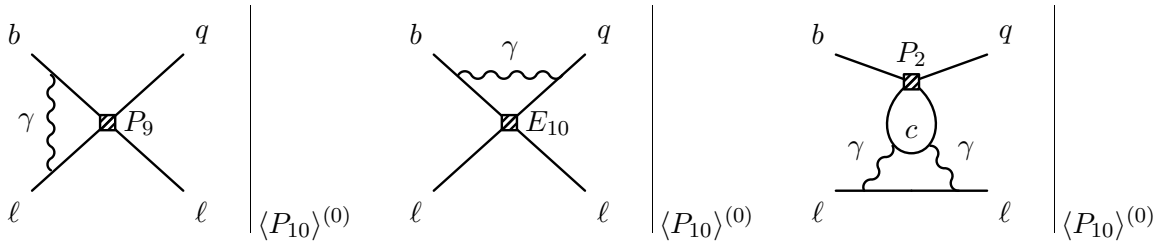

Figure C.1: *One- and two-loop diagrams of operator insertions projected on the tree-level matrix element $\langle P_{10}\rangle^{(0)}$. Their UV poles are subtracted by mixing-renormalisation constants. Finite terms are also subtracted in evanescent-operator insertions. P_2 mixes at two-loop in P_{10}, a true penguin indeed.*

with

$$Z_d^{(1)} = -\frac{1}{9\varepsilon}\,, \qquad Z_\ell^{(1)} = -\frac{1}{\varepsilon}\,, \qquad Z_e^{(1)} = -\frac{40}{9\varepsilon}\,.$$

We proceed similarly for the constants governing the mixing of operators into P_{10}. We calculate the UV poles of all one-loop insertions of given operator, project on the tree-level matrix element of P_{10} and absorb the left-over pole in the renormalisation constants of the Wilson coefficients.

For the case of physical operators mixing into physical ones, we absorb only the divergences into the constants $\hat{Z}_{P,P}$. For evanescent operators this is not the case. Evanescent operators vanish in four dimensions and at each order in perturbation theory their operator basis needs to be extended. To ensure that the Wilson coefficients at a given fixed order are independent from the choice of evanescent operators in some higher order, we include finite terms in $\hat{Z}_{E,P}$ and completely cancel the mixing of evanescent to physical operators.

We have calculated all contributing one-loop mixing renormalisation constants. The mixing of physical operators can also be extracted from the anomalous dimension matrices in [83, 81]. Here, we also report constants for the mixing of evanescent to physical operators

$$\begin{aligned} \hat{Z}_{2,10}^{(1)} &= 0\,, \\ \hat{Z}_{9,10}^{(1)} &= -\frac{2}{\varepsilon}\,, \qquad & \hat{Z}_{10,10}^{(1)} &= 0\,, \\ \hat{Z}_{E_9,10}^{(1)} &= \frac{32}{3}\,, \qquad & \hat{Z}_{E_{10},10}^{(1)} &= 0\,. \end{aligned} \tag{C.4}$$

The only two-loop renormalisation needed is the two-loop mixing of P_2 into P_{10}, $\hat{Z}_{2,10}^{(2)}$. We extract its $1/\varepsilon$-part from the corresponding anomalous dimension in [83] and calculated the $1/\varepsilon^2$-term ourselves

$$\hat{Z}_{2,10}^{(2)} = \frac{4}{9\varepsilon^2} - \frac{26}{27\varepsilon}\,. \tag{C.5}$$

Fig. C.1 shows a sample of the diagrams whose UV poles we absorb in mixing-renormalisation constants.

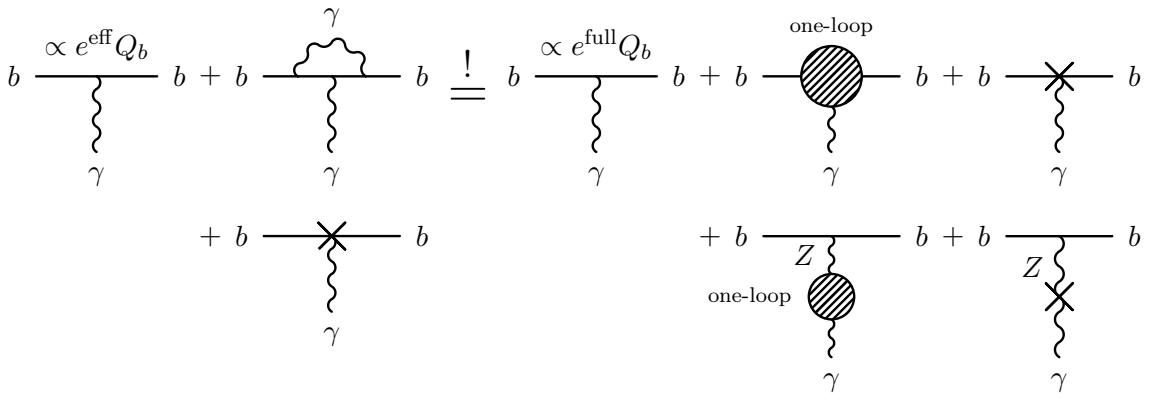

Figure C.2: *The one-loop matching for the $b \to b\gamma$ amplitude. On the left the effective theory amplitudes, on the right the SM amplitudes. Crosses refer to counterterm insertions and hatched blobs to the sum of all corresponding diagrams. e^{full} and e^{eff} are the electromagnetic-coupling constants in the two theories and Q_b the electric charge of the b quark.*

C.3 Threshold Corrections for α_e

The $\overline{\text{MS}}$ coupling α_e in the SM is not the same as the $\overline{\text{MS}}$ coupling α_e in the five-flavour effective theory. And none of them is the $\overline{\text{MS}}$ coupling reported in Ref. [39] that we use as a numerical input (Tab. 8.1). The running of the six-flavour coupling, α_e^{full}, is controlled by the β functions of the full $\text{SU}(3)_c \times \text{SU}(2)_L \times \text{U}(1)_Y$ theory, the five-flavour coupling, α_e^{eff}, by the QCD and QED β functions only, and the PDG coupling, α_e^{PDG}, is the $\overline{\text{MS}}$ coupling in the SM with the top-quark decoupled.

Therefore, to apply Eq. (7.1) and obtain the Wilson coefficients we need to relate α_e^{full} to α_e^{eff}. The relation depends on the renormalisation scheme for α_e. One possibility is to impose the equality of the coupling constant at the matching scale:

$$\alpha_e^{\text{eff}}(\mu_0) \stackrel{!}{=} \alpha_e^{\text{full}}(\mu_0)\,. \tag{C.6}$$

This procedure requires us to absorb contributions from heavy particles in the finite part of the coupling-renormalisation constant Z_e^{full}, it is not $\overline{\text{MS}}$ renormalisation. We prefer to renormalise both couplings α_e^{full} and α_e^{eff} in the $\overline{\text{MS}}$ scheme in which case

$$\alpha_e^{\text{eff}}(\mu_0) \neq \alpha_e^{\text{full}}(\mu_0)\,. \tag{C.7}$$

The couplings are related through threshold corrections that affect the analytic expression of $\mathcal{C}_{10}^{(22)}$ in the single-G_F normalisation. In the quadratic-G_F normalisation the LO Wilson coefficient is free from α_e and $\mathcal{C}_{10}^{(22)}$ is unaffected.

We calculate the threshold corrections by matching the amplitudes of the effective theory to the SM ones for the process $b \to b\,\gamma$ at $\mathcal{O}(\alpha_e)$. Fig. C.2 shows a diagrammatic interpretation of the matching. The photon is an external state in this matching. Therefore, following our discussion in App. C.1, we calculate the $Z-\gamma$ and $\gamma-\gamma$ two-point functions and fix the finite

terms of the corresponding field-renormalisation constants. The result of the matching yields

$$\begin{aligned} \alpha_e^{\text{full}} &= \alpha_e^{\text{eff}} \left(1 + \frac{\alpha_e^{\text{eff}}}{4\pi}\Delta\alpha_e\right), \qquad \text{with} \\ \Delta\alpha_e &= -\frac{2}{3} - 7\ln\frac{\mu^2}{M_W^2} + \frac{16}{9}\ln\frac{\mu^2}{M_t^2}\,. \end{aligned} \tag{C.8}$$

The first two terms come from the decoupling of the weak gauge bosons. The last one from the decoupling of the top quark. Therefore, we also obtain the relation to the PDG coupling, α_e^{PDG}:

$$\alpha_e^{\text{full}} = \alpha_e^{\text{PDG}} \left(1 + \frac{\alpha_e^{\text{PDG}}}{4\pi}\Delta^{\text{top}}\alpha_e\right), \tag{C.9}$$

$$\alpha_e^{\text{eff}} = \alpha_e^{\text{PDG}} \left(1 + \frac{\alpha_e^{\text{PDG}}}{4\pi}\Delta^{\text{gauge}}\alpha_e\right), \tag{C.10}$$

with

$$\Delta^{\text{top}}\alpha_e = \frac{16}{9}\ln\frac{\mu^2}{M_t^2} \qquad \text{and} \qquad \Delta^{\text{gauge}}\alpha_e = \frac{2}{3} + 7\ln\frac{\mu^2}{M_W^2}. \tag{C.11}$$

We use Eqs. (C.9) and (C.10) to obtain $\alpha_e^{\text{full}}(M_Z^{\text{pole}})$ and $\alpha_e^{\text{eff}}(M_Z^{\text{pole}})$ from the PDG input in Tab. 8.1. In the matching, we apply Eq. (C.8) to substitute $\alpha_e^{\text{full}} \to \alpha_e^{\text{eff}}$ in the expansion of the SM amplitude in Eq. (7.11):

$$\tilde{\alpha}_e^{\text{full}} A^{(1)}_{\text{full},\,10} + \left(\tilde{\alpha}_e^{\text{full}}\right)^2 A^{(2)}_{\text{full},\,10} = \tilde{\alpha}_e^{\text{eff}} A^{(1)}_{\text{full},\,10} + \left(\tilde{\alpha}_e^{\text{eff}}\right)^2 \left[A^{(2)}_{\text{full},\,10} + \Delta\alpha_e\, A^{(1)}_{\text{full},\,10}\right], \tag{C.12}$$

after which we can consistently extract $\mathcal{C}_{10}^{(22)}$ from equating SM with effective theory amplitudes at $\mathcal{O}(\alpha_e^2)$.

C.4 Details on the Renormalisation Group Evolution

General

The dependence of the Wilson coefficients $\mathcal{C}_i$ on the renormalisation scale μ is governed by the anomalous dimension matrix (ADM) $\hat{\gamma}$:

$$\mu\frac{d}{d\mu}\mathcal{C}_i(\mu) = \left[\hat{\gamma}^T(\mu)\right]_{ij}\mathcal{C}_j(\mu)\,, \tag{C.13}$$

with the expansion in the couplings

$$\hat{\gamma}(\mu) = \sum_{\substack{m,n=0 \\ m+n\geq 1}} \tilde{\alpha}_s(\mu)^m \tilde{\alpha}_e(\mu)^n\, \hat{\gamma}_{(mn)}\,, \tag{C.14}$$

which is known up to and including relevant entries in $(mn) = (30)$ and (21). It has been solved as an expansion in terms of the small quantities [81]

$$\omega \equiv 2\beta_{00}^s\,\tilde{\alpha}_s(\mu_0), \tag{C.15}$$

$$\lambda \equiv \frac{\beta_{00}^e}{\beta_{00}^s}\frac{\tilde{\alpha}_e(\mu_0)}{\tilde{\alpha}_s(\mu_0)} \equiv \frac{\beta_{00}^e}{\beta_{00}^s}\kappa(\mu_0)\,, \tag{C.16}$$

with $\beta^e_{(00)}$ and $\beta^s_{(00)}$ the leading terms in the β function of the electromagnetic and strong coupling, respectively. In this new expansion, the evolution operator (7.24) is

$$U(\mu_b, \mu_0) = \sum_{m,n\geq 0}^{2} \omega^m \lambda^n U_{(mn)}\,, \tag{C.17}$$

excluding the term $(mn) = (22)$ that requires the knowledge of higher-order contributions to the ADM. The $U_{(mn)}$'s are given in Ref. [81], whereas the initial Wilson coefficients of the single-G_F normalisation at the scale μ_0 have the expansion

$$\begin{aligned} c_i(\mu_0) = c_i^{(00)} &+ \omega \frac{c_i^{(10)}}{2\beta^s_{00}} + \omega^2 \frac{c_i^{(20)}}{(2\beta^s_{00})^2} \\ &+ \omega\lambda \frac{c_i^{(11)}}{2\beta^e_{00}} + \omega^2\lambda \frac{c_i^{(21)}}{4\beta^e_{00}\beta^s_{00}} + \omega^2\lambda^2 \frac{c_i^{(22)}}{(\beta^e_{00})^2}\,. \end{aligned} \tag{C.18}$$

The components $C_{i,(mn)}$ of the downscaled Wilson coefficients in Eq. (7.25) are then obtained from the reexpansion of Eq. (7.24) in the new parameters $\tilde{\alpha}_s(\mu_b)$ from

$$\omega = 2\beta^s_{00}\,\eta\,\tilde{\alpha}_s(\mu_b)\,, \tag{C.19}$$

and $\kappa(\mu_b)$ from

$$\begin{aligned} \lambda = \frac{\beta^e_{00}}{\beta^s_{00}} \frac{\kappa(\mu_b)}{\eta} \Big[1 &+ \kappa(\mu_b) A_1(\eta) \\ &+ \tilde{\alpha}_s(\mu_b)\kappa(\mu_b) A_2(\eta) + \mathcal{O}\left(\kappa^2, \tilde{\alpha}_s^2\right)\Big] \end{aligned} \tag{C.20}$$

by inserting them in Eqs. (C.17) and (C.18). The coefficients $A_{1,2}(\eta)$ are listed Ref. [81].

Solution

We present the full solution of the components $c_{10,(mn)}$ from Eq. (7.24) for the single-G_F normalisation. At the low scale μ_b they are functions of $\eta = \alpha_s(\mu_0)/\alpha_s(\mu_b)$ and their initial components $c_i^{(mn)}$ at the matching scale μ_0. We discussed the derivation of the according results $\widetilde{c}_{10,(mn)}$ for the quadratic-G_F normalisation in Sec. 7.2.

The numerical diagonalisation of the LO anomalous dimension yields the exponents

$$a_i = (-2,\, -1,\, -0.899395,\, -0.521739,\, -0.422989,\, 0.145649,\, 0.260870,\, 0.408619)\,. \tag{C.21}$$

i	1	2	3	4	5	6	7	8
b_i	0.00354	0.01223	−0.00977	−0.01070	−0.00572	0.00022	0.01137	−0.00117
$d_i^{(2a)}$	0	0	0.61602	0.44627	0.57472	0.08573	−0.48807	−0.24089
$d_i^{(2b)}$	−1.18162	0.22940	0.06522	−0.04380	−0.02201	−0.00316	−0.03366	−0.00414
$d_i^{(1)}$	0.01117	−0.03088	0.00411	0.00713	0.00478	0.00012	0.00379	−0.00023
$d_i^{(4)}$	−0.00799	−0.03666	0.06300	0	−0.01519	−0.00071	0	−0.00344
$e_i^{(1a)}$	0	0	−0.25941	−0.29751	−0.48014	0.04647	−0.16269	−0.04728
$e_i^{(1b)}$	1.13374	0.09381	−0.03041	0.00781	0.01838	−0.00138	−0.02259	0.00121
$e_i^{(4a)}$	0	0	−4.03683	0	1.52565	−0.27461	0	−0.70642
$e_i^{(4b)}$	3.38669	−0.10885	0.16283	0	0.06697	−0.01681	0	0.00137
$e_i^{(1)}$	0.01117	−0.03088	0.00411	0.00713	0.00478	0.00012	0.00379	−0.00023
$e_i^{(2)}$	0.00354	0.01223	−0.00977	−0.01070	−0.00572	0.00022	0.01137	−0.00117
$e_i^{(3)}$	0.02179	−0.12336	0.07870	0	0.01930	0.00873	0	−0.00516
$e_i^{(4)}$	−0.00799	−0.03666	0.06400	0	−0.01519	−0.00071	0	−0.00344
$e_i^{(5)}$	0.19550	−0.93249	0.37858	0	0.39909	0.05921	0	−0.09989
$e_i^{(6)}$	−0.17154	0.39616	0.01201	0	−0.19423	0.00357	0	−0.04597

Table C.1: *Numerical values of b_i, $d_i^{(j)}$ and $e_i^{(j)}$ entering the RGE solution in Eq. (C.22).*

and the explicit expressions for the down-scaled components are:

$$c_{10,(11)} = c_{10}^{(11)}, \qquad c_{10,(21)} = \eta\, c_{10}^{(21)}, \qquad c_{10,(02)} = \sum_{i=1}^{8} b_i \eta^{a_i}\, c_2^{(00)},$$

$$\begin{aligned}
c_{10,(12)} &= \sum_{i=1}^{8} \eta^{a_i+1} \Big[\left(d_i^{(2a)} \eta^{-1} + d_i^{(2b)} \right) c_2^{(00)} + d_i^{(1)} c_1^{(10)} + d_i^{(4)} c_4^{(10)} \Big] \\
&\quad - 0.11060 \frac{\ln \eta}{\eta} c_2^{(00)} + \left(\eta^{-1} - 1\right) \left(0.26087\, c_9^{(11)} + 1.15942\, c_{10}^{(11)} \right), \\
c_{10,(22)} &= \sum_{i=1}^{8} \eta^{a_i+2} \left[\left(e_i^{(1a)} \eta^{-1} + e_i^{(1b)} \right) c_1^{(10)} + \left(e_i^{(4a)} \eta^{-1} + e_i^{(4b)} \right) c_4^{(10)} + \sum_{j=1}^{6} e_i^{(j)} c_j^{(20)} \right] \\
&\quad + \left(0.27924\, c_1^{(10)} + 0.33157\, c_4^{(10)} + 2.35917\, c_9^{(11)} + 3.29679\, c_{10}^{(11)} \right) \ln \eta \\
&\quad + (1-\eta) \left(0.26087\, c_9^{(21)} + 1.15942\, c_{10}^{(21)} \right) + c_{10}^{(22)} .
\end{aligned} \tag{C.22}$$

We list the coefficients b_i, $d_i^{(j)}$ and $e_i^{(j)}$ in Tab. C.1.

C.5 Numerical Study of $\mathcal{C}_{10}$ in the OS-1 Scheme

In this appendix we estimate higher-order corrections in the OS-1 scheme and supplement in this context the discussion of the OS-2 and HY schemes from Sec. 10.1. We proceed as for Figures 10.2 and 10.3 to vary the matching scale μ_0 and estimate in this way higher-order QCD corrections via the dependence on the running top-quark mass. The result is shown in Fig. C.3 at NLO QCD and NLO (EW + QCD) order normalised to the OS-2 result at the respective order.

The different μ_0 dependence of the NLO QCD result for the OS-1 and OS-2 schemes originates from the different normalisations (Eq. (4.14)), which bear a μ_0 dependence due to the m_t dependence of the determination of $M_W^{\text{on-shell}}$ and consequently $s_W^{\text{on-shell}}$. As mentioned in Sec. 7.1.1, we compute $M_W^{\text{on-shell}}$ with the aid of result [86], which incorporates higher-order corrections. These contribute beyond the NLO EW calculation of $\mathcal{C}_{10}$ in this work, especially those that require the choice of a particular renormalisation scheme for the top-quark mass. Throughout, we use the pole mass as in Ref. [86].

At NLO (EW + QCD) the OS-1 scheme exhibits a much different μ_0 dependence with respect to OS-2 and HY schemes. The main reason is the large EW two-loop correction to $c_{10}^{(22)}$ from the s_W-on-shell counterterm that we discussed in connection with Fig. 10.1. The counterterm has a strong top-quark-mass dependence. To illustrate the latter, we present in Fig. C.3 also the NLO (EW + QCD) result (dashed-dotted line) when keeping the scale of the running top-quark mass in the counterterm contribution fixed at $\mu_0 = 160$ GeV. We observe that the large shift caused by the electroweak two-loop correction in the OS-1 scheme is accompanied with an artificially large top-quark-mass dependence that we results to the μ_0 dependence of the solid line. As a consequence, we do not consider the OS-1 scheme in

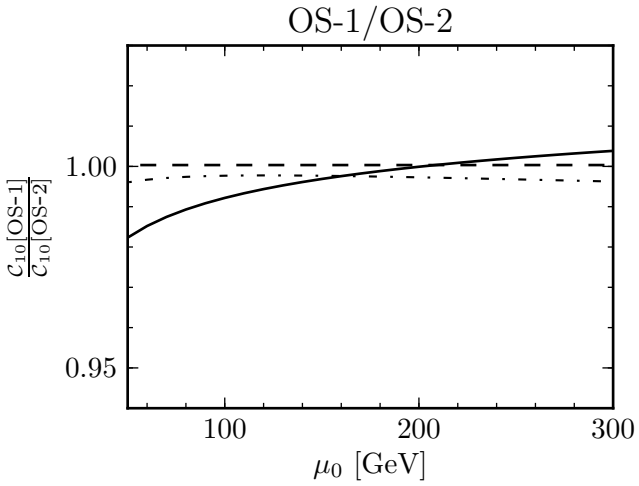

Figure C.3: *The μ_0 dependence of the ratio of the Wilson coefficient $\mathcal{C}_{10}(\mu_b = 5\,GeV)$ in OS-1 and OS-2 scheme. The LO and NLO QCD result coincide (dashed). The full μ_0 dependence of NLO (QCD + EW) (solid) and partial μ_0 dependence for fixed $m_t(160\,GeV)$ in the s_W-on-shell counterterm (dashed dotted).*

our estimate of higher-order uncertainties. It would artificially increase the estimate from μ_0 variation from the $\pm 0.3\%$ estimate given in Sec. 10.1, to around $+0.4\%$ and -1.7%.

Bibliography

[1] **ATLAS Collaboration**, G. Aad et al., *Observation of a new particle in the search for the Standard Model Higgs boson with the ATLAS detector at the LHC*, *Phys.Lett.* **B716** (2012) 1–29, [arXiv:1207.7214].

[2] **CMS Collaboration**, S. Chatrchyan et al., *Observation of a new boson at a mass of 125 GeV with the CMS experiment at the LHC*, *Phys.Lett.* **B716** (2012) 30–61, [arXiv:1207.7235].

[3] R. S. Chivukula and H. Georgi, *Composite Technicolor Standard Model*, *Phys. Lett.* **B188** (1987) 99, [doi:10.1016/0370-2693(87)90713-1].

[4] L. Hall and L. Randall, *Weak scale effective supersymmetry*, *Phys.Rev.Lett.* **65** (1990) 2939–2942, [doi:10.1103/PhysRevLett.65.2939].

[5] M. Ciuchini, G. Degrassi, P. Gambino, and G. F. Giudice, *Next-To-Leading (QCD) Corrections to $\bar{B} \to X_s\gamma$ in Supersymmetry*, *Nucl. Phys.* **B534** (1998) 3–20, [hep-ph/9806308].

[6] A. J. Buras, P. Gambino, M. Gorbahn, S. Jager, and L. Silvestrini, *Universal Unitarity Triangle and Physics Beyond the Standard Model*, *Phys. Lett.* **B500** (2001) 161–167, [hep-ph/0007085].

[7] G. D'Ambrosio, G. F. Giudice, G. Isidori, and A. Strumia, *Minimal Flavour Violation: an Effective Field Theory Approach*, *Nucl. Phys.* **B645** (2002) 155–187, [hep-ph/0207036].

[8] V. Cirigliano, B. Grinstein, G. Isidori, and M. B. Wise, *Minimal flavor violation in the lepton sector*, *Nucl. Phys.* **B728** (2005) 121–134, [hep-ph/0507001].

[9] S. Davidson and F. Palorini, *Various Definitions of Minimal Flavour Violation for Leptons*, *Phys. Lett.* **B642** (2006) 72–80, [hep-ph/0607329].

[10] N. Arkani-Hamed, L. J. Hall, D. Tucker-Smith, and N. Weiner, *Flavor at the TeV scale with extra dimensions*, *Phys.Rev.* **D61** (2000) 116003, [hep-ph/9909326].

[11] B. Grinstein, M. Redi, and G. Villadoro, *Low Scale Flavor Gauge Symmetries*, *JHEP* **1011** (2010) 067, [arXiv:1009.2049].

[12] Z. Berezhiani, *The Weak Mixing Angles in Gauge Models with Horizontal Symmetry: A New Approach to Quark and Lepton Masses*, *Phys.Lett.* **B129** (1983) 99–102, [doi:10.1016/0370-2693(83)90737-2].

[13] Z. Berezhiani and J. Chkareuli, *Quark-Leptonic Families in a Model with $SU(5) \times SU(3)$ Symmetry (in russian)*, *Sov.J.Nucl.Phys.* **37** (1983) 618–626.

[14] Z. Berezhiani and M. Y. Khlopov, *The Theory of broken gauge symmetry of families (in russian)*, *Sov.J.Nucl.Phys.* **51** (1990) 739–746.

[15] T. Feldmann, *See-Saw Masses for Quarks and Leptons in $SU(5)$*, *JHEP* **04** (2011) 043, [arXiv:1010.2116].

[16] D. Guadagnoli, R. N. Mohapatra, and I. Sung, *Gauged Flavor Group with Left-Right Symmetry*, *JHEP* **04** (2011) 093, [arXiv:1103.4170].

[17] R. T. D'Agnolo and D. M. Straub, *Gauged flavour symmetry for the light generations*, *JHEP* **1205** (2012) 034, [arXiv:1202.4759].

[18] R. Alonso, M. B. Gavela, L. Merlo, and S. Rigolin, *On the Scalar Potential of Minimal Flavour Violation*, *JHEP* **07** (2011) 012, [arXiv:1103.2915].

[19] A. J. Buras, M. V. Carlucci, L. Merlo, and E. Stamou, *Phenomenology of a Gauged $SU(3)^3$ Flavour Model*, *JHEP* **1203** (2012) 088, [arXiv:1112.4477].

[20] A. J. Buras, C. Grojean, S. Pokorski, and R. Ziegler, *FCNC Effects in a Minimal Theory of Fermion Masses*, *JHEP* **1108** (2011) 028, [arXiv:1105.3725].

[21] A. J. Buras, L. Merlo, and E. Stamou, *The Impact of Flavour Changing Neutral Gauge Bosons on $\bar{B} \to X_s\gamma$*, *JHEP* **1108** (2011) 124, [arXiv:1105.5146].

[22] M. Dine, A. Kagan, and S. Samuel, *Naturalness in supersymmetry, or raising the supersymmetry breaking scale*, *Phys.Lett.* **B243** (1990) 250–256, [doi:10.1016/0370-2693(90)90847-Y].

[23] A. Azatov, J. Galloway, and M. A. Luty, *Superconformal Technicolor*, *Phys.Rev.Lett.* **108** (2012) 041802, [arXiv:1106.3346].

[24] A. Azatov, J. Galloway, and M. A. Luty, *Superconformal Technicolor: Models and Phenomenology*, *Phys.Rev.* **D85** (2012) 015018, [arXiv:1106.4815].

[25] J. Galloway, M. A. Luty, Y. Tsai, and Y. Zhao, *Induced Electroweak Symmetry Breaking and Supersymmetric Naturalness*, [arXiv:1306.6354].

[26] J. F. Kamenik, J. Shu, and J. Zupan, *Review of New Physics Effects in $t\bar{t}$ Production*, *Eur.Phys.J.* **C72** (2012) 2102, [arXiv:1107.5257].

[27] B. Grinstein, A. L. Kagan, M. Trott, and J. Zupan, *Forward-backward asymmetry in $t\bar{t}$ production from flavour symmetries*, *Phys.Rev.Lett.* **107** (2011) 012002, [arXiv:1102.3374].

[28] B. Grinstein, A. L. Kagan, J. Zupan, and M. Trott, *Flavor Symmetric Sectors and Collider Physics*, *JHEP* **1110** (2011) 072, [arXiv:1108.4027].

[29] J. Brod, J. Drobnak, A. L. Kagan, E. Stamou, and J. Zupan, *New Strong Interactions from $t\bar{t}$ Asymmetries*, *to be published* (2013).

[30] Y. Grossman, Y. Nir, J. Thaler, T. Volansky, and J. Zupan, *Probing minimal flavor violation at the LHC*, *Phys.Rev.* **D76** (2007) 096006, [arXiv:0706.1845].

[31] **LHCb Collaboration**, R. Aaij et al., *First evidence for the decay $B_s \to \mu^+\mu^-$*, *Phys.Rev.Lett.* **110** (2013) 021801, [arXiv:1211.2674].

[32] **LHCb Collaboration**, R. Aaij et al., *Measurement of the $B_s^0 \to \mu^+\mu^-$ branching fraction and search for $B^0 \to \mu^+\mu^-$ decays at the LHCb experiment*, [arXiv:1307.5024].

[33] **CMS Collaboration**, S. Chatrchyan et al., *Measurement of the $B_s \to \mu^+\mu^-$ branching fraction and search for $B^0 \to \mu^+\mu^-$ with the CMS Experiment*, [arXiv:1307.5025].

[34] S. Hansmann-Menzemer, *Experimental results on flavour physics*, EPS-HEP 2013, European Physical Society Conference on High Energy Physics, Jul, 2013.

[35] K. De Bruyn, R. Fleischer, R. Knegjens, P. Koppenburg, M. Merk, et al., *Probing New Physics via the $B_s^0 \to \mu^+\mu^-$ Effective Lifetime*, *Phys.Rev.Lett.* **109** (2012) 041801, [arXiv:1204.1737].

[36] **LHCb Collaboration**, G. Raven, *Measurement of the CP violation phase ϕ_s in the B_s system at LHCb*, [arXiv:1212.4140].

[37] **LHCb Collaboration**, R. Aaij et al., *Measurement of the CP-violating phase ϕ_s in $B_s \to J/\psi\pi^+\pi^-$ decays*, *Phys.Lett.* **B713** (2012) 378–386, [arXiv:1204.5675].

[38] **LHCb Collaboration**, R. Aaij et al., *Determination of the sign of the decay width difference in the B_s system*, *Phys.Rev.Lett.* **108** (2012) 241801, [arXiv:1202.4717].

[39] **Particle Data Group Collaboration**, J. Beringer et al., *Review of Particle Physics (RPP)*, *Phys.Rev.* **D86** (2012) 010001, [doi:10.1103/PhysRevD.86.010001].

[40] **LHCb Collaboration**, R. Aaij et al., *Implications of LHCb measurements and future prospects*, *Eur.Phys.J.* **C73** (2013) 2373, [arXiv:1208.3355].

[41] C. McNeile, C. Davies, E. Follana, K. Hornbostel, and G. Lepage, *High-Precision f_{B_s} and HQET from Relativistic Lattice QCD*, *Phys.Rev.* **D85** (2012) 031503, [arXiv:1110.4510].

[42] **Fermilab Lattice Collaboration, MILC Collaboration**, A. Bazavov et al., *B- and D-meson decay constants from three-flavor lattice QCD*, *Phys.Rev.* **D85** (2012) 114506, [arXiv:1112.3051].

[43] H. Na, C. J. Monahan, C. T. Davies, R. Horgan, G. P. Lepage, et al., *The B and B_s Meson Decay Constants from Lattice QCD*, *Phys.Rev.* **D86** (2012) 034506, [arXiv:1202.4914].

[44] **HPQCD Collaboration**, R. Dowdall, C. Davies, R. Horgan, C. Monahan, and J. Shigemitsu, *B-meson decay constants from improved lattice NRQCD and physical u, d, s and c sea quarks*, *Phys.Rev.Lett.* **110** (2013) 222003, [arXiv:1302.2644].

[45] A. J. Buras, R. Fleischer, J. Girrbach, and R. Knegjens, *Probing New Physics with the $B_s \to \mu^+\mu^-$ Time-Dependent Rate*, [arXiv:1303.3820].

[46] T. Inami and C. S. Lim, *Effects of Superheavy Quarks and Leptons in Low-Energy Weak Processes $K_L \to \mu\bar{\mu}$, $K^+ \to \pi^+\nu\bar{\nu}$ and $K^0 \leftrightarrow \bar{K}^0$*, *Prog. Theor. Phys.* **65** (1981) 297, [doi:10.1143/PTP.65.297].

[47] M. Misiak, *Rare B-Meson Decays*, [arXiv:1112.5978].

[48] G. Buchalla and A. J. Buras, *QCD corrections to the $\bar{s}dZ$ vertex for arbitrary top quark mass*, *Nucl.Phys.* **B398** (1993) 285–300, [doi:10.1016/0550-3213(93)90110-B].

[49] G. Buchalla and A. J. Buras, *QCD corrections to rare K and B decays for arbitrary top quark mass*, *Nucl.Phys.* **B400** (1993) 225–239, [doi:10.1016/0550-3213(93)90405-E].

[50] M. Misiak and J. Urban, *QCD corrections to FCNC decays mediated by Z penguins and W boxes*, *Phys.Lett.* **B451** (1999) 161–169, [hep-ph/9901278].

[51] G. Buchalla and A. J. Buras, *The rare decays $K \to \pi\nu\bar{\nu}$, $B \to X\nu\bar{\nu}$ and $B \to \ell^+\ell^-$: An Update*, *Nucl.Phys.* **B548** (1999) 309–327, [hep-ph/9901288].

[52] T. Hermann, M. Misiak, and M. Steinhauser, *NNLO QCD corrections to $B_s \to \mu^+\mu^-$*, *to be published* (2013).

[53] A. J. Buras, J. Girrbach, D. Guadagnoli, and G. Isidori, *On the Standard Model prediction for $BR(B_{s,d} \to \mu^+\mu^-)$*, *Eur.Phys.J.* **C72** (2012) 2172, [arXiv:1208.0934].

[54] G. Buchalla and A. J. Buras, *Two loop large m_t electroweak corrections to $K \to \pi\nu\bar{\nu}$ for arbitrary Higgs boson mass*, *Phys.Rev.* **D57** (1998) 216–223, [hep-ph/9707243].

[55] J. Brod, M. Gorbahn, and E. Stamou, *Two-Loop Electroweak Corrections for the $K \to \pi\nu\bar{\nu}$ Decays*, *Phys.Rev.* **D83** (2011) 034030, [arXiv:1009.0947].

[56] A. J. Buras, M. Misiak, and J. Urban, *Two-Loop QCD Anomalous Dimensions of Flavour-Changing Four-Quark Operators Within and Beyond the Standard Model*, *Nucl. Phys.* **B586** (2000) 397–426, [hep-ph/0005183].

[57] M. Misiak, H. Asatrian, K. Bieri, M. Czakon, A. Czarnecki, et al., *Estimate of $B(\bar{B} \to X_s\gamma)$ at $\mathcal{O}(\alpha_s^2)$*, *Phys.Rev.Lett.* **98** (2007) 022002, [hep-ph/0609232].

[58] G. Buchalla, A. J. Buras, and M. K. Harlander, *The Anatomy of ϵ'/ϵ in the Standard Model*, *Nucl.Phys.* **B337** (1990) 313–362, [doi:10.1016/0550-3213(90)90275-I].

[59] A. J. Buras, M. Jamin, and M. E. Lautenbacher, *The Anatomy of ϵ'/ϵ beyond leading logarithms with improved hadronic matrix elements*, *Nucl.Phys.* **B408** (1993) 209–285, [hep-ph/9303284].

[60] A. J. Buras, S. Jager, and J. Urban, *Master Formulae for $\Delta F = 2$ NLO-QCD Factors in the Standard Model and Beyond*, *Nucl. Phys.* **B605** (2001) 600–624, [hep-ph/0102316].

[61] R. Babich et al., *K^0–$\bar{K}^0$ Mixing Beyond the Standard Model and CP-Violating Electroweak Penguins in Quenched QCD with Exact Chiral Symmetry*, *Phys. Rev.* **D74** (2006) 073009, [hep-lat/0605016].

[62] D. Becirevic, V. Gimenez, G. Martinelli, M. Papinutto, and J. Reyes, *B-Parameters of the Complete Set of Matrix Elements of $\Delta B = 2$ Operators from the Lattice*, *JHEP* **04** (2002) 025, [hep-lat/0110091].

[63] M. Blanke, A. J. Buras, K. Gemmler, and T. Heidsieck, *$\Delta F = 2$ observables and $B \to X_q\gamma$ decays in the Left-Right Model: Higgs particles striking back*, *JHEP* **1203** (2012) 024, [arXiv:1111.5014].

[64] A. J. Buras, F. De Fazio, and J. Girrbach, *The Anatomy of Z' and Z with Flavour Changing Neutral Currents in the Flavour Precision Era*, *JHEP* **1302** (2013) 116, [arXiv:1211.1896].

[65] A. J. Buras, *Weak Hamiltonian, CP violation and rare decays*, [hep-ph/9806471].

[66] M. Ciuchini, E. Franco, L. Reina, and L. Silvestrini, *Leading order QCD corrections to $b \to s\gamma$ and $b \to sg$ decays in three regularization schemes*, *Nucl.Phys.* **B421** (1994) 41–64, [hep-ph/9311357].

[67] G. Buchalla, A. J. Buras, and M. E. Lautenbacher, *Weak decays beyond leading logarithms*, *Rev.Mod.Phys.* **68** (1996) 1125–1144, [hep-ph/9512380].

[68] M. Ciuchini, E. Franco, G. Martinelli, L. Reina, and L. Silvestrini, *Scheme independence of the effective Hamiltonian for $b \to s\gamma$ and $b \to sg$ decays*, *Phys.Lett.* **B316** (1993) 127–136, [hep-ph/9307364].

[69] P. Gambino and M. Misiak, *Quark mass effects in $\bar{B} \to X_s\gamma$*, *Nucl.Phys.* **B611** (2001) 338–366, [hep-ph/0104034].

[70] M. Misiak and M. Steinhauser, *NNLO QCD Corrections to the $\bar{B} \to X_s\gamma$ Matrix Elements Using Interpolation in m_c*, *Nucl. Phys.* **B764** (2007) 62–82, [hep-ph/0609241].

[71] C. McNeile, A. Bazavov, C. Davies, R. Dowdall, K. Hornbostel, et al., *Direct determination of the strange and light quark condensates from full lattice QCD*, *Phys.Rev.* **D87** (2013), no. 3 034503, [arXiv:1211.6577].

[72] M. Beneke, J. Rohrer, and D. Yang, *Branching fractions, polarisation and asymmetries of $B \to VV$ decays*, *Nucl.Phys.* **B774** (2007) 64–101, [hep-ph/0612290].

[73] K.-C. Yang, *Form-Factors of B(u,d,s) Decays into P-Wave Axial-Vector Mesons in the Light-Cone Sum Rule Approach*, *Phys.Rev.* **D78** (2008) 034018, [arXiv:0807.1171].

[74] H.-Y. Cheng and R. Shrock, *Some Results on Vector and Tensor Meson Mixing in a Generalized QCD-like Theory*, *Phys.Rev.* **D84** (2011) 094008, [arXiv:1109.3877].

[75] J. Drobnak, A. L. Kagan, J. F. Kamenik, G. Perez, and J. Zupan, *Forward Tevatron Tops and Backward LHC Tops with Associates*, *Phys.Rev.* **D86** (2012) 094040, [arXiv:1209.4872].

[76] L. Roca, J. Palomar, and E. Oset, *Decay of axial vector mesons into VP and P gamma*, *Phys.Rev.* **D70** (2004) 094006, [hep-ph/0306188].

[77] H.-Y. Cheng, Y. Koike, and K.-C. Yang, *Two-parton Light-cone Distribution Amplitudes of Tensor Mesons*, *Phys.Rev.* **D82** (2010) 054019, [arXiv:1007.3541].

[78] J. Kuipers, T. Ueda, J. A. M. Vermaseren, and J. Vollinga, *Form version 4.0*, *CoRR* **abs/1203.6543** (2012).

[79] N. D. Christensen and C. Duhr, *FeynRules - Feynman rules made easy*, *Comput.Phys.Commun.* **180** (2009) 1614–1641, [arXiv:0806.4194].

[80] J. Alwall, M. Herquet, F. Maltoni, O. Mattelaer, and T. Stelzer, *MadGraph 5 : Going Beyond*, *JHEP* **1106** (2011) 128, [arXiv:1106.0522].

[81] T. Huber, E. Lunghi, M. Misiak, and D. Wyler, *Electromagnetic logarithms in* $\bar{B} \to X_s \ell^+ \ell^-$, *Nucl.Phys.* **B740** (2006) 105–137, [hep-ph/0512066].

[82] C. Bobeth, M. Gorbahn, and E. Stamou, *Electroweak Corrections to* $B_s \to \mu^+ \mu^-$, *to be published* (2013).

[83] C. Bobeth, P. Gambino, M. Gorbahn, and U. Haisch, *Complete NNLO QCD analysis of* $\bar{B} \to X_s \ell^+ \ell^-$ *and higher order electroweak effects*, *JHEP* **0404** (2004) 071, [hep-ph/0312090].

[84] **CDF Collaboration, D0 Collaboration**, Tevatron-Electroweak-Working-Group, *Combination of CDF and DØ results on the mass of the top quark using up to 5.8* fb^{-1} *of data*, [arXiv:1107.5255].

[85] **CDF Collaboration, D0 Collaboration**, T. Aaltonen et al., *Combination of the top-quark mass measurements from the Tevatron collider*, *Phys.Rev.* **D86** (2012) 092003, [arXiv:1207.1069].

[86] M. Awramik, M. Czakon, A. Freitas, and G. Weiglein, *Precise prediction for the W boson mass in the standard model*, *Phys.Rev.* **D69** (2004) 053006, [hep-ph/0311148].

[87] F. Jegerlehner, M. Y. Kalmykov, and O. Veretin, *MS versus pole masses of gauge bosons: Electroweak bosonic two loop corrections*, *Nucl.Phys.* **B641** (2002) 285–326, [hep-ph/0105304].

[88] F. Jegerlehner, M. Y. Kalmykov, and O. Veretin, $\overline{MS}$ *versus pole masses of gauge bosons. 2. Two loop electroweak fermion corrections*, *Nucl.Phys.* **B658** (2003) 49–112, [hep-ph/0212319].

[89] J. Fleischer and F. Jegerlehner, *Radiative Corrections to Higgs Decays in the Extended Weinberg-Salam Model*, *Phys.Rev.* **D23** (1981) 2001–2026, [doi:10.1103/PhysRevD.23.2001].

[90] C. Bobeth, M. Misiak, and J. Urban, *Photonic penguins at two loops and* m_{top} *dependence of* $BR[B \to X_s \ell^+ \ell^-]$, *Nucl.Phys.* **B574** (2000) 291–330, [hep-ph/9910220].

[91] A. Sirlin, *Radiative Corrections in the* $SU(2)_L \times U(1)$ *Theory: A Simple Renormalization Framework*, *Phys.Rev.* **D22** (1980) 971–981, [doi:10.1103/PhysRevD.22.971].

[92] F. Bezrukov, M. Y. Kalmykov, B. A. Kniehl, and M. Shaposhnikov, *Higgs Boson Mass and New Physics*, *JHEP* **1210** (2012) 140, [arXiv:1205.2893].

[93] J. Fleischer, O. Tarasov, and F. Jegerlehner, *Two loop large top mass corrections to electroweak parameters: Analytic results valid for arbitrary Higgs mass*, *Phys.Rev.* **D51** (1995) 3820–3837, [doi:10.1103/PhysRevD.51.3820].

[94] **LHCb Collaboration**, *Improved constraints on γ from $B^{\pm} \to DK^{\pm}$ decays including first results on 2012 data*, . Linked to LHCb-ANA-2013-012.

[95] A. J. Buras and J. Girrbach, *Towards the Identification of New Physics through Quark Flavour Violating Processes*, [arXiv:1306.3775].

[96] **Particle Data Group Collaboration**, K. Nakamura et al., *Review of Particle Physics*, *J. Phys.* **G37** (2010) 075021, [doi:10.1088/0954-3899/37/7A/075021].

[97] J. Laiho, E. Lunghi, and R. S. Van de Water, *Lattice QCD inputs to the CKM unitarity triangle analysis*, *Phys.Rev.* **D81** (2010) 034503, [arXiv:0910.2928] [http://www.latticeaverages.org].

[98] K. G. Chetyrkin et al., *Charm and Bottom Quark Masses: an Update*, *Phys. Rev.* **D80** (2009) 074010, [arXiv:0907.2110].

[99] A. J. Buras, M. Jamin, and P. H. Weisz, *Leading and Next-to-Leading QCD Corrections to ϵ Parameter and $B^0 - \bar{B}^0$ Mixing in the Presence of a Heavy Top Quark*, *Nucl.Phys.* **B347** (1990) 491–536, [doi:10.1016/0550-3213(90)90373-L].

[100] J. Urban, F. Krauss, U. Jentschura, and G. Soff, *Next-to-leading order QCD corrections for the $B^0 - \bar{B}^0$ mixing with an extended Higgs sector*, *Nucl.Phys.* **B523** (1998) 40–58, [hep-ph/9710245].

[101] A. J. Buras, D. Guadagnoli, and G. Isidori, *On ϵ_K beyond lowest order in the Operator Product Expansion*, *Phys.Lett.* **B688** (2010) 309–313, [arXiv:1002.3612].

[102] A. J. Buras and D. Guadagnoli, *Correlations among new CP violating effects in $\Delta F = 2$ observables*, *Phys.Rev.* **D78** (2008) 033005, [arXiv:0805.3887].

[103] J. Brod and M. Gorbahn, *The NNLO Charm-Quark Contribution to ϵ_K and ΔM_K*, [arXiv:1108.2036].

[104] J. Brod and M. Gorbahn, *ϵ_K at Next-to-Next-to-Leading Order: The Charm-Top-Quark Contribution*, *Phys.Rev.* **D82** (2010) 094026, [arXiv:1007.0684].

[105] T. Blum, P. Boyle, N. Christ, N. Garron, E. Goode, et al., *The $K \to (\pi\pi)_{I=2}$ Decay Amplitude from Lattice QCD*, *Phys.Rev.Lett.* **108** (2012) 141601, [arXiv:1111.1699].

[106] S. Durr, Z. Fodor, C. Hoelbling, S. Katz, S. Krieg, et al., *Precision computation of the kaon bag parameter*, *Phys.Lett.* **B705** (2011) 477–481, [arXiv:1106.3230].

[107] **HPQCD Collaboration, UKQCD Collaboration**, E. Gamiz et al., *Unquenched determination of the kaon parameter $B(K)$ from improved staggered fermions*, *Phys.Rev.* **D73** (2006) 114502, [hep-lat/0603023].

[108] J. Laiho and R. S. Van de Water, *Pseudoscalar decay constants, light-quark masses, and B_K from mixed-action lattice QCD*, [arXiv:1112.4861].

[109] C. Kelly, *Continuum Results for Light Hadronic Quantities using Domain Wall Fermions with the Iwasaki and DSDR Gauge Actions*, [arXiv:1201.0706]. Contribution to The XXIX International Symposium on Lattice Field Theory, July 10-16, 2011.

[110] T. Bae, Y.-C. Jang, C. Jung, H.-J. Kim, J. Kim, et al., *Kaon B-parameter from improved staggered fermions in $N_f = 2 + 1$ QCD*, [arXiv:1111.5698].

[111] C. Bouchard, E. Freeland, C. Bernard, A. El-Khadra, E. Gamiz, et al., *Neutral B mixing from $2 + 1$ flavor lattice-QCD: the Standard Model and beyond*, [arXiv:1112.5642]. Proceedings of the XXIX International Symposium on Lattice Field Theory - Lattice 2011, July 10-16, 2011, Squaw Valley, Lake Tahoe, California.

[112] **HPQCD Collaboration**, E. Gamiz, C. T. Davies, G. P. Lepage, J. Shigemitsu, and M. Wingate, *Neutral B Meson Mixing in Unquenched Lattice QCD*, *Phys.Rev.* **D80** (2009) 014503, [arXiv:0902.1815].

[113] R. Evans, A. El-Khadra, and E. Gamiz, *A determination of the B_s^0 and B_d^0 mixing matrix elements in 2+1 lattice QCD*, *PoS* **LATTICE2008** (2008) 052.

[114] C. Albertus, Y. Aoki, P. Boyle, N. Christ, T. Dumitrescu, et al., *Neutral B-meson mixing from unquenched lattice QCD with domain-wall light quarks and static b-quarks*, *Phys.Rev.* **D82** (2010) 014505, [arXiv:1001.2023].

[115] **UTfit Collaboration**, M. Bona et al., *The Utfit Collaboration Report on the Status of the Unitarity Triangle Beyond the Standard Model. I: Model- Independent Analysis and Minimal Flavour Violation*, *JHEP* **03** (2006) 080, [hep-ph/0509219].

[116] **BaBar Collaboration**, B. Aubert et al., *A Search for $B^+ \to \tau^+\nu$ with Hadronic B tags*, *Phys.Rev.* **D77** (2008) 011107, [arXiv:0708.2260].

[117] **Belle Collaboration**, K. Ikado et al., *Evidence of the Purely Leptonic Decay $B^- \to \tau^- \bar{\nu}_\tau$*, *Phys.Rev.Lett.* **97** (2006) 251802, [hep-ex/0604018].

[118] **Belle Collaboration**, I. Adachi et al., *Measurement of $B^- \to \tau^- \bar{\nu}_\tau$ with a Hadronic Tagging Method Using the Full Data Sample of Belle*, *Phys.Rev.Lett.* **110** (2013) 131801, [arXiv:1208.4678].

[119] G. Isidori and P. Paradisi, *Hints of Large $\tan\beta$ in Flavour Physics*, *Phys. Lett.* **B639** (2006) 499–507, [hep-ph/0605012].

[120] E. Lunghi and A. Soni, *Possible Indications of New Physics in B_d-mixing and in $\sin(2\beta)$ Determinations*, *Phys.Lett.* **B666** (2008) 162–165, [arXiv:0803.4340].

[121] **Heavy Flavor Averaging Group Collaboration**, Y. Amhis et al., *Averages of B-Hadron, C-Hadron, and tau-lepton properties as of early 2012*, [arXiv:1207.1158].

[122] **LHCb Collaboration**, R. Aaij et al., *Measurement of CP violation and the B_s^0 meson decay width difference with $B_s^0 \to J/\psi K^+K^-$ and $B_s^0 \to J/\psi\pi^+\pi^-$ decays*, *Phys.Rev.* **D87** (2013) 112010, [arXiv:1304.2600].

[123] A. J. Buras, M. Spranger, and A. Weiler, *The Impact of Universal Extra Dimensions on the Unitarity Triangle and Rare K and B Decays*, *Nucl. Phys.* **B660** (2003) 225–268, [hep-ph/0212143].

[124] M. Blanke, A. J. Buras, D. Guadagnoli, and C. Tarantino, *Minimal Flavour Violation Waiting for Precise Measurements of ΔM_s, $S_{\Psi\Phi}$, A^s_{sl}, $|V_{ub}|$, γ and $B^0_{s,d} \to \mu^+\mu^-$*, *JHEP* **10** (2006) 003, [hep-ph/0604057].

[125] M. Blanke and A. J. Buras, *Lower Bounds on $\Delta M_{s,d}$ from Constrained Minimal Flavour Violation*, *JHEP* **05** (2007) 061, [hep-ph/0610037].

[126] A. J. Buras, A. Poschenrieder, M. Spranger, and A. Weiler, *The Impact of Universal Extra Dimensions on $\bar{B} \to X_s\gamma$, $\bar{B} \to X_s g$, $\bar{B} \to X_s\mu^+\mu^-$, $K_L \to \pi^0 e^+ e^-$, and ϵ'/ϵ*, *Nucl. Phys.* **B678** (2004) 455–490, [hep-ph/0306158].

[127] A. J. Buras, M. V. Carlucci, S. Gori, and G. Isidori, *Higgs-mediated FCNCs: Natural Flavour Conservation vs. Minimal Flavour Violation*, *JHEP* **1010** (2010) 009, [arXiv:1005.5310].

[128] V. Ahrens, A. Ferroglia, M. Neubert, B. D. Pecjak, and L. L. Yang, *The top-pair forward-backward asymmetry beyond NLO*, *Phys.Rev.* **D84** (2011) 074004, [arXiv:1106.6051].

[129] A. V. Manohar and M. Trott, *Electroweak Sudakov Corrections and the Top Quark Forward-Backward Asymmetry*, *Phys.Lett.* **B711** (2012) 313–316, [arXiv:1201.3926].

[130] W. Hollik and D. Pagani, *The electroweak contribution to the top quark forward-backward asymmetry at the Tevatron*, *Phys.Rev.* **D84** (2011) 093003, [arXiv:1107.2606].

[131] W. Bernreuther and Z.-G. Si, *Top quark and leptonic charge asymmetries for the Tevatron and LHC*, *Phys.Rev.* **D86** (2012) 034026, [arXiv:1205.6580].

[132] P. M. Nadolsky, H.-L. Lai, Q.-H. Cao, J. Huston, J. Pumplin, et al., *Implications of CTEQ global analysis for collider observables*, *Phys.Rev.* **D78** (2008) 013004, [arXiv:0802.0007].

[133] **CDF Collaboration**, T. Aaltonen et al., *Evidence for a Mass Dependent Forward-Backward Asymmetry in Top Quark Pair Production*, *Phys.Rev.* **D83** (2011) 112003, [arXiv:1101.0034].

[134] **CDF Collaboration**, *Measurement of the Forward Backward Asymmetry in Top Pair Production in the Dilepton Decay Channel using 5.1 fb^{-1}*, tech. rep., 2011.

[135] **D0 Collaboration**, V. M. Abazov et al., *Forward-backward asymmetry in top quark-antiquark production*, *Phys.Rev.* **D84** (2011) 112005, [arXiv:1107.4995].

[136] **CDF Collaboration**, T. Aaltonen et al., *Measurement of the top quark forward-backward production asymmetry and its dependence on event kinematic properties*, *Phys.Rev.* **D87** (2013) 092002, [arXiv:1211.1003].

[137] **ATLAS Collaboration**, *Measurement of the top quark pair production charge asymmetry in proton-proton collisions at $\sqrt{s} = 7$ TeV using the ATLAS detector*, Tech. Rep. ATLAS-CONF-2013-078, CERN, Geneva, Jul, 2013.

[138] **ATLAS Collaboration**, *Measurement of the charge asymmetry in dileptonic decay of top quark pairs in pp collisions at $\sqrt{s} = 7$ TeV using the ATLAS detector*, . ATLAS-CONF-2012-057, ATLAS-COM-CONF-2012-060.

[139] **CMS Collaboration**, S. Chatrchyan et al., *Measurement of the charge asymmetry in top-quark pair production in proton-proton collisions at $\sqrt{s} = 7$ TeV*, *Phys.Lett.* **B709** (2012) 28–49, [arXiv:1112.5100].

[140] **CMS Collaboration**, *Top charge asymmetry measurement in dileptons at 7 TeV*, Tech. Rep. CMS-PAS-TOP-12-010, CERN, Geneva, 2012.

[141] **CDF Collaboration**, *Combination of CDF top quark production cross section measurements with up to* 4.6 fb^{-1}, *CDF note 9913* (2009).

[142] **ATLAS Collaboration**, *Statistical combination of top quark pair production cross-section measurements using dilepton, single-lepton, and all-hadronic final states at $\sqrt{s} = 7$ TeV with the ATLAS detector*, .

[143] **CMS Collaboration**, *Combination of top pair production cross section measurements*, Tech. Rep. CMS-PAS-TOP-11-024, CERN, Geneva, 2011.

[144] M. Czakon, M. L. Mangano, A. Mitov, and J. Rojo, *Constraints on the gluon PDF from top quark pair production at hadron colliders*, [arXiv:1303.7215].

[145] J. Aguilar-Saavedra and M. Perez-Victoria, *Asymmetries in $t\,\bar{t}$ production: LHC versus Tevatron*, *Phys.Rev.* **D84** (2011) 115013, [arXiv:1105.4606].

[146] J. Cao, K. Hikasa, L. Wang, L. Wu, and J. M. Yang, *Testing new physics models by top charge asymmetry and polarization at the LHC*, *Phys.Rev.* **D85** (2012) 014025, [arXiv:1109.6543].

[147] S. Fajfer, J. F. Kamenik, and B. Melic, *Discerning New Physics in Top-Antitop Production using Top Spin Observables at Hadron Colliders*, *JHEP* **1208** (2012) 114, [arXiv:1205.0264].

[148] M. J. D. Powell, *Direct search algorithms for optimization calculations*, *Acta Numerica* **7** (1, 1998) 287–336, [doi:10.1017/S0962492900002841].

[149] **CDF Collaboration**, T. Aaltonen et al., *First Measurement of the t anti-t Differential Cross Section $d\sigma/dM_{t\bar{t}}$ in $p\bar{p}$ Collisions at $\sqrt{s} = 1.96$ TeV*, *Phys.Rev.Lett.* **102** (2009) 222003, [arXiv:0903.2850].

[150] S. Jung, H. Murayama, A. Pierce, and J. D. Wells, *Top quark forward-backward asymmetry from new t-channel physics*, *Phys.Rev.* **D81** (2010) 015004, [arXiv:0907.4112].

[151] M. I. Gresham, I.-W. Kim, S. Tulin, and K. M. Zurek, *Confronting Top AFB with Parity Violation Constraints*, *Phys.Rev.* **D86** (2012) 034029, [arXiv:1203.1320].

[152] **ATLAS Collaboration Collaboration**, G. Aad et al., *Measurements of top quark pair relative differential cross-sections with ATLAS in pp collisions at* $\sqrt{s} = 7$ *TeV*, *Eur.Phys.J.* **C73** (2013) 2261, [arXiv:1207.5644].

[153] **CMS Collaboration**, *Measurement of differential top-quark pair production cross sections in the lepton+jets channel in pp collisions at 8 TeV*, Tech. Rep. CMS-PAS-TOP-12-027, CERN, Geneva, 2013.

[154] **CDF Collaboration Collaboration**, T. Aaltonen et al., *Search for pair-production of strongly-interacting particles decaying to pairs of jets in* $p\bar{p}$ *collisions at* $\sqrt{s} = 1.96$ *TeV*, *Phys.Rev.Lett.* **111** (2013) 031802, [arXiv:1303.2699].

[155] **CDF Collaboration**, T. Aaltonen et al., *Search for Maximal Flavor Violating Scalars in Same-Charge Lepton Pairs in* $p\bar{p}$ *Collisions at* $\sqrt{s} = 1.96$*-TeV*, *Phys.Rev.Lett.* **102** (2009) 041801, [arXiv:0809.4903].

[156] **CDF Collaboration**, T. Aaltonen et al., *Search for new particles decaying into dijets in proton-antiproton collisions at* $\sqrt{s} = 1.96$ *TeV*, *Phys.Rev.* **D79** (2009) 112002, [arXiv:0812.4036].

[157] **D0 Collaboration**, V. Abazov et al., *Measurement of dijet angular distributions at* $\sqrt{s} = 1.96$ *TeV and searches for quark compositeness and extra spatial dimensions*, *Phys.Rev.Lett.* **103** (2009) 191803, [arXiv:0906.4819].

[158] **CMS Collaboration Collaboration**, S. Chatrchyan et al., *Search for narrow resonances using the dijet mass spectrum in pp collisions at* $\sqrt{s} = 8$ *TeV*, [arXiv:1302.4794].

[159] C. Bobeth, M. Gorbahn, T. Hermann, M. Misiak, E. Stamou, and M. Steinhauser, $B_s \to \mu^+\mu^-$ *at NNLO in strong and NLO in electroweak interactions*, *to be published* (2013).

[160] K. Chetyrkin, J. H. Kuhn, and M. Steinhauser, *RunDec: A Mathematica package for running and decoupling of the strong coupling and quark masses*, *Comput.Phys.Commun.* **133** (2000) 43–65, [hep-ph/0004189].

[161] M. Ciuchini, G. D'Agostini, E. Franco, V. Lubicz, G. Martinelli, et al., *2000 CKM triangle analysis: A Critical review with updated experimental inputs and theoretical parameters*, *JHEP* **0107** (2001) 013, [hep-ph/0012308].

[162] W. R. Frazer and J. R. Fulco, *Effect of a Pion-Pion Scattering Resonance on Nucleon Structure. II*, *Phys.Rev.* **117** (1960) 1609–1614, [doi:10.1103/PhysRev.117.1609].

[163] Y. Nambu, *Possible existence of a heavy neutral meson*, *Phys.Rev.* **106** (1957) 1366–1367, [doi:10.1103/PhysRev.106.1366].

[164] J. Sakurai, *Theory of strong interactions*, *Annals Phys.* **11** (1960) 1–48, [doi:10.1016/0003-4916(60)90126-3].

[165] H. B. O'Connell, B. Pearce, A. W. Thomas, and A. G. Williams, $\rho - \omega$ *mixing, vector meson dominance and the pion form-factor*, *Prog.Part.Nucl.Phys.* **39** (1997) 201–252, [hep-ph/9501251].

[166] P. Nogueira, *Automatic feynman graph generation*, *Journal of Computational Physics* **105** (1993), no. 2 279 – 289, [doi:10.1006/jcph.1993.1074].

[167] T. Hahn, *Generating Feynman diagrams and amplitudes with FeynArts 3*, *Comput.Phys.Commun.* **140** (2001) 418–431, [hep-ph/0012260].

[168] A. I. Davydychev and J. Tausk, *Two loop selfenergy diagrams with different masses and the momentum expansion*, *Nucl.Phys.* **B397** (1993) 123–142, [doi:10.1016/0550-3213(93)90338-P].

[169] A. Denner, *Techniques for calculation of electroweak radiative corrections at the one loop level and results for W physics at LEP-200*, *Fortsch.Phys.* **41** (1993) 307–420, [arXiv:0709.1075].

[170] G. 't Hooft and M. Veltman, *Regularization and Renormalization of Gauge Fields*, *Nucl.Phys.* **B44** (1972) 189–213, [doi:10.1016/0550-3213(72)90279-9].

[171] T. Trueman, *Spurious anomalies in dimensional renormalization*, *Z.Phys.* **C69** (1996) 525–536, [hep-ph/9504315].

[172] S. Larin, *The Renormalization of the axial anomaly in dimensional regularization*, *Phys.Lett.* **B303** (1993) 113–118, [hep-ph/9302240].

Acknowledgements

Four years are a long time and yet they have passed so fast. They would not have been as productive, rewarding and, definitely, not as exciting without the support and understanding of the people who accompanied me. I am sincerely grateful to Prof. Andrzej Buras for including me in his group, teaching, guiding, and working with me. Andrzej was the first to awaken my interest in particle physics and he still does. He was always there for me, supporting and motivating me. I am also greatly indebted to Martin Gorbahn who made me feel at home in the Excellence Cluster, collaborated with me and helped in many aspects of this research without losing his patience. Without his deep insight into the field this thesis would not have been the same. I wish to explicitly thank both Andrzej and Martin for giving me so many opportunities to travel and research abroad. I do not consider this self-evident and feel much obliged and privileged. Many thanks are reserved for Joachim Brod and Luca Merlo who accompanied me throughout this time as close friends and collaborators trying their best to help me understand as much physics I could handle. Joachim invited me to Cincinnati and Luca to Padua, where most fruitful collaborations developed. I warmly thank Prof. Alexander L. Kagan and Prof. Jure Zupan on whom I imposed myself in Cincinnati and at CERN. The collaboration with them has been most exciting and refreshing for me. I thank Prof. Guido Altarelli and Prof. Ferruccio Feruglio for inspiring discussions and a fruitful collaboration. Thanks to Sandro Casagrande and Stefan Vickers for their help and company in the cluster, to Minoru Nagai for his valuable explanations and for teaching me *go*, and, in particular, to Christoph Bobeth who has been so helpful in these last stages of this work. Also, I thank Andreas Weiss and Jure Drobnak for their support. I thank Robert Ziegler for the many, most interesting and elaborate, discussions on physics. Without my friends I would not have made it. I thank Alexander, Andrew, Andrianos, Annalisa, Aris, Christoph, Dan, Johannes, Natalai, Rodrigo and Stefanos, who all helped me in their own way these last years. I thank Julia, Lorenz and Melissa for standing by my side. I did not make it easy for them. I am wholeheartedly grateful to my family for their constant support and understanding.